Dissertation

submitted to the

Combined Faculty of Natural Sciences and Mathematics

of the Ruperto Carola University Heidelberg, Germany

for the degree of

Doctor of Natural Sciences

Presented by

M.Sc. Xin Li

born in: Enshi, China 28th September 1990

Oral examination: 2nd November 2021

Endoplasmic reticulum stress sensor ATF6 as an immunometabolic modulator in hepatic tumorigenesis

Referees:

Prof. Dr. Ralf Bartenschlager

Prof. Dr. Mathias Heikenwälder

Table of Contents

1 Abbreviations

µl	microliter
µm	micrometer
ALP	alkaline phosphatase
ALT	alanine aminotransferase
AP1	activator protein-1
ASH	alcoholic steatohepatitis
AST	aspartate aminotransferase
ATF6	activating transcription factor 6
BECs	biliary epithelial cells
BIP	binding immunoglobulin protein
CCA	cholangiocarcinoma
cDNA	complementary desoxyribonucleic acid
CHOP	CCAAT/enhancer-binding protein homologous protein
CREBH	cyclic AMP response element-binding protein H
CREBP	cyclic AMP response element-binding protein
CRTC2	CREB-regulated transcription coactivator 2
DAMP	damage-associated molecular pattern
DCs	dendritic cells
DEN	N-nitrosodiethylamine
DR	ductular reaction
eIF2α	eukaryotic translation initiation factor 2α
EM	electron microscopy
ER	endoplasmic reticulum
ERAD	endoplasmic reticulum–associated protein degradation
ERO1α	ER oxidase 1α
FACS	fluorescence-activated cell sorting
FFAs	free fatty acids

GP73	Golgi protein 73
GPX	glutathione peroxidase
GRP	glucose-regulated protein
H&E	hematoxylin-eosin
HBP	hexosamine biosynthetic pathway
HBV	Hepatitis-B-Virus
HCC	hepatocellular carcinoma
HCV	Hepatitis-C-Virus
HFD	high-fat diet
HIF-1α	hypoxia-inducible factor-1α
HSC	hepatic stellate cell
i.p.	intraperitoneal
ICAM-1	Intercellular adhesion molecule 1
IL	interleukin
IRE1α	inositol requiring enzyme 1α
KC	kupffer cell
LSEC	liver sinusoidal endothelial cell
MAMPs	microbe-associated molecular patterns
MCD diet	methionine–choline-deficient diet
MDSCs	myeloid-derived suppressor cells
MHC	major histocompatibility complex
MRI	magnetic resonance imaging
NAFLD	nonalcoholic fatty liver disease
NASH	nonalcoholic steatohepatitis
nATF6	nuclear ATF6
ND	normal diet
NK cells	natural killer cells
NKT cells	natural killer T cells
NQO1	NAD(P)H quinone dehydrogenase 1

NRF2	nuclear factor erythroid 2–related factor 2
NT	non-tumoral tissue
PAMPs	pathogen-associated molecular patterns
PDI	protein disulfide isomerase
PDL1	programmed death ligand 1
PERK	protein kinase R (PKR)–like ER kinase
PKR	protein kinase R
RNS	reactive nitrogen species
ROS	reactive oxygen species
RT	room temperature
SCD1	stearoyl-CoA desaturase 1
SDS	sodium dodecyl sulfate
T	tumoral tissue
TACE	transarterial chemoembolization
TG	triglyceride
tg	transgenic
TGFβ	transforming growth factor-b
TME	tumor microenvironment
TNF	tumor necrosis factor
Treg	regulatory T cell
UPR	unfolded protein response
VCAM-1	vascular cell adhesion molecule 1
VEGF	vascular endothelial growth factor
WD	western-diet
WT	wild-type
XBP1	X-box binding protein 1

2 Summary

The liver is the site of the sixth most common form of primary cancer - represented mainly by hepatocellular carcinoma (HCC) and cholangiocarcinoma (CCA). Although the recent increment of knowledge on immunological, metabolic, and genetic mechanisms - from a systemic to a single cell level approach - led to consistent implementation of the therapeutic management of liver diseases and improved quality of life in patients, new challenges became apparent in the development of arising therapeutic strategies for pathologies accompanied by chronic inflammation, like liver cancer.

Elevated endoplasmic reticulum (ER) stress and the unfolded protein response (UPR) have been observed in precancerous diseases associated with the development of liver cancer, such as hepatic viral infection and nonalcoholic steatohepatitis (NASH)[1]. In the context of liver diseases, the inositol requiring enzyme 1α (IRE1α) and the protein kinase R (PKR)–like ER kinase (PERK) branches of UPR have been intensively investigated, whereas the role of activating transcription factor 6 (ATF6) in hepatic diseases has remained elusive[2]. In this study, by employing different genetically modified mouse models and cell lines, I tried to examine and illustrate the role of ATF6 in hepatic tumorigenesis.

In the first place, I analyzed the publicly available databases of liver cancer, the liver biopsy from healthy donors and NASH-diagnosed patients, para-tumor and tumor tissue from liver cancer patients, and tissues from liver cancer mouse models for the expression of ATF6 at both mRNA and protein levels. Strikingly, I detected a significant increase in ATF6 mRNA and protein expression in the diseased areas compared to their corresponding controls. Moreover, by doing immunohistochemistry, I identified the activation of ATF6 in the diseased tissues, indicated by the nuclear localization of ATF6. Based on these observations, I worked on the generation of hepatocyte-specific nuclear-ATF6 (nATF6) overexpression mice.

In a mouse model of hepatocyte-specific activation of the ATF6 branch of UPR, I observed that transgenic homozygous mice die shortly after birth, whereas their heterozygous counterparts can survive for more than one year instead, suggesting a dose-effect. Heterozygous mice develop hepatomegaly, liver damage, and cholestasis at their young ages. Strikingly, the heterozygous mice progress to liver cancer with a tumor incidence of 100% at 12 months. To investigate the underlying mechanisms of the pro-tumorigenic effects by persistent ATF6 activation, I performed RNA-seq, proteomic and metabolic analysis on the liver of the heterozygous animals. I found out that ATF6 is intensively involved in the regulation of hepatic glucose, lipid, and amino acid

metabolism. The sustained activation of the ATF6 arm of UPR in hepatocytes induces hepatocyte cell death and shifts the cellular metabolism to support the energy and building blocks requirements for compensatory proliferation. The high rate of hepatocyte turnover and constant ER stress lead to oxidative stress and hepatic inflammation, resulting in hepatic tumor onset. Meanwhile, the metabolic switch in hepatocytes deprives nutrients in the surrounding environment and further suppresses the anti-tumor function of immune cells.

In the end, I generated hepatocyte-specific ATF6 knockout mice, and I challenged this mouse model with different carcinogenic treatments. Surprisingly, I found ATF6 knockout confers general hepato-protection to mice in response to these treatments, indicating a potential clinical application of ATF6 inhibition in anti-tumor therapies.

3 Zusammenfassung

Die Leber ist der Ort der sechsthäufigsten Krebserkrankung – hauptsächlich representiert durch das Hepatozelluläre Karzinom (HCC) und das Cholangiokarzinom (CCA). Obwohl unsere wachsenden Kenntnisse über die immunologischen, metabolischen und genetischen Mechanismen, von der systematischen bis zur zellulären Ebene zu einem besseren therapeutischen Management der Lebererkrankung geführt sowie die Lebensqualität der Patienten verbessert haben, treten ständig neue Herausforderungen bei der Entwicklung der therapeutischen Strategien für die chronischen Lebererkrankungen wie Leberkrebs auf.

Der erhöhte Endoplasmatischem Retikulumstress (ER Stress) und die ungefaltete Protein-Antwort (UPR) wurden in verschiedenen präkanzerösen Erkrankungen im Zusammenhang mit der Leberkrebsentwicklung - wie hepatische virale Infektion und nicht-alkoholische Steatohepatitis (NASH) - beobachtet. In Lebererkrankung werden die UPR-Signalzweige des Inositol Requiring Enzym 1α (IRE1α und der Proteinkinase (PKR)–ähnliche ER Kinase (PERK) intensiv untersucht, während die Rolle des aktivierenden Transkriptionsfaktor 6 (ATF6) unbekannt bleibt. In dieser von mir vorgelegten Studie wurde die Rolle des ATF6-Zweigs des UPRs in der hepatischen Tumorgenese untersucht, mit Hilfe von genetisch modifizierten Organismen und Zelllinien.

Als erstes untersuchten wir mit Expressionsanalyse von ATF6 von der öffentlichen Datenbank, die Leberbiopsien von den gesunden Probanden und NASH Patienten sowie die Paratumor- und Tumorproben stammt aus Leberkrebspatienten und Mäusen. Überraschend wurde eine signifikante Steigerung der ATF6-Expression auf mRNA- und Proteinebene im kranken Gewebe im Vergleich zu den Kontrollen beobachtet. Darüber hinaus ist aus der Immunohistochemie zu entnehmen, dass die Aktivierung von ATF6 durch seine Nukleus-Translokation manifestiert wurde. Aufgrund dieser Beobachtung haben wir eine Mauslinie generiert, das kerntranslozierende Protein ATF6 (nATF6) spezifisch nur in Hepatozyten überexprimiert.

Anhand dieses Mausmodells, in dem der ATF6-Signalzweig von UPR spezifisch in Hepatozyten aktiviert wird, haben wir festgestellt, dass alle Homozygoten Tiere kurz nach Geburt gestorben sind. Die Heterozygoten Tiere überleben im Gegensatz dazu mehr als ein Jahr, jedoch mit der Entwicklung von Hepatomegalie, Leberschädigung und Cholestase, schon mit früherem Alter. Interessanterweise zeigen die Heterozygoten eine Tumorinzidenz von 100% im Alter von 12 Monaten.

Um die Mechanismen dieses prä-tumorgenen Effekts der ATF6-Aktivierung zu untersuchen, wurden RNA-Sequenzierung, proteomische sowie metabolische Analysen durchgeführt. Ich konnte entdecken, dass die kontinuierliche Aktivierung von ATF6-Zweig des UPRs in hepatischen Glucose-, Lipid- und Aminosäuremetabolismus beteiligt hat. Die anhaltende Aktivierung der UPR des ATF6-Arms in Hepatozyten induziert den Tod von Hepatozyten und verschiebt den Zellstoffwechsel, um den Energie- und Bausteinbedarf der kompensatorischen Proliferation zu decken. Die hohe Umsatzrate der Hepatozyten und der ständige ER-Stress führen zu oxidativem Stress und Leberentzündungen, was zur Entstehung von Lebertumoren führt. Gleichzeitig beutet diese metabolische Umstellung in Hepatozyten auch die Nährstoffe in der Umgebung aus und unterdrückt die Anti-Tumor Funktion der Immunzellen.

Am Ende haben wir noch die hepatozyt-spezifisch ATF6 knockout Mäuse generiert und die mit unterschiedlichen Tumorgenen behandelt. Erstaunlicherweise haben wir gefunden, dass die Abwesenheit von ATF6 einen Schutzeffekt auf die behandelten Mäuse hatte- dies gibt der ATF6-Inhibition einen klinischen Wert in der Entwicklung der anti-tumor Therapie.

4 Introduction

4.1 The liver

4.1.1 The physiological nature of the liver

The liver is a metabolically essential organ found exclusively in vertebrates. It is the second-largest organ located in the upper-right area of the abdomen of the human body[3]. Morphologically, the liver can be split into left, right, caudate, and quadrate lobes from the posterior position[3]. The Couinaud classification further divides the liver lobes into eight functionally independent segments based on the hepatic vascular supply[4] (**Figure 1**). Each segment is equipped with its own vascular system (portal vein and hepatic artery) and biliary tree (bile ducts), according to this system.

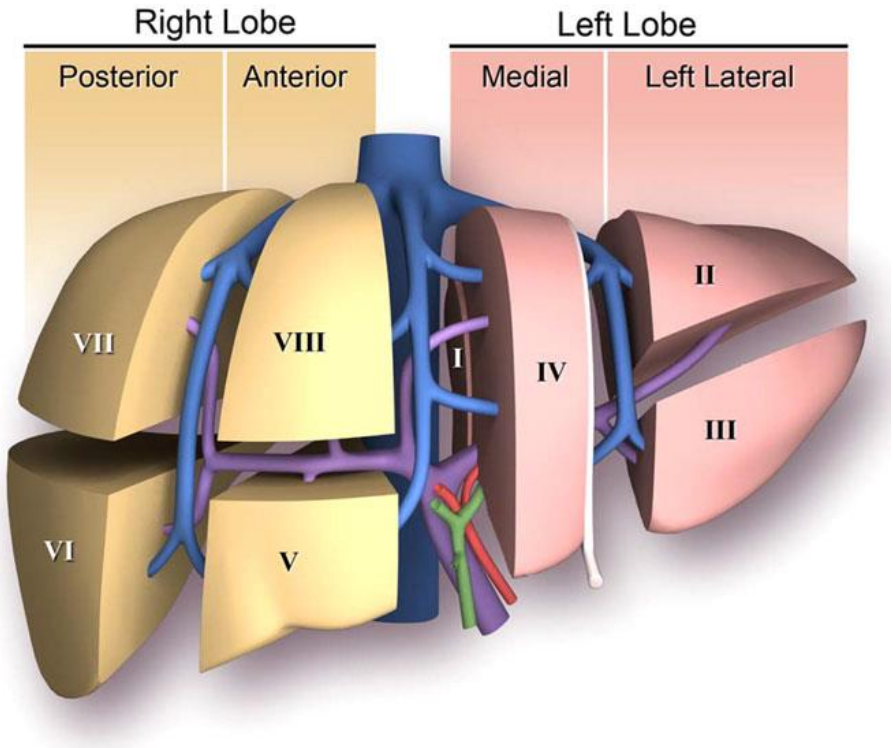

Figure 1: **The Couinaud classification: segmental anatomy of the liver** (adapted from Lena Sibulesky[5]). The Couinaud categorization system divides the functional regions of the liver based on their circulatory supply (segment I to segment VIII).

Microscopically, the building blocks of liver tissue are termed hepatic lobules, which are hexagonal structures composed of plates of hepatocytes, liver sinusoids, portal triads, and a central vein. Hepatic lobules are bound by a connective tissue layer called Glisson's capsule, covering the entire liver[6]. Glisson's capsule further stretches into the liver as sheaths accompanying the hepatic vascular supply. In fact, the hepatic portal vein and hepatic artery

constitute the blood supply of the liver and converge with hepatic ducts at the hepatic hilum. Around 25% of the blood flow to the liver is oxygenated arterial blood, whereas 75% of the blood entering the liver is venous blood[3]. The nutrient-enriched venous blood flowing through the gastrointestinal tract converges the oxygenated arterial blood in the 'liver sinusoid' – a unique fenestrated capillary that slows the blood flow and provides the platform for substance exchanging[7].

The liver governs up to 500 different functions in both humans and mice, including metabolite detoxification, protein synthesis, and secretion of biochemicals required for digestion and growth[8]. These various functions are carried out by distinct crosstalks between hepatic parenchymal cells (e.g. hepatocytes and cholangiocytes) and non-parenchymal cells (e.g. Kupffer cells (KCs), hepatic stellate cells (HSCs), liver sinusoidal endothelial cells (LSECs), and adaptive immune cells). The primary parenchymal cell type in the liver is hepatocytes, which account for approximately 78% of the liver volume[9] and exert the principal functions of the liver (e.g. cholesterol synthesis, bile salts synthesis, phospholipids synthesis, and nutrients metabolism)[10]. The second-largest cell population in the liver is represented by cholangiocytes, which mainly support hepatocytes to transport bile acids by releasing bicarbonate and H_2O[11]. Other resident cells, including HSCs, KCs, natural killer (NK) cells, and natural killer T (NKT) cells, together with other myeloid lineage cells, maintain the immune-suppressive character of the liver[12].

4.1.2 Primary Liver cancer

New treatment options, understanding disease mechanisms, and broader prevention programs (e.g. screening of defined risk-groups of patients) led to reduced mortality rates, decreased incidence, and an increased 5-year survival rate in most solid cancers[13]. Nevertheless, liver cancer opposes these trends[14]. Primary liver cancer originates in the form of different entities: HCC accounts for 80-90% of all primary liver cancers, whereas 10-15% results from CCA. Non-epithelial tumors (angiosarcoma) and pediatric hepatoblastoma make for a comparatively insignificant fraction of primary liver cancer[15] **(Figure 2)**.

The most relevant risk factors for the development of primary liver cancer are chronic inflammatory etiologies leading to chronic necro-inflammation, originating from viral infections (e.g. Hepatitis-B-Virus (HBV), and Hepatitis-C-Virus (HCV)), metabolic alterations (e.g. alcoholic, and non-alcoholic steatohepatitis[16]), chronic toxin exposure or parasite infection (e.g. flukes, and aflatoxin)[12]. Hepatocellular carcinoma, hence the name, was thought to originate from hepatocytes. However, the cellular origin of liver cancer is controversial, although the traditional

assumption " HCC and CCA are transformed from distinct parenchymal cell populations" is widely accepted[17]. Globally, the major risk factor of HCC is still viral infection, which leads to a geographical, region-depend HCC epidemiology; whereas prophylactic immunization and new therapeutic techniques have slowed the increase of HBV and HCV-related liver cancer, lifestyle-related and environmental variables such as sterile inflammation or inflammation induced by alcohol or excessive nutrition show an elevated contribution to HCC formation[15,18]. In fact, chronic liver inflammation is believed to lead to necro-inflammation and to give rise to a pathological state like fibrosis and cirrhosis[12,19], which are strong correlative drivers of primary liver cancer[16]. Furthermore, classical risk factors common to the majority of cancers, namely age, sex, lifestyle, genetic risk factors (e.g. Kras/Braf, C-reactive protein polymorphism activation), also play an important role in liver cancer formation.

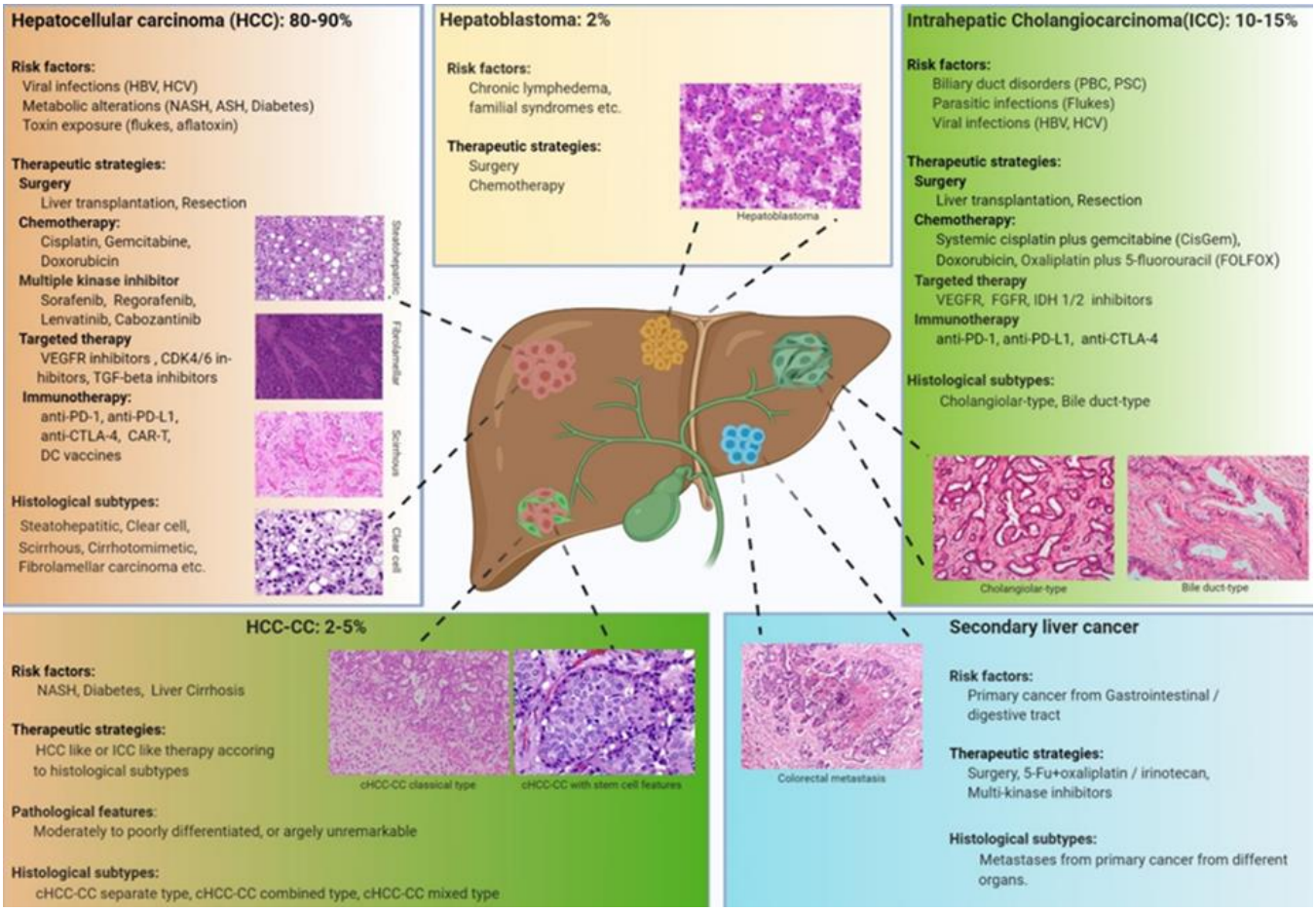

Figure 2: **The incidence, risk factors, and pathological features of hepatic cancer.** Cartoon representing the incidence of different forms of primary liver cancer correlated to their specific risk factors and currently approved therapies, described in detail in the text.

4.1.3 Primary liver cancer treatments

Primary liver cancer is difficult to treat, and only a few therapeutic options have been standardized[20,21] **(Figure 3)**. Generally, a treatment approach is established according to cancer progression, size, and aggressiveness. Treatment options for early-stage liver cancer include liver transplantation as the curative approach with <10% recurrence and approximately 70% 5-years survival[15]. Other treatment options are tumor resections, potentially combined with tumor-reducing therapies (e.g. transarterial chemoembolization (TACE), ablation strategies using radio-frequency or microwaves, thermal approaches, intratumoral ethanol injection, or high dose rate brachytherapy, and selective internal radiotherapy with beta-emitter yttrium-90). Liver cancer chemotherapy (e.g. cisplatin, gemcitabine) or multikinase inhibition with sorafenib, regorafenib, or lenvatinib, however, results in just a modest survival benefit[14,22-28].

Current therapeutic approaches still suffer from a relevant lack of efficacy, and until a few years ago, the only possible therapeutic option for advanced liver cancer was limited to the multi-kinase inhibitor sorafenib[18]. 50-70% of patients successfully treated for liver cancer recidivate in the form of newly formed primary liver cancer or micro-metastasis if the whole cancer-affected lobe cannot be resected[15]. Moreover, the cirrhotic microenvironment of the tumor-bearing liver often prevents sufficient liver tissue removal by resection without compromising the remaining intact liver tissue[13].

To maximize treatment benefits for primary liver cancer, besides careful and individual assignment of anti-cancer therapy, it is opportune to eradicate the underlying cause. In the case of primary liver cancer, it seems reasonable to target the chronic inflammatory stimuli, either by anti-viral therapy (e.g. interferon-based, eradication of HCV by direct-anti-viral agents (DAA and and HBV-load by nucleic-analogs), life-style intervention (e.g. limiting alcohol consumption, diet), reduction of oxidative stress (e.g. vitamin E/C or analogs like raxofelast, silymarin, metadoxine, mitoquinone mesylate) or liver fluke eradication[14,29]. Additionally, during the last 10 years, increased understanding of the complicated cellular and molecular immunological network in the hepatic milieu has resulted in the development of innovative treatment strategies such as immunotherapy[15]. New therapeutic interventions recently reached the clinical phase of FDA approval, like immunotherapy and combinatorial microenvironmental-targeted immunotherapeutic approaches, which might be promising strategies for future first-line liver cancer therapy[14,18,25,28,30,31] (**Figure 3**). Interestingly, an aetiology-dependent efficacy of immunotherapy has been observed in NASH-mediated liver cancer, giving that NASH is a liver disease triggered by metabolic activation of T cells[32].

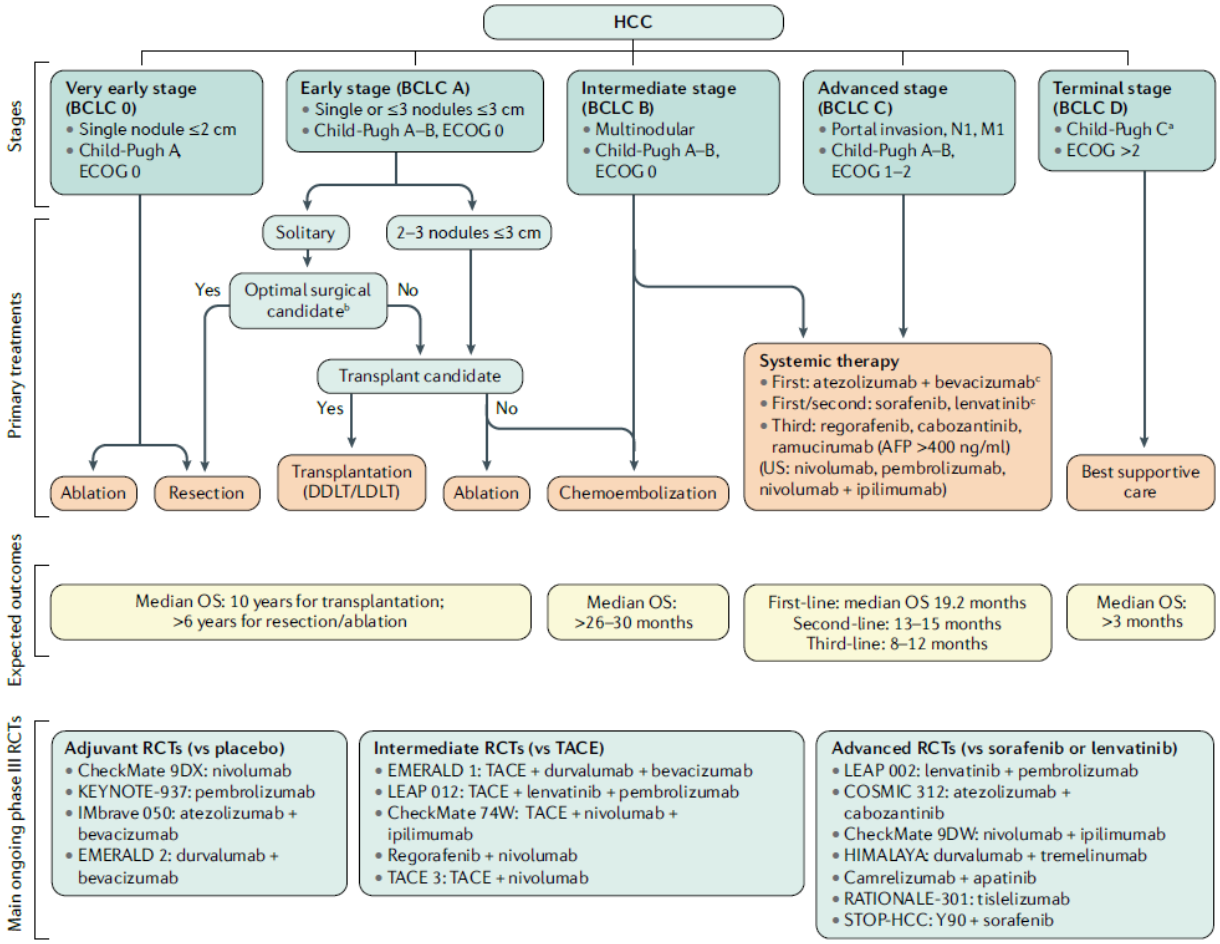

Figure 3. Current HCC treatments in the clinic (Adapted from Llovet et al.[13]). The Barcelona Clinic Liver Cancer (BCLC) staging system classifies liver cancer into five stages, and the figure depicts the treatment techniques for each stage of liver cancer.

4.2 The immunological landscape in liver cancer

4.2.1 The immunotolerant nature of the liver

As evidenced by the fact that hepatic portal blood contains approximately 100 times more microbe-associated molecular patterns (MAMPs) than peripheral blood, the liver is the prophase and powerful organ for clearing pathogen-associated molecular patterns (PAMPs) and MAMPs produced from the gastrointestinal tract[12]. Consequently, distinct regulatory mechanisms to maintain liver immunotolerance against various external stimuli are critical to avoid liver injury[33].

The induction and maintenance of liver immunotolerance are mediated by crosstalks between liver-resident cells and circulating immune cells **(Figure 4)**. A group of endothelial cells covers the liver sinusoid termed LSECs with up to 100 nm fenestration. As a result, the extracellular matrix

rejects particles or antigens larger than 20 nm in blood[34]. A diverse array of pattern recognition receptors (e.g. Toll-like receptors), costimulatory molecules (e.g. CD80, CD86, and major histocompatibility complex (MHC) class I/II), and adhesion molecules (e.g. intercellular adhesion molecule 1 (ICAM-1) and vascular cell adhesion molecule 1 (VCAM-1)) expressed on LSECs endowed them with the ability to serve as efficiency monitors for immune response[12]. Indeed, antigens presented by LSECs via MHC class I stimulate naive $CD8^+$ T cells, resulting in T cell tolerance and maturation of a subpopulation of LSCEs with increased PDL1 expression[35]. KCs account for approximately 80% of macrophages in the body and scavenge the majority of circulating particulate antigens[12]. Depletion of KCs abolishes the immunotolerant character of the liver, indicating the crucial role of KCs in maintaining liver homeostasis[36]. Mechanistically, KCs express high levels of PDL1 but low levels of co-stimulatory molecules, which enable them to dominate the maintaining of immunosuppressive character and anti-inflammatory microenvironment of the liver[36]. Additionally, phagocytosis of host apoptotic cells by KCs is a critical mechanism for suppressing immunological responses induced by inflammatory mediators produced by dying cells. Hepatic dendritic cells (DCs) are less effective in activating T cells than their splenic counterparts; this is mainly due to the high IL-10 and low IL-12 hepatic milieu[37]. Interestingly, liver DCs themselves are a rich source of IL-10[38].

Apart from the regulatory mechanisms outlined previously, it has been shown that other cell types in the healthy liver contribute to its immunotolerant orientation. For instance, regulatory T cell (Treg) expresses a high level of CD25 and CTLA-4 to compete with T cells to bind IL2, CD80, and CD86. Meanwhile, Treg can also secret anti-inflammatory cytokines like transforming growth factor-β (TGF-β) and IL-10[12]. HSCs are also rich sources of anti-inflammatory cytokines (e.g. TGF-β)[39]. Myeloid-derived suppressor cells (MDSCs), which release immunosuppressive cytokines (IL10 and TGFβ) and deplete amino acids essential for T cell proliferation, are also found in the healthy liver[40].

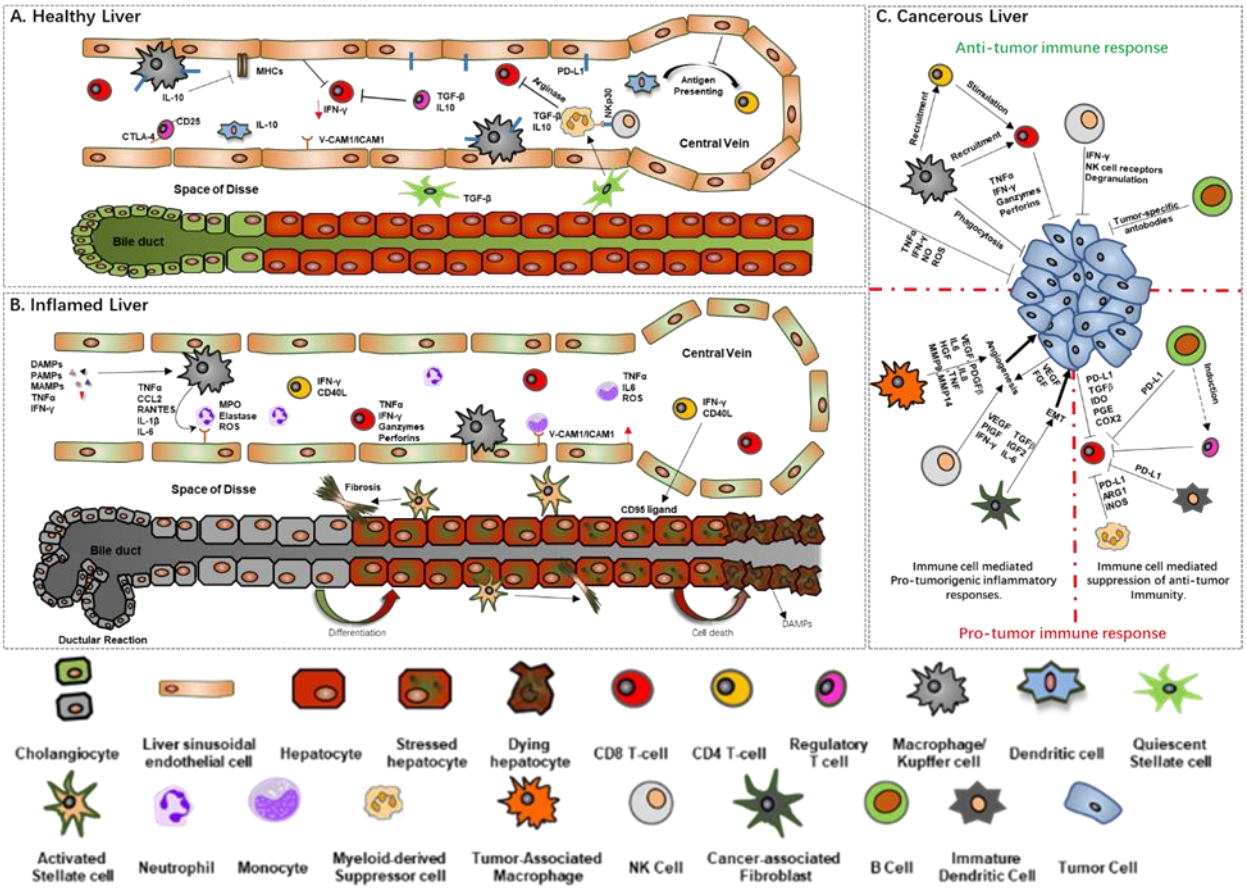

Figure 4: **The healthy, inflammatory, and malignant liver's immune microenvironment** (original figure of Figure.1 in Li et al.[15]). **a).** The maintenance of immune-suppressive character in a healthy liver. **b).** The immunological landscape of inflammatory liver. **c).** Pro- and anti-tumor immune response in the liver microenvironment.[15]

4.2.2 The protumorigenic inflammatory liver microenvironment

HCC was identified as the most prevalent malignancy caused by inflammation[12]. To effectively treat primary liver cancer, it is critical first to understand how it develops nearly entirely due to underlying chronic inflammation[15]. Chronic inflammation in the liver is initiated and maintained by events such as immune cell activation in response to viral infections, proinflammatory cytokines released by the innate immune cells in response to chronic injury, exogenous toxins induced destabilization of intrinsic hepatic cell types (e.g. hepatocytes, and LSECs), lipotoxicity and increased iron deposition[15]. All of the aforementioned etiological variables contribute to an abnormally high level of reactive oxygen species (ROS) and reactive nitrogen species (RNS), resulting in DNA damage and cell death in hepatocytes over time[15].

Hepatocyte cell death acts as a hallmark of chronic inflammation-related liver disorders such as NASH, viral hepatitis, and liver cirrhosis[41]. It is mostly accomplished by two different types of cell

death: apoptosis and necroptosis/necrosis, both of which can be distinguished into further subtypes[41,42]. Recent studies show that additional cell-death processes (e.g. oxeiptosis, pyroptosis, and ferroptosis) may resculpt the liver microenvironment in chronic hepatitis. These are of particular interest but remain understudied in the context of chronic hepatitis[43]. As a result of the loss of an intact cell membrane, dying hepatocytes produce a large concentration of damage-associated molecular patterns (DAMPs)[44]. In conjunction with bio-products derived from excessive lipids or alcohol intake, these 'antigen-like factors' lead to the breakdown of the stabilized immune tolerance[37,45]. In response to exogenous pathogens invasion, KCs activate pattern-recognition receptor signaling and secret a diverse array of pro-inflammatory cytokines (e.g. interleukin (IL)-1, and tumor necrosis factor (TNF)) and chemokines (e.g. CCL1, CCL2, and CCL5/RANTES)[37]. The activation of KCs results in enhanced expression of adhesion molecules (e.g. ICAM-1, and VCAM-1) and decreased platelet endothelial cell adhesion molecule-1 expression on LSECs, which is crucial for the recruitment and transmigration of neutrophils and monocytes[46]. Following the activation of innate immune cells, besides constant monocytes also adaptive immune cells are recruited to the liver, both contributing to the inflammatory hepatic microenvironment.

Prolonged and unresolved inflammation alters the microenvironment of the liver, reshaping it towards a pro-carcinogenic direction[18]. In particular, the crosstalks of cytokines, chemokines, growth factors, and proangiogenic factors in the inflamed liver facilitate cell proliferation and dedifferentiation in a regenerative organ like the liver, an essential process for oncogenic transformation[47,48]. For instance, it has been demonstrated that pro-inflammatory TNF released by KCs promotes hepatic cancer by activating JNK signaling in response to oxidative stress and by enhancing Wnt/-catenin signaling[49]. Other inflammatory cytokines, like IL-1, IL-6, and IL-23, have also been implicated in the tumor-promoting process[50]. Besides, pro-angiogenic factors (e.g. angiopoietin-2, vascular endothelial growth factors (VEGFs)) that are abundant in the inflammatory milieu are required for angiogenesis, a vital step in carcinogenesis[15].

Tumor initiation is a process in which normal cells gain survival benefits and accumulate oncogenic mutations over time[50]. A distinct hepatic biliary phenotype, characterized by hyperproliferation of progenitor-like cells, has often been detected in the injured or inflamed liver, termed ductular reaction (DR)[15]. Accelerated expansion in a mutation-prone environment favors the accumulation of genetic mutations[51], activates oncogenic signaling pathways, and confers malignant potential to the cells[52,53].

Collectively, the diverse surrounding microenvironment shaped by chronic inflammation contributes to its pro-tumorigenic character via different mechanisms. In line with the clinical observations, the diversity of tumor surroundings contributes to the malignant and lethal characters of the tumor. Indeed, liver cancer patients with elevated levels of diversity and heterogeneity in the tumor microenvironment (TME) are negatively associated with cytolytic activities of T lymphocytes and patient outcome[54].

4.2.3 The surveillance of primary tumors

The activation of certain oncogenes and mutation of specific tumor suppressors are commonly recognized origins of malignant cells. They steer the host cell in a premalignant direction and trigger multiple cellular introspective surveillance processes such as apoptosis and senescence[55]. Apoptosis is the most typical way for oncogene/stress-driven malignant cells to be eliminated[56]. The best-known instance operates via the DNA-damage/p53 pathway. The wild-type (WT) p53 protein attaches to damaged DNA and causes hepatocytes to undergo growth arrest until a successful DNA repair is performed. Resting cells that do not mend themselves undergo apoptosis triggered by p53. Mechanisms that inactivate the apoptotic and cell cycle arrest functions of p53, such as inhibition of MDM2 phosphorylation/nuclear translocation by CD44 or loss of function or mutation of p53, effectively shutting down p53's genomic surveillance activity and hastening the onset of HCC[57]. Indeed, in a murine model, loss of p53 accelerates dedifferentiation in hepatocytes and hepatic carcinogenesis[17].

In case the intrinsic “genetic surveillance” of primary carcinogenesis is ineffective, surveillance by immune cells will be employed[15]. The immune system fights against carcinogenesis in multiple manners, for example, by eliminating viruses (e.g. HBV and HPV) and pathogens that directly contribute to tumorigenesis or by scavenging pathogens that could contribute to the pro-carcinogenic inflammatory microenvironment. Apart from these fundamental functions, immune effectors can direct their attention to pre-malignant or nascent tumor cells that have evolved as a result of ineffective intrinsic tumor suppression mechanisms via tumor-associated antigens or stress-induced antigens (e.g. cyclophilin B, SART2, p53, MRP3, AFP, and hTERT)[52]. A significant increase in senescent hepatocytes was observed after antibody-mediated $CD4^+$ T cell depletion in a $Tak1^{-/-}$ mouse model, indicating that the adaptive immune response is critical for the surveillance of malignant cells[58].

4.3 The metabolic landscape in liver cancer

4.3.1 The liver as the central metabolic organ

For centuries, the liver has been recognized as a critical metabolic organ that regulates the body's energy metabolism. It serves as a metabolic hub that connects different tissues (e.g. skeletal muscle, and adipose tissue). In general, the digestion of food in the gastrointestinal tract releases nutrients such as glucose and amino acids, which are further delivered to the liver through the portal vein. During the postprandial period, glucose condenses into glycogen or packs into lipid droplets in the form of triglycerides (TG) in hepatocytes[59]. Amino acids are either digested for energy metabolism or employed in the synthesis of proteins and other bioactive substances. During fasting, the liver releases glucose (glycogenolysis and gluconeogenesis) or TG into the bloodstream to fulfill the energetic demand of extrahepatic organs[8]. These fuel substrates are metabolized in extrahepatic tissues (e.g. muscle) and result in metabolites like lactate and alanine, which in turn go back to the liver and serve as building blocks for gluconeogenesis[8]. Meanwhile, the nonesterified fatty acids released by the adipose tissue go through β-oxidation and ketogenesis in the mitochondria of hepatocytes[8].

In the setting of hepatic vascularity, hepatic zonation is determined by the oxygen gradient and characterized by a distinct distribution of functions within the hepatic lobule **(Figure 5)**[60]. Consequently, whereas all hepatocytes appear to be similar phenotypically, their location along the lobule exposes them to distinct microenvironments, resulting in functional differentiation[15]. In particular, the oxygen gradient divides the hepatic lobule into oxygen-rich Zone-1 in the portal area, oxygen-medium Zone-2, and oxygen-low Zone-3 around the pericentral vein. Functionally, ATP-consuming tasks, including synthesis and secretion of the protein, fatty acid β-oxidation, and gluconeogenesis, are carried out in Zone-1; Iron metabolism and maintenance of insulin-like growth factor homeostasis take place in Zone-2; And low energy-demanding activities such as glycolysis, detoxification, and lipogenesis are mainly executed in hepatocytes located in Zone-3[61]. Indeed, the metabolism-related sequential enzymes in hepatocytes reveal a unique distribution along the Porto-central axis in the hepatic sinusoid[15].

Given the intimate relationship between parenchymal and non-parenchymal cells in the liver, it was demonstrated that the latter cells also exhibit a distinctive spatial distribution. For instance, the pericentral LSECs and periportal LSECs show differences in the expression of at least 60% of their genes. The zonation of KCs has also been reported, given that KCs located in Zone-3 show more cytotoxic activity and are more potent in the production of IL-1β, whereas their

counterparts in the portal area are offering a protective niche by secreting TNF and elevate their phagocytic activity[62,63]. In addition, the gene expression profile and functionality of HSCs are also spatially regulated. As reported, the HSCs associated with Zone 1 express a high level of NGFR; instead, their counterparts in Zone 3 express ADAMTSL2 and are critical for collagen secretion upon CCL4 challenge[64].

This spatial-temporal arrangement of hepatic metabolism defines an appropriate evolutionary degree of organization, which generates a milieu that specifies the functional communication of hepatic parenchymal and non-parenchymal cells[15]. Disturbance in the balanced interaction is fundamental in inducing liver inflammation and contributing to the acceleration of disease-promoting cancerogenic changes[15].

4.3.2 The metabolic landscape in the inflamed liver

The spatial organization of hepatocyte functions can be changed in different settings of liver disorders or can specifically characterize the development of a given pathology[15]. For instance, alcohol-induced hepatic injury is primarily restricted to pericentral Zone-3, where the enzymes and genes involved in detoxification and lipogenesis are most abundant[65]. Similarly, excessive calory intake-induced metabolic stress results in hepatic steatosis, and hepatocyte dysfunction also favors the pericentral area due to the high expression of enzymes involved in glucose and lipid metabolism[15]. It was discovered, however, hepatic zonation is gradually lost as the disease progresses, implying that alterations in the metabolic milieu result in decreased organ functionality[66].

NASH has developed into one of the most representative and widespread metabolic dysfunctions in the liver[67]. Accumulated free fatty acids (FFAs) and FFAs-related byproducts in hepatocytes result in lipotoxicity, which facilitates cellular damage and hepatocyte death. The continuous hepatocyte cell death and compensatory proliferation lead to KCs activation and ROS generation, further accelerate the progression of chronic hepatitis. Interestingly, oxidative stress and hypoxia may arise due to metabolic changes associated with the oxygen gradient generated by hepatic zonation, giving that the expression of two master regulators involved in oxidative stress and hypoxia (namely nuclear factor erythroid 2–related factor 2 (NRF2) and Hypoxia-inducible factor 1-α (HIF-1α), respectively) is spatially regulated in chronic hepatitis induced by NASH[68,69] or hepatic viral infections[70]. In fact, the induction of hepatic steatosis via changing the hepatic zonation and modulating lipogenic genes' expression has been often observed in HCV-infected livers, implying that liver metabolic zonation might suggest a specific tropism for viral infections[71].

On the other hand, chronic inflammation, in turn, could reshape liver metabolic programs via the secretion of cytokines by infiltrating lymphocytes to inhibit β-oxidation and lipid turnover in hepatocytes[72].

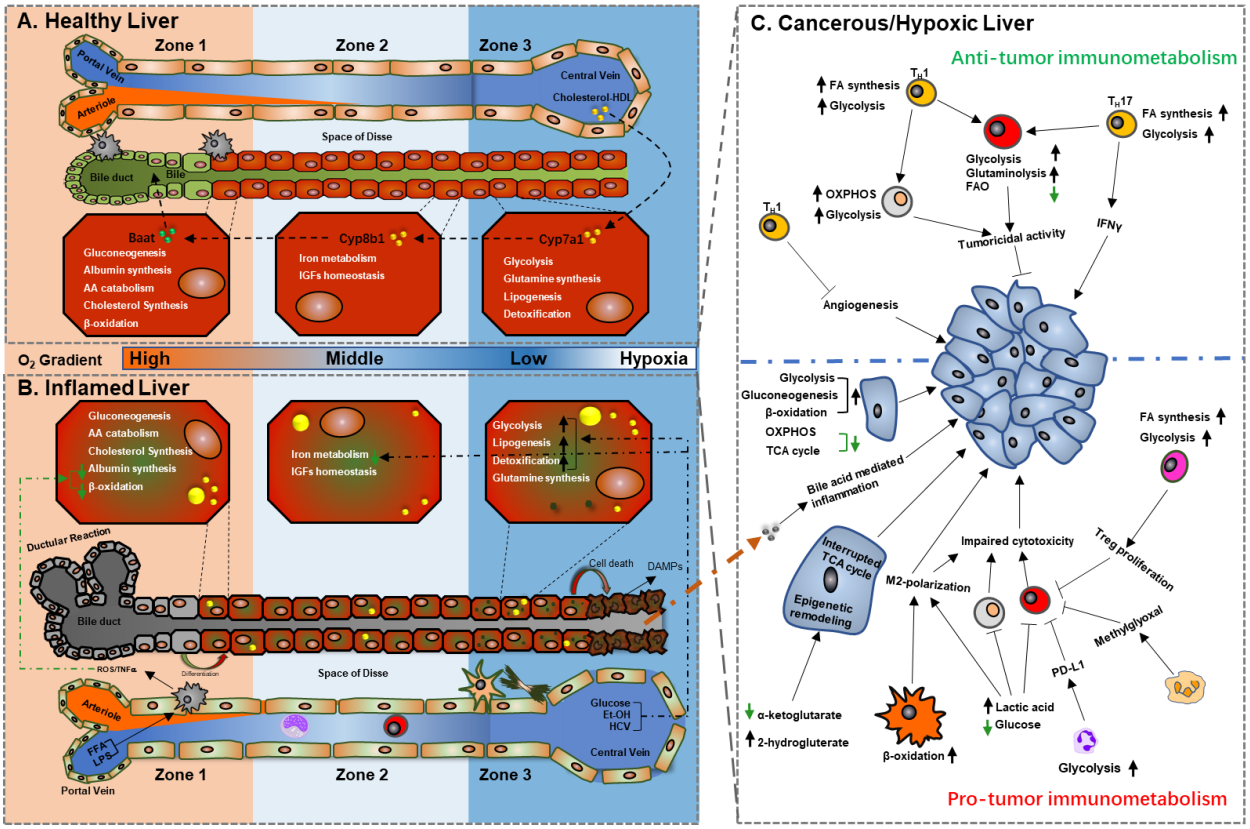

Figure 5: **The healthy, inflammatory, and malignant liver's metabolic microenvironment** (the original figure of Figure.2 in Li et al.[15]). **a).** The spatial distribution of hepatocytes enables the liver to perform its metabolic, detoxifying, and synthesis tasks in a healthy liver. **b).** The metabolic landscape of inflammatory liver. **c).** The metabolic reprogramming of tumor cells and tumor-associated immune cells rewire the anti-tumor immune responses in the TME.[15]

4.3.3 The metabolic landscape in the cancerous liver

Regardless of the etiologies, metabolic modulation in glucose, nucleotide, and lipid metabolism has been recurrently identified in hepatic malignancies. Tumor cells utilize aerobic glycolysis, which burns glucose in a way 15 times more inefficient compared to oxidative phosphorylation, to meet their metabolic and anabolic demands for malignant expansion[59]. In this setting, malignant cells are compelled to uptake a significantly greater quantity of glucose from the environment, leading to a nutrition-deprived surrounding for other cell types in the milieu[73]. The elevated rate of glycolysis results in accumulated metabolites such as lactate, which is immunosuppressive and leads to an acidic microenvironment. Glycolytic intermediates can be further diverted to other

glucose metabolic pathways, including the hexosamine biosynthetic pathway (HBP), the pentose phosphate pathway, the citrate cycle, and other metabolism pathways[15]; which are affected by the elevated glycolytic rate and are found commonly dysregulated in liver cancer[59].

Mechanisms of metabolic reprogramming are critical in treating hepatic cancers, especially for those whose etiology is primarily related to metabolic reprogramming, such as NASH and alcoholic steatohepatitis (ASH) induced HCC. For example, elevated levels of circulating fatty acid or glucose as a result of adipose tissue mobilization of fatty acids in response to an imbalanced lipid intake shift the energy metabolism of cancer cells toward glucose and fat catabolism as the primary energy sources[74]; conferring tumor cells enhanced ability in malignant expansion and resistance to anti-tumor therapies[75].

The alterations in metabolism affect not only the host cells (hepatocytes or tumor cells) but also the immune cells of their functionality in the same hepatic milieu. The altered metabolic environment can potentially change the liver's immunological responses, allowing tumor cells to avoid immune surveillance mechanisms. Indeed, in a mouse model of nonalcoholic fatty liver disease (NAFLD), in which the animals were fed a methionine–choline-deficient diet (MCD diet), the excessive linoleic acid induces lipotoxicity and results in a selective loss of $CD4^+$ T cells, contributing to the collapse of anti-tumor immune surveillance and hepatocarcinogenesis[76].

In the context of liver cancer, tumor cells exhaust nutrients and leave other cell types in a nutrition-deprived milieu. Thus, as a consequence, metabolic reprogramming has been recurrently observed in tumor-associated immune cells with altered functionality **(Figure 5c)**. For instance, macrophages in the HCC microenvironment acquire an M2-phenotype, which is associated with higher fatty acid oxidation capacity and promotes tumor cell motility[77]. The increased ability of Tregs to consume energy substrates such as lipids and glucose appears to be associated with their development in the HCC microenvironment, which suppresses the host anti-tumor immune response[78]. Clinical observations have also implied the phenotypes as mentioned above; HCC patients with high expression of pyruvate kinase 2 were associated with a robust pro-inflammatory polarization of $CD8^+$ T-cells, T-regs, and M2 macrophages[79]. Thus, cancer cells may become susceptible to complementary therapies when specific enzymes involved in crucial metabolic pathways are targeted. In this direction, inhibition of stearoyl-CoA-desaturase and acetyl-CoA-carboxylase has already achieved promising results in animal models[15].

4.4 Endoplasmic Reticulum Stress

4.4.1 ER stress and the UPR

The ER is a membrane-bound subcellular organelle with an intricate three-dimensional structure comprised of a diverse array of structural domains (**Figure 6**)[80]. As the primary subcellular compartment engaged in protein folding and maturation, the ER synthesizes approximately one-third of the total proteome[81]. The majority of the secreted proteins or membrane proteins are processed and quality-checked in the lumen of ER prior to being released to the extracellular environment or displayed on the cell surface[82]. Consequently, the maintenance of physiological functions of the ER provides vital significance for cellular homeostasis.

Perturbations that can affect ER function vary from the change of nutrition status (e.g. feeding, or starvation) to acute stress (e.g. Ischemia/reperfusion damage or inflammation), leading to fluctuations in ER's ability for protein folding and abnormal increase of misfolded proteins inside the lumen[2]. This biological status is termed ER stress, whose role has been widely reflected in different diseases, including diabetes, Alzheimer's disease, and cancer of various origins[81].

The constant monitoring of ER lumen conditions, the sensing of stress-inducing stimuli, and the adaptive regulation of ER's protein-folding capacity are conducted via a collection of integrated signaling pathways termed the UPR[82]. Mammalian cells orchestrate three branches of UPR, which are defined by the transmembrane ER stress sensors: IRE1α, PERK, and ATF6 **(Figure 7)**[82]. Each branch's activation results in the production of b-ZIP transcription factors and the activation of UPR target genes, but the processes and outcomes differ. IRE1α activation requires its conformational change (dimerization, oligomerization, and trans-autophosphorylation) of this molecule to induce its RNase activity, enabling it to excise a 26-nucleotide fragment on the mRNA of X-box binding protein 1 (XBP1) to express XBP1s (spliced form) and to degrade a subset of mRNAs via regulated IRE1α-dependent decay of mRNA. XBP1s' expression regulates genes related to protein folding, translocation, secretion, and endoplasmic reticulum-associated protein degradation (ERAD)[83].

PERK shares a similar activation procedure as IRE1α; activation of PERK facilitates phosphorylation of eukaryotic translation initiaton factor 2α (eIF2α), which inhibits protein synthesis and thus reduces the entry of proteins into the ER, therefore is beneficial for the cells to resolve stress[84]. Importantly, phospho-eIF2α permits the mRNAs with specific open reading frames in their 5´-UTR (untranslated regions), including ATF4, to translate into transcriptional

factors. ATF4 regulates the expression of genes that participate in various biological processes, including cellular redox balance, amino acid metabolism, cell growth arrest (e.g. GADD34), apoptosis (e.g. CCAAT/enhancer-binding protein homologous protein (CHOP)), and ER chaperones' production[81]. The role and function of the ATF6 branch of UPR will be discussed in section 4.4.5 of this thesis.

UPR activation expands the ER membrane to restore protein-folding ability and to maintain cellular homeostasis[81,82]. In 1988, an innovative study demonstrated that upregulation of critical ER chaperone proteins (e.g. glucose-regulated protein (GRP) 78 and GRP94) maintains cellular homeostasis in the presence of protein folding stress in mammalian cells[85]. GRP78, which falls into the heat shock protein HSP70 family and is also known as binding immunoglobulin protein (BIP), was considered the most critical chaperone and a master regulator of the UPR during ER stress. BIP binds to unfolded/misfolded proteins to facilitate proper assembling and prevent their transportation. Meanwhile, it also binds Ca^{2+} to regulate the UPR signaling. Early studies suggested that BIP is bounded with ATF6, PERK, or IRE1α to keep these ER sensors in an inactivated state in non-stressed cells. Upon stress, BIP releases from these sensors to initiate the UPR[86] **(Figure 7)**. However, recent finding reveals that the IRE1α branch of UPR can be regulated independently of BIP[82].

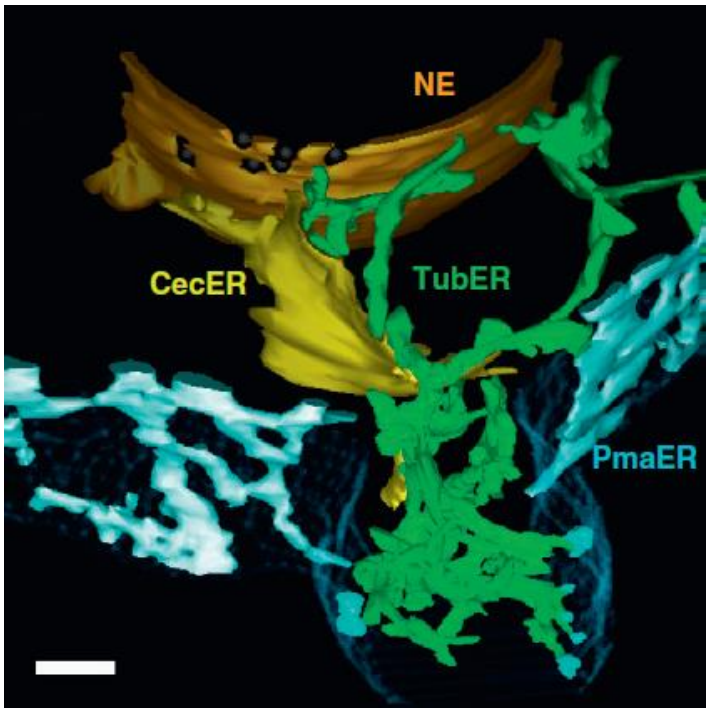

Figure 6. The three-dimensional architecture of the ER (adapted from Friedman et al.[80]). A representative image from electron microscopy reveals the three-dimensional architecture of the ER. CecER: central cisternal ER, TubER: tubular ER, PmaER: PM-associated ER, NE: nuclear envelope.

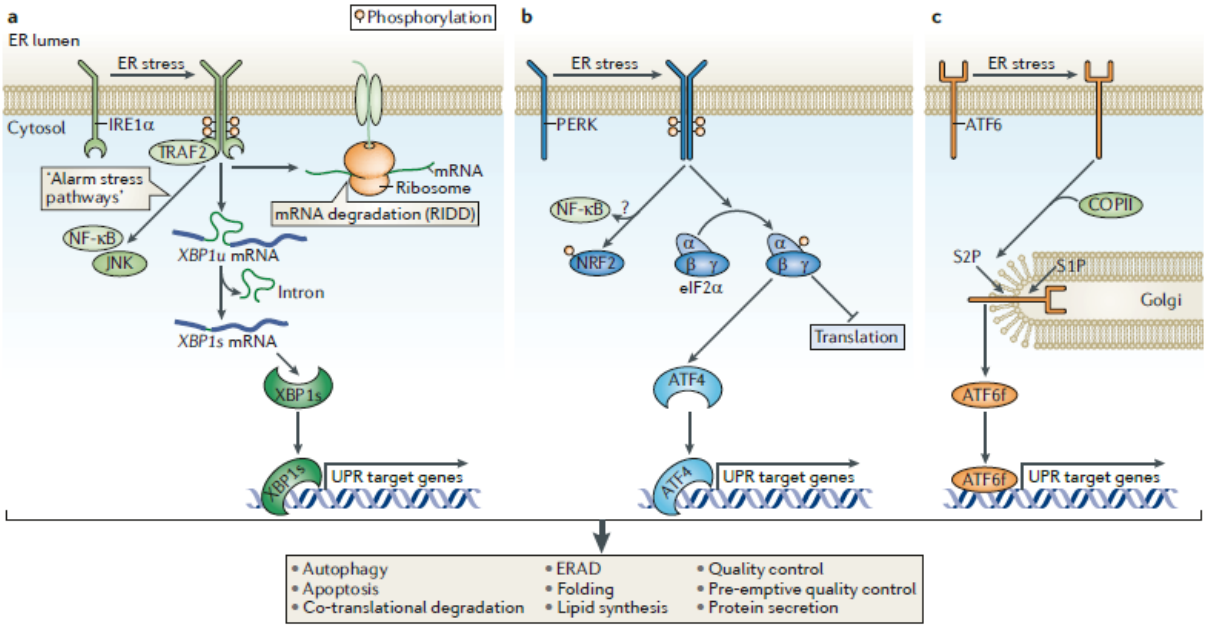

Figure 7: The different branches of the UPR (adapted from Claudio Hetz[83]). The activation of a distinct branch of the UPR transmits information about the ER's folding status, triggering a cascade of biological actions that restore the ER's protein-folding capacity.

4.4.2 ER stress in inflammation and immune response

Conventionally, the activation of the UPR networks was thought to control cellular homeostasis and aid tissue damage. Emerging evidence suggests that ER stress-induced UPR is also closely associated with various inflammatory and stress signalings, which are commonly identified in inflammatory diseases such as diabetes, atherosclerosis, and cancer[87]. In the context of liver diseases, persistent and unresolved ER stress induces UPR-mediated cell death in hepatocytes, which release DAMPS, eliciting an inflammatory response and contributing to disease progression[15].

Both ER stress and inflammation are transitorily adaptive mechanisms for cell survival and restoring organ functions, and both are deleterious when chronically activated. All three branches of the UPR are able to mediate pro-inflammatory programs, mainly through the activation of NF-κB signaling, AP-1 pathway, and generation of ROS **(Figure 8)**. As the central mechanism of the inflammatory response, NF-κB can be induced by three branches of UPR via distinct means[87]. IkB proteins keep NF-κB in an inactive status in non-stressed cells and prevent its nuclear translocation. Upon the UPR activation, IRE1α initiates a program that could degrade IkB and promote NF-κB translocation to the nucleus[88]. Interestingly, the activation of the PERK branch of UPR phosphorylates eIF-2α, which translationally suppresses the expression of IkB and leads to

the activation of NF-κB. Moreover, the activation of PERK-eIF2α also activates CHOP to induce apoptosis of the stressed cells, as the initial step of inflammation onset[89]. In 2009, a link between the ATF6 branch of UPR with the activation of the canonical NF-κB pathway had been reported. However, the exact mechanism remains elusive[90].

Besides the NF-κB pathway, the IRE1α branch of UPR was responsible for ER stress-induced activation of JNK-AP1 signaling. AP-1 is a dimerized complex consisting of peptides from the JUN, FOS, ATF, and MAF families. It serves as a transcriptional factor that facilitates the release of pro-inflammatory cytokines like TNF, IL-6, keratinocyte growth factor, and IL-8[89]. Notably, the IRE1α branch of UPR acts as an important modulator for the secretion of inflammatory cytokines in multiple cell types (e.g. endothelial cells, lymphocytes, and macrophages), as the activation of XBP1 by IRE1α is indispensable for the optimal expression of IL-6, CXCL-3, and monocyte chemoattractant protein 1[91].

In inflammatory liver disorders (e.g. viral hepatitis and NASH), ROS/RNS and the UPR have been frequently observed; it seems that they often co-occur[15], probably due to the tight connection between mitochondria and ER through mitochondria-associated ER membranes[92]. The ROS originated from the ER is mainly controlled by protein disulfide isomerase (PDI) and ER oxidase 1α (ERO1α), given their ability to regulate the formation of disulfide bonds in ER-resident proteins[93,94]. PDIs receive electrons from substrates involved in protein folding to oxidize the thiol group in protein cysteine residues to generate disulfide bonds; the reduced PDIs can further reduce and isomerize disulfide bonds[95]. Meanwhile, ERO1α catalyzes the transfer of electrons from PDIs to oxygen molecules, recycles PDIs, and generates ROS[95]. ER-induced ROS can mediate calcium release, given that the ER act as a calcium-storage organelle, and calcium channels are targets of ROS in the ER. Released calcium could be taken by the mitochondria and stimulate mitochondrial ROS production[96]. Other ER-resident transcription factors, such as cyclic AMP response element-binding protein H (CREBH), might also participate in the UPR-mediated inflammatory response. Both CREBH and CHOP have been reported to be involved in iron metabolism and inflammatory pathogenesis via regulating hepcidin secretion[97].

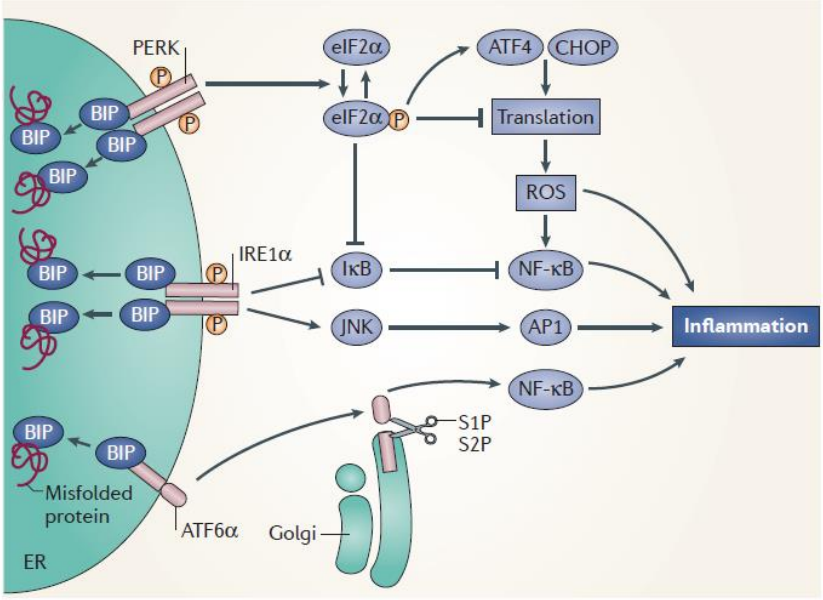

Figure 8: The different branches of UPR and inflammation (adapted from Wang et al.[98]). The three branches of UPR are connected to the induction of inflammation via distinct mechanisms.

Besides above mentioned ER-inflammation links, it is worth noting that hepatic ER stress is more pro-inflammatory due to the increased susceptibility of stressed hepatocytes to TNF-induced cell death[99]; and the stress signal generated by a single cell in the liver can be conveyed to the adjoining milieu[15]. This can be accomplished through the use of effective mediators such as the soluble version of Golgi protein 73 (GP73), which activates the UPR in adjacent non-parenchymal cells like macrophages to induce the activation of pro-inflammatory GSK-3, NF-κB, and MAPK pathways[100,101].

4.4.3 ER-stress and metabolism

Emerging evidence suggests that the activating UPR signaling modulates a variety of physiological processes in addition to homeostatic maintenance and protein quality control, reflecting the intricate communications between the UPR and other cellular signaling pathways[83]. Given that ER and Golgi apparatus cooperate to transport and release correctly assembled proteins involved in various biological events, the disturbances related to ER dysfunction have been commonly thought of as a consequence of ER's adaption to protein folding requirements. However, critical and emerging perspectives pointed out that these consequences can not simply be addressed by cell-autonomous responses to restore protein folding capacity and cellular homeostasis[87]. The types of the UPR may differ in distinct cell types in response to the same challenge or in the same cell type in response to different challenges. For example, in cells that display high secretion rate (e.g. B cell, and pancreatic β cell), activation of the UPR is meant to

restore or increase the protein-folding capacity of ER to meet the demand for protein folding and secretion[102]. Whereas in metabolically active cells such as hepatocytes and adipocytes, which synthesize a large number of lipoproteins, activation of the UPR tends more to maintain the ER homeostasis to couple with lipid status[87].

Hepatocytes are highly activated in glucose and lipid metabolism, and they serve as the primary source of glucose and lipid for other systemic organs. All three branches of UPR are involved in glucose metabolism; the first set of UPR target genes are chaperones from the GRP family. An emerging amount of literature suggests the pivotal role of the UPR in monitoring glucose fluctuations and maintaining glucose levels[83]. For example, whole-body PERK-deficient mice or mice harboring functionally mutated eIF2α were shown defective gluconeogenesis phenotype in the liver[103]. Indeed, hepatic overexpression of the C-terminal domain of Gadd34, which enforces the dephosphorylation of eIF2α, diminishes glycogen storage and impairs gluconeogenesis in the liver of transgenic mice under high-fat diet (HFD) feeding. This work further suggests that translational regulation of metabolic regulators by eIF2α adds to deleterious effects of food excess[33]. XBP1, the downstream target of IRE1α, has been shown to regulate lipogenesis, glycogen synthesis, and glucose output[104,105]. Interestingly, the activation of the ATF6 branch of UPR has been linked to glucose metabolism by competing with cyclic AMP response element-binding protein (CREBP) to bind CREB-regulated transcription coactivator 2 (CRTC2). In response to ER stress, activated ATF6 binds to CRTC2 to form a complex that occupies the promoter of XBP1. Therefore, the CREB-CRTC2 interaction is disrupted together with its downstream target genes that are involved in gluconeogenesis[106].

Not surprisingly, all three branches of UPR pathways are implicated in fatty acid and cholesterol metabolism. In a liver-specific XBP1 deletion model, mice are protected from developing hepatic steatosis under a high-fructose diet feeding. Mechanisms involved are transcriptional regulations of genes that participated in the synthesis of fatty acid (e.g. stearoyl-CoA desaturase 1 (SCD1), acetyl-CoA carboxylases 2, and diacylglycerol acyltransferase 2) by XBP1 activation[104]. On a similar note, an in vivo study shows that depletion of PERK in mouse mammary epithelial cells results in reduced content of FFA in the milk due to the compromised expression of genes including FAS, ACL, and SCD1[107].

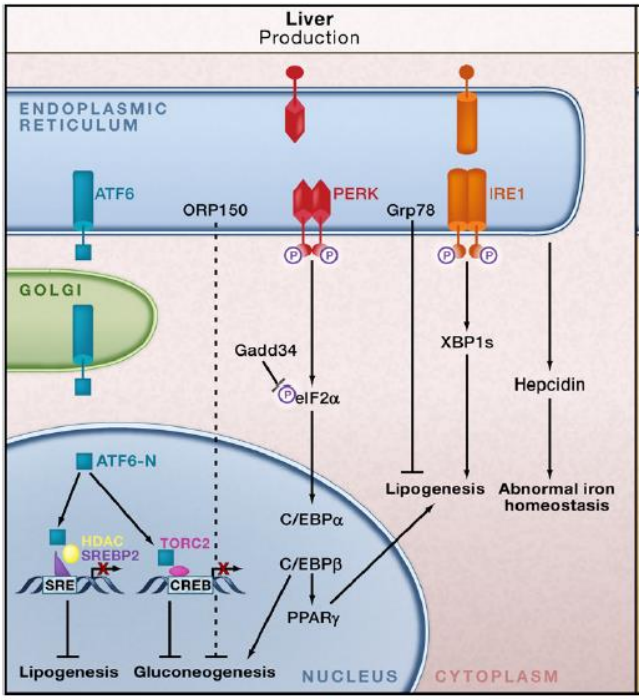

Figure 9:The UPR and metabolic homeostasis (adapted from Hotamisligil[87]). ER stress disrupts the metabolism of lipids, glucose, and iron in the liver via distinct mechanisms.

In a model which mice are exposed to an extreme level of ER stress induced by tunicamycin, hepatic depletion of ATF6, IRE1α, or p58IK or functionally mutate eIF2α (inhibition the PERK branch of UPR) in mice all compromise their ability to recover from tunicamycin-induced hepatic steotosis[108]. This study reveals the roles of three branches of UPR on lipid metabolism; however, as the extreme stress induced by tunicamycin is not comparable or even not relevant to the physiological situation, the actual impacts of the distinct UPR branches in hepatic lipid metabolism in physiological or pertinent pathological settings remain elusive and demand further experimentation.

The UPR controls not only molecules involved in glucose and lipid metabolism but also signaling networks involved in the metabolic destination of other nutrients (e.g. amino acid). Therefore, in addition to a protein-folding unit, the ER also functions as a nutrient-sensing organelle and is closely linked to other metabolic regulatory mechanisms such as mTOR signaling[109]. In fact, with our knowledge gaining in ER stress, the UPR is turning into a promising strategy for dealing with metabolic diseases (e.g. obesity, NASH, and diabetes) and cancer.

4.4.4 ER stress and cancer

Tumor growth persists regardless of various cell-intrinsic and cell-extrinsic challenges, such as oxidative stress, nutrient deprivation, hypoxia, and acidic extracellular environment[110]. Despite the

different types of stress, persistent and robust ER stress has been frequently detected in different types of cancer, including pancreatic, lung, liver, brain, and even non-solid tumors[98].

In the previous two sections of this chapter, I discussed the UPR in promoting inflammation and remodeling glucose/lipid metabolism in host cells, which serve as the major mechanistic underpinnings for the pro-tumorigenic effect of the UPR. This could be explained by the built-in pro-survival character of the UPR, as cells exposed to stress may obtain different oncogenic potentials (e.g. DNA damage, genetic mutation, chromosome instability, etc.). Therefore, pro-survival benefits to these cells offering them the opportunity to accumulate cellular oncogenic signatures and become cancerous. Indeed, PERK knockout mice show delayed tumorigenesis in MMTV-*Neu*-induced mammary tumor[111], while PERK activation accelerates MYC-mediated malignancy transformation in cells via ATF4-CHOP-induced autophagy[98]. The role of the IRE1α branch of UPR in tumorigenesis has been investigated intensively in multiple myeloma, where the elevated XBP1s level has been frequently detected. Indeed, overexpression of XBP1s drives multiple myeloma pathogenesis in mice[112]. Notably, tumor cells harboring mutated IRE1α or XBP1 have been identified in patients suffering from multiple myeloma and connected with drug resistance towards proteasome inhibition[98]. The anti-tumorigenic function of ER stress in host cells has been less documented compared to its protumorigenic effect. XBP1 depletion in small intestinal epithelium accelerates intestinal tumorigenesis in mice[113], emphasizing a tumor-inhibiting role of the IRE1α branch of UPR. Conventionally, CHOP was thought to be a downstream target of the PERK-ATF4 axis, whereas recent evidence suggests that this concept might not be comprehensive, as the activation of CHOP can be independent of the PERK branch of UPR. In chronic ER stress, induction of CHOP may induce apoptosis in premalignant cells and prevent malignant transformation. In a Kras-induced lung cancer model, knockout of CHOP elevates the tumor incidence. A similar phenotype has also been seen in a HCC mouse model[98], suggesting a different role of CHOP in tumorigenesis compared to the PERK-ATF4 axis. However, although the stressed cells or premalignant cells can go through the UPR-mediated cell death, the DAMPs released by dead cells can still initiate immune responses and promote the inflammatory environment, which benefits tumorigenesis and tumor growth.

In the established TME, the deprivation of oxygen and nutrition together with the acidic surrounding pH predominantly burst ER-stress[110]. Mechanistically, oxygen shortage leads to cellular ROS accumulation, which further contributes to ER stress and stabilizes HIF1α - a fundamental transcriptional factor in response to hypoxia[114]. Meanwhile, highly reactive peroxidized lipids, which are generated as byproducts of ROS, could destroy ER chaprone[115].

Glucose and glutamine deprivation, which is commonly detected in the TME and probably mainly due to the Warburg effect, restricts the HBP. Given that HBP generates UDP-sugars, which are essential for protein glycosylation and protein folding. Besides the environmental factors, the cell-intrinsic factors such as the activation of oncogenic signaling and enhanced protein synthesis/secretion rate induce or aggravate ER stress. Indeed, malignant transformation mediated by suppression/loss of tumor suppressors (e.g. p53, PTEN, or TSC 1/2) significantly promotes the protein synthesis, contributing to ER stress[110].

4.4.5 Activating Transcription Factor 6

Compared to the IRE1α and PERK arm of UPR, the ATF6 branch of UPR is the most underinvestigated. Mammalian cells express two ATF6 isoforms – ATF6 (known as ATF6α, 670 aa) and ATF6β (703 aa); both share a high degree of sequence similarity in their b-Zip domains for binding to ER stress-response element but exhibit distinct transcriptional activation N-terminal domains. It has been documented that the α form of ATF6 is a more potent but more labile transcriptional activator compared with its β form homo-isomer, and the activation of ATF6α occurs earlier than ATF6β upon ER-stress[116]. Therefore, in my study and this thesis, I investigate and focus on the role of ATF6α in liver tumorigenesis.

Unlike IRE1α and PERK (type I transmembrane protein), ATF6 is a type II transmembrane glycoprotein with a molecule weight around 90 kDa, which falls into the bZIP transcription factor family[117]. Under phycological conditions, ATF6 is kept in an inactive form via interaction with BIP. Upon ER stress, ATF6 disassociates from BIP and exposes its Golgi-localisation sequences (GLS) at 468–475 aa and 476–500 aa within the ER-luminal domain, eliciting its Golgi apparatus translocation. Notably, the successful transportation of ATF6 from ER lumen to Golgi apparatus requires coat protein II endosomes[118]. ATF6 is produced both in monomers and in oligomers, probably due to the coexistence of intra- and inter-disulfide bridges in its ER luminal domain. However, only ATF6 in its reduced monomeric form may enter the Golgi apparatus[87], suggesting the importance of the redox status in activating the ATF6 arm of UPR and a potential link of ATF6 to cellular redox regulation[87]. The full-length ATF6 is cleaved successively by Site-1 protease (S1P) and S2P to remove its luminal domain and the transmembrane anchor, respectively[117]. The remaining 50 kDa N-terminal cytoplasmic domain (nATF6) containing the nucleus translocation sequence could enter the nucleus and bind to the promoter of ER stress element-containing genes, UPR element-containing genes, and cAMP response element-containing genes[119].

According to certain researches, ATF6 may accelerate hepatocarcinogenesis via modulating the expression of its target genes[98]. A missense variation in ATF6 increases the host's susceptibility to HCC by enhancing the mRNA expression of its downstream genes[120]. Indeed, it has been discovered that BIP, the most important target of ATF6 and a master regulator of ER stress, could indicate the malignancy of tumor cells[98]. In response to ER stress, ATF6 rapidly promotes the production of BIP, and the latter binds to unfolded or misfolded proteins, alleviating ER stress[98]. In unstressed cells, BIP is usually restricted to the ER lumen and maintained at a physiological expression level, however, it has been detected on the cell surface of many human malignant cells, probably due to the overexpression of BIP in these cells[98].

Although studies have documented a potential link between ATF6 and liver cancer, the actual role of ATF6 in hepatic tumorigenesis and the underlying molecular mechanisms remain elusive. In this study, I aimed at exploring the potential relationship between ATF6 expression, its impact on the liver microenvironment, and hepatic tumorigenesis.

5 Hypothesis and aims

In my Ph.D. project, three main questions regarding the ATF6 branch of UPR were addressed in the context of liver cancer.

First, what is the role of persistent activation of ATF6 in the development of liver cancer?

Second, what are the underlying mechanisms of the ATF6 activation-mediated tumor-promoting effects?

Last, how could our knowledge about hepatic ER stress in different etiologies be employed to guide therapeutical interventions for liver cancer treatments?

Increasing evidence suggests that activation of the ATF6 branch of UPR is closely related to liver pathogenesis, including liver cancer[2]. However, the reported role of the ATF6 branch of UPR in liver cancer is controversial, and also the underlying mechanisms require further understanding. In order to decipher the role of the ATF6 branch of UPR in liver tumorigenesis, I generated hepatocyte-specific ATF6 activation mice and hepatocyte-specific ATF6 knockout mice. I analyzed the hepatocyte-specific ATF6 activation mice with or without oncogenic challenges, focusing on whether the presence of activated ATF6 affects hepatic tumor onset and progression. In parallel, I characterized hepatocyte-specific ATF6 knockout mice in the face of dietary, chemical, and genetic oncogenic challenges to see if the absence of ATF6 could alleviate the hepatic tumor burden.

The inflammatory liver microenvironment has been long recognized as one of the main factors contributing to the onset of liver cancer. The presence of oxidative stress and metabolic remodeling in the inflammatory hepatic milieu continues to draw the scientific and medical communities' attention. Given the fact that the ATF6 arm of UPR is closely related to oxidative stress and energy metabolism, I characterized the hepatocyte-specific ATF6 activation mice under dietary anti-oxidative stress treatment. I also analyzed the transcriptome, proteome, and metabolome of mice with hepatocyte-specific ATF6 activation to address these hypotheses.

6 Materials and methods

6.1 Mice, diets, and treatments

The R26-LSL-nATF6-HA mouse line was a kind gift from Prof. Dirk Haller from Technische Universität München (TUM); the generation of this mouse line has been published previously[121]. The animals were bred with C57BL/6J mice for at least 10 generations to keep this line in C57BL/6J genetic background. Alb-Cre mice, $Rag1^{-/-}$ mice, $SPP1^{-/-}$ mice, and $ATF6^{flox/flox}$ mice are obtained from The Jackson Laboratory and are all in C57BL/6J genetic background.

The R26-LSL-nATF6-HA mice were cross with Alb-Cre mice to generate hepatocyte-specific nATF6-HA–overexpressing heterozygous mice ($nATF6^{tg/wt}$). Hepatocyte-specific nATF6-HA–overexpressing heterozygous mice ($nATF6^{tg/wt}$) were bred with $Rag1^{-/-}$ mice and $SPP1^{-/-}$ mice to generate $nATF6^{tg/wt}Rag1^{-/-}$ mice and $nATF6^{tg/wt}SPP1^{-/-}$ mice, respectively. The $ATF6^{flox/flox}$ mice were cross with Alb-Cre mice to generate hepatocyte-specific ATF6 knockout mice (homozygous, $ATF6^{\Delta Hep}$). All control mice were age, sex, and genetic background matched.

The breeding and housing of the mouse lines mentioned above took place at German Cancer Research Center (DKFZ), Heidelberg. Mice were maintained under specific pathogen-free (SPF) conditions. Treatments to the mice were performed in accordance with German Law (G-178/19, G-80/17, G-279/16, G-141/19, and DKFZ332).

6.2 Measurements of serum parameters

Blood was drawn from the heart of the mice after dissection, and centrifugation was used to isolate serum using serum isolation gel tubes (Sarstedt, Z/1.1). The serology parameters were measured with FUJIFILM DRI-CHEM NX500i machine and commercially available FUJIFILM DRI-CHEM slides for ALT, AST, TCHO, TBIL, ALB, and ALP.

6.3 Measurement of hepatic triglycerides

The measurement of hepatic TG was described previously[122]. In brief, around 30 mg of frozen liver tissue was crushed in liquid nitrogen. Then 250µl 0.9% NaCl buffer was added, the samples are collected and incubated on a heating block for 10 min at RT, 450 rpm. Afterward, 250µl 0.5M KOH was added to the sample, mixed by vortexing, and incubated on a heat blocking for 30 min at 71°C, 450rpm, followed by an addition of 500µl 0.15M $MgSO_4$, vortexed and centrifugation at 13,000g for 10min, RT. The supernatants from each sample were collected and 1:4 diluted before being measured by optical densitometry O.D. 505 with GPO-PAP from Roche Diagnostics.

6.4 Intraperitoneal glucose tolerance test

The protocol for the intraperitoneal glucose tolerance test was described previously[122]. In brief, before the experiment, mice were fasting for 8 hours, and their blood glucose concentrations were checked before injecting glucose solution. Then, the mice were injected i.p. with 5µl/g body weight glucose solution(20%). At the given time intervals, blood glucose was tested with the "Accu-chek Performa Glucometer" by puncturing the facial vein.

6.5 Intraperitoneal insulin tolerance test

The protocol for the intraperitoneal glucose tolerance test was described previously[122]. In brief, before the experiment, mice were fasting for 6 hours, and their blood glucose concentrations were checked before injecting insulin solution. Then the mice were given 1U/Kg body weight insulin solution via i.p. injection. At the given time intervals, blood glucose was tested with the "Accu-chek Performa Glucometer" by puncturing the facial vein.

6.6 Protein isolation and western blot

The protocols for protein isolation and western blot analysis were described previously[72]. In short, liver homogenates and cell lysis were prepared in RIPA buffer (Cell Signaling Technology #9806S), which contains Protease Inhibitor Cocktail (Thermo Scientific) and Phosphatase Inhibitor Cocktail (Thermo Scientific). The BCA assay was used to determine the protein concentrations. A total of 30 ug of protein was denatured at 95°C for 5 min in Laemmli buffer containing 5% β-mercaptoethanol and loaded in sodium dodecyl sulfate (SDS)-gel for electrophoresis. Following that, the protein was deposited onto PVDF membranes (Immobilon-P, Merck Millipore) by semi-dry electroblotting (Trans-Blot Turbo Transfer, Bio-Rad). The PVDF membranes were further incubated in 5% BSA solution (in PBST) overnight before primary antibody incubation. Primary antibodies (Table 1) were incubated overnight at 4°C in a shaking environment. After 3 times wash with PBST, corresponded secondary antibody solution (Table 1) was incubated with the membrane for 1.5h. The detection was accomplished using the Clarity Western ECL Substrate (Bio-Rad) in conjunction with the ChemiDoc Touch imaging equipment (Bio-Rad).

Table 1: Antibodies used for WB.

Antibody	Host	Dilution	Company	Number
Anti-mouse IgG, HRP-linked	horse	1:10000	CST	7076

Anti-O-Linked N-Acetylglucosamine	Mouse	1:1000	Abcam	ab2739
Anti-rabbit IgG, HRP-linked	goat	1:10000	CST	7074
ATF6	Rabbit	1:1000	CST	65880
ATF6	Rabbit	1:1000	SAB	32008
ATF6	Mouse	1:1000	NOVUS	NBP-40256
BIP	rabbit	1:1000	CST	3177
CHOP	rabbit	1:100	CST	5554
Cyclin D1	rabbit	1:1000	CST	55506
EIF2a	rabbit	1:1000	CST	9722
GAPDH	rabbit	1:1000	CST	2118
HA	rabbit	1:2000	Abcam	ab9110
P38	rabbit	1:1000	CST	9212
PARP	rabbit	1:1000	CST	9532
PCNA	rabbit	1:1000	CST	13110
PDL1	rabbit	1:1000	CST	60475
p-EIF2a	rabbit	1:1000	CST	3597
PERK	rabbit	1:1000	CST	5683
p-P38	rabbit	1:1000	CST	9211
Vinculin	mouse	1:500	Santa Cruz	sc-73614

6.7 Isolation of RNA, quantitative real-time PCR and RNA sequencing

According to the manufacturer's protocol, total RNA isolation from snap-frozen liver tissue or cultured cells was performed with RNeasy Mini Kit (Qiagen). The on-column digestion was carried out using an RNase-free DNase kit (Qiagen) according to the manufacturer's protocol to completely remove genomic DNA. RNA concentration and quality were determined by Nanodrop (Thermo Scientific) for quantitative real-time PCR and by Qubit for RNA sequencing. In a 384-well plate, qRT-PCR was performed in duplicates using Fast Start SYBR Green Master Rox (Roche) and Eurofins supplied custom-made primers using a 7900 HT qRT-PCR equipment (Applied Biosystems, Life Technologies Darmstadt, Germany)[122]. RNA-seq was performed in collaboration with Genomics & Proteomics Core Facility in DKFZ.

6.8 Isolation and staining of lymphocytes for flow cytometry

The Isolation and staining of lymphocytes for flow cytometry were following the protocol described in the article[72]. The animals were sacrificed, and the livers were perfused with 0.9% NaCl buffer. Then livers were collected, minced, digested with Collagenase and DNase, and subsequently passed through a 100µm filter. Then hepatic lymphocytes were purified by a 2-step Percoll gradient. Spleens were passed through a 100m mesh and then washed to isolate splenic

lymphocytes. The samples were then treated with red blood cell lysis buffer for 5 minutes at RT, followed by a washing step.

For stimulation of lymphocytes, cells were cultured in RPMI 1640 supplemented with 2%(v/v) fetal calf serum. Cell Activation Cocktail with Brefeldin A (Biolegend #423304) and Monensin Solution (Biolegend #420701) were diluted in the medium at the rate of 1:500 and 1:1000, respectively. Antibody staining was done in the presence of Fc receptor blockade in flow cytometry-activated cell sorting (FACS) buffer. For live/dead discrimination, the ZombieDyeNIR dye was stained according to the manufacturer's specifications. After washing with FACS buffer and centrifugation (400g, 5min, 4°C), cells were stained for 40 minutes at 4°C with 25µl of titrated antibody master mix and then washed. For sorting experiments, the samples were then sorted using FACS. eBioscience IC fixation (#00-8222-49) was used to fix samples for samples that only need surface staining for flow cytometry, as directed by the manufacturer's instruction. For samples that need intracellular staining, eBioscience Perm buffer (#00-8333-56) was used. BD FACSFortessa was used to analyze the stained cells, and FlowJo was used to analyze data. In collaboration with the DKFZ FACS core facility, a FACS Aria II machine and a FACS Aria FUSION machine were employed for sorting.

6.9 Histology, immunohistochemistry and scanning

The histology, immunohistochemistry, and scanning were described previously[32]. Mice were killed and tissues were collected and fixed in 4% paraformaldehyde for 24 hours. Then the tissues were paraffin-embedded, cut, and stained in collaboration with the technical team from the Department of Chronic Inflammation and Cancer at German Cancer Research Center (DKFZ), Heidelberg. In brief, FFPE and cryo-preserved tissues were cut to prepare 2µm sections. These sections were stained with Hematoxylin/Eosin or immunohistochemistry staining with antibodies listed in Table 2 on a Bond-MAX machine (Leica).

Table 2: Antibodies used for IHC.

Antibody	Host	Dilution	Company	Number
A6	rat	1:50	Hybridoma Bank	-
AFP	goat	1:100	R&D	AF5369
ATF6 (human)	mouse	1:100	Abnova	H00022926
B220	rat	1:3000	BD	553084
BIP	rabbit	1:200	CST	3177
CD3	rabbit	1:500	Invitrogen	MA1-90582
CD4	rat	1:50	BD	550278
CD44v6	rat	1:500	eBioscience	BMS145

CD8	rat	1:200	BD	553027
CD8	rat	1:200	Invitrogen	14-0808-82
CHOP	rabbit	1:100	CST	5554
CK19	rat	1:500	Hybridoma Bank	-
cl-Caspase 3	rabbit	1:300	CST	9661
Collagen IV	rabbit	1:100	Cedarlane	CL50451AP-1
F4/80	rabbit	1:400	CST	70076
g H2AX	rabbit	1:500	Novus Biologicals	NB100-2280
GP73	Mouse	1:100	Santa Cruz	sc48011
GS	rabbit	1:1000	Abcam	ab16802
HA	rabbit	1:300	Abcam	ab9110
Ki67	rabbit	1:200	Thermo scientific	RM-9106-S1
Ly6G	rat	1:800	BD	551459
MPO	rabbit	1:50	Abcam	ab9535
NKP46	Goat	1:60	R&D	BAF2225
NQO1	rabbit	1:800	Abcam	ab34173
p 21	rabbit	1:1000	Abcam	ab188224
p 62	rabbit	1:500	Biozol	MBL-PM045
PD1	goat	1:100	R&D	AF1021
PDL1	rabbit	1:50	CST	64988
Phospho c-Jun	rabbit	1:200	CST	3270
p-STAT3	rabbit	1:100	CST	9145
SPP1	goat	1:1000	R&D	AF808

For lipid droplets staining, 5µm sections from cryo-preserved tissues were stained with Sudan Red (0.25% Sudan IV in ethanolic solution). All stained slides were scanned with the Aperio AT2 DX System (Leica) and analyzed by macro-based analysis by ImageJ.

6.10 Immunofluorescence microscopy

The Immunofluorescence microscopy was described previously[32]. Immunofluorescence microscopy was performed in collaboration with Danijela Heide, Jenny Hetzer at German Cancer Research Center (DKFZ), Department of Chronic Inflammation and Cancer (Heidelberg). In brief, mice were dissected, and tissues were embedded in OCT for the preparation of 25µm slices. The sections were permeabilized and blocked with 0.3% Triton X-100 (Sigma-Aldrich) and 10% FBS in PBS. Primary antibodies CD3 (Invitrogen, MA1-90582), CD8 (BD, 553027), and PD1 (R&D, AF1021) were used to stain the samples. Stained slides were covered with fluorescence mounting medium (DAKO), the stained slides were scanned with the NanoZoomer S60 Digital slide scanner (hamamatsu photonics).

6.11 Lipid extraction from mouse liver tissue and LC-MS analysis

Lipid extraction from mouse liver tissue and LC-MS analysis was done in collaboration with Dr. Lisa Schlicker at the German Cancer Research Center (DKFZ), Department of Tumor Metabolism and Microenvironment (Heidelberg). Liver tissues from WT and ATF6 overexpression were harvested at 3 months age (Ctrl: n= 5, Exp: n=7) were extracted according to Matyash et al[123]. MTBE extracts were dried with a constant nitrogen airflow at 35°C. Lipids were dissolved in 200 µl isopropanol and subjected to LC-MS analysis.

Lipids were separated on a C8 column (Accucore C8 column, 2.6 µm particle size, 50 x 2.1 mm, Thermo Fisher Scientific) mounted on an Ulitmate 3000 HPLC (Thermo Fisher Scientific) and heated to 40°C. The mobile phase buffer A consisted of 0.1% formic acid in CH_3CN/H_2O (10/90, v/v) and buffer B consisted of 0.1% formic acid in $CH_3CN/IPOH/H_2O$ (45/45/10, v/v/v). Following the injection of 3 µl lipid sample, a concentration of 20% solvent B was maintained for two minutes.

Following that, a linear increase to 99.5 % B occurred within five minutes and was maintained for 27 minutes. After returning to 20% B within 1 minute, the column went through re-equilibration at 20% B for 5 minutes, thus the total run time is 40 minutes. From 2 to 35 minutes, the flow rate was kept at 350 l/min and the eluent was directed to the QE Plus's ESI source. MS analysis was carried out using a Thermo Fisher Scientific Q Exactive Plus mass spectrometer. Data analyses were carried out by Dr. Lisa Schlicker using EI-Maven.

6.12 Electron microscopy

The electron microcopy was described previously[32] and performed in collaboration with Prof.Dr.Marco Prinz from the Universitätsklinikum Freiburg. In short, freshly isolated liver samples were fixed with glutaraldehyde. Then the liver samples were stained with toluidine blue followed by epon-embedding and cutting. Following trimming and ultrathin cutting, liver tissues were treated with uranyl acetate and lead citrate as previously described[32].

6.13 Positron emission tomography–computed tomography (PET-CT) and Magnetic resonance Imaging (MRI)

The PET-CT and MRI were done in collaboration with Dr. Jugold Manfred from the core facility of DKFZ.

The PET / CT examinations are carried out on a special small animal scanner (Inveon PET/SPECT/CT, Siemens) in the Core Facility Small Animal Imaging (DKFZ). Before the PET-CT measurement, the animals are injected with the F18 radioactively labeled tracer FDG via a tail

catheter. The maximum injection quantity is 100µl and the total activity applied is between 3-8 MBq. Shortly before the examination, the animals are deprived of their food for four hours in order to ensure targeted absorption of the tracer into the tumors. The mice are anesthetized with sevoflurane (2.5% v / v in air) for immobilization.

The MRI examinations are carried out on a preclinical 1 Tesla small-animal tomograph (ICON, Bruker, Ettlingen, Germany). First, the mice are anesthetized [inhalation anesthesia with sevoflurane (3–3.5% by volume) and air (0.5 l / min)] before 0.1 ml of contrast medium (Prohance® (Gadoteridol, Bracco)), 0.5 mmol / kg body weight, Bayer Schering Pharma) is administered intraperitoneally.

6.14 High-Throughput 16S Ribosomal RNA (rRNA) Gene Sequence Analysis

High-Throughput 16S Ribosomal RNA (rRNA) Gene Sequence Analysis was performed in collaboration with Dr. Olivia Coleman and Prof. Dirk Haller from Technische Universität München. DNA was extracted from mouse caecal content using a modified procedure by Godon et al., for high-throughput 16S rRNA Gene Amplicon Sequencing[124]. Briefly, mouse caecal contents were mechanically lysed using 0.1-mm glass beads and a bead beater (FastPrep-24 fitted with a cooling adapter) and followed by purification of DNA using NucleoSpin gDNA columns (Machery-Nagel, No. 740230.250). PCR (25 cycles) was employed to amplify amplicon libraries (V3/V4 regions of 16S rRNA genes), which were further purified with the AMPure XP system (Beckmann Coulter, Indianapolis, IN). The purified libraries were pooled in an equimolar amount before sending for sequencing with a MiSeq system (Illumina, San Diego, CA) in paired-end mode (PE275).

The data analysis (Amplicon Sequence Analysis Sequencing data) was performed on the website www.imngs.org (the IMNGS pipeline)[125]. For the R1 and R2 read, 5 nucleotides from the 5' end and another 5 nucleotides from the 3' end are trimmed, respectively (trim score 5). To remove an expected error rate (1. Chimera), UCHIME is employed[126]. The readings from de-multiplexed samples were combined and grouped using UPARSE v8.1.1861_i86 by 97% similarity[127].As the last step, to achieve a OTU table for all samples, all sequences were remapped to their representative sequences. R programming environment (R Core Group, Vienna Austria) with the use of Rhea[128] was employed for further analysis of the sequencing data.

6.15 Generation of nATF6 overexpression and ATF6 knockout cell lines

nATF6 overexpression and ATF6 knockout cell lines were generated in collaboration with Dr. Jan Kosla from our group.

For nATF6 overexpression cells, the CDS coding activated form of murine Atf6 (nAtf6, AA 1-373) and HA-tag on the C-terminus of nAtf6 was cloned between XhoI and EcoRI restriction sides of the retroviral plasmid MSCV-linker-IRES-GFP, resulting in MSCV-nAtf6-IRES-GFP vector. nATF6 overexpressing (FL83B nATF oe) and control (FL83B MLIG) cells were prepared by transduction of FL83B cells with retroviral particles containing MSCV-nAtf6-IRES-GFP and MSCV-linker-IRES-GFP construct respectively. Viral particles were produced in Phoenix GP cells (ATCC CRL-3215) after transfection with either MSCV-nAtf6-IRES-GFP or MSCV-linker-IRES-GFP vector together with VSV-G (Clontech) vector. Cells were expanded and sorted for Green fluorescent protein (GFP) using a FACS Aria II (BD).

The FL83B Atf6 knock-out (ko) cells were prepared by transient transfection (Lipofectamine™ 3000 Transfection Reagent, ThermoFisher) of FL83B cells with vectors derived from pSpCas9(BB)-2A-Puro (PX459) V2.0 and following selection with puromycine (10 μg/ml) for 3 days. Sequences for single guide RNAs (sgRNAs) and primers for verification of indel formation were designed using CRISPOR.org webtool. Control cells for FL83B Atf6 ko cells were transfected with PX459 V2.0 without any sgRNA cloned in. The indel formation was verified by TIDE assay.

Phoenix GP cells were grown in Dulbecco modified eagle medium (DMEM) containing GlutaMAX, 10 % FCS, 1 % PS in a P100 (TPP) dish until they reach 80 % confluence in an incubator with 37°C, 5% CO2 and 21% oxygen.

6.16 Statistical analysis

Data in the thesis are presented as the mean±SEM. For statistical analyses, GraphPad Prism software version 7.04 (GraphPad, La Jolla, CA) was employeed. For all data requires only two groups comparison, unpaired, parametric t-test was employed. When comparing multiple groups by ordinary one-way ANOVA with Turkey's multiple comparison. Fisher's exact test was used to calculate the incidence of HCC. Statistical significance is either indicated as p values in the figure or showed as follows:*$p < 0.05$, **$p < 0.01$, ***$p < 0.001$ and ****$p < 0.0001$.

7 Results

7.1 ATF6 expression and activation in human and mouse liver pathologies

ER stress has been frequently observed in pre-malignant diseases and various tumors. In my first few analyses (in collaboration with Lukas Frick), I analyzed the expression levels of ER stress-related genes in existing databases. Notably, I found several genes involved in ER stress were dysregulated in the context of liver cancer (Data not shown). Among them, ATF6 drew my main interest, given its vital role in mediating the UPR while its function in hepatic pathogenesis remains largely elusive. As shown in Figure 10a – 10d, I next investigated the expression of ATF6 at the mRNA level from different databases. Surprisingly, in most of the tested databases, ATF6 is significantly upregulated in hepatic tumor samples compared to normal liver tissues.

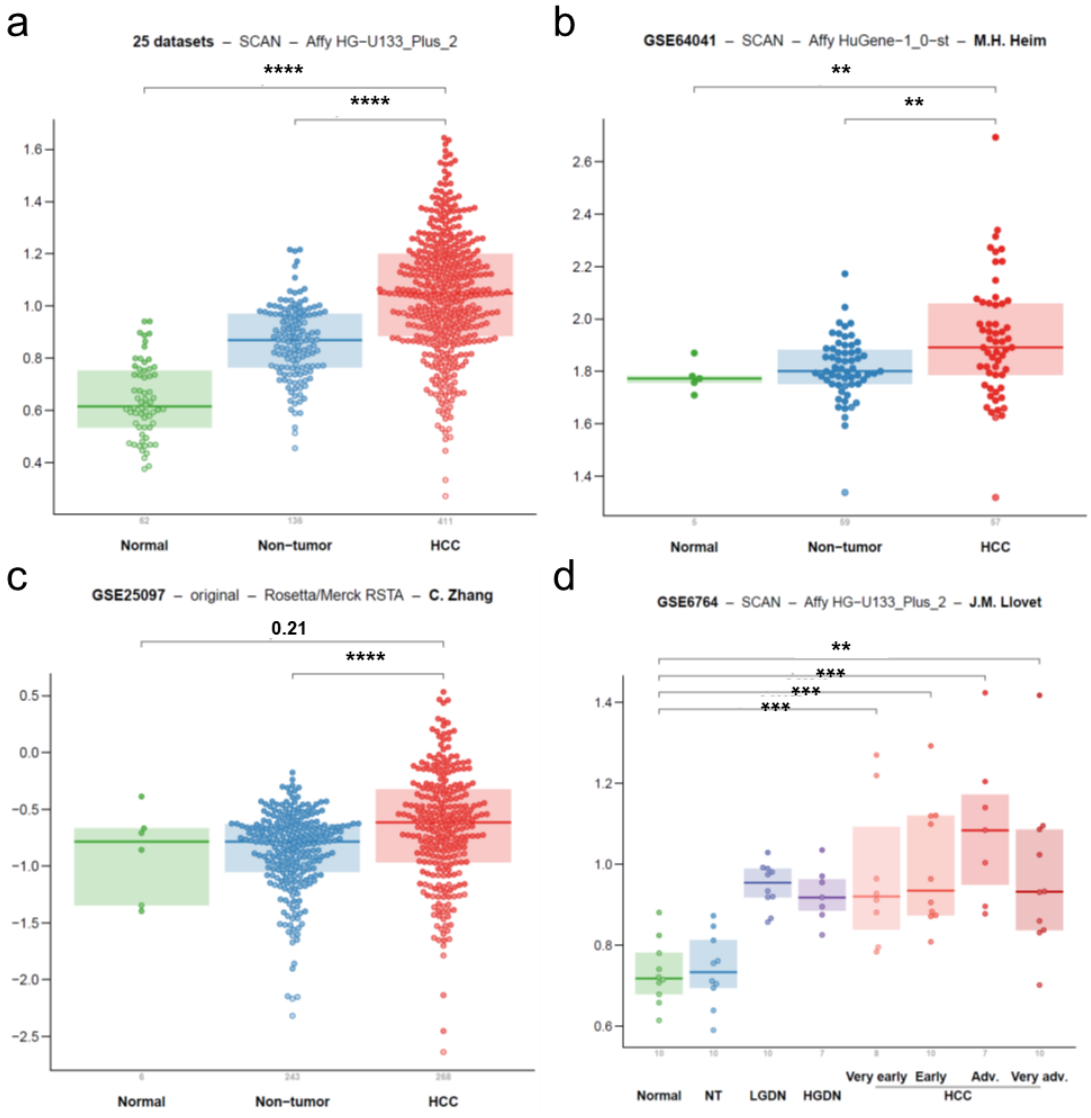

Figure 10: Elevated ATF6 mRNA expression in hepatic tumors in human. a) - **d).** ATF6 expression signature in normal liver, non-tumor tissue, and HCC tissue. Data obtained from existing databases. All data are shown as mean ± SEM. All data were analyzed by unpaired T-test, one-way ANOVA, and Tukey`s multiple comparison test. p values are indicated or represented as *, *p<0.05;**p<0.01; ***p<0.001; ****p<0.0001.

Additionally, I employed a publically available dataset from the Cancer Genome Atlas (TCGA) to conduct the gene expression profiling interactive analysis (GEPIA), which shows a consistently elevated ATF6 expression in mRNA in both HCC and CCA (Data not shown).

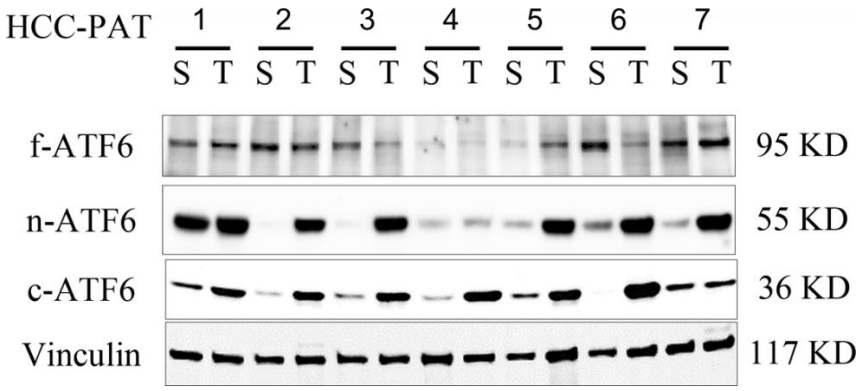

Figure 11: ATF6 protein expression and activation status are altered in HCC. Patient samples were subjected to western blot analysis. Each patient set includes tumoral tissue (T) as well as surrounding non-tumoral tissue (S).

To corroborate my findings from the databases, I first performed quantitative real-time PCR(qPCR) and western blot analyses of tumoral and tumor-surrounding tissue from HCC patients. In line with what I observed in the bioinformatics analysis, qPCR analysis shows the ATF6 mRNA expression is significantly higher in hepatic tumoral tissues compared to the tumor surrounding tissues (Data not shown). Strikingly, by western blot analysis, showing different forms of ATF6, I found that the activated form of ATF6 (nATF6) is mainly accumulated in the tumoral tissues compared to the surrounding tissues (Figure 11), indicating that not only the expression level of ATF6 but also its activation status is vital for disease progression.

Successively, I collected a set of tissue microarrays containing 197 non-tumoral tissues and 393 HCC tissues. I performed IHC staining of ATF6 to better observe the activation and expression status of ATF6 in these samples. As shown in Figure 12, both representative pictures (Figure 12a) and the quantification of all stained tissue microarrays (Figure 12b) indicate the expression level and the activation extent of ATF6 is stronger in HCC tissues compared to non-tumoral tissues.

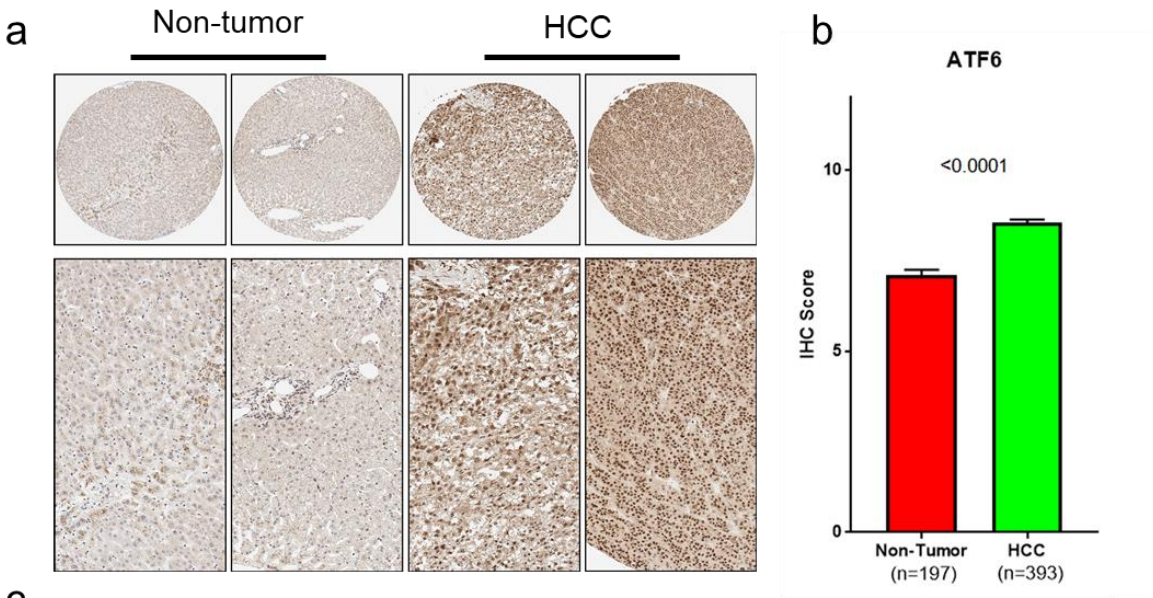

c

ATF6 Scoring									
Cytoplasm					Nuclear				
	Qualitative		Quantitative			Qualitative		Quantitative	
	Score	Standard	Score	Standard		Score	Standard	Score	Standard
	0	Negative	0	Negative		0	Negative	0	Negative
	1	Weak	1	1-10%		1	Weak	2	1-10%
	2	Middle	2	10-50%		2	Middle	4	10-50%
	3	Strong	3	>50%		3	Strong	6	>50%

Figure 12: Activation and elevated expression of ATF6 protein in HCC tissues. a). Representative pictures of ATF6 IHC staining in 197 non-HCC samples and 393 HCC samples. **b).** Quantification of ATF6 IHC scores from IHC staining in **a**. **c).** The criterion for ATF6 IHC scoring in **b**. All data are shown as mean ± SEM. All data were analyzed by unpaired T-test, p value is indicated.

The elevated ATF6 expression and activation in HCC tissues indicate that the quality of ER stress in ATF6^{high} tissues and ATF6^{low} tissues is different. Then I reasoned whether the activation of the ATF6 arm of UPR is a consequence or a cause of hepatic carcinogenesis. Thus I performed ATF6 IHC staining in liver tissues from NASH patients, as NASH is known as a pre-tumor stage disease. Strikingly, in control samples, biopsies from healthy livers qualified for liver transplantation, I noted that the ATF6 expression is kept at a low level and evenly distributed in the cytoplasm of hepatocytes. However, in all tested NASH samples, regardless of the stage of the disease (referred to the NAFLD Activity Score (NAS)), the expression of ATF6 protein is significantly increased, and a large proportion of the protein is condensed in the nucleus (Figure 13), indicating that ER stress already exists in the pre-tumor stage.

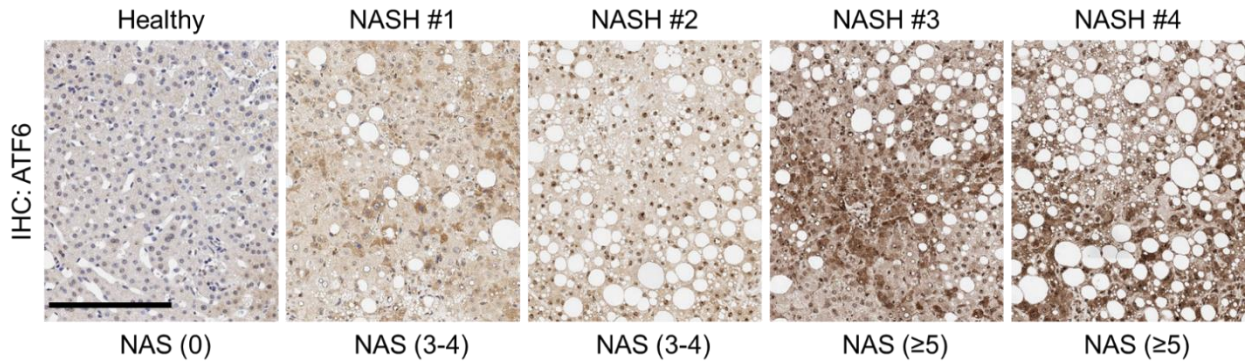

Figure 13: Elevated ATF6 protein expression and activation in human NASH livers. Representative pictures of ATF6 IHC staining in healthy and NASH livers.

To further validate and confirm the same expression and activation pattern of ATF6 in murine experimental models, I checked ATF6 expression in liver and tumor tissues from hydrodynamic tail vein injection (HDTVi)-induced liver cancer models by qPCR. In these models, ATF6 expression largely depends on the oncogenes/tumor suppressors that drive tumorigenesis, as ATF6 upregulation at mRNA level was clearly detectable in mice injected with Notch/Akt and Kras/p19, but not in YAP/Akt model (Figure 14). Accordingly, I hypothesized that the expression level and the activation status of ATF6 could be important in both human and murine hepatocarcinogenesis.

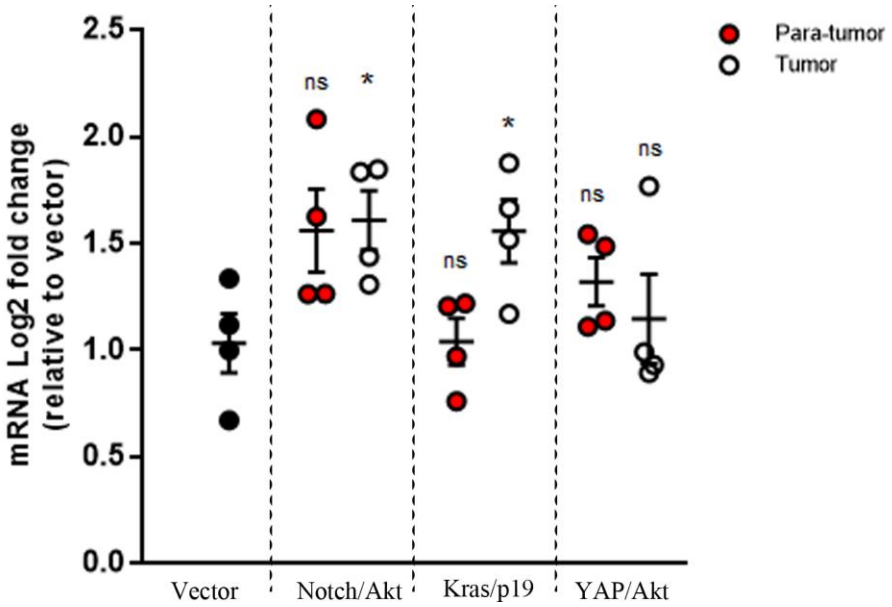

Figure 14: ATF6 mRNA expression in HDTVi mouse models. qPCR analysis of ATF6 expression in oncogenes induced liver cancer in mice. All data are shown as mean ± SEM. All data were analyzed by unpaired T-test and compared to 'Vector' group. p values are indicated or represented as *, *p<0.05;**p<0.01; ***p<0.001; ****p<0.0001.

7.2 Generation of mice with liver-specific nATF6 overexpression

7.2.1 Generation of hepatic nATF6 overexpression mice

To validate my hypothesis and further investigate the role of ATF6 activation in liver pathologies, I generated a mouse model carrying ATF6 activation specifically and persistently in hepatocytes (Figure 15). Specifically, a fragment containing two loxP sites, a stop castle, and the activated form of ATF6 (nATF6) tagged by hemagglutinin (HA) was inserted under the ROSA-26 locus of the R26-LSL-nATF6 animal[121]. This mouse line was further bred with another line overexpressing Cre recombinase under the albumin promoter (Figure 15a).

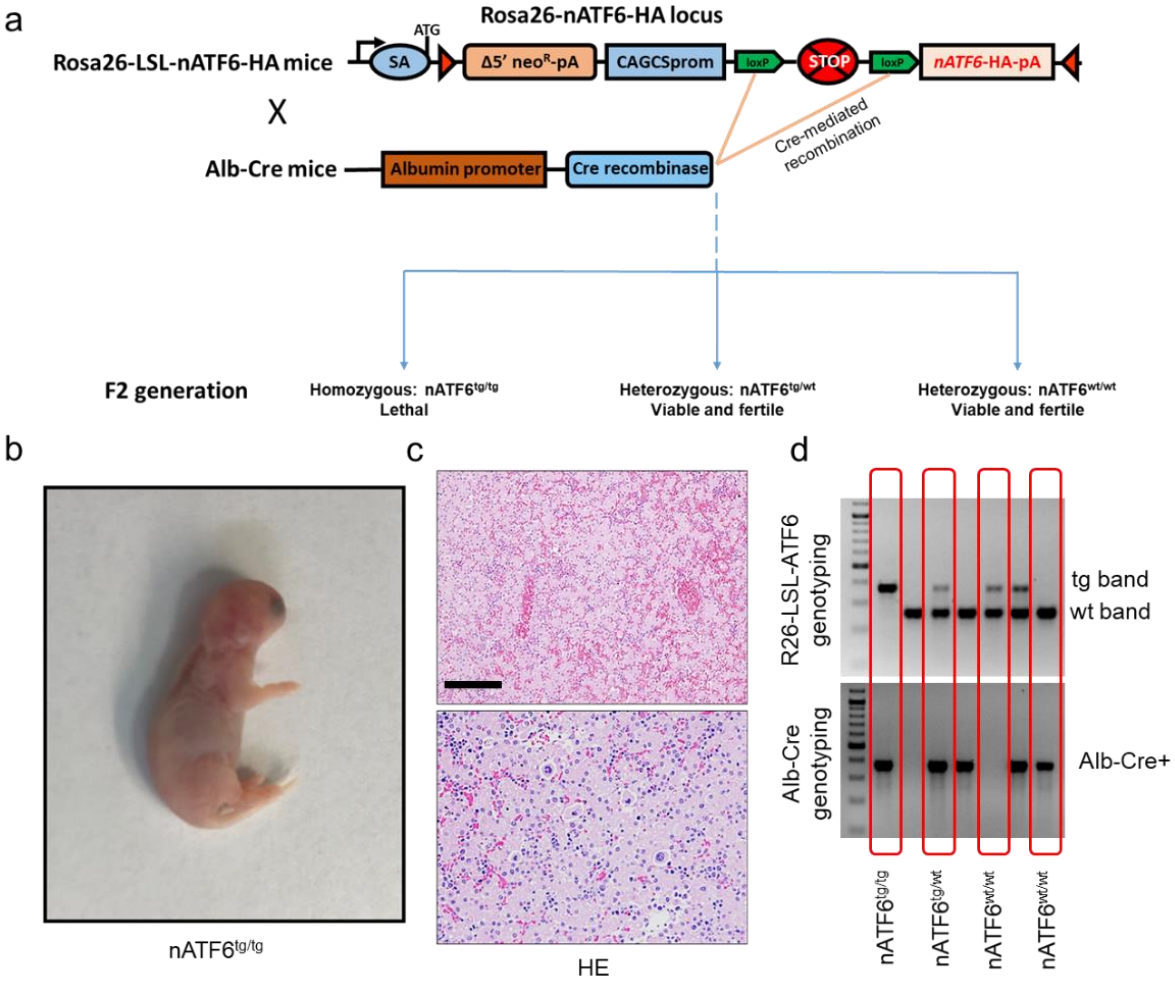

Figure 15: Generation of hepatocyte-specific nATF6 overexpression mice. a). A schematic representation to show the generation of hepatocyte-specific nATF6 overexpression mice. **b).** Representative picture to show the homozygous lethal phenotype in R26-LSL-ATF6 x Alb-Cre mouse line. **c).** Hematoxylin-Eosin (H&E) staining of the liver from **b**. **d).** Genotyping analysis of R26-LSL-ATF6 x Alb-Cre mice cohort. The presence of nATF6 transgene and Albumin-Cre were tested by PCR in each mouse.

Theoretically, animals with three genotypes should be generated at F2 generation; namely, mice with homozygous overexpression of nATF6 transgene ($nATF6^{tg/tg}$), mice with heterozygous overexpression of nATF6 transgene ($nATF6^{tg/wt}$), and mice without nATF6 transgene expression ($nATF6^{wt/wt}$). However, I found that $nATF6^{tg/tg}$ mice are lethal (Figure 15b), and I only received control mice without transgene expression ($nATF6^{wt/wt}$) and animals expressing heterozygous ATF6 transgene ($nATF6^{tg/wt}$) (Figure 15d). The homozygous mice ($nATF6^{tg/tg}$) probably die either embryonically or shortly after birth and show an obvious liver failure phenotype (Figure 15c).

Both control mice ($nATF6^{wt/wt}$) and heterozygous mice ($nATF6^{tg/wt}$) grow and behave normally until 6 months of age, when I start to register a difference in body weight between control ($nATF6^{wt/wt}$) and heterozygous animals ($nATF6^{tg/wt}$) (Figure 16).

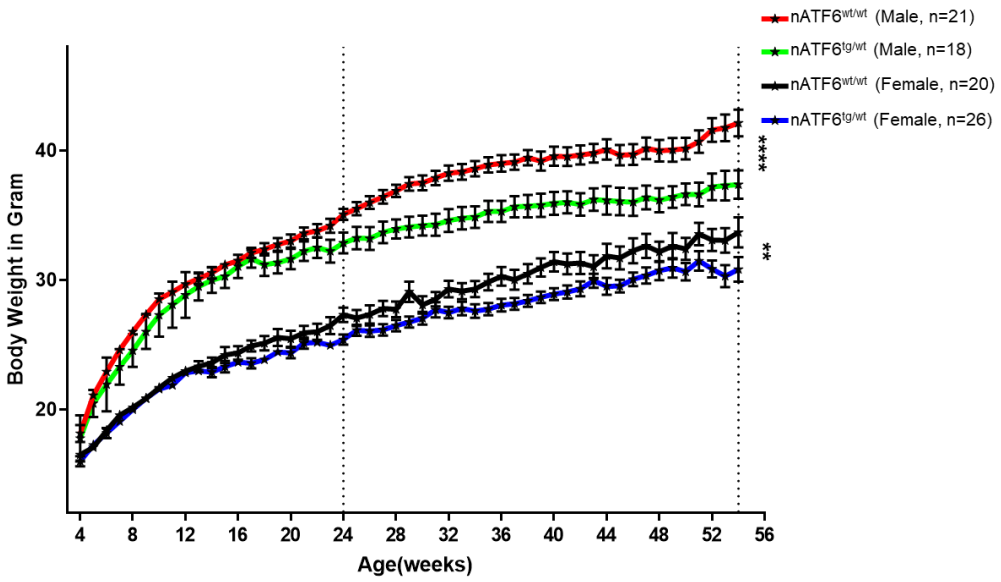

Figure 16: Bodyweight curve of $nATF6^{wt/wt}$ and $nATF6^{tg/wt}$ mice. The body weight of $nATF6^{wt/wt}$ and $nATF6^{tg/wt}$ mice was traced on a weekly basis. All data are shown as mean ± SEM. Mice body weight at the end time point was compared by unpaired T-test. p values are represented as *, *p<0.05;**p<0.01; ***p<0.001; ****p<0.0001.

7.2.2 Functional characterization of hepatic ATF6 activation in mouse liver

To confirm nATF6 overexpression in this mouse model and to investigate its effects on the UPR activation. I sacrificed control animals ($nATF6^{wt/wt}$) and heterozygous animals ($nATF6^{tg/wt}$) at 4-week and 12-week of age, respectively. The qPCR results targeting endogenous and exogenous ATF6 suggest that overexpression of nATF6 works as expected. The overexpressed nATF6 appears to have a suppressive effect on the expression of endogenous ATF6 at the mRNA level (Figure 17a) – similar to a feedback mechanism.

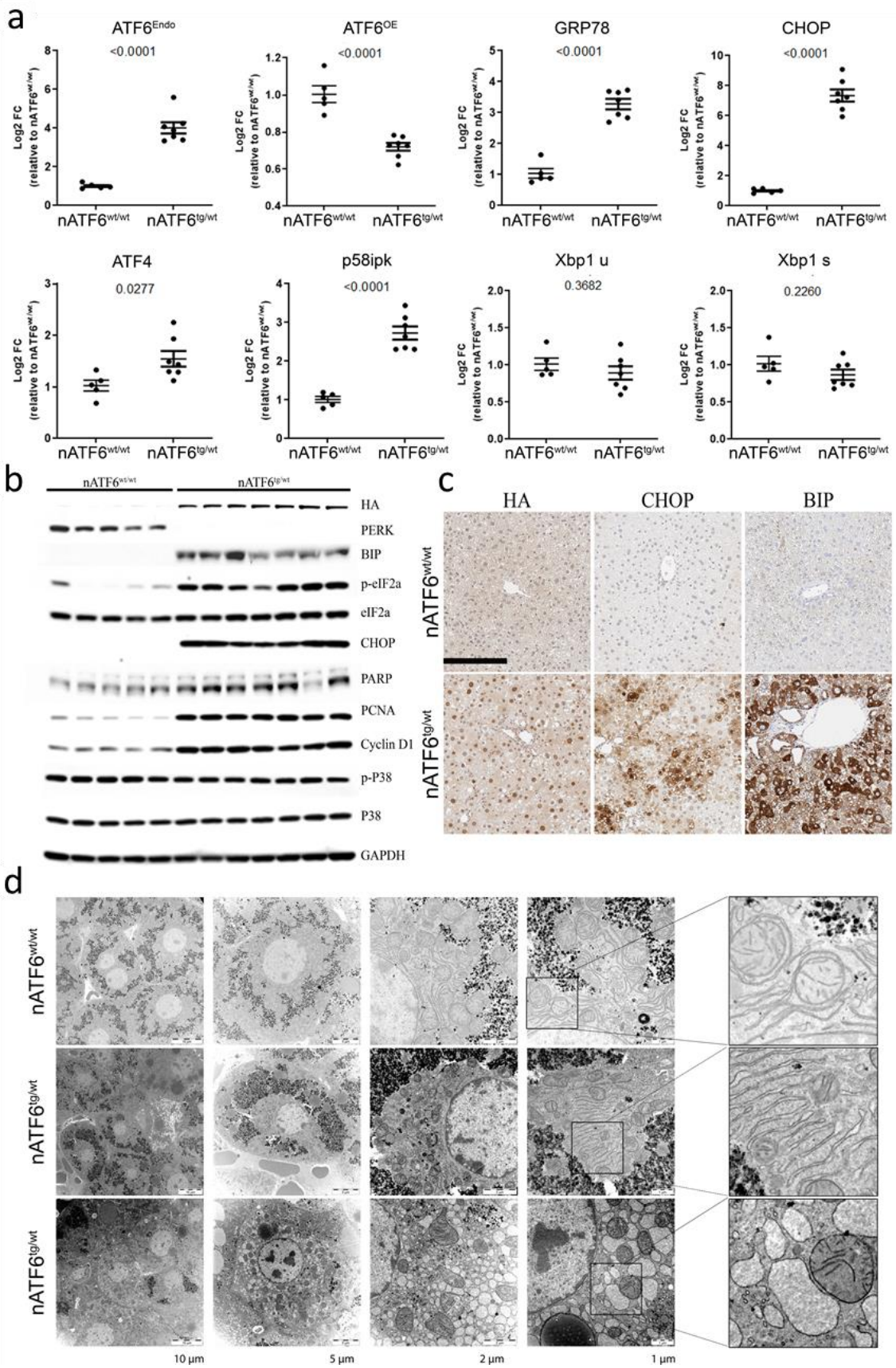
a
ATF6Endo
<0.0001
ATF6OE
<0.0001
GRP78
<0.0001
CHOP
<0.0001
ATF4
0.0277
p58ipk
<0.0001
Xbp1 u
0.3682
Xbp1 s
0.2260
Log2 FC (relative to nATF6wt/wt)
nATF6wt/wt
nATF6tg/wt
b
nATF6wt/wt
nATF6tg/wt
HA
PERK
BIP
p-eIF2a
eIF2a
CHOP
PARP
PCNA
Cyclin D1
p-P38
P38
GAPDH
c
HA
CHOP
BIP
nATF6wt/wt
nATF6tg/wt
d
nATF6wt/wt
nATF6tg/wt
nATF6tg/wt
10 µm
5 µm
2 µm
1 µm

Figure 17: Functional verification of hepatocyte-specific ATF6 overexpression in mice liver. a). Real-time qPCR analysis of the expression levels of indicated UPR-related genes in livers of nATF6$^{wt/wt}$ and nATF6$^{tg/wt}$ mice. **b).** Western blot analyses of the expression of UPR-related molecules in livers of nATF6$^{wt/wt}$ and nATF6$^{tg/wt}$ mice. **c).** Representative pictures show IHC staining of HA, CHOP, and BIP in livers of nATF6$^{wt/wt}$ and nATF6$^{tg/wt}$ mice. HA staining indicates overexpressed nATF6, BIP staining suggests the extent of ER stress, and BIP itself is also a target of ATF6; CHOP staining indicates the induction of apoptotic pathways. **d).** Electron microscopy of hepatocytes from nATF6$^{wt/wt}$ and nATF6$^{tg/wt}$ mice. All data were shown as mean ± SEM. All data were analyzed by unpaired T-test. p values are indicated in the graph.

Taking advantage of HA-tag labeling on the exogenous overexpressed nATF6 fragment, I was able to detect the overexpression of nATF6 quantitatively and qualitatively. By performing western blot analyses, I could observe the overexpressed nATF6 with an HA-tag in livers of heterozygous mice (nATF6$^{tg/wt}$) but not in controls (nATF6$^{wt/wt}$) (Figure 17b). Importantly, from the histological analysis for HA expression (Figure 17c, IHC: HA), I could see that the overexpressed nATF6 was mainly condensed in the nucleus of hepatocytes, indicating the nuclear translocation of exogenous nATF6 – an essential procedure for the function of transcriptional factors — is successful. Further, combined with the qPCR results of ATF6 target genes (e.g. Bip, and p58ipk), I could see the apparent activation of the ATF6 branch of UPR after nATF6 overexpression (Figure 17a - 17c). Lastly, as a golden standard for proving the UPR activation, I employed electron microscopy (EM) analyses to observe the subcellular structure of the ER in hepatocytes of nATF6$^{wt/wt}$ and nATF6$^{tg/wt}$ mice. From the EM pictures, I could see well-structured ERs in the hepatocytes from nATF6$^{wt/wt}$ mice. In contrast, ERs from hepatocytes of nATF6$^{tg/wt}$ mice show much tension, as revealed by the enlarged ER lumen in hepatocytes trying to increase ER capacity. Some hepatocytes failed this attempt and resulted in ER dysfunction (Figure 17d).

In summary, using the R26-LSL-nATF6 x Alb-Cre mouse model, I have successfully overexpressed nATF6 in hepatocytes, and the overexpressed nATF6 functions as a transcriptional factor to activate the ATF6 arm of UPR.

7.3 Persistent ATF6 activation in mouse liver induces ROS-mediated liver damage

7.3.1 Persistent ATF6 activation in hepatocytes induces hepatocyte turnover and hepatomegaly in mouse liver

The survival analysis of nATF6$^{wt/wt}$ and nATF6$^{tg/wt}$ mice suggests that the nATF6$^{tg/wt}$ mice did not survive the first 1.5 years of life (Figure 26b). I collected livers of the mice at 3-month and 6-month time points, respectively (Figure 18a). Notably, at both time points, livers from nATF6$^{tg/wt}$ mice show a hepatomegaly phenotype compared to healthy controls, as revealed by the liver weight and liver-to-body weight ratio (Figure 18b).

By checking serology parameters, I found the alanine transaminase (ALT) level and alanine transaminase (AST) level in the serum are significantly elevated in nATF6$^{tg/wt}$ mice at both 3-month and 6-month time points (Figure 19). In healthy livers, these transaminases are usually expressed by hepatocytes and rarely released into the serum. These enzymes are released to the blood upon acute stress or under pathologic conditions, which leads to cell death in hepatocytes. The increased serum ALT and AST levels serve as golden standard markers for detecting liver disease in the clinic for years. Indeed, in livers of nATF6$^{tg/wt}$ mice, which show an incredibly high level of ALT and AST in the serum, I have observed elevated apoptosis as shown by western blot analyses for the activation of apoptosis-related molecules – cleaved-Caspase 3 and poly(ADP-ribose) polymerase (PARP) (Figure 17b). Similar results have been obtained by histological staining of the cleaved form of Caspase 3 (Figure 20, IHC: cl-Caspase 3).

Besides dying hepatocytes, I have seen a larger proportion of hepatocytes with proliferative potential, as revealed by the histological staining of Ki-67, a generally accepted marker for proliferating cells (Figure 20). Indeed, western blot analyses of proliferating cell nuclear antigen (PCNA) and cyclin D1 show significant upregulation of these two proteins (Figure 17b), indicating that cell death and proliferation of hepatocyte occurs in parallel in the liver of nATF6$^{tg/wt}$ mice. Moreover, similar hepatic phenotypes of hepatomegaly and increased hepatocyte turnover have been observed also in 6-month old animals. Notably, I found a gender difference in cystic liver phenotype, which will be discussed later in section 7.4.2 (Figure 18a).

7.3.2 Persistent ATF6 activation leads to DNA damage and chromosome instability in hepatocytes

The rapid compensatory proliferation of hepatocytes has been frequently linked to oxidative stress, DNA damage, and chromosome instability. As I have observed obvious liver damage and increased hepatocyte turnover in livers of nATF6$^{tg/wt}$ mice. I checked the DNA damage in livers of nATF6$^{tg/wt}$ mice by IHC staining of γ-H2AX. Indeed, I could identify hepatocytes displaying positive staining for γ-H2AX staining, indicating damaged DNA existing in these cells (Figure 21a – 21b). Moreover, by employing a microarray-based comparative genomic hybridization (aCGH) assay, I tested the genomic DNA from hepatic tissues of nATF6$^{wt/wt}$ and nATF6$^{tg/wt}$ mice. Strikingly, gain and loss of fragments have been detected in different regions of chromosomes in the liver of nATF6$^{tg/wt}$ mice, indicating these animals' liver already has chromosome instability at 3-month age (Figure 21c).

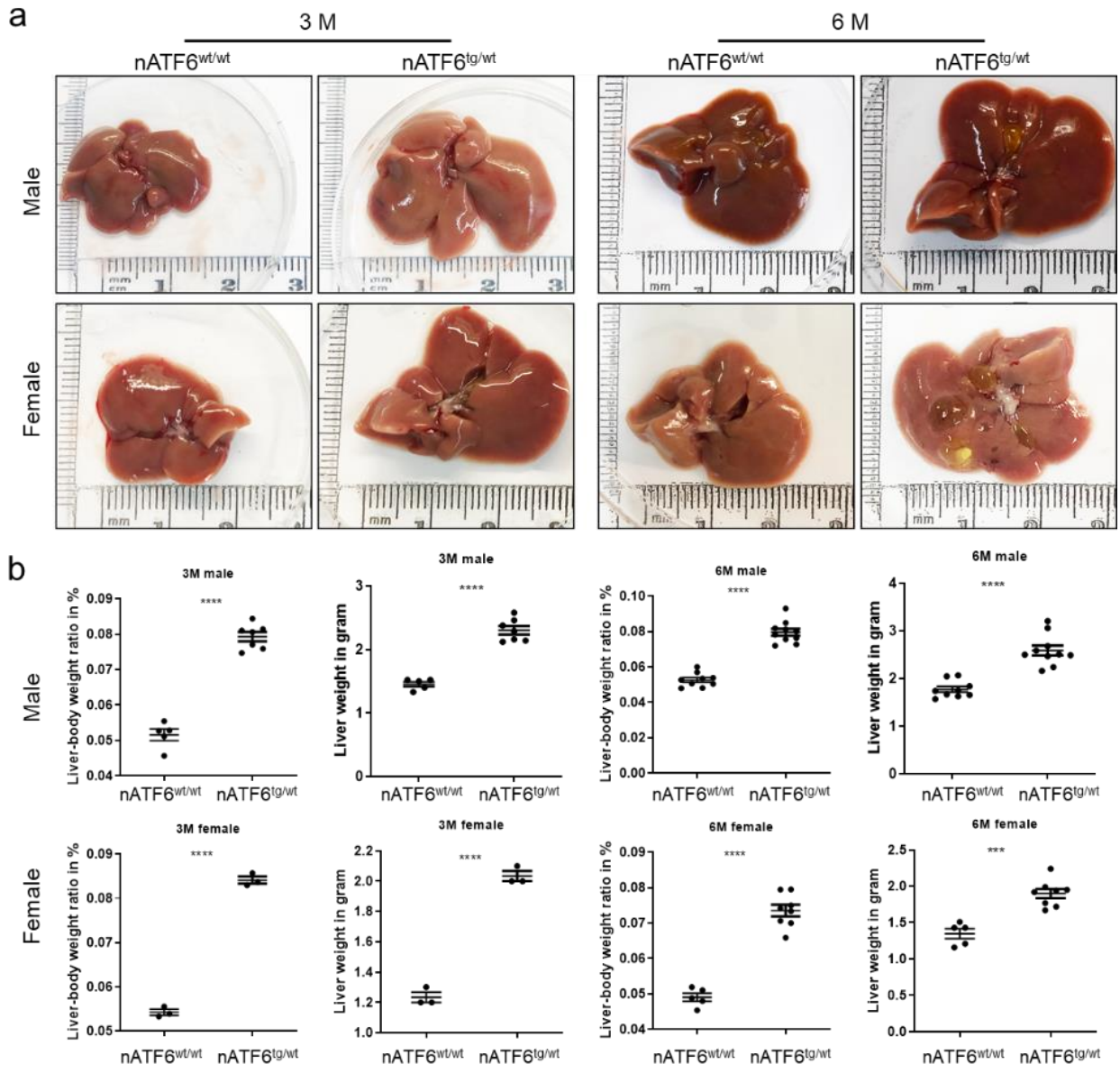

Figure 18: Persistent ATF6 activation in hepatocytes induces hepatomegaly in mouse liver. a). Representative liver pictures from indicated mice group at 3-month and 6-month age. **b).** Liver weight and liver to body weight ratio of mice in the indicated groups at 3-month and 6-month age. All data were shown as mean ± SEM. All data were analyzed by unpaired T-test. p values are represented as *, *p<0.05;**p<0.01; ***p<0.001; ****p<0.0001.

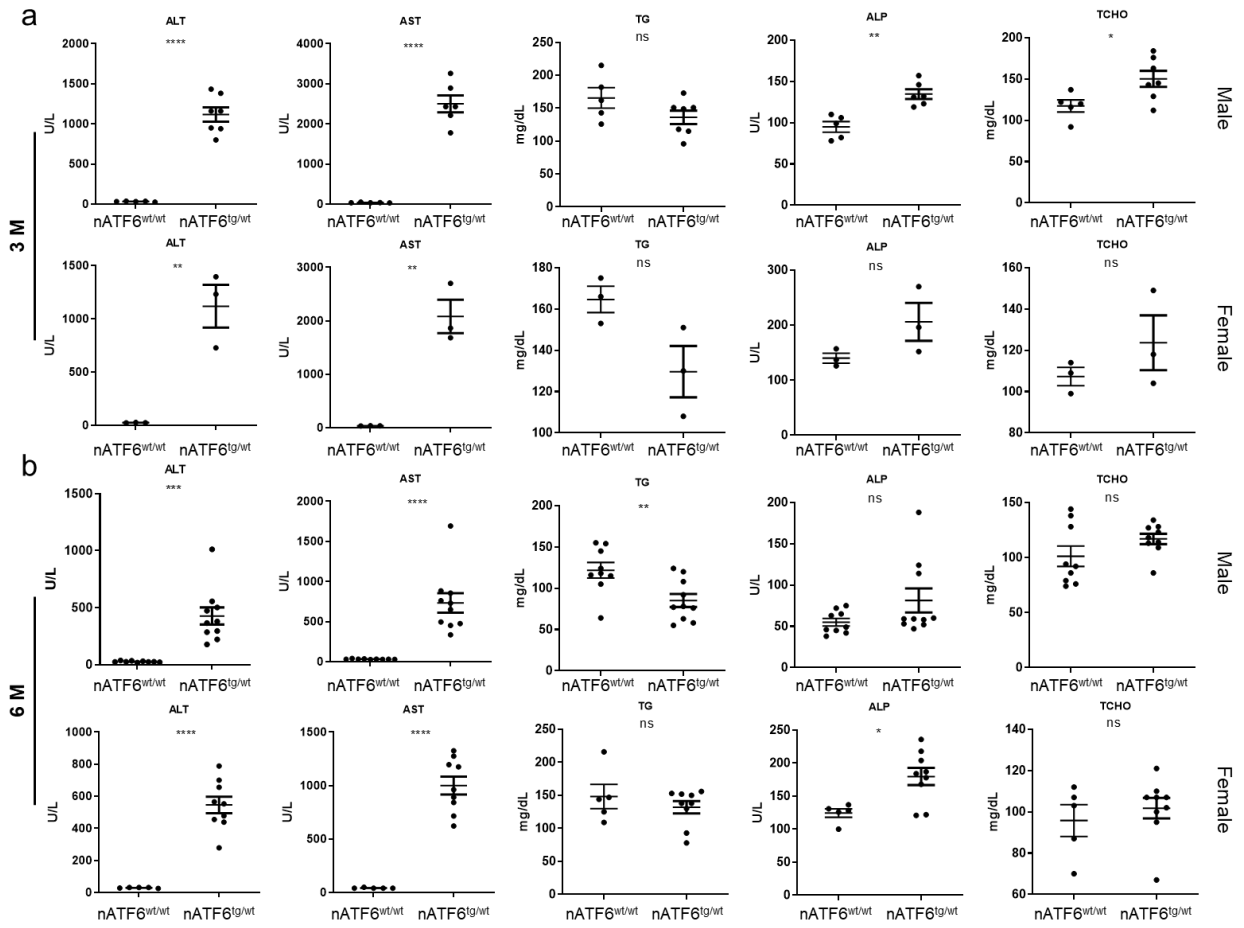

Figure 19: Persistent ATF6 activation in hepatocytes induces liver damage in mice. a). Serology parameters from the male (upper panel) and female (lower panel) mice in indicated groups at 3-month age. **b).** Serology parameters from the male (upper panel) and female (lower panel) mice in indicated mice group at 6-month age. All data were shown as mean ± SEM. All data were analyzed by unpaired T-test. p values are indicated as *, *p<0.05;**p<0.01; ***p<0.001; ****p<0.0001.

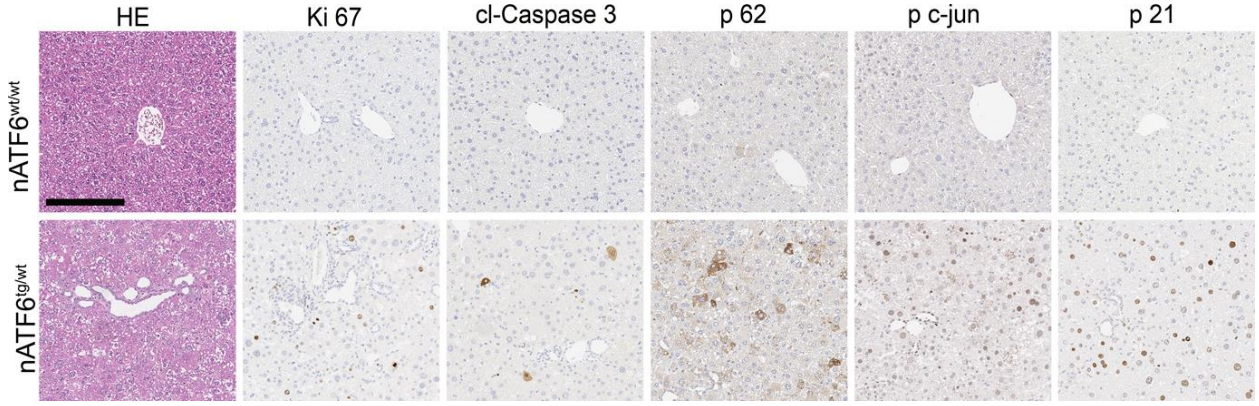

Figure 20: Persistent ATF6 activation in hepatocytes induces hepatocyte turnover. IHC staining of indicated molecules. HE staining shows the histological features of the liver, Ki 67 staining shows proliferative hepatocytes, cl-Caspase 3 staining shows apoptotic hepatocytes, p 62 staining shows

autophagosome cargos, p c-Jun staining shows activation of JNK signaling, p 21 staining shows cell cycle arrest in the liver.

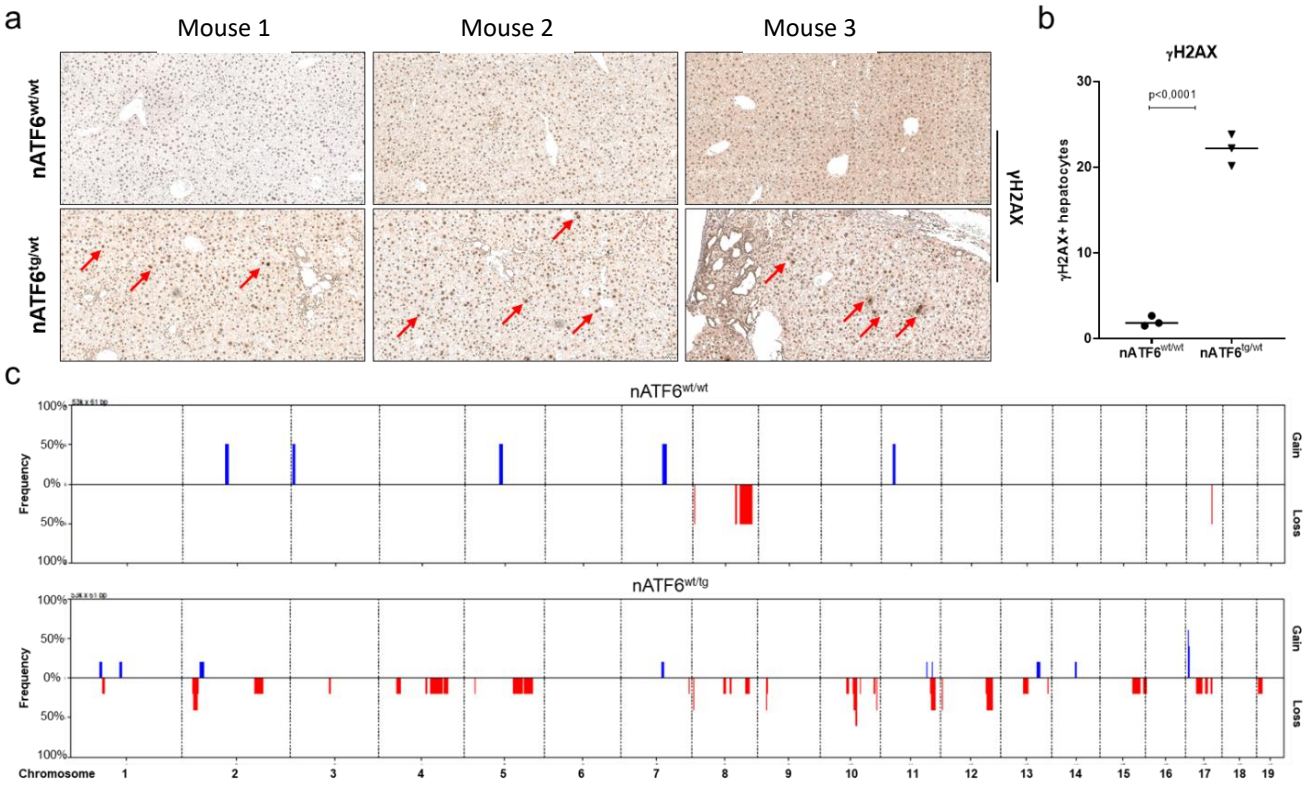

Figure 21: Persistent ATF6 activation in hepatocytes induces DNA damage and chromosome instability in nATF6$^{tg/wt}$ mice liver. a). IHC staining of g-H2AX in liver sections from nATF6$^{wt/wt}$ (n=3) and nATF6$^{tg/wt}$ (n=3) mice. **b).** Quantification of g-H2AX positive cells in **a**. **c).** aCGH analysis of liver samples from nATF6$^{wt/wt}$ (n=5) and nATF6$^{tg/wt}$ (n=7) mice, blue bars indicate the gained fragments in the chromosome and red bars indicate the lost fragments in the chromosome.

7.3.3 Persistent ATF6 activation in hepatocytes re-modulates the transcriptomic and proteomic profiles of the liver

To understand the underlying mechanisms of the phenotype I observed in nATF6$^{tg/wt}$ mice, I prepared mRNA samples and protein lysate from livers of 3-month and 6-month old animals (including both genotypes) for bulk RNA-seq and mass spec-based proteomics analyses.

For both RNA-seq and proteomic analyses, the control and experimental groups clustered quite well in the unsupervised clustering analysis (Figure 22a and Figure 23a). Strikingly, hepatic overexpression of nATF6 significantly changed the transcriptomic and proteomic profiles in mouse liver. The MA-plot (Figure 22b) of RNA-seq and the volcano graph (Figure 23b) of proteomics indicate the expression of many molecules is changed at both transcriptional and translational levels.

Gene Set Enrichment Analysis (GSEA) of RNA-seq and mass spec data revealed multiple biological events in mouse liver, including the UPR, apoptosis, p53 pathway, and cell-cycle regulation, have changed upon nATF6 overexpression. Interestingly, events related to inflammatory responses, including TNF-NKκB signaling, also arose in the GSEA. Additionally, events associated with malignant transformation, such as angiogenesis and epithelial-mesenchymal transition (EMT), also showed up in the analysis (Figure 22c and Figure 23c). Metabolic changes have also been identified and are involved in driving pathology but will be discussed later in this thesis.

7.3.4 ATF6-mediated liver damage is ROS-dependent and can be alleviated by anti-ROS treatment

As I have detected significant cell cycle alteration, DNA damage, and chromosome instability in livers of nATF6$^{tg/wt}$ mice, I reasoned which intermediator could mediate the liver phenotypes induced by persistent ATF6 activation.

As discussed in the introduction, the UPR activation is closely related to ROS generation due to the function of ER and its close contact with mitochondria. Thus, I checked the expression of critical molecules involved in oxidative stress. Surprisingly, I found ROS-related genes, including glutathione peroxidase 1 (GPX1), GPX2, GPX3, GPX7, and NAD(P)H Quinone Dehydrogenase 1 (Nqo1), are significantly upregulated upon ATF6 activation (Figure 24a); indicating the involvement or at least the induction of oxidative stress in livers of nATF6$^{tg/wt}$ mice. Among these ROS-related genes, the GPX family catalyzes the process of organic hydroperoxides and hydrogen peroxide (H_2O_2) reduction by glutathione, thereby protecting cells from oxidative damage. To ensure what I saw in RNA-seq data is accurate, I further performed IHC staining of P62 and NQO1, which are key molecules in NRF2 mediated anti-oxidative stress response; and MPO, which are mainly released by neutrophils and are able to cause oxidative damage in host tissue (Figure 24b). As expected, all these oxidative stress-related molecules are dramatically accumulated in livers of nATF6$^{tg/wt}$ mice over time, implying strong ROS induction, potentially crucial for driving pathology.

To address whether ROS is the primary mediator for ATF6 activation-induced hepatic phenotypes, I treated 4-week old nATF6$^{wt/wt}$ and nATF6$^{tg/wt}$ mice with a chow diet containing butylated hydroxyanisole (BHA). Mice fed a nutrition-matched normal diet (ND) served as controls. All mice behaved as expected despite different diet treatments - when it comes to the macroscopic feature of the movement, the food and water intake, etc. But mice fed the BHA diet did not gain weight at the same speed as those treated with the control diet (Data not shown).

I further tracked the serology parameters of these animals on a monthly basis. At the age of 4 weeks (before initiation of BHA-diet treatment), all serology parameters in nATF6$^{wt/wt}$ mice fell into the healthy range. In contrast, nATF6$^{tg/wt}$ mice showed significant indications of liver damage, as I have illustrated before. Strikingly, just 1-month of BHA-diet treatment is sufficient to maintain the ALT and AST in the serum of nATF6$^{tg/wt}$ mice at a significantly lower level compared to nATF6$^{tg/wt}$ mice receiving control diet (Figure 25a); indicating amelioration of liver damage in nATF6$^{tg/wt}$ mice by BHA-diet treatment. Further serology analyses revealed that the BHA-diet is capable of maintaining the liver damage in nATF6$^{tg/wt}$ mice constantly at a relatively low level throughout the whole life of the animals (Figure 25a).

To gain more comprehensive knowledge about the effect of BHA on the liver of nATF6$^{tg/wt}$ mice, I dissected a group of animals after 3 months of BHA-diet feeding. Interestingly, beyond our expectations, although the liver damage seems to be relieved according to the serology parameters, the hepatomegaly showed in nATF6$^{tg/wt}$ mice was not rescued but became even worse under BHA treatment (Data not shown).

However, histologically, I have observed that the expression levels of BIP (revealing the level of ER stress), phosphorylated c-Jun, and p21 (indicating the cell cycle arrest) were all significantly diminished by BHA-diet treatment (Figure 25b), suggesting reduced liver damage.

In summary, these data suggest that oxidative stress plays a critical role in nATF6 overexpression-mediated liver damage.

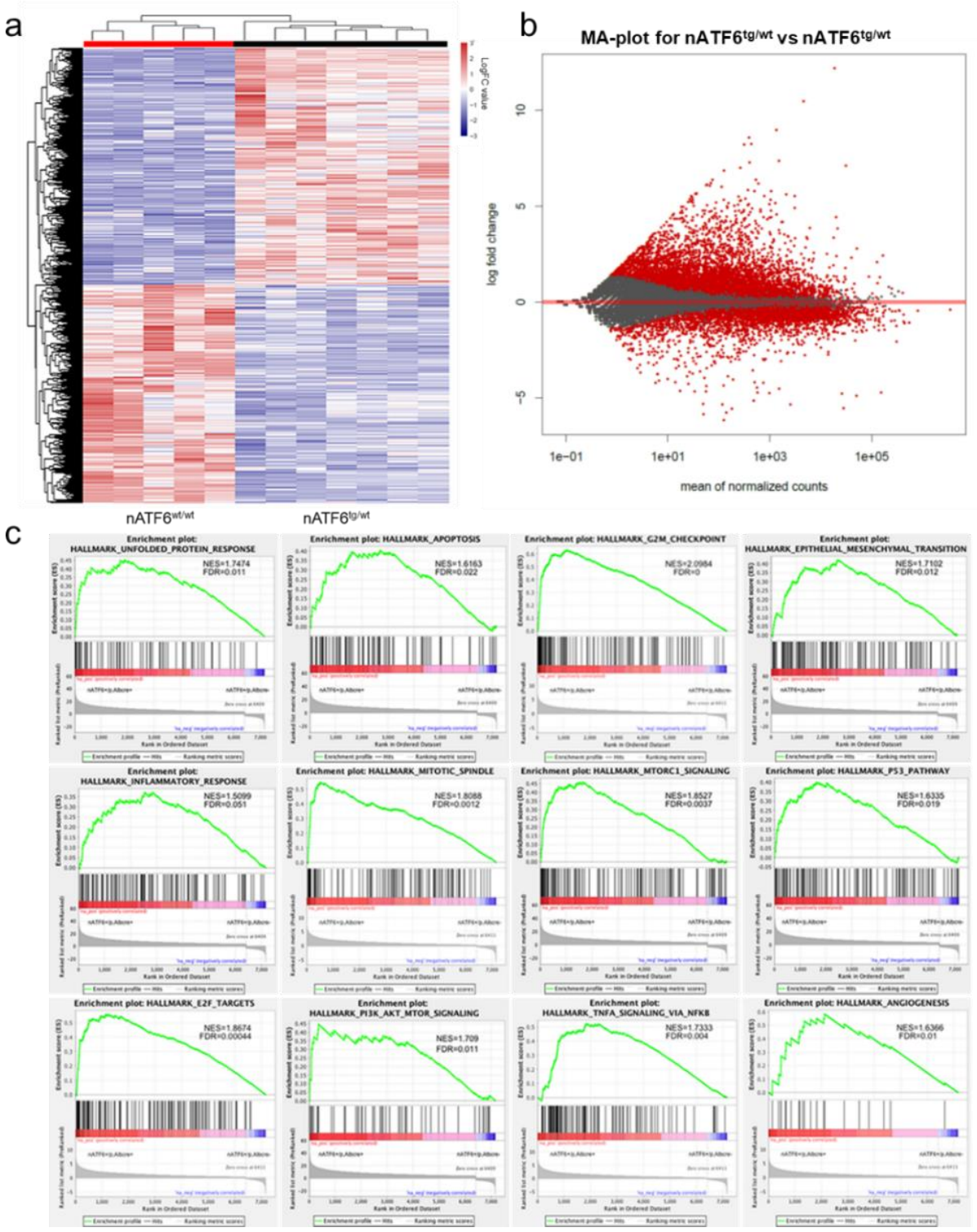

Figure 22: Persistent ATF6 activation in hepatocytes alters the transcriptional profile in mice liver. a). The unsupervised cluster of RNA-seq data from nATF6$^{wt/wt}$ (n=5) and nATF6$^{tg/wt}$ (n=7) mice liver shows in a heatmap. **b).** MA-plot shows the differently expressed genes from **a**. **c).** Gene Set Enrichment Analysis (GSEA) of RNA-seq data shows significantly changed pathways, including the UPR, apoptosis, cell cycle-related regulation, inflammation-related pathways, etc.

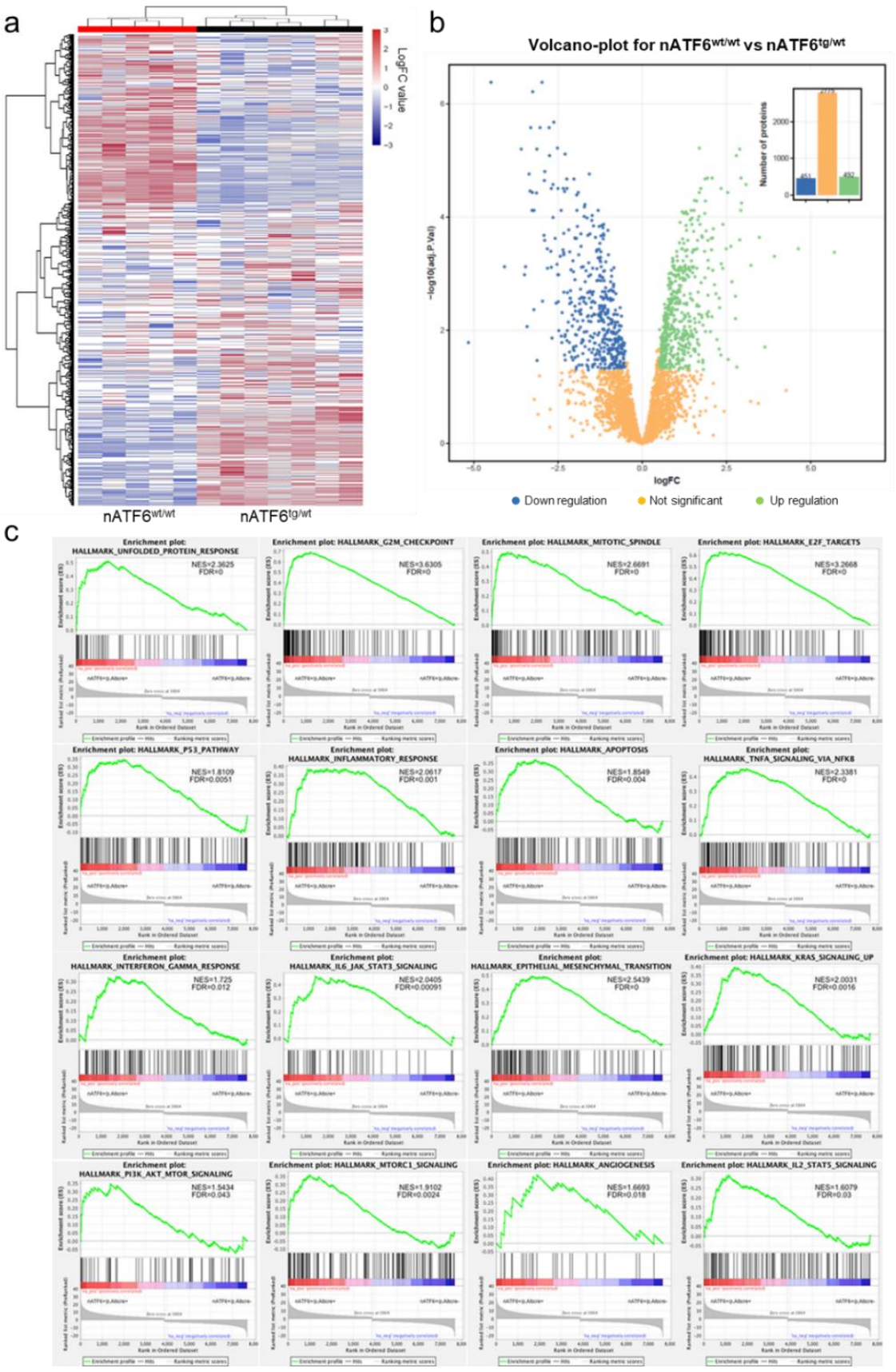
a
LogFC value
nATF6wt/wt
nATF6tg/wt
b
Volcano-plot for nATF6wt/wt vs nATF6tg/wt
−log10(adj.P.Val)
logFC
Number of proteins
451
432
Down regulation
Not significant
Up regulation
c
Enrichment plot: HALLMARK_UNFOLDED_PROTEIN_RESPONSE
NES=2.3625
FDR=0
Enrichment plot: HALLMARK_G2M_CHECKPOINT
NES=3.6305
FDR=0
Enrichment plot: HALLMARK_MITOTIC_SPINDLE
NES=2.6691
FDR=0
Enrichment plot: HALLMARK_E2F_TARGETS
NES=3.2668
FDR=0
Enrichment plot: HALLMARK_P53_PATHWAY
NES=1.8109
FDR=0.0051
Enrichment plot: HALLMARK_INFLAMMATORY_RESPONSE
NES=2.0617
FDR=0.001
Enrichment plot: HALLMARK_APOPTOSIS
NES=1.8549
FDR=0.004
Enrichment plot: HALLMARK_TNFA_SIGNALING_VIA_NFKB
NES=2.3381
FDR=0
Enrichment plot: HALLMARK_INTERFERON_GAMMA_RESPONSE
NES=1.725
FDR=0.012
Enrichment plot: HALLMARK_IL6_JAK_STAT3_SIGNALING
NES=2.0405
FDR=0.00091
Enrichment plot: HALLMARK_EPITHELIAL_MESENCHYMAL_TRANSITION
NES=2.5439
FDR=0
Enrichment plot: HALLMARK_KRAS_SIGNALING_UP
NES=2.0031
FDR=0.0016
Enrichment plot: HALLMARK_PI3K_AKT_MTOR_SIGNALING
NES=1.5434
FDR=0.043
Enrichment plot: HALLMARK_MTORC1_SIGNALING
NES=1.9102
FDR=0.0024
Enrichment plot: HALLMARK_ANGIOGENESIS
NES=1.6693
FDR=0.018
Enrichment plot: HALLMARK_IL2_STAT5_SIGNALING
NES=1.6079
FDR=0.03

Figure 23: Persistent ATF6 activation in hepatocytes alters hepatic proteome. a). The unsupervised cluster of proteomics data from the liver of nATF6$^{wt/wt}$ (n=5) and nATF6$^{tg/wt}$ (n=7) mice shows in a heatmap. **b).** Volcano-plot shows the differently expressed proteins from **a**. **c).** Gene Set Enrichment Analysis (GSEA) of proteomics data shows the significantly changed pathways, including the UPR, E2F targets, cell cycle-related regulation, inflammation-related pathways, etc.

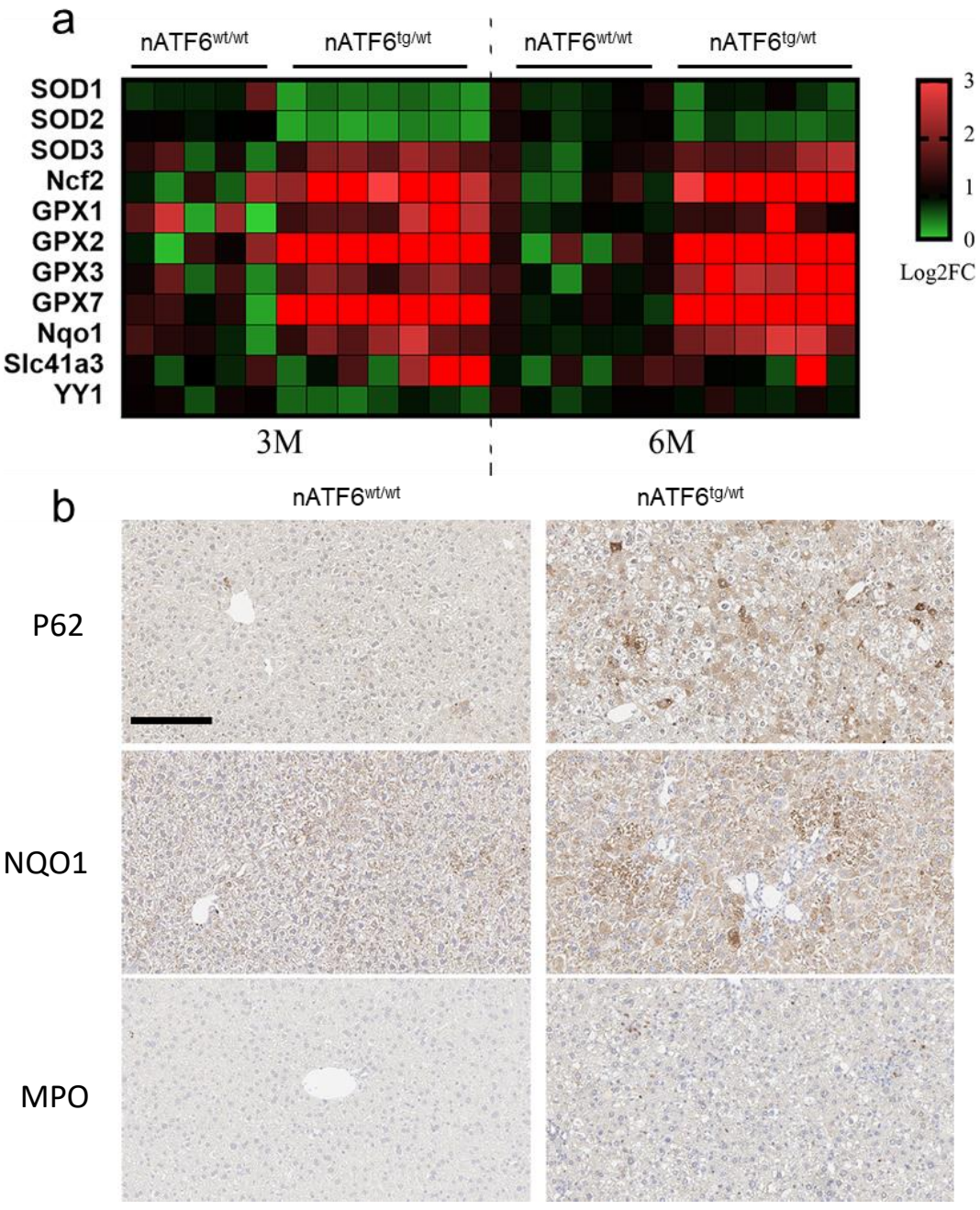

Figure 24: Persistent ATF6 activation in mouse liver induces ROS production. a). A heat-map shows the expression of indicated genes in the nATF6$^{wt/wt}$ (n=5) and nATF6$^{tg/wt}$ (n=7) mice liver at 3-month and 6-month age. **b).** Representative IHC staining of indicated molecules in the liver of nATF6$^{wt/wt}$ and nATF6$^{tg/wt}$ mice at 3-month age, P62 staining shows autophagosome cargos, NQO1 staining indicates change of cellular redox state, MPO staining indicates activation of neutrophil granulocytes.

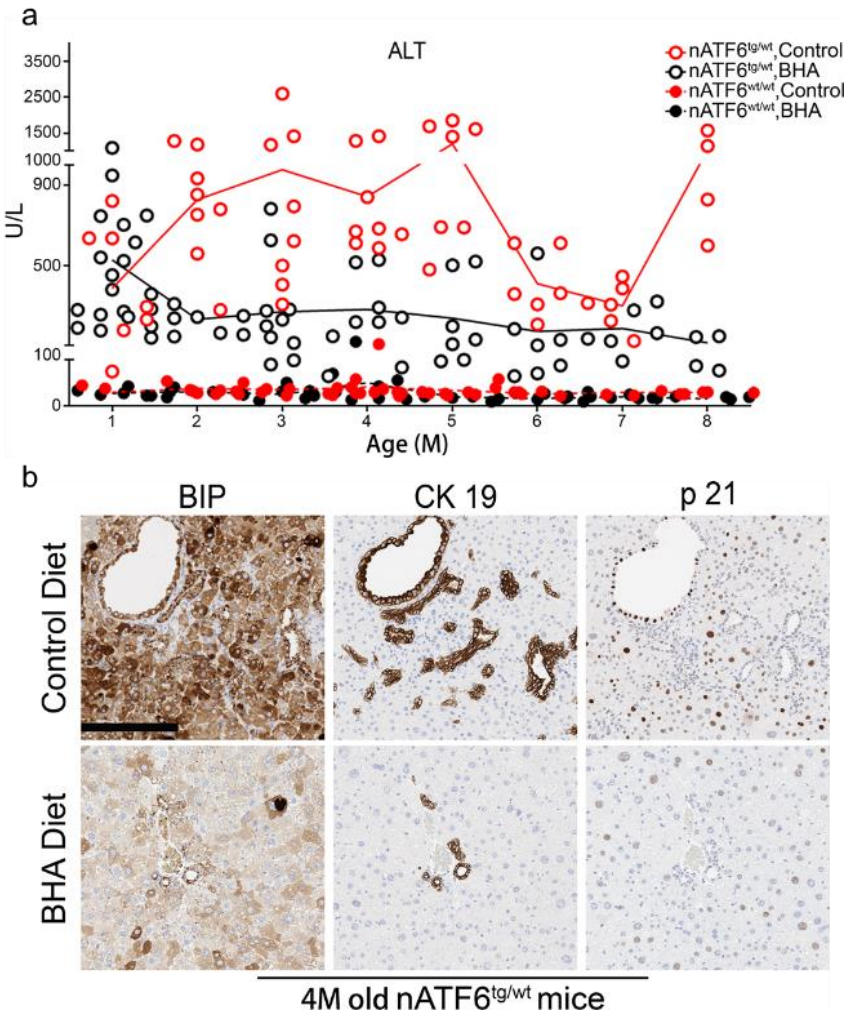

Figure 25: Anti-ROS BHA diet alleviates liver damage in nATF6$^{tg/wt}$ mice. a). Serum ALT levels of nATF6$^{wt/wt}$ and nATF6$^{tg/wt}$ mice treated with control diet or BHA-containing diet at different time points. **b).** Representative IHC staining of indicated molecules in nATF6$^{tg/wt}$ mice treated with control diet or BHA-containing diet at 4-month age, BIP staining reveals the levels of ER stress, CK 19 staining indicates expansion of BECs, P 21 staining shows cell cycle arrest.

7.4 Hepatic ATF6 activation induces tumorigenesis in mouse liver

7.4.1 Persistent ATF6 activation in mouse liver leads to hepatic tumor formation

From the dissection of 3-month and 6-month old nATF6$^{tg/wt}$ and control mice, I found that persistent activation of nATF6 induces ROS-mediated liver damage. By comparing the survival data of nATF6$^{tg/wt}$ mice to that of nATF6$^{wt/wt}$ mice, I observed a significant decrease in the survival rate in nATF6$^{tg/wt}$ mice at the age of 1 year (Figure 26b). Most of the nATF6$^{tg/wt}$ mice had to be sacrificed at around 1-year-old. They show an obvious harmful phenotype (tumor-suspicious big belly), which reaches the termination criterion according to my approved animal protocols, whereas the control animals remained healthy. To understand what was happening in livers of

nATF6$^{tg/wt}$ mice at their old ages, I sent 9-month-old animals for positron emission tomography-computed tomography (PET-CT) and MRI to view their livers non-invasively.

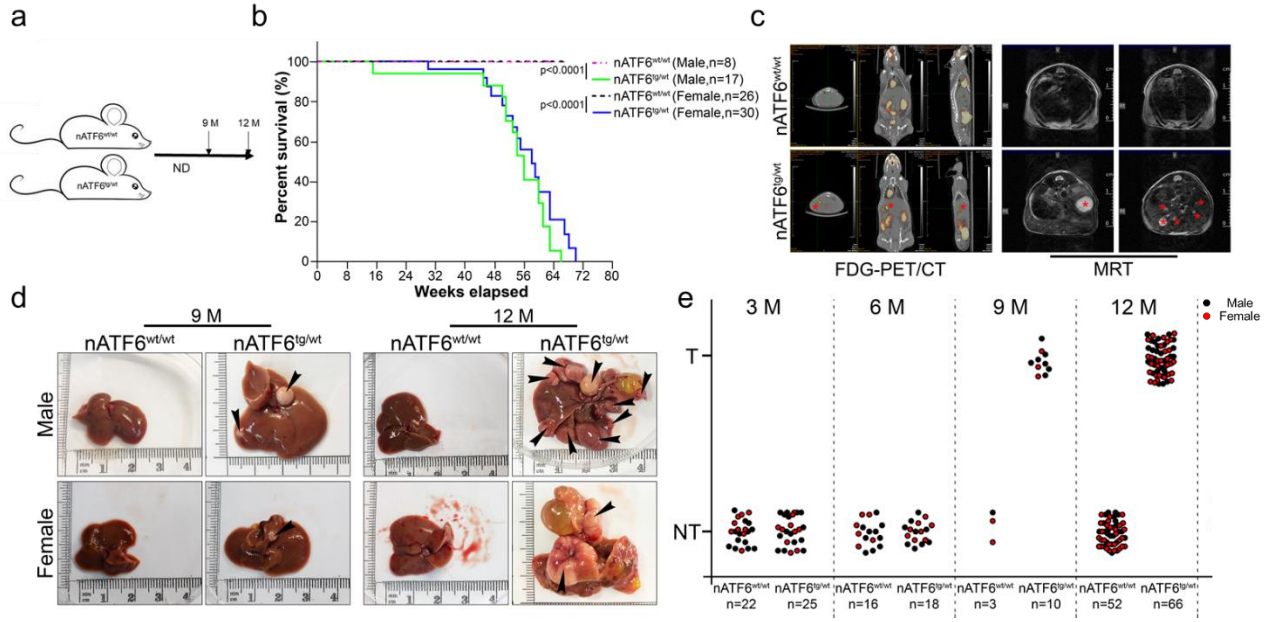

Figure 26: Persistent nATF6 expression in mouse liver leads to liver cancer formation. a). A schematic representation shows the experimental strategy. **b).** The survival curve of the nATF6$^{wt/wt}$ and nATF6$^{tg/wt}$ mice. **c).** Representative PET-CT (left panel) and MRI (right panel) images from nATF6$^{wt/wt}$ and nATF6$^{tg/wt}$ mice. **d).** Representative liver pictures from indicated mice groups at 9-month and 12-month age, tumors were indicated by black arrows. **e).** Hepatic tumor incidence of nATF6$^{wt/wt}$ and nATF6$^{tg/wt}$ mice at different ages.

Interestingly, livers of nATF6$^{tg/wt}$ mice show suspicious malignant lesions due to increased absorption of Fluorodeoxyglucose (^{18}F) in the hepatic areas, indicating a changed glucose metabolism and high demands for glucose in these areas. The MRI has detected areas with abnormal density, in line with the PET-CT results, suggesting nodules or premalignant lesions in livers of 9-month-old nATF6$^{tg/wt}$ mice (Figure 26c). Indeed, after dissection of 9-month-old nATF6$^{tg/wt}$ mice, I found multiple visible tumors exclusively in livers of nATF6$^{tg/wt}$ mice but not in nATF6$^{wt/wt}$ control mice (Figure 26d). A similar but more severe phenotype has been observed in 12-month-old animals as well (Figure 26d). I summed up the tumor incidence in nATF6$^{tg/wt}$ mice; Surprisingly, I found that all male mice from nATF6$^{tg/wt}$ group developed liver cancer at 9-month age; while some female animals did not have visible tumors in the liver (data not shown). However, livers from female nATF6$^{tg/wt}$ mice display a more severe cystic phenotype, indicating a non-negligible gender disparity in nATF6 expression-induced hepatic phenotypes in mice. In both male and female nATF6$^{tg/wt}$ mice, the tumor incidence is 100% at 12 months of age (Figure 26e).

7.4.2 Hepatic nATF6 expression-induced liver phenotypes show gender disparity in mice

As mentioned in the previous section, a prominent sex disparity in the liver phenotype of nATF6$^{tg/wt}$ mice is displayed. Indeed, female nATF6$^{tg/wt}$ mice seem to suffer mainly from liver cysts rather than tumors (Figure 27a). The earliest time I detected hepatic cysts in female nATF6$^{tg/wt}$ mice was at 6 months of their age, at which stage no tumor has been observed in livers of nATF6$^{tg/wt}$ mice (Figure 18a). When female nATF6$^{tg/wt}$ mice reach a 12-month age, the cystic burden becomes obvious and severe as these animals show an enlarged belly. I had to terminate them according to my approved animal protocols (Figure 27a). I collected the liquid content in hepatic cysts of female nATF6$^{tg/wt}$ mice and sent it for LC-MS base analyses; the data shows the liquid content in hepatic cysts from female nATF6$^{tg/wt}$ mice are bile acids (Figure 27b).

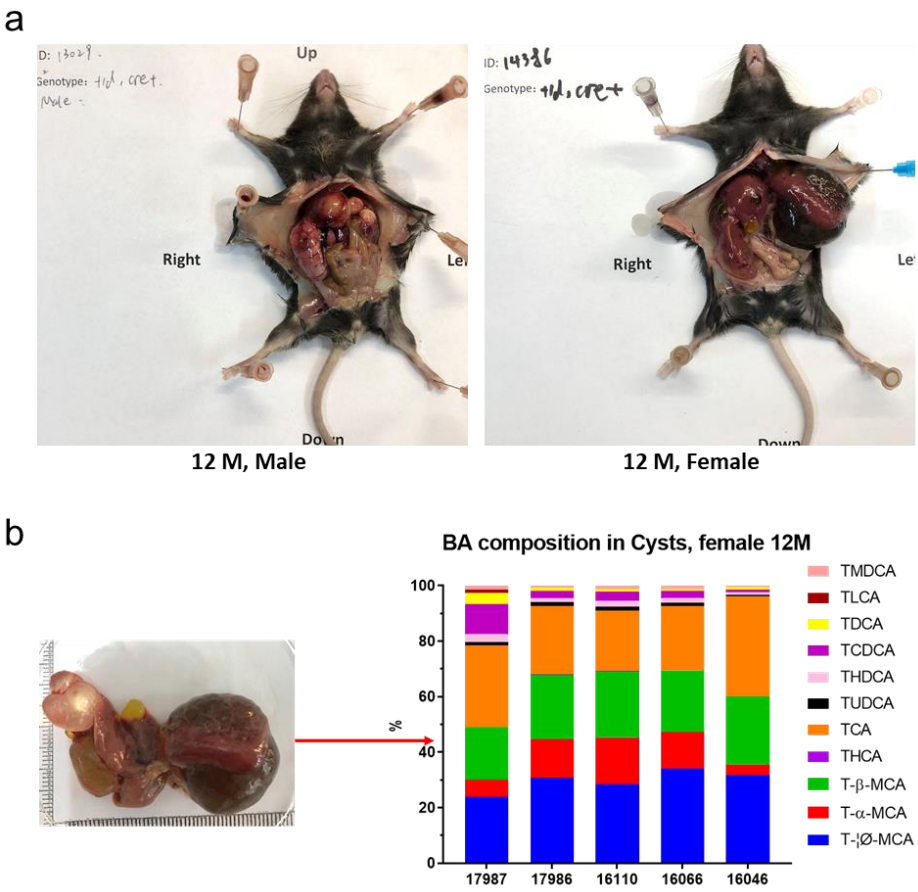

Figure 27: Sex disparity in nATF6 expression-induced liver phenotypes. a). Representative pictures of male and female nATF6$^{tg/wt}$ mice dissected at 12-month age. **b).** Liquid content in hepatic cysts of female nATF6$^{tg/wt}$ mice was analyzed by LC-MS, indicating that the liquid components in cysts of female nATF6$^{tg/wt}$ mice are bile acids.

To better understand the gender disparity in the cystic phenotype, I performed bulk RNA-seq analysis of livers from male and female nATF6$^{wt/wt}$ and nATF6$^{tg/wt}$ mice at 6-month age.

It has been evidenced that male and female nATF6$^{tg/wt}$ mice show distinct gene expression patterns, as shown in the c-net style GSEA analysis (Figure 28). Under persistent ATF6 activation, livers from female mice have more robust activation in anti-oxidative stress and immune response-related biological events. In contrast, these events have no difference in the normal situation with the male mice (Figure 29).

In addition, serology analyses and metabolic analyses show a gender disparity of nATF6$^{tg/wt}$ mice in liver cholesterol and bile acid metabolism (Figure 19a and Figure 36). Further studies are needed to understand the underlying mechanisms.

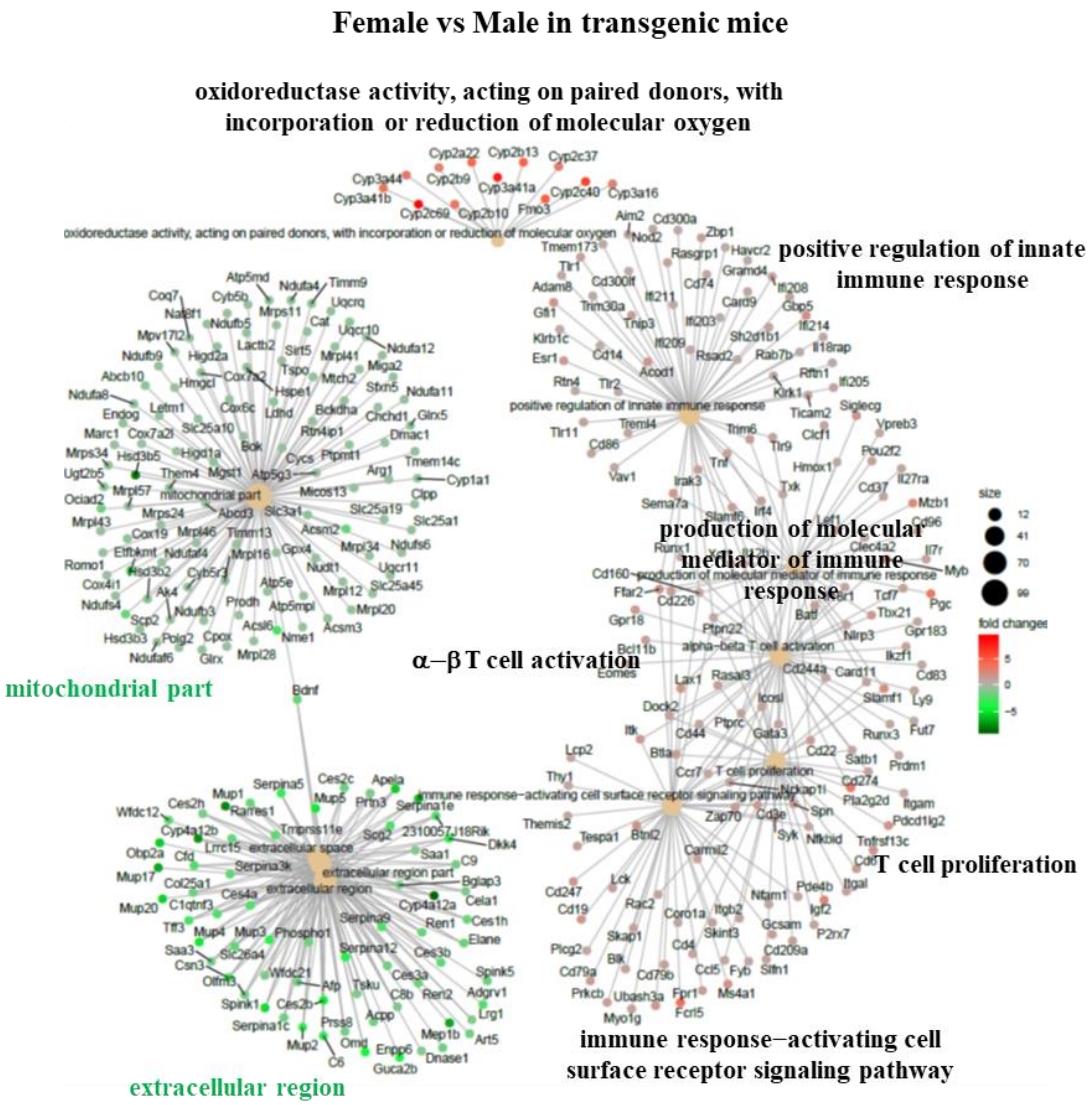

Figure 28: Sex disparity in gene expression profiles in nATF6$^{tg/wt}$ mice. GSEA analysis of RNA-seq data from male and female nATF6$^{tg/wt}$ mice liver shows an apparent gender disparity in the transcriptional networks in livers of nATF6$^{tg/wt}$ mice. Genes located on sex chromosomes have been excluded from the analysis.

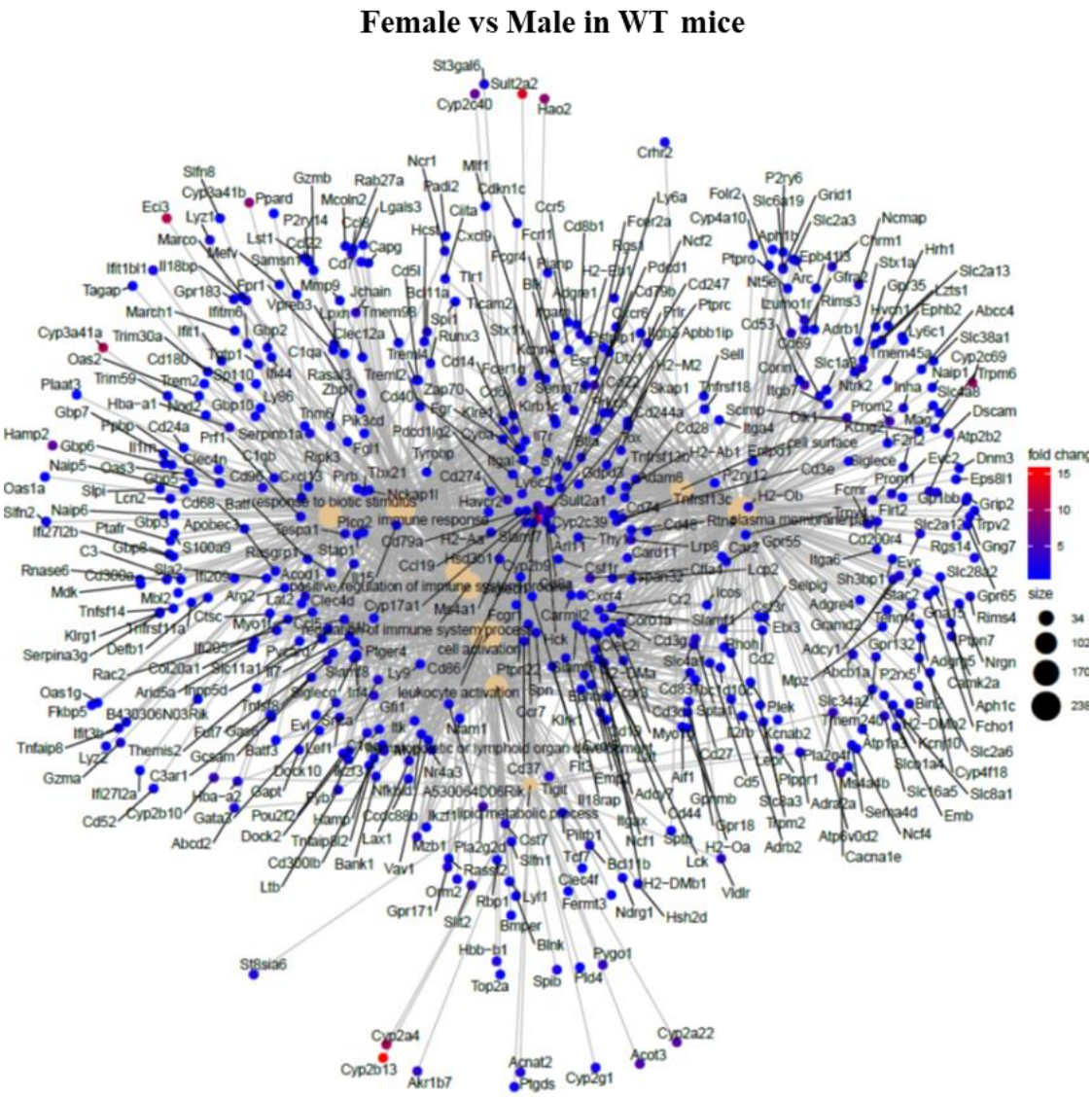

Figure 29: Gene expression profiles in male and female nATF6$^{wt/wt}$ mice. GSEA analysis of RNA-seq data from male and female nATF6$^{wt/wt}$ mice liver. No significant changes in pathways had been identified between livers of male and female nATF6$^{wt/wt}$ mice. Genes located on sex chromosomes have been excluded from the analysis.

7.4.3 ATF6 activation-induced hepatic tumors show both HCC and CCA phenotype and are similar to human liver cancers in genetic patterns

I focused on the connection between ATF6 activation and hepatic tumorigenesis in this project. For characterizing the growth pattern of ATF6 activation-induced hepatic tumors, I performed a series of IHC staining for hepatic sections from nATF6$^{tg/wt}$ mice. As shown in Figure 30a, the HE staining clearly shows the tumoral and non-tumoral areas; the tumoral area is more obvious in IHC staining of collagen IV, where the distribution of collagen IV is massively disrupted. Interestingly, hepatic tumors induced by ATF6 activation not only have an HCC phenotype (as

shown by AFP staining) but also contain tumors reminiscent of CCA (as shown by CK19 staining). Notably, HA staining shows the major proportion of cells within the HCC area expresses nATF6 transgene, indicating the tumor originated from nATF6-overexpressed hepatocytes. However, in the CCA tumor, a considerable amount of cells either have no transgene expression or only have a low-level expression of nATF6 transgene, implying this tumor may originate from cells without ATF6 activation due to the environmental stress (Figure 30a).

Besides the histological stainings, which shows typical characters of HCC and CCA in nATF6$^{tg/wt}$ mouse liver. I further isolated the genomic DNA from tumor areas and performed aCGH assay. As revealed in Figure 30b, the genome of the tumor cells shows significant genomic instability, indicated by the lost and gained fragments in their chromosome regions. Moreover, by comparing the aCGH data with human tumors from established databases, I concluded the hepatic tumors in nATF6$^{tg/wt}$ mice are genetically mimicking the human situation (Figure 30c).

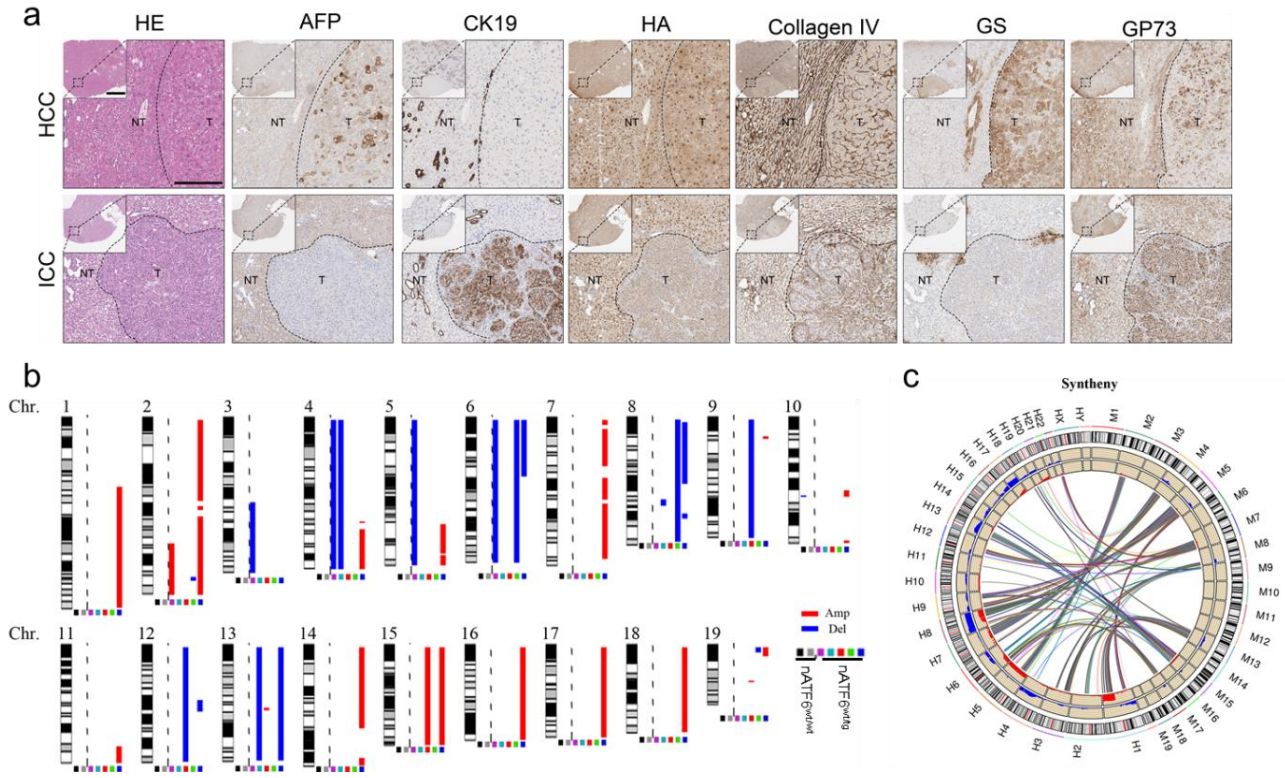

Figure 30: Characterization of ATF6 activation-induced hepatic tumors. a). IHC staining of indicated molecules in the hepatic tumor sections from nATF6$^{tg/wt}$ mice; NT: non-tumoral area; T: Tumoral area. **b).** A microarray-based comparative genomic hybridization (aCGH) assay of liver tissue from nATF6$^{wt/wt}$ mice and tumoral tissue from nATF6$^{tg/wt}$ mice. **c).** Synteny analysis of chromosomal aberrations in tumors from nATF6$^{tg/wt}$ mice liver and human HCC shows the genetic instability in ATF6 activation-induced HCC in mice is similar to that in human HCC.

7.5 Liver-specific ATF6 activation reshapes hepatic metabolism and generates a nutrition-deprived microenvironment

7.5.1 Liver-specific ATF6 activation re-modulates the glucose and amino acid metabolism in the liver of nATF6$^{tg/wt}$ mice

To further uncover the underlying mechanisms of the pro-tumorigenic effect of ATF6 activation, I went back to the transcriptome and proteome data at 3-month and 6-month time points. At that stage, tumors are not established in livers of nATF6$^{tg/wt}$ mice. Among the enriched GSEA pathways, besides those I have discussed in previous sections, the misregulation of metabolism-related pathways drew my attention (Figure 31c), given the liver and the ER play critical roles in systemic and cellular metabolism, respectively.

The liver is the primary site for glucose storage, and its functionality is vital for maintaining blood glucose at a stable level. I checked the molecules involved in glucose metabolism in my RNA-seq data. Strikingly, the expression of key regulators involved in glucose metabolism was affected by ATF6 activation and changed significantly in livers of nATF6$^{tg/wt}$ mice (Figure 31a). Further analyses suggested that the activation of nATF6 tends to shift glucose metabolism in livers of nATF6$^{tg/wt}$ mice from oxidative phosphorylation towards aerobic glycolysis. The critical enzymes for aerobic glycolysis were upregulated upon hepatic ATF6 activation (Figure 31a). To functionally validate this finding, I first performed periodic acid-schiff stain (PAS) staining with liver sections from nATF6$^{tg/wt}$ and nATF6$^{wt/wt}$ mice. Strikingly, the PAS staining shows glycogen storage in livers of nATF6$^{tg/wt}$ mice has been massively depleted (Figure 32b). The change of glucose metabolism in the liver also affects nATF6$^{tg/wt}$ mice systematically. As shown in the glucose tolerance test, nATF6$^{tg/wt}$ mice are less susceptible to high-dose glucose injection, and the fasting glucose level in nATF6$^{tg/wt}$ animals is also lower than in nATF6$^{wt/wt}$ animals (Figure 32a).

Indeed, NMR-based analyses of liver metabolites indicate the glucose metabolism in nATF6$^{tg/wt}$ mice liver has been fundamentally re-modulated. The lack of glucose in livers of nATF6$^{tg/wt}$ mice is the most predominant phenotype identified by NMR-based metabolic analyses (Figure 33); Indicating that persistent ATF6 activation shifts the glucose metabolism towards aerobic glycolysis rather than oxidative phosphorylation. Except for the glucose and lipid metabolism, the NMR metabolic analyses also provide information about changes in amino-acid metabolism in livers of nATF6$^{tg/wt}$ mice (Figure 33).

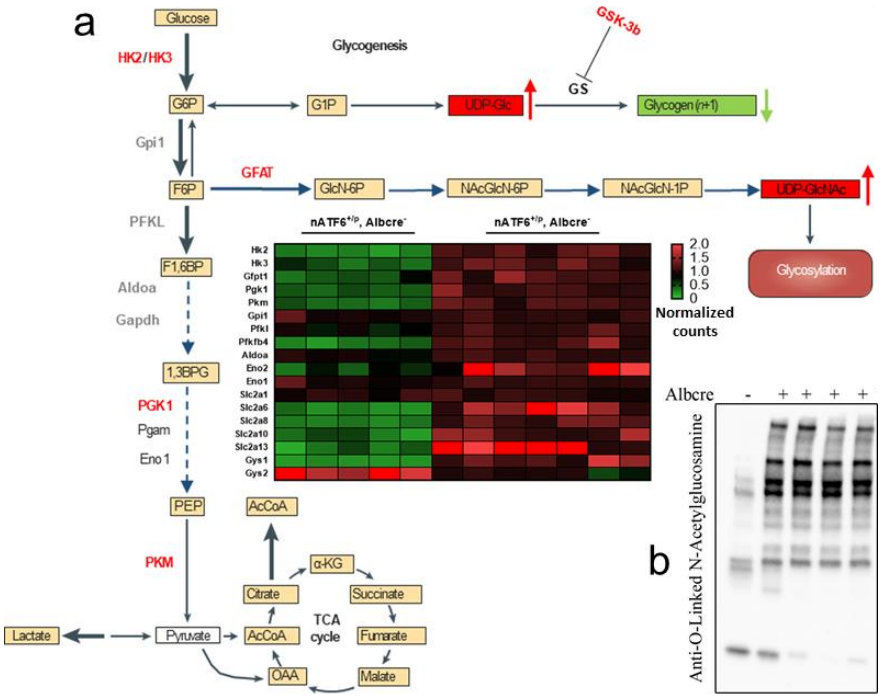
a
Glucose
HK2/HK3
Glycogenesis
GSK-3b
GS
G6P
G1P
UDP-Glc
Glycogen (n+1)
Gpi1
F6P
GFAT
GlcN-6P
NAcGlcN-6P
NAcGlcN-1P
UDP-GlcNAc
PFKL
nATF6+/p, Albcre-
nATF6+/p, Albcre-
F1,6BP
Aldoa
Gapdh
1,3BPG
PGK1
Pgam
Eno1
PEP
AcCoA
PKM
α-KG
Citrate
Succinate
TCA cycle
Lactate
Pyruvate
AcCoA
Fumarate
OAA
Malate
Hk2
Hk3
Gfpt1
Pgk1
Pkm
Gpi1
Pfkl
Pfkfb4
Aldoa
Eno2
Eno1
Slc2a1
Slc2a6
Slc2a8
Slc2a10
Slc2a13
Gys1
Gys2
2.0
1.5
1.0
0.5
0
Normalized counts
Glycosylation
b
Albcre - + + + +
Anti-O-Linked N-Acetylglucosamine
c
Transcriptome
Proteome
Enrichment plot: HALLMARK_OXIDATIVE_PHOSPHORYLATION
NES=-2.484
FDR=0
Enrichment plot: HALLMARK_BILE_ACID_METABOLISM
NES=-3.9195
FDR=0
Enrichment plot: HALLMARK_ADIPOGENESIS
NES=-2.0031
FDR=0.0054
Enrichment plot: HALLMARK_FATTY_ACID_METABOLISM
NES=-1.7369
FDR=0.0061
Enrichment plot: HALLMARK_GLYCOLYSIS
NES=1.3536
FDR=0.14
Enrichment plot: HALLMARK_CHOLESTEROL_HOMEOSTASIS
NES=1.6738
FDR=0.014
Enrichment plot: HALLMARK_OXIDATIVE_PHOSPHORYLATION
NES=-3.9157
FDR=0
Enrichment plot: HALLMARK_BILE_ACID_METABOLISM
NES=-3.9663
FDR=0
Enrichment plot: HALLMARK_ADIPOGENESIS
NES=-3.3675
FDR=0
Enrichment plot: HALLMARK_FATTY_ACID_METABOLISM
NES=-3.2444
FDR=0
NES=1.3289
FDR=0.1418
Enrichment plot: HALLMARK_CHOLESTEROL_HOMEOSTASIS
NES=1.4777
FDR=0.061

Figure 31: Hepatic nATF6 expression remodels liver glucose metabolism in mice. a). A schematic representation shows the glucose metabolism network and the changed expression of glucose metabolism-related genes in nATF6$^{tg/wt}$ mice liver. **b).** The expression of O-linked N-acetylglucosamine in nATF6$^{wt/wt}$ and nATF6$^{tg/wt}$ mice was checked by western blot. **c).** Gene Set Enrichment Analysis (GSEA) of RNA-seq data from livers of nATF6$^{wt/wt}$ (n=5) and nATF6$^{tg/wt}$ (n=7) mice at 3-month age shows the enrichment of metabolism-related pathways, including oxidative phosphorylation, bile acid metabolism, fatty acid metabolism, glycolysis, cholesterol homeostasis, etc.

To exclude other factors that might affect hepatic metabolisms, such as difference in movements or food/water intake between nATF6$^{tg/wt}$ and nATF6$^{wt/wt}$ mice, I transferred the animals into metabolic cages (TSE systems) to track their metabolic parameters (including O_2 consumption, moving activity, food/water intake, etc.). As showing in Figure 32c, no noticeable difference in O_2 consumption, food/water intake, and movement between nATF6$^{tg/wt}$ and nATF6$^{wt/wt}$ mice had been recorded. Thus, I concluded the metabolic remodeling founded in livers of nATF6$^{tg/wt}$ mice is due to activation of the ATF6 branch of UPR.

7.5.2 Liver-specific ATF6 activation re-modulates hepatic lipid metabolism in mice

Besides glucose metabolism, lipid metabolism in hepatocytes is also of vital importance for maintaining body homeostasis. Due to significant changes in serum TG and cholesterol content, which I reported in section 7.3, linking ATF6 activation to lipid metabolism in livers of nATF6$^{tg/wt}$ mice is reasonable. As the initial step, I performed Sudan Red staining for lipids in liver sections of nATF6$^{wt/wt}$ and nATF6$^{tg/wt}$ mice. Impressively, a pronounced accumulation of lipid contents has been found in nATF6$^{tg/wt}$ mice liver at 3-month age (Figure 34a). Further study has shown this steatotic phenotype already exists in livers of nATF6$^{tg/wt}$ mice at 4-week age (data not shown).

Additionally, I aimed to understand which lipid components are accumulated in livers of nATF6$^{tg/wt}$ mice. I performed a hepatic TG assay and a hepatic cholesterol assay with liver homogenate from nATF6$^{wt/wt}$ and nATF6$^{tg/wt}$ mice. Surprisingly, no difference in hepatic TG has been observed (Figure 34b), but a clear-cut increase in hepatic cholesterol level occurs in livers of nATF6$^{tg/wt}$ mice at 3-month age (Figure 34c), indicating a modification on cholesterol metabolism by ATF6 activation. Indeed, genes involved in cholesterol and lipid metabolism, such as IL36, CD36, ACAT2, SQLE, SREBP1, DGAT2, and SCD1, were changed significantly upon ATF6 activation (Figure 34d).

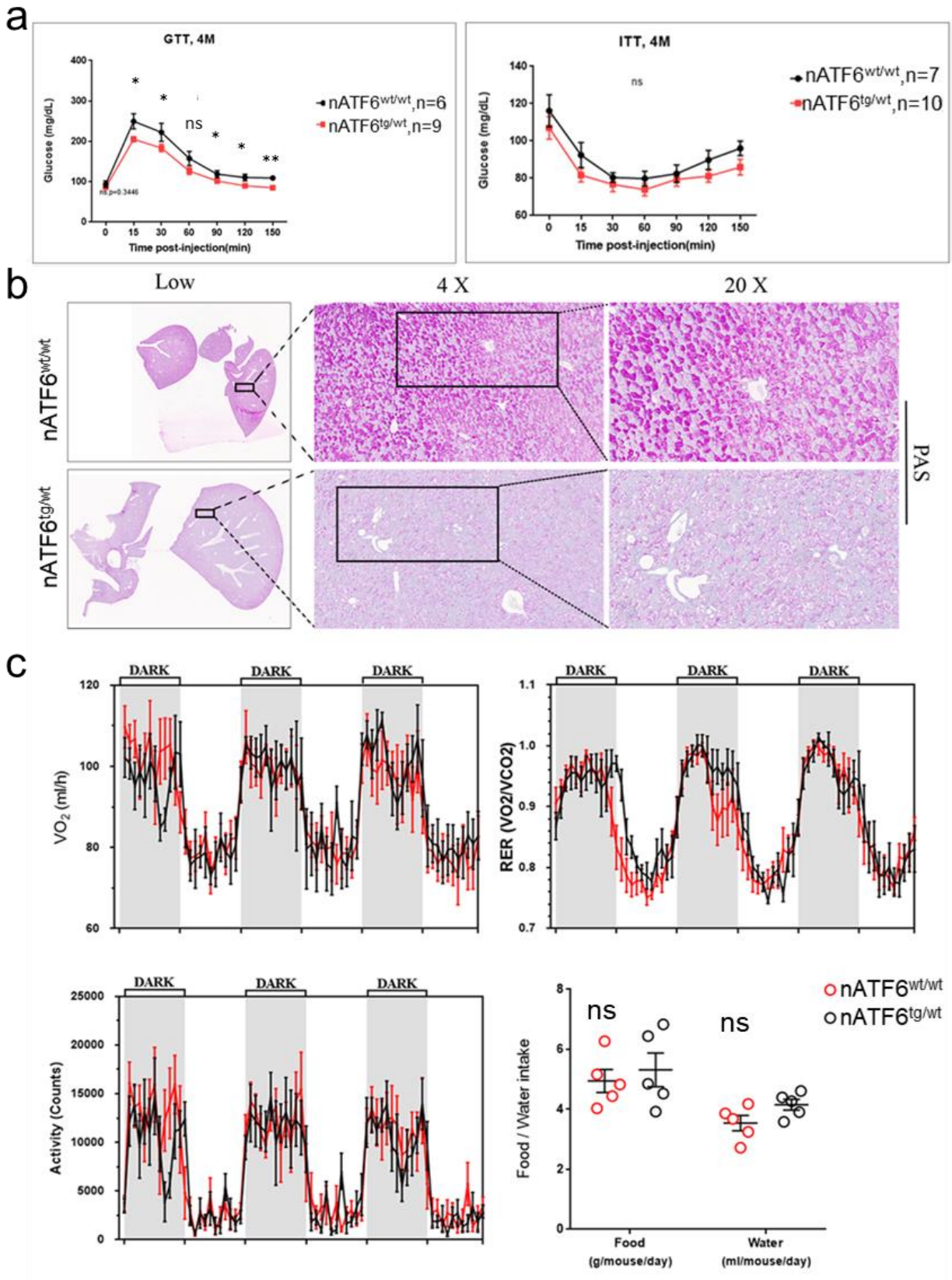
a
GTT, 4M
Glucose (mg/dL)
Time post-injection(min)
nATF6wt/wt,n=6
nATF6tg/wt,n=9
ns
ITT, 4M
nATF6wt/wt,n=7
nATF6tg/wt,n=10
b
Low
4 X
20 X
nATF6wt/wt
nATF6tg/wt
PAS
c
DARK
VO2 (ml/h)
RER (VO2/VCO2)
Activity (Counts)
Food / Water intake
Food
(g/mouse/day)
Water
(ml/mouse/day)

Figure 32: Hepatic nATF6 expression affects systematic glucose metabolism in mice. a). The glucose tolerance test (left panel) and the insulin tolerance test (right panel) were performed in nATF6$^{wt/wt}$ and nATF6$^{tg/wt}$ mice at 4-month age. **b).** Histological PAS staining in liver sections from nATF6$^{wt/wt}$ and nATF6$^{tg/wt}$ mice at 3-month age. **c).** Metabolic cages analysis shows the O_2 consumption, moving activity, and food/water intake in nATF6$^{wt/wt}$ and nATF6$^{tg/wt}$ mice at 3-month age. All data were shown as mean ± SEM. All data were analyzed by unpaired T-test. p values are indicated as *, *p<0.05;**p<0.01; ***p<0.001; ****p<0.0001.

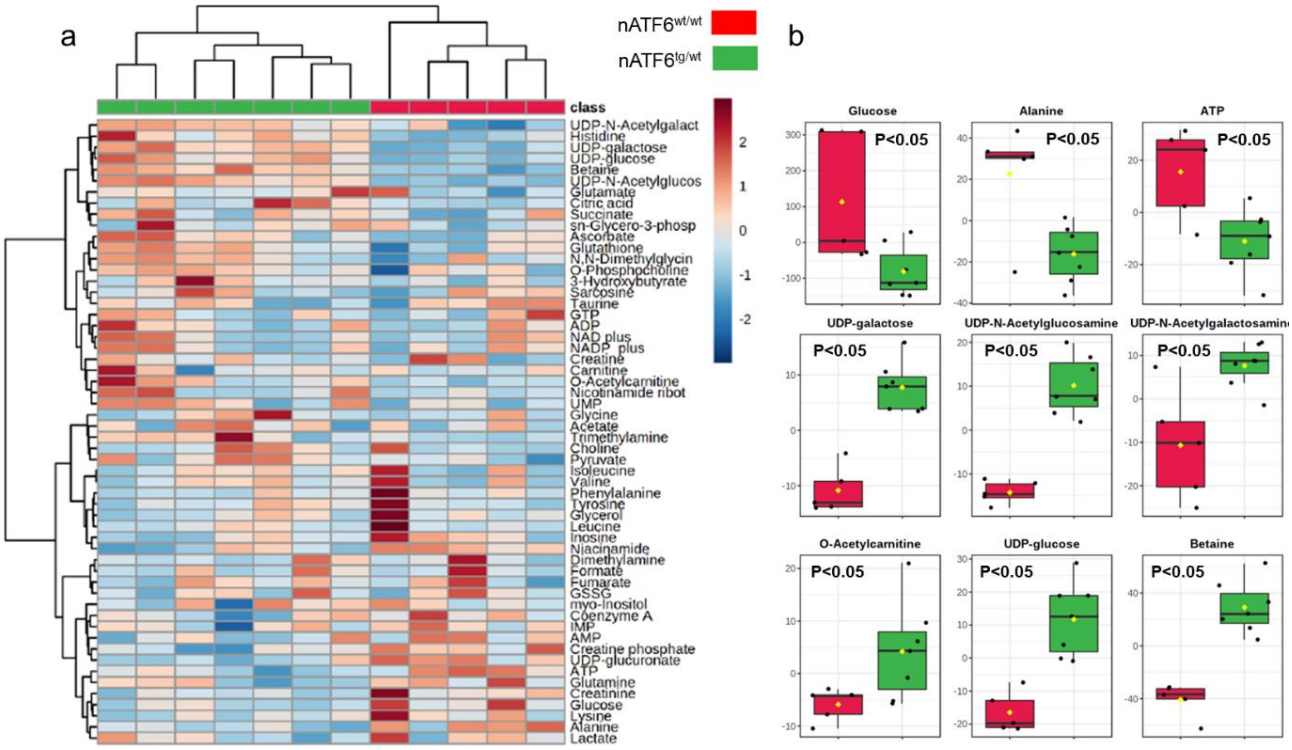

Figure 33: Hepatic nATF6 expression alters glucose and amino acid metabolism in mice. a). The unsupervised cluster of NMR-based metabolic data from nATF6$^{wt/wt}$ (n=5) and nATF6$^{tg/wt}$ (n=7) mice at 3-month age showed in a heatmap. **b).** The bar graph shows the significantly changed metabolites in nATF6$^{wt/wt}$ (n=5) and nATF6$^{tg/wt}$ (n=7) mice at 3-month age. All data are shown as mean ± SEM. All data were analyzed by unpaired T-test. p values are indicated in the graph.

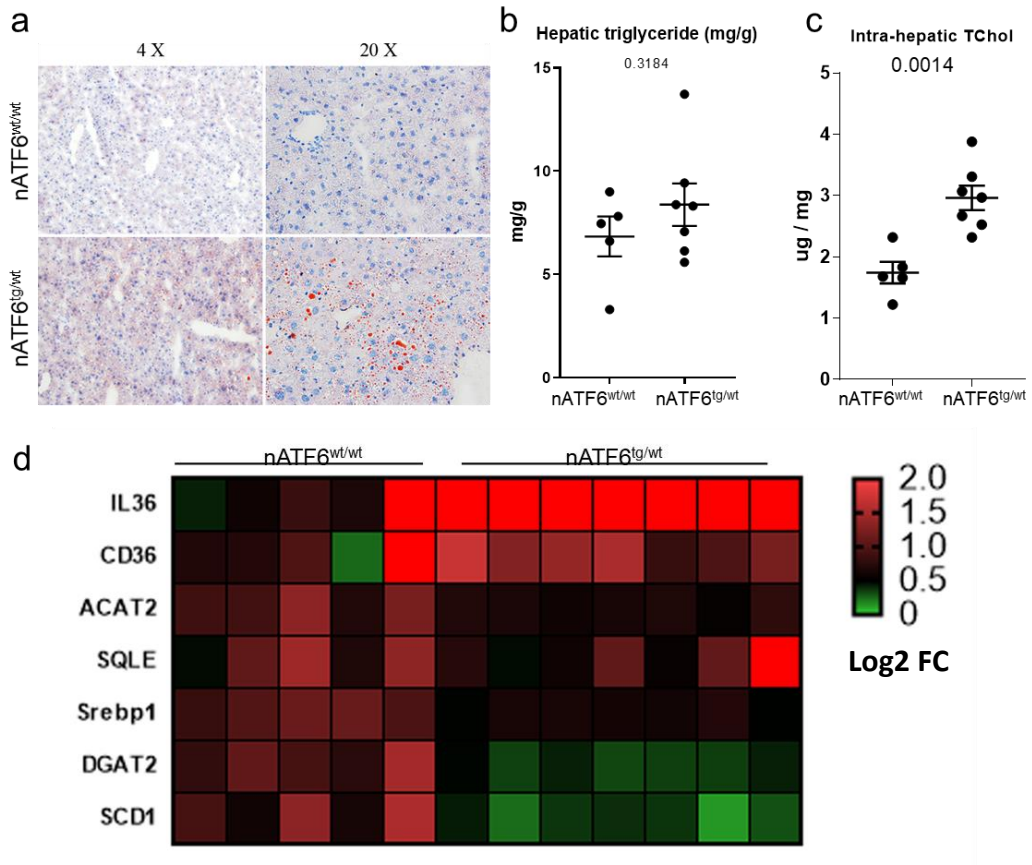

Figure 34: Hepatic nATF6 expression alters cholesterol metabolism in mouse liver. a). Histological Sudan-red staining of liver sections from nATF6$^{wt/wt}$ and nATF6$^{tg/wt}$ mice at 3-month age. **b).** Graphs show intrahepatic triglyceride and cholesterol concentrations in livers of nATF6$^{wt/wt}$ and nATF6$^{tg/wt}$ mice at 3-month age. **c).** A heatmap shows the expression of lipid metabolism-related genes in livers of nATF6$^{wt/wt}$ and nATF6$^{tg/wt}$ mice at 3-month age. All data are shown as mean ± SEM. All data were analyzed by unpaired T-test. p values are indicated in the graph.

For a better characterization of ATF6 activation-induced changes in lipid metabolism, I performed LC-MS-based lipidomic analyses. Surprisingly, I also found ether lipids O-Phosphatidylcholine (O-PC) and O-Posphatidylethanolamine (O-PE) are overrepresented in the experimental condition (Figure 35a and 35b). The transcriptome and proteomics data indicate that the fatty acid metabolism and cholesterol metabolism are attenuated in nATF6$^{tg/wt}$ mice liver. To further confirm this finding, I put nATF6$^{wt/wt}$ and nATF6$^{tg/wt}$ mice on a high-fat, high cholesterol diet - western diet (WD) (Figure 35c). Strikingly, the WD treatment accelerated hepatic tumorigenesis in nATF6$^{tg/wt}$ mice, as visible tumors already exist in livers of nATF6$^{tg/wt}$ mice at 6-month age (Figure 35d - 35h).

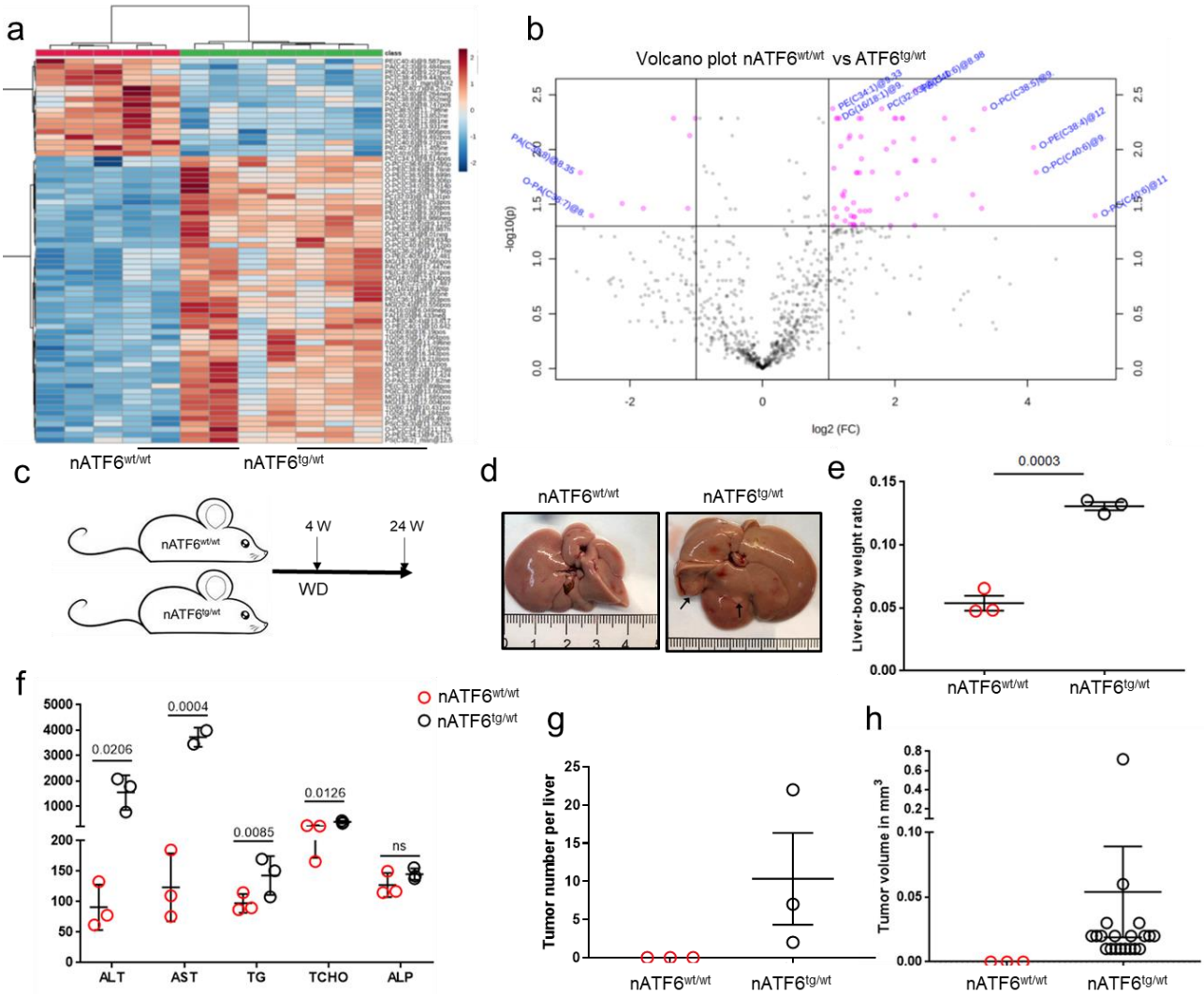

Figure 35: Hepatic nATF6 expression remodels lipid metabolism in mouse liver. a). A heatmap shows significantly changed lipid components in nATF6$^{wt/wt}$ (n=5) and nATF6$^{tg/wt}$ (n=7) mice liver. **b).** Volcano-plot shows significantly changed lipid components in nATF6$^{wt/wt}$ (n=5) and nATF6$^{tg/wt}$ (n=7) mice liver. **c).** A schematic representation shows the experimental strategy. **d).** Representative liver pictures from nATF6$^{wt/wt}$ (n=3) and nATF6$^{tg/wt}$ (n=3) mice fed the western diet for 20 weeks. Tumors are indicated with black arrows. **e).** Liver to body weight ratio of nATF6$^{wt/wt}$ and nATF6$^{tg/wt}$ mice in **d**. **f).** Serology parameters of mice in **d**. **g).** Hepatic tumor numbers and **h).** Hepatic tumor volumes of mice in **d**. All data are shown as mean ± SEM. All data were analyzed by unpaired T-test. p values are indicated in the graph.

7.5.3 Persistent ATF6 activation in hepatocytes changes hepatic bile acids metabolism and induces a cholestatic liver phenotype in nATF6$^{tg/wt}$ mice

Given that the hepatocyte is the primary site for bile acid secretion and bile acid act as the end product of cholesterol metabolism in the liver, I analyzed the bile acid components in livers and in serum of nATF6$^{tg/wt}$ mice by mass spectrometry. Interestingly, the bile acid concentration and the

bile acid composition have been massively changed upon ATF6 activation in the liver and the serum of nATF6$^{tg/wt}$ mice (Figure 36 and Figure 37).

The difference in bile acid composition could be affected by two factors. The first one is ATF6 activation in hepatocytes remodels bile acid metabolism as I have proposed. Indeed, the transcriptome and proteome data indicate activation of the ATF6 branch of UPR significantly affects bile acid metabolism. The second factor would be ATF6 activation in the liver remodels bacteria composition in the gut, given that secondary bile acids are products of bacterial modification in the colon. To test this hypothesis, I collected the feces content in mouse cecum and performed a 16s rRNA gene sequencing to illustrate the microbiota profile. However, no significant difference in microbiota components between nATF6$^{wt/wt}$ and nATF6$^{tg/wt}$ mice has been detected (Figure 38). Thus, I confirmed that the re-modulation of bile acid metabolism is directly caused by ATF6 activation in hepatocytes but not affected by the gut microbiota.

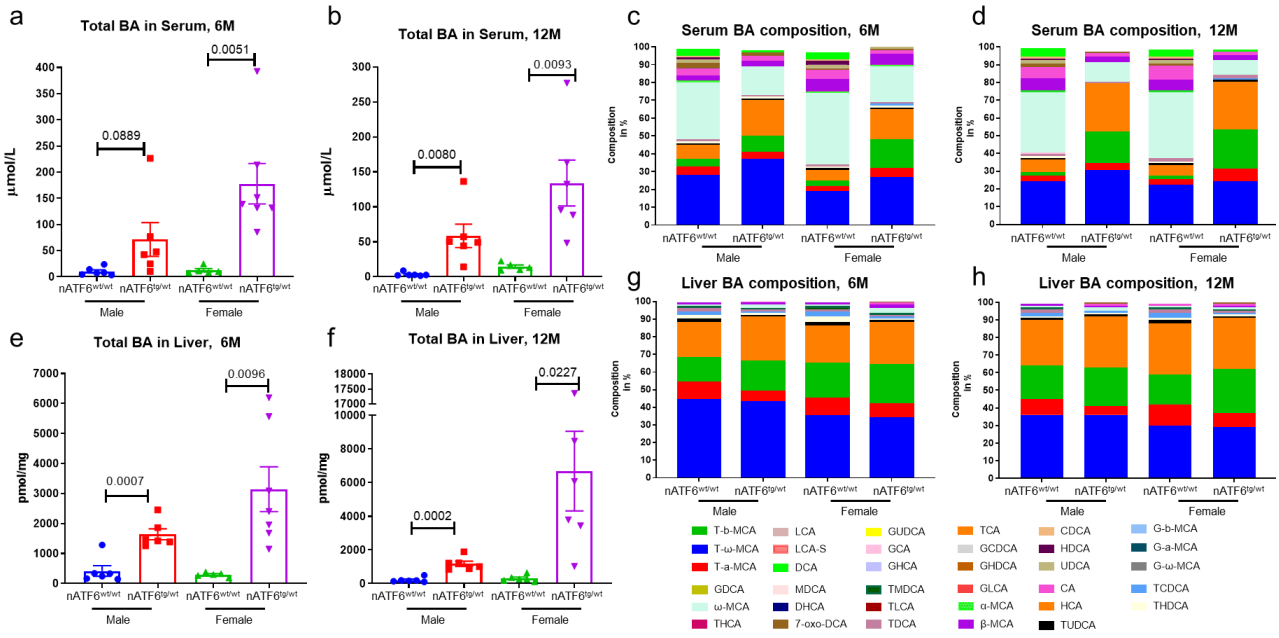

Figure 36: nATF6 expression in hepatocytes changes bile acids metabolism in mouse liver. a). Bile acid concentration in the serum of 6-month old nATF6$^{wt/wt}$ and nATF6$^{tg/wt}$ mice. **b).** Bile acid concentration in the serum of 12-month old nATF6$^{wt/wt}$ and nATF6$^{tg/wt}$ mice. **c).** Bile acid composition in the serum of 6-month old nATF6$^{wt/wt}$ and nATF6$^{tg/wt}$ mice. **d).** Bile acid composition in the serum of 12-month old nATF6$^{wt/wt}$ and nATF6$^{tg/wt}$ mice. **e).** Bile acid concentration in the liver of 6-month old nATF6$^{wt/wt}$ and nATF6$^{tg/wt}$ mice. **f).** Bile acid concentration in the liver of 12-month old nATF6$^{wt/wt}$ and nATF6$^{tg/wt}$ mice. **g).** Bile acid composition in the liver of 6-month old nATF6$^{wt/wt}$ and nATF6$^{tg/wt}$ mice. **h).** Bile acid composition in the liver of 12-month old nATF6$^{wt/wt}$ and nATF6$^{tg/wt}$ mice. All data are shown as mean ± SEM. All data were analyzed by unpaired T-test. p values are indicated in the graph.

Interestingly, bile acid concentrations in both the serum and the livers show a gender disparity upon ATF6 activation. As shown in Figure 36, bile acid is more concentrated in serum and livers of female nATF6$^{tg/wt}$ mice compared to their male counterparts. This is in line with what I have mentioned in the previous section - the female nATF6$^{tg/wt}$ mice show a severe cystic liver phenotype.

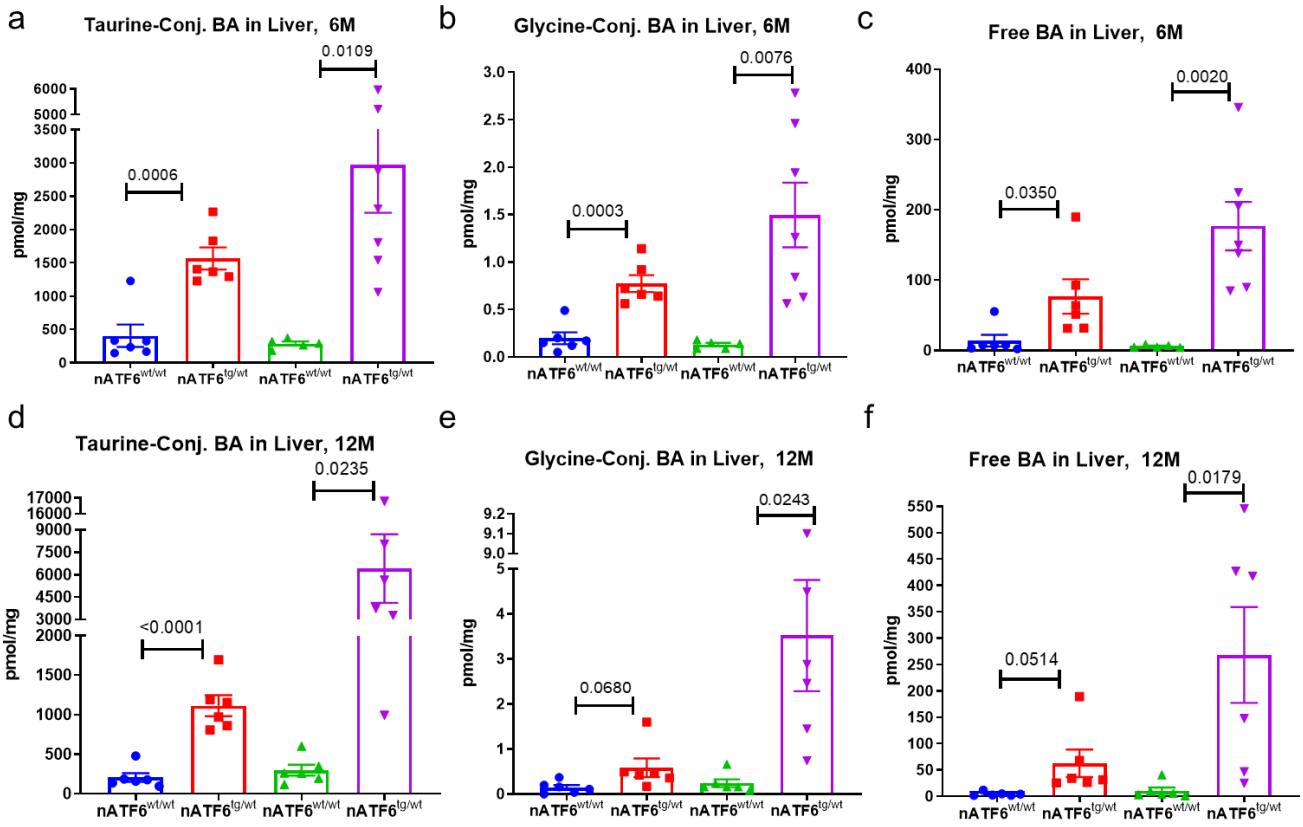

Figure 37: nATF6 expression in hepatocytes changes bile acids components in mouse liver. a). Taurine-conjugated bile acids in livers of 6-month old nATF6$^{wt/wt}$ and nATF6$^{tg/wt}$ mice. **b).** Glycine-conjugated bile acids in livers of 6-month old nATF6$^{wt/wt}$ and nATF6$^{tg/wt}$ mice. **c).** Free bile acids in livers of 6-month old nATF6$^{wt/wt}$ and nATF6$^{tg/wt}$ mice. **d).** Taurine-conjugated bile acids in livers of 6-month old nATF6$^{wt/wt}$ and nATF6$^{tg/wt}$ mice. **e).** Glycine-conjugated bile acids in livers of 6-month old nATF6$^{wt/wt}$ and nATF6$^{tg/wt}$ mice. **f).** Free bile acids in livers of 6-month old nATF6$^{wt/wt}$ and nATF6$^{tg/wt}$ mice. All data are shown as mean ± SEM. All data were analyzed by unpaired T-test. p values are indicated in the graph.

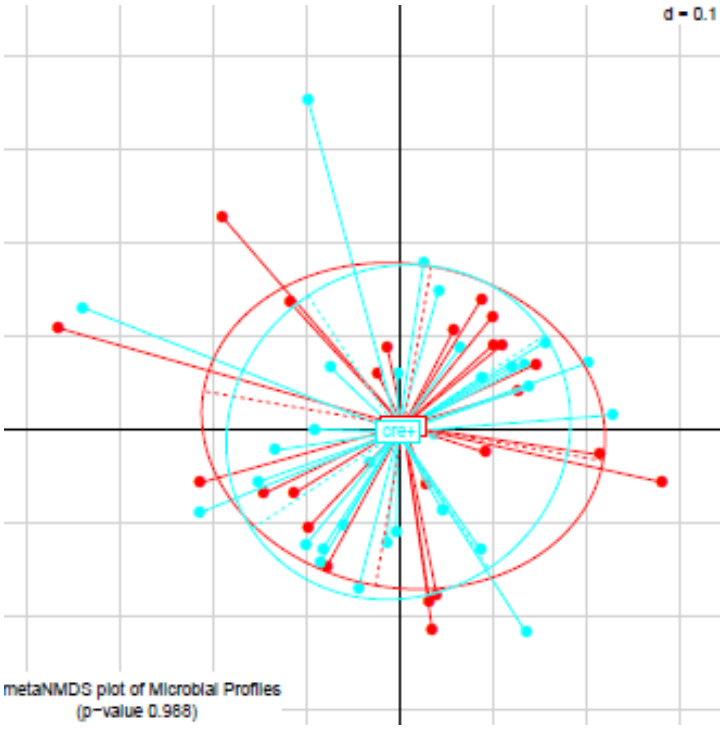

Figure 38: ATF6 activation in the liver does not affect microbiota composition in the gut. 16s rRNA gene sequencing of the caecal content from nATF6$^{wt/wt}$ mice and nATF6$^{tg/wt}$ mice, indicating no difference in microbiota components in nATF6$^{wt/wt}$ and nATF6$^{tg/wt}$ mice. p value is indicated in the graph.

7.5.4 The metabolic reprogramming in livers of nATF6$^{tg/wt}$ mice is a direct consequence of ATF6 activation

To figure out whether the metabolic reprogramming in livers of nATF6$^{tg/wt}$ mice is a consequence of cellular activation of the ATF6 branch of UPR or a result of the altered hepatic microenvironment. I generated nATF6-overexpression cells and ATF6 knockout cells from FL83B mouse hepatocyte cell line.

Further studies using NMR-based metabolic analyses in nATF6-overexpression cells have shown that activation of nATF6 shifts cellular metabolism towards aerobic glycolysis, as the metabolic end product, lactic acid, was accumulated in nATF6-overexpression cells (Figure 39a - 39b). However, the knockout of ATF6 in FL83B cells shows the opposite trend (Figure 40a - 40b). Interestingly, in line with the in-vivo study, activation of the ATF6 arm of UPR leads to the accumulation of UDP-species which are vital for protein glycosylation. Moreover, overexpression of nATF6 results in accumulated serine, alanine, and succinate in FL83B cells, whereas the knockout of ATF6 reverses these phenotypes (Figure 39b and Figure 40b).

Taken together, I concluded that the metabolic reprogramming in livers of nATF6$^{tg/wt}$ mice is a direct consequence of ATF6 activation.

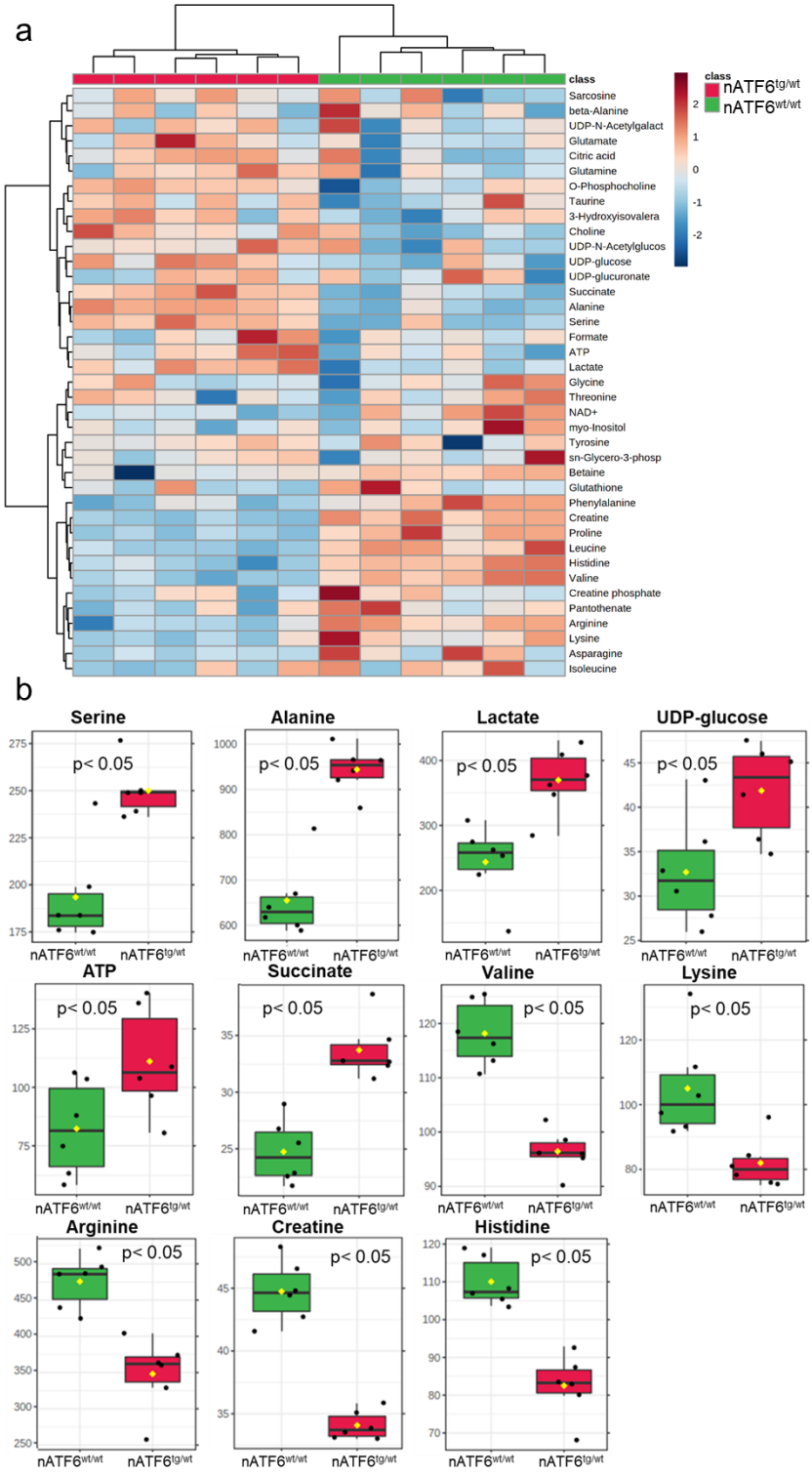

Figure 39: nATF6 expression shifts cellular metabolism towards aerobic glycolysis in vitro. a). The unsupervised cluster of NMR-based metabolic data from the control (n=6) and nATF6 overexpression (n=6) FL83B cells showed in a heatmap. **b).** Bar graphs show the significantly changed metabolites in the control (n=6) and nATF6 overexpression (n=6) FL83B cells. All data are shown as mean ± SEM. All data were analyzed by unpaired T-test. p values are indicated in the graph.

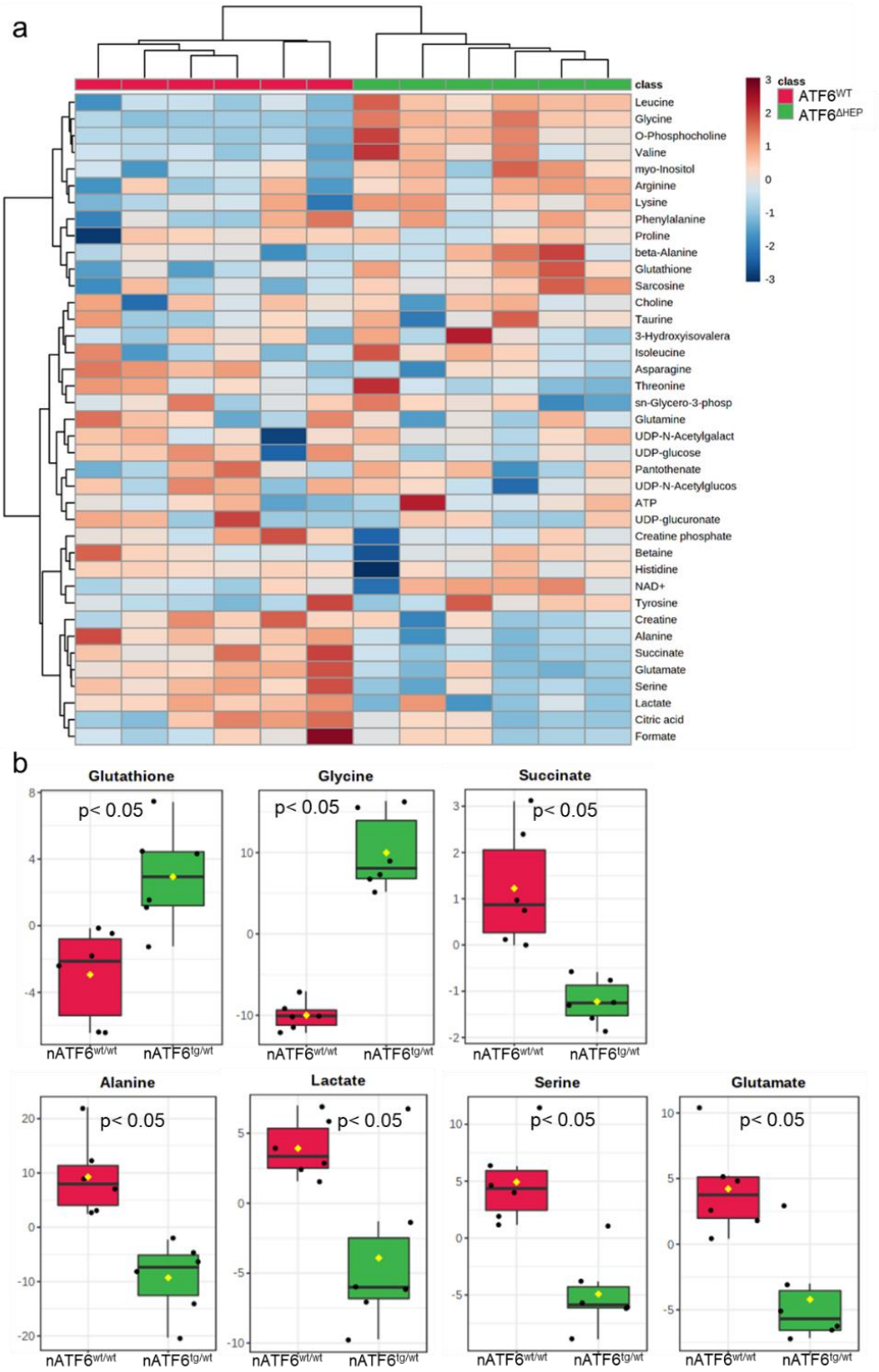

Figure 40: ATF6 knockout prevents aerobic glycolysis in vitro. a). The unsupervised cluster of NMR-based metabolic data from the control (n=6) and ATF6 knockout (n=6) FL83B cells showed in a heatmap. **b).** The bar graph shows the significantly changed metabolites in the control (n=6) and ATF6 knockout (n=6) FL83B cells. All data are shown as mean ± SEM. All data were analyzed by unpaired T-test. p values are indicated in the graph.

7.6 Liver-specific ATF6 activation contributes to the immunosuppressive liver microenvironment

7.6.1 Persistent ATF6 activation generates an inflammatory hepatic microenvironment

In hepatic nATF6-overexpression mice, I saw apparent liver damage and cell death, which has often been linked to hepatic inflammation due to the release of DAMPs. IHC staining of innate and adaptive immune cells confirms that persistent activation of nATF6 in mice liver induces chronic inflammation, characterized by noticeable accumulation of immune cells (Figure 41e). Further studies quantitatively confirmed my findings by fluorescence-activated cell sorting (FACS) analyses (Figure 41a - 41d). Interestingly, among these changed immune cells, the alteration in iNKT (Invariant natural killer T) cells represents the most striking change in livers of nATF6$^{tg/wt}$ mice.

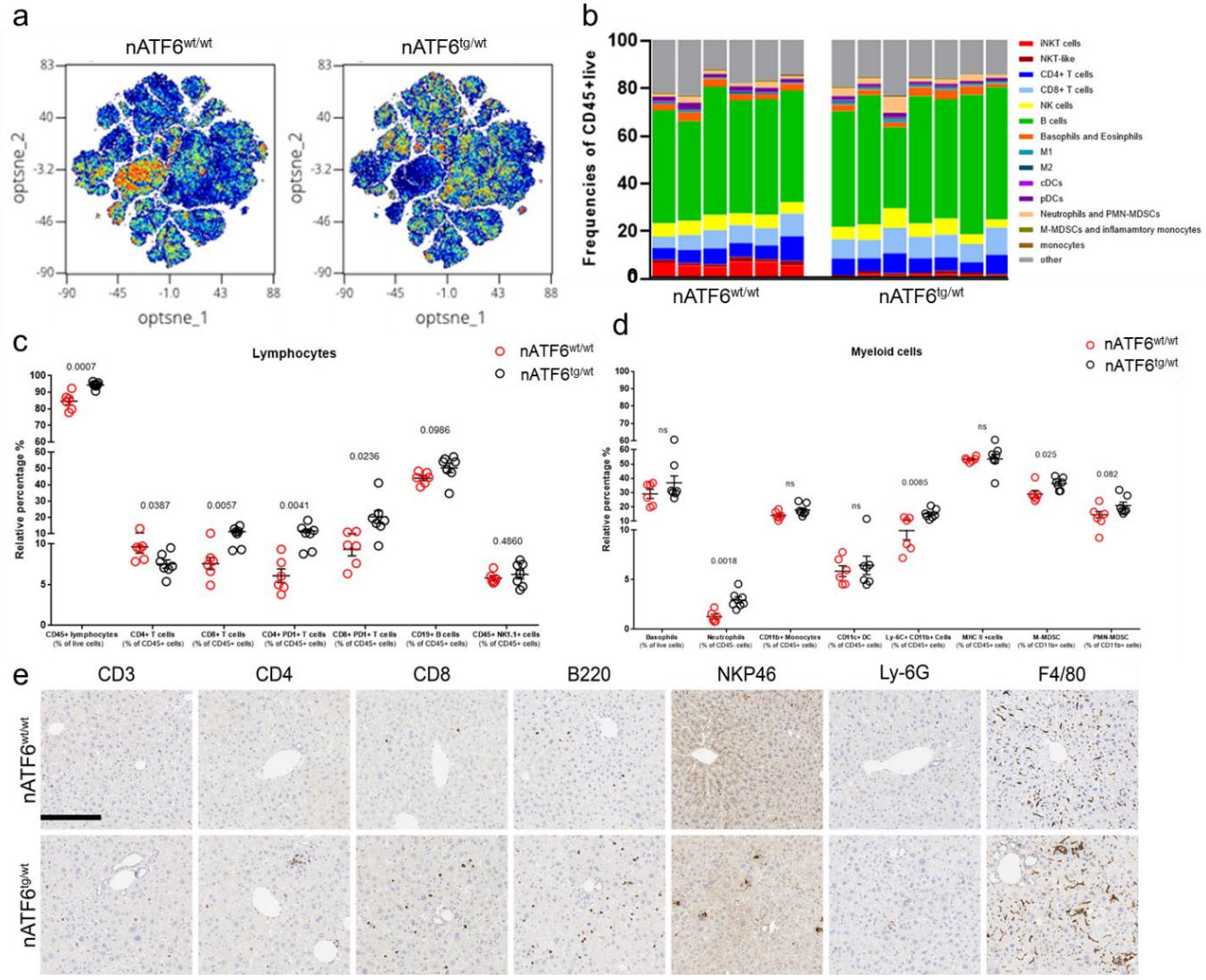

Figure 41: ATF6 activation in mouse liver induces hepatic immune cells activation and inflammation. a). TSNE representation of immune-cell populations in livers of 6-month old nATF6$^{wt/wt}$ and nATF6$^{tg/wt}$ mice. **b).** Bar graphs show the immune-cell composition in livers of 6-month old nATF6$^{wt/wt}$ and nATF6$^{tg/wt}$ mice. **c)** - **d).** FACS analysis shows the indicated immune-cell percentages in livers of 6-month old nATF6$^{wt/wt}$ and nATF6$^{tg/wt}$ mice. **e).** IHC staining of indicated molecules shows different immune-cell populations in livers of 6-month old nATF6$^{wt/wt}$ and nATF6$^{tg/wt}$ mice. All data are shown as mean ± SEM. All data were analyzed by unpaired T-test. p values are indicated in the graph.

7.6.2 The adaptive immune response, but not the innate immune response, is important for the anti-tumor immunosurveillance in livers of nATF6$^{tg/wt}$ mice

In the previous section, I have detected obvious signs of activation of innate and adaptive immune responses, both of which are key players in the immunosurveillance of tumorigenesis. To further understand their roles in nATF6-mediated tumorigenesis, I designed strategies to block these two immune responses in livers of nATF6$^{tg/wt}$ mice.

My previous data suggest that activation of the innate immune response is not decisively involved in the anti-tumor immunosurveillance in livers of nATF6$^{tg/wt}$ mice (data not shown). Thus I focused on the role of the adaptive immune response. I crossed R26-LSL-nATF6 x Alb-Cre mice with Rag1 whole-body knockout mice (Rag1$^{-/-}$) to generate mice that have heterozygous nATF6 expression in the hepatocytes under the R26 locus, but the whole body lacks mature T and B cells (nATF6$^{tg/wt}$Rag1$^{-/-}$). As shown in Figure 43, the CD3 positive T cells have been largely depleted in this mouse model harboring defects in the adaptive immune response. I dissected the first group of nATF6$^{tg/wt}$Rag1$^{-/-}$ mice and their controls nATF6$^{tg/wt}$Rag1$^{+/+}$ when they reach 9 months time point (Figure 42a). Both the nATF6$^{tg/wt}$Rag1$^{-/-}$ mice and their controls (nATF6$^{tg/wt}$Rag1$^{+/+}$ mice) developed liver cancer at 9-month age, but the tumor burden in nATF6$^{tg/wt}$Rag1$^{-/-}$ mice is much more severe compared to their control counterparts (Figure 42e - 42f). Strikingly, when summarizing the overall survival rate in nATF6$^{tg/wt}$Rag1$^{-/-}$ and nATF6$^{tg/wt}$Rag1$^{+/+}$ mice, I found the whole-body knockout of Rag1 significantly reduces the lifespan of nATF6$^{tg/wt}$ mice. Around half of the nATF6$^{tg/wt}$Rag1$^{-/-}$ mice reached the termination criteria at around 8-month age (Figure 42b), which occurs much earlier compared to nATF6$^{tg/wt}$ mice who need approximately 12 months to reach the termination criteria (Figure 42b). More importantly, I found many of the nATF6$^{tg/wt}$Rag1$^{-/-}$ mice have already had visible tumors in their livers at 6-month age (Figure 42c), whereas in nATF6$^{tg/wt}$Rag1$^{+/+}$ mice, no tumor can be detected under the microscope at the same age (Figure 18a). These data strongly suggest that the adaptive immune response is of vital importance for anti-tumor immunosurveillance in livers of nATF6$^{tg/wt}$ mice. By IHC staining, I can identify that tumors induced by ATF6 activation in the Rag1 knockout background show typical HCC characters (Figure 43).

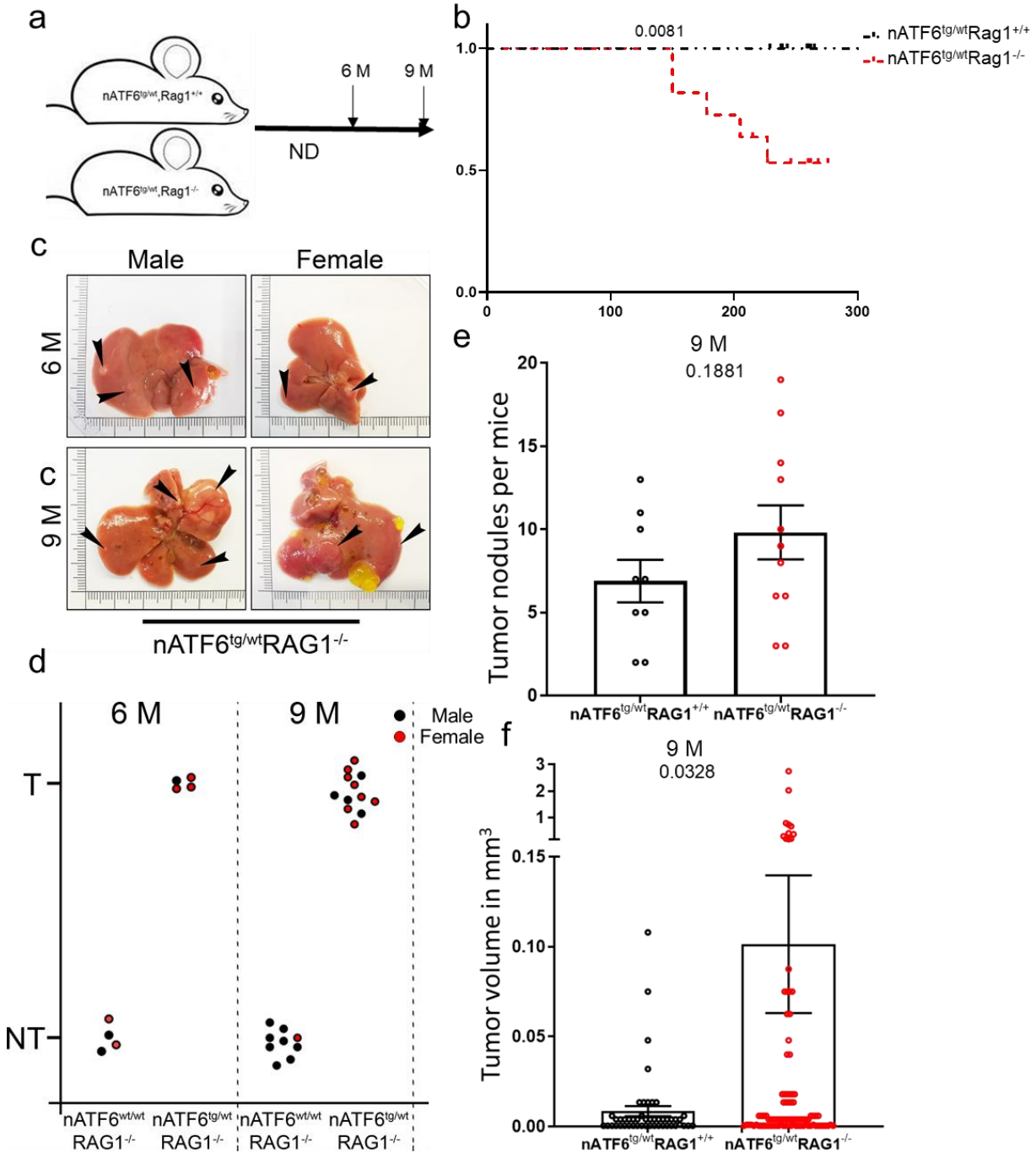

Figure 42: The adaptive immune response is vital for anti-tumor immunosurveillance in ATF6 activation-induced liver cancer. a). A schematic representation shows the experimental strategy. **b).** Survival curve of nATF6$^{tg/wt}$Rag1$^{+/+}$ mice and the nATF6$^{tg/wt}$Rag1$^{-/-}$ mice. **c).** Representative liver pictures from indicated mice groups at 6-month and 9-month age. Black arrows indicate tumors. **d).** Tumor incidence of nATF6$^{tg/wt}$Rag1$^{+/+}$ mice and the nATF6$^{tg/wt}$Rag1$^{-/-}$ mice at different ages. **e).** Hepatic tumor numbers and **f).** Hepatic tumor volumes in 9-month old nATF6$^{tg/wt}$Rag1$^{+/+}$ mice and nATF6$^{tg/wt}$Rag1$^{-/-}$ mice. All data are shown as mean ± SEM. All data were analyzed by unpaired T-test. p values are indicated in the graph.

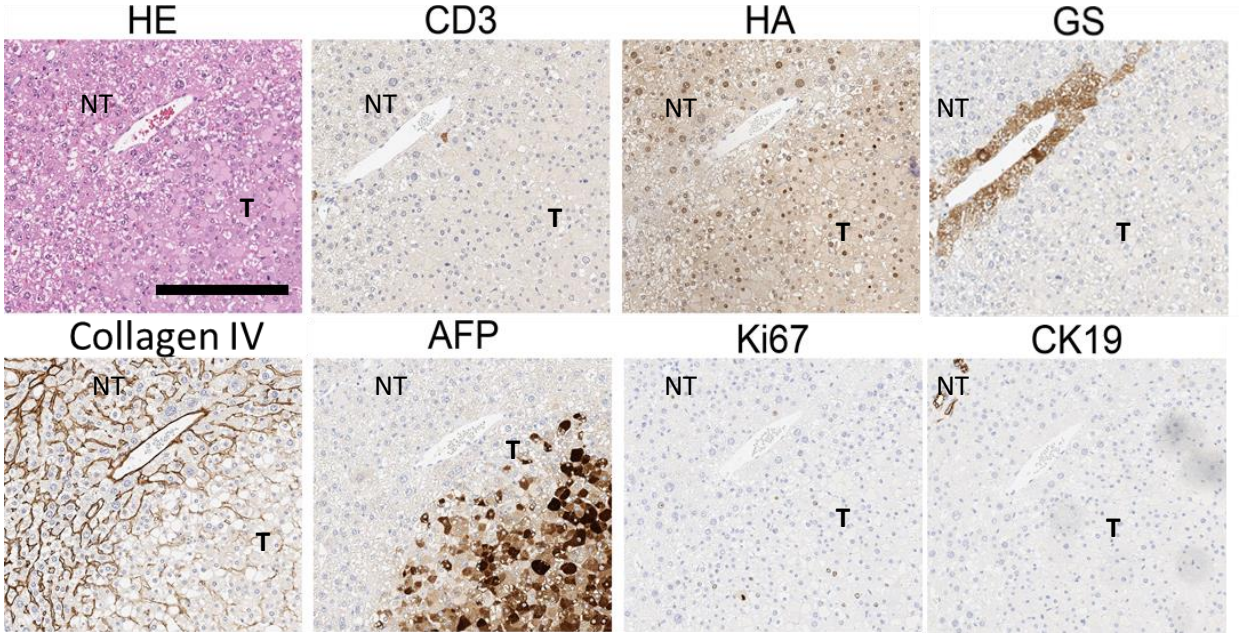

Figure 43: Histological characterization of ATF6 activation-induced liver cancer in nATF6$^{tg/wt}$Rag1$^{-/-}$ mice. IHC staining of indicated molecules in tumor sections from nATF6$^{tg/wt}$Rag1$^{-/-}$ mice. HE staining shows the tumoral and non-tumoral area; CD3 staining indicates the successful removal of mature T cells in nATF6$^{tg/wt}$Rag1$^{-/-}$ mice; HA staining indicates cells with overexpressed nATF6; Collagen IV shows the disrupted collagen in the extracellular matrix; AFP staining as a biomarker for HCC; Ki67 staining shows the proliferating cells.

7.6.3 Co-existence of pro-inflammatory and immunosuppressive mechanisms in nATF6$^{tg/wt}$ mice liver

Flow cytometry analyses showed that T lymphocytes isolated from livers of nATF6$^{tg/wt}$ mice livers are more potent to secrete cytokines (e.g. TNF, and IFNγ) upon activation (Figure 44a). Indicating a pro-inflammatory phenotype of these cells in the inflammatory microenvironment. To better understand the mechanisms of how tumor cells escape the immunosurveillance mediated by adaptive immune cells, I performed histological staining of PD-1 and PDL1 in liver sections from nATF6$^{tg/wt}$ mice.

Interestingly, IHC staining shows an increased proportion of PD-1 positive cells (Figure 44c), including a large proportion of T lymphocytes as represented by further flow cytometry analyses (Figure 41c). Indicating that T cells in livers of nATF6$^{tg/wt}$ mice undergo exhaustion and activation processes simultaneously. Immunofluorescence staining further shows the colocalization of PD-1 positive cells with CD8 positive cells, corroborating the exhaustion of cytotoxic T lymphocytes - the main force to execute anti-tumor immunosurveillance (Figure 44b).

Additionally, with the histological staining of PDL1 - the key molecule mediating T cell apoptosis through PD1-PDL1 interaction, I observed the expression of PDL1 is significantly enhanced in

livers of nATF6$^{tg/wt}$ mice compared to control animals(Figure 44d - 44e). Interestingly, the expression of PDL1 seems not only restricted in myeloid cells as customarily suggested, I also identified PDL1 signaling in hepatocytes in livers of nATF6$^{tg/wt}$ mice (Figure 44d). This means a potential role of the ATF6 arm of UPR to regulate PDL1 expression in hepatic parenchymal cells.

With these data, I concluded that in livers of nATF6$^{tg/wt}$ mice, the pro-inflammatory immune response and the pro-tumorigenic immunosuppressive microenvironment exist simultaneously.

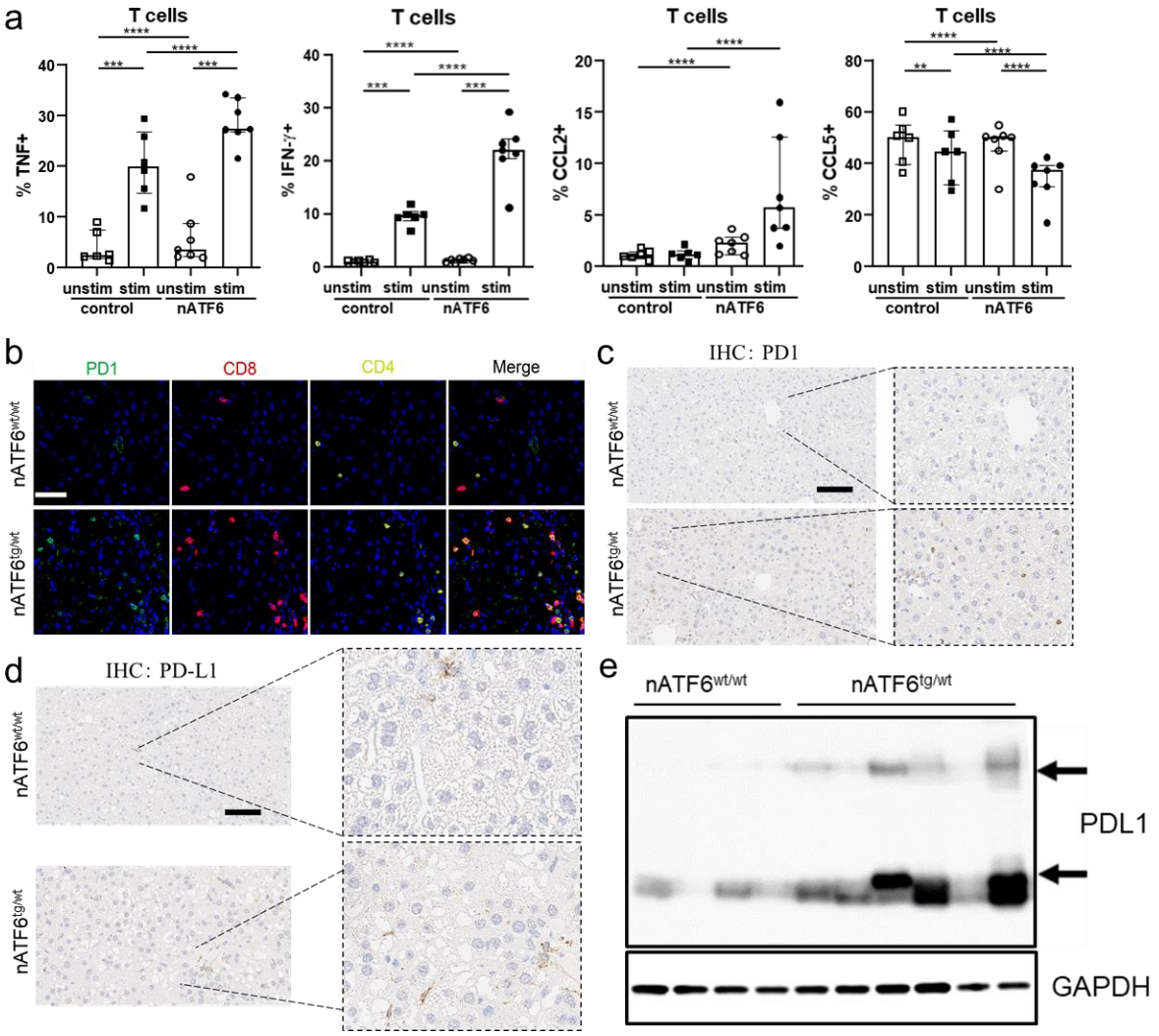

Figure 44: Co-existence of the inflammatory and immunosuppressive mechanisms in livers of nATF6$^{tg/wt}$ mice. a). Bar graphs show the indicated cytokine secretion by T cells isolated from livers of 6-month old nATF6$^{wt/wt}$ and nATF6$^{tg/wt}$ mice with or without stimulation. **b).** Immunofluorescence staining of indicated molecules in liver sections from 6-month old nATF6$^{wt/wt}$ and nATF6$^{tg/wt}$ mice. **c).** IHC staining of PD1 in liver sections from 6-month old nATF6$^{wt/wt}$ and nATF6$^{tg/wt}$ mice. **d).** IHC staining of PDL1 in liver sections from 6-month old nATF6$^{wt/wt}$ and nATF6$^{tg/wt}$ mice. **e).** Western blot analysis of PDL1 in liver homogenate from 6-month old nATF6$^{wt/wt}$ and nATF6$^{tg/wt}$ mice. All data are shown as mean ± SEM. All data were analyzed by unpaired T-test. *p<0.05;**p<0.01; ***p<0.001; ****p<0.0001.

7.7 BECs contribute to ATF6-mediated tumorigenesis in the liver of nATF6$^{tg/wt}$ mice

7.7.1 Persistent ATF6 activation in hepatocytes induces expansion of BECs in the liver of nATF6$^{tg/wt}$ mice

Besides the hepatomegaly liver phenotype, nATF6$^{tg/wt}$ mice also show yellowish serum, indicating a potential biliary disease in these animals; this hypothesis is further supported by the ALP levels in serum of nATF6$^{tg/wt}$ mice (Figure 19).

Indeed, through histological staining of cytokeratin-19 (CK-19), which serves as a marker for the hepatic biliary cells, I could identify a pronounced expansion of the biliary cells/progenitor cells around the portal area (Figure 45). This phenotype (hyperproliferation of biliary cells) is termed ductular reaction and is commonly found in the injured liver. Strikingly, with IHC staining of CD44v6, A6, p-STAT3, and GP73, I could identify biliary epithelial cells (BECs) with high expression of these molecules (Figure 45 and Figure 46), which could be essential for their expansion and the malignant transformation of the hepatocytes.

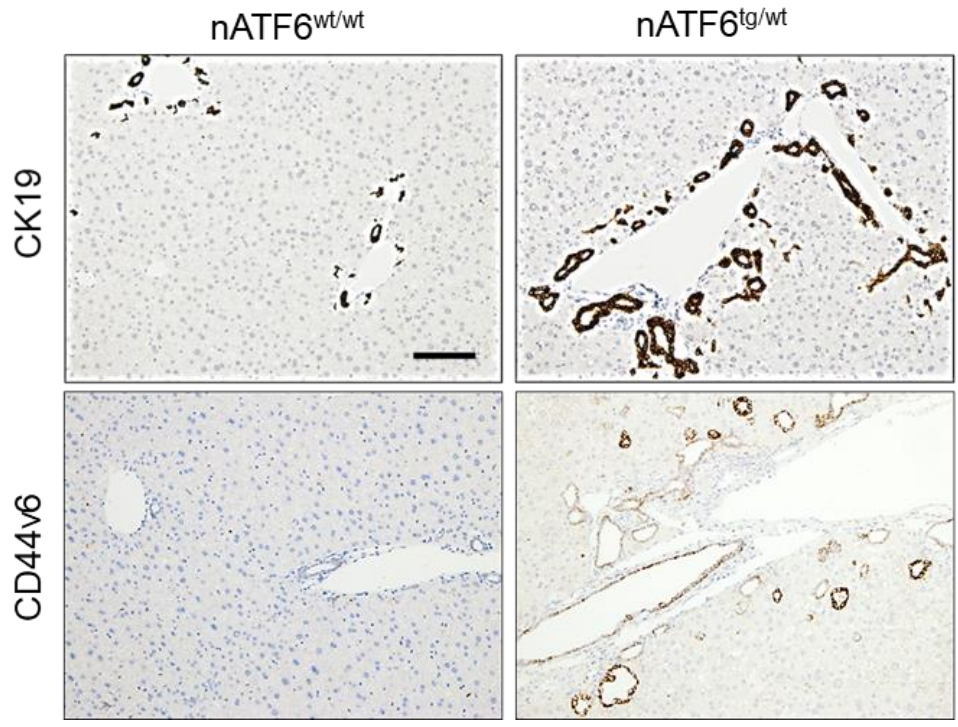

Figure 45: Persistent ATF6 activation in hepatocytes induces expansion of BECs. IHC staining of CK19 and CD44v6 in liver sections from 3-month old nATF6$^{wt/wt}$ and nATF6$^{tg/wt}$ mice.

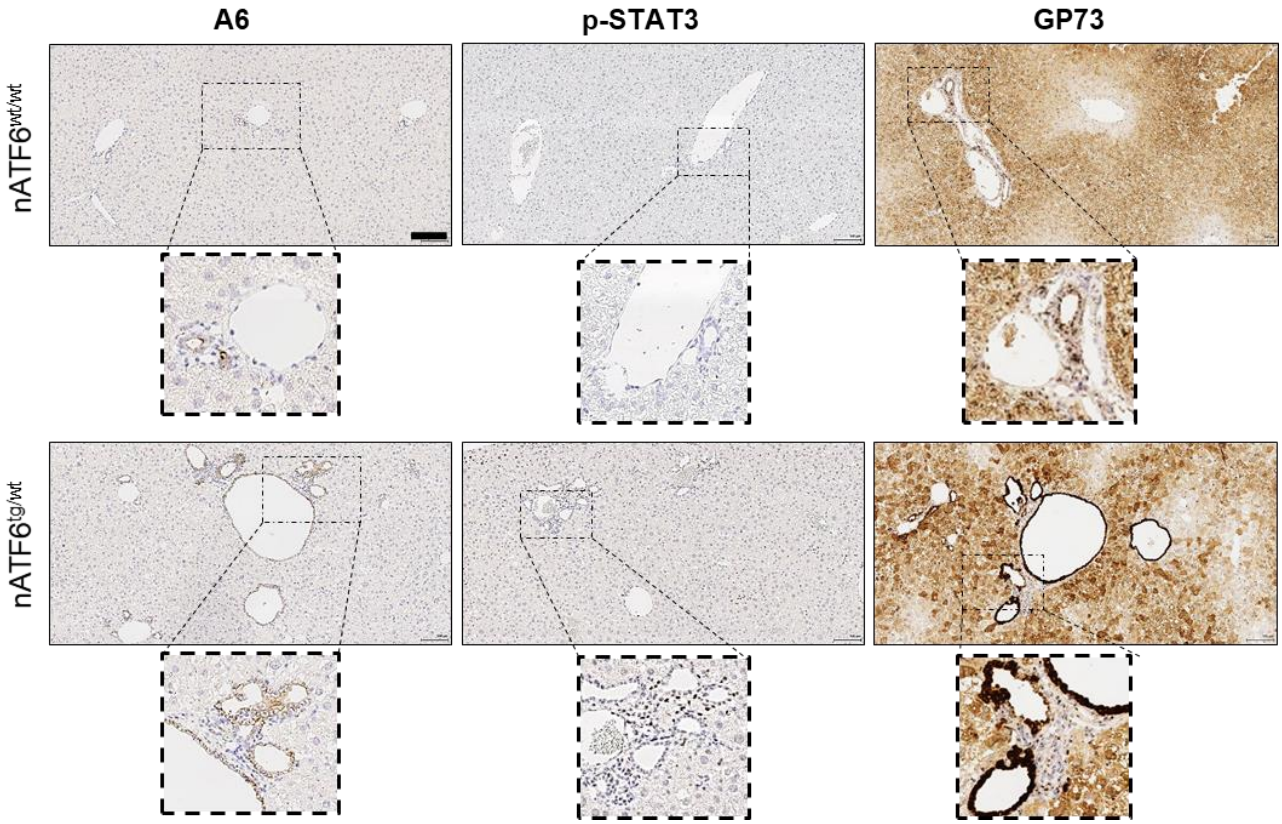

Figure 46: Hyperactive phenotype of BECs in livers of nATF6$^{tg/wt}$ mice. IHC staining of indicated molecules in liver sections from 3-month old nATF6$^{wt/wt}$ and nATF6$^{tg/wt}$ mice. A6 staining indicates the progenitor-like BECs, p-STAT3 positive cells and GP73 positive cells are mainly BECs.

7.7.2 Secretion of SPP1 by BECs in the liver of nATF6$^{tg/wt}$ mice

After seeing the hepatomegaly and liver damage phenotype in nATF6$^{tg/wt}$ mice at a young age (3 months), I performed cytokine and chemokine profiles to illustrate which cytokines or chemokines were changed significantly in livers of nATF6$^{tg/wt}$ mice. Strikingly, among the cytokines and chemokines, I found the expression of a batch of candidates, including SPP1, ICAM-1, VCAM-1, IGFBP-1, CCL5, IL-33, and others, have changed significantly upon ATF6 activation (Figure 47a).

Further, I checked the relationship between the upregulated cytokines and hepatic tumorigenesis from already published works. The molecule SPP1 (also known as Osteopontin, H19/20 in the cytokine array) drew my attention. SPP1 has been shown in many cases linked with hepatic pathogenesis. As the first step, I want to understand which cell types in the liver secretes SPP1. By employing IHC staining of SPP1, I could identify that SPP1 is expressed mainly by the BECs upon ATF6 activation. At the same time, other non-parenchymal cells also represent a small amount of SPP1 secretion (Figure 47b).

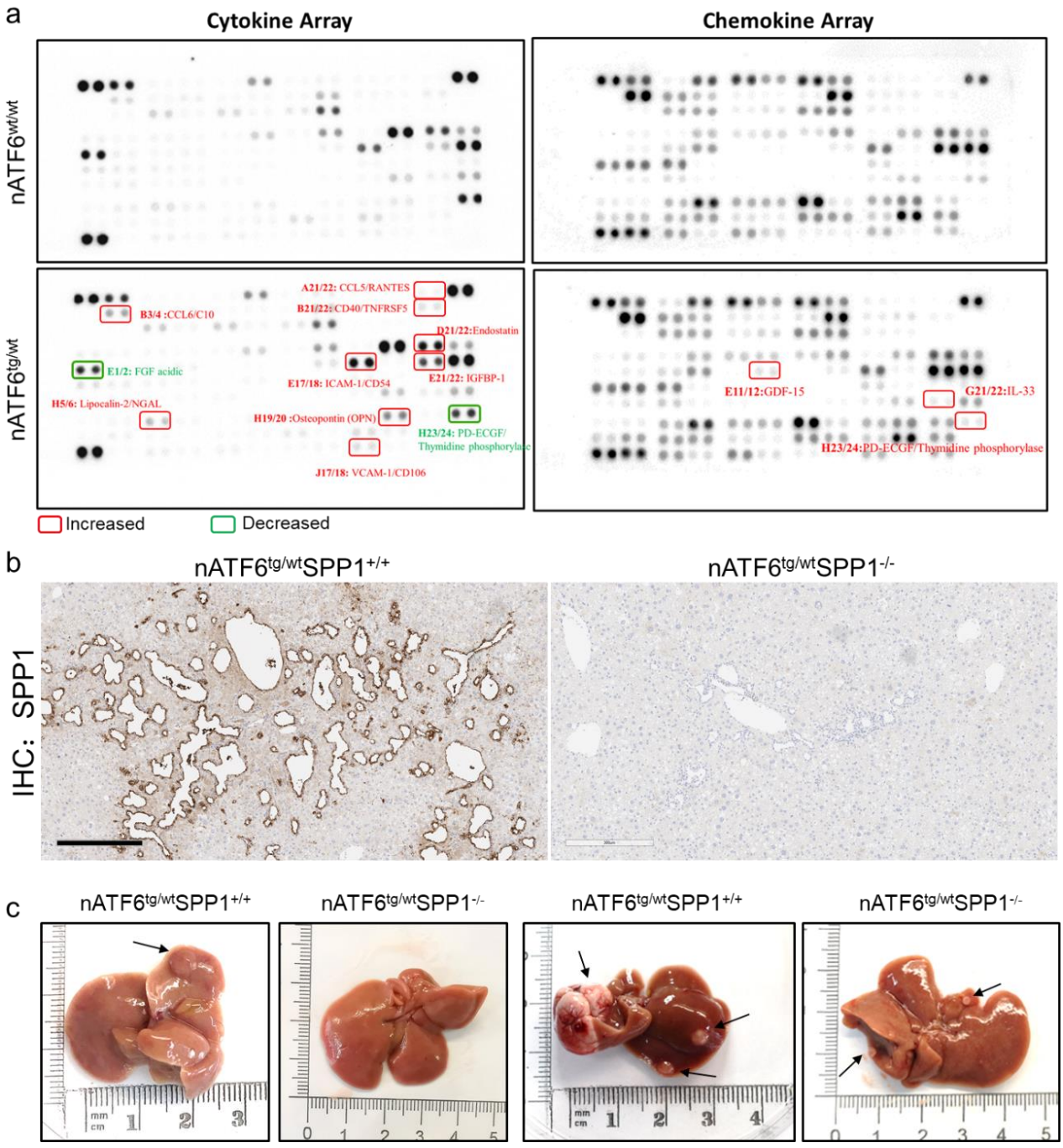

Figure 47: BECs derived SPP1 contributes to hepatic tumorigenesis in nATF6$^{tg/wt}$ mice. a). Elisa-based cytokine array and chemokine array analyses of liver homogenate from 3-month old nATF6$^{wt/wt}$ and nATF6$^{tg/wt}$ mice. **b).** IHC staining of SPP1 in liver sections from 9-month old nATF6$^{tg/wt}$SPP1$^{+/+}$ and nATF6$^{tg/wt}$SPP1$^{-/-}$ mice. **c).** Representative liver pictures from indicated mice group at 8-month (left panel) and 9-month (right panel) age. Black arrows indicate tumors.

7.7.3 BECs derived SPP1 contributes to ATF6-mediated tumorigenesis in mouse liver

To validate whether elevated secretion of SPP1 in livers of nATF6$^{tg/wt}$ mice is crucial for ATF6 activation-mediated hepatic tumorigenesis or not, I crossed R26-LSL-nATF6 x Alb-Cre mice with

SPP1 whole-body knockout mice (SPP1$^{-/-}$ mice). Thus, mice with heterozygous nATF6 expression in hepatocytes under the R26 locus, while the whole body lacks SPP1 expression (nATF6$^{tg/wt}$SPP1$^{-/-}$ mice) were generated. As shown in Figure 47b, the SPP1 expression has been completely abolished in nATF6$^{tg/wt}$SPP1$^{-/-}$ mice, suggesting a successful removal of SPP1 by cross the R26-LSL-nATF6 x Alb-Cre mice with SPP1$^{-/-}$ mice.

I dissected the first group of nATF6$^{tg/wt}$SPP1$^{-/-}$ mice and their controls nATF6$^{tg/wt}$SPP1$^{+/+}$ when they reach 9-month age. Both nATF6$^{tg/wt}$SPP1$^{-/-}$ mice and their controls (nATF6$^{tg/wt}$SPP1$^{+/+}$ mice) developed liver cancer at 9 months. However, the tumor burden in nATF6$^{tg/wt}$SPP1$^{-/-}$ mice seems to be reduced compared to their control counterparts (Figure 47c).

7.8 Hepatic ATF6 deletion ameliorates the tumor burden of mice in different models

7.8.1 Generation and validation of hepatocyte-specific ATF6 knockout mice

In previous sections, I have detailed the phenotypes and related mechanisms in hepatocyte-specific nATF6-activation mice. To further confirm the protumorigenic effect of the ATF6 arm of UPR, which I observed in the transgenic mice, I generated hepatocyte-specific ATF6 knockout mice (ATF6$^{\Delta Hep}$ mice) by crossing ATF6$^{flox/flox}$ mice with Alb-Cre mice (Figure 48).

The ATF6$^{flox/flox}$ mice with loxP sites bordering the exons 8-9 of ATF6 gene, when bred ATF6$^{flox/flox}$ mice with Alb-Cre mice, the Cre mediated recombination results in a depletion of the fragment from exon 8 to exon 9 in ATF6 gene (Figure 48a). The homozygosity of floxed ATF6 gene and the presence of Alb-Cre were determined using PCR analysis (Figure 48b). The ATF6$^{\Delta Hep}$ mice grow normally and do not show any apparent phenotypes by themselves without challenge (data not shown).

7.8.2 Knockout of ATF6 protects mice from chemical carcinogen-induced liver cancer

In previous sections of my thesis, I have discussed my data suggesting that ATF6 activation plays a vital role in tumorigenesis and lipid metabolism, particularly cholesterol metabolism. To address whether loss of ATF6 would exert beneficial functions, I employed a well-established NASH and DEN (N-nitrosodiethylamine)-induced HCC model. According to the literature[129], DEN plus HFD mediates HCC formation by inducing oxidative stress. I injected ATF6$^{\Delta Hep}$ mice and ATF6^{wt} mice with 25 mg/kg (body weight) DEN at the age of 14 days. 4 weeks after DEN injection, the animals were treated with WD for 26 weeks (Figure 49a). The ATF6$^{\Delta Hep}$ mice and ATF6^{wt} mice did not show a difference in animal body weight during the whole period of diet feeding (data not shown).

I dissected the animals when they were 32 weeks old. Surprisingly, I found all the ATF6^{wt} mice developed visible liver cancer, while in ATF6$^{\Delta Hep}$ mice, no tumor or only small spots could be found in the liver (Figure 49b).

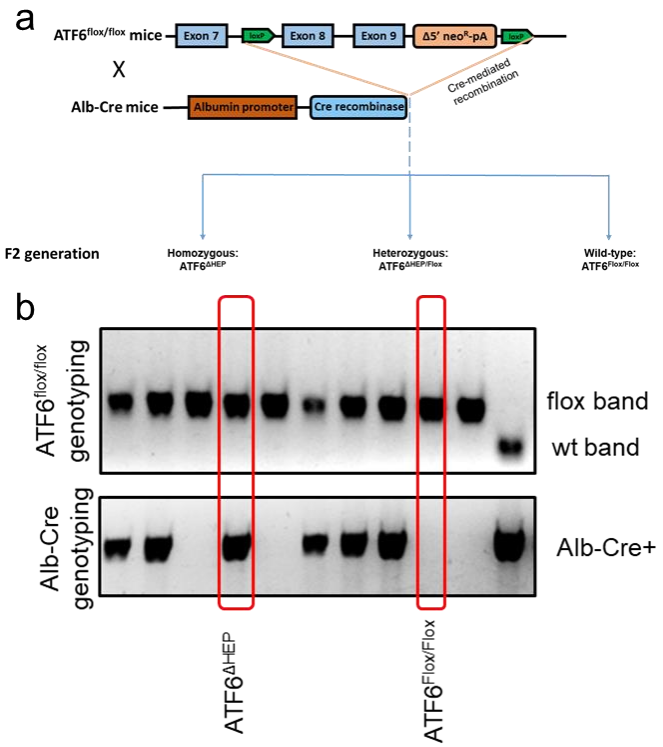

Figure 48: Generation of hepatocyte-specific ATF6 knockout mouse model. a). A schematic representation shows the generation of hepatocyte-specific ATF6 knockout mice. **b).** Representative genotyping results of ATF6$^{Flox/Flox}$ x Alb-Cre mice. PCR tested the floxed ATF6 gene and Albumin-Cre transgene in each mouse.

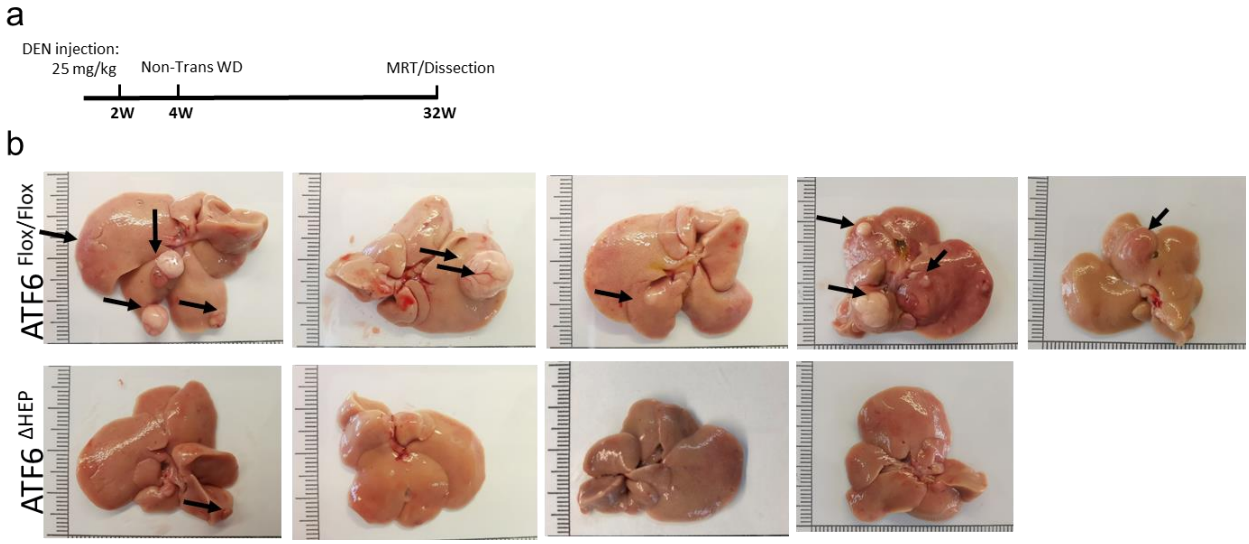

Figure 49: ATF6 knockout protects mice from NASH and chemical carcinogen-induced HCC. a). A schematic representation shows the experimental strategy. **b).** Representative liver pictures from indicated mice groups treated with DEN and western diet as explained in **a**. Black arrows indicate tumors.

7.8.3 Knockout of ATF6 conditionally protects mice from oncogene activation-induced liver cancer

To validate whether the protective effect of ATF6 knockout is only restricted in DEN/NASH-induced liver cancer or not. I used hydrodynamic tail vein injection for delivery of oncogene-containing plasmids. Specifically, I used the plasmids combination of Kras overexpression plus p53 knockdown (Kras/p53). 12-week old ATF6$^{\Delta Hep}$ mice and ATF6^{wt} mice were hydrodynamically injected with Kras/p53 plasmids. Interestingly, the ATF6 knockout mice showed a prolonged survival upon Kras/p53 plasmids injection, indicating a protective role of ATF6 knockout (Figure 50a). Moreover, when I dissected a group of mice 6 weeks after plasmids injection, I found that the tumor burden in ATF6$^{\Delta Hep}$ mice is significantly lower compared to ATF6^{wt} mice (Figure 50b – 50f).

To sum up, by employing animal models mentioned above, I concluded that ATF6 knockout could be beneficial for mice under oncogenic challenges.

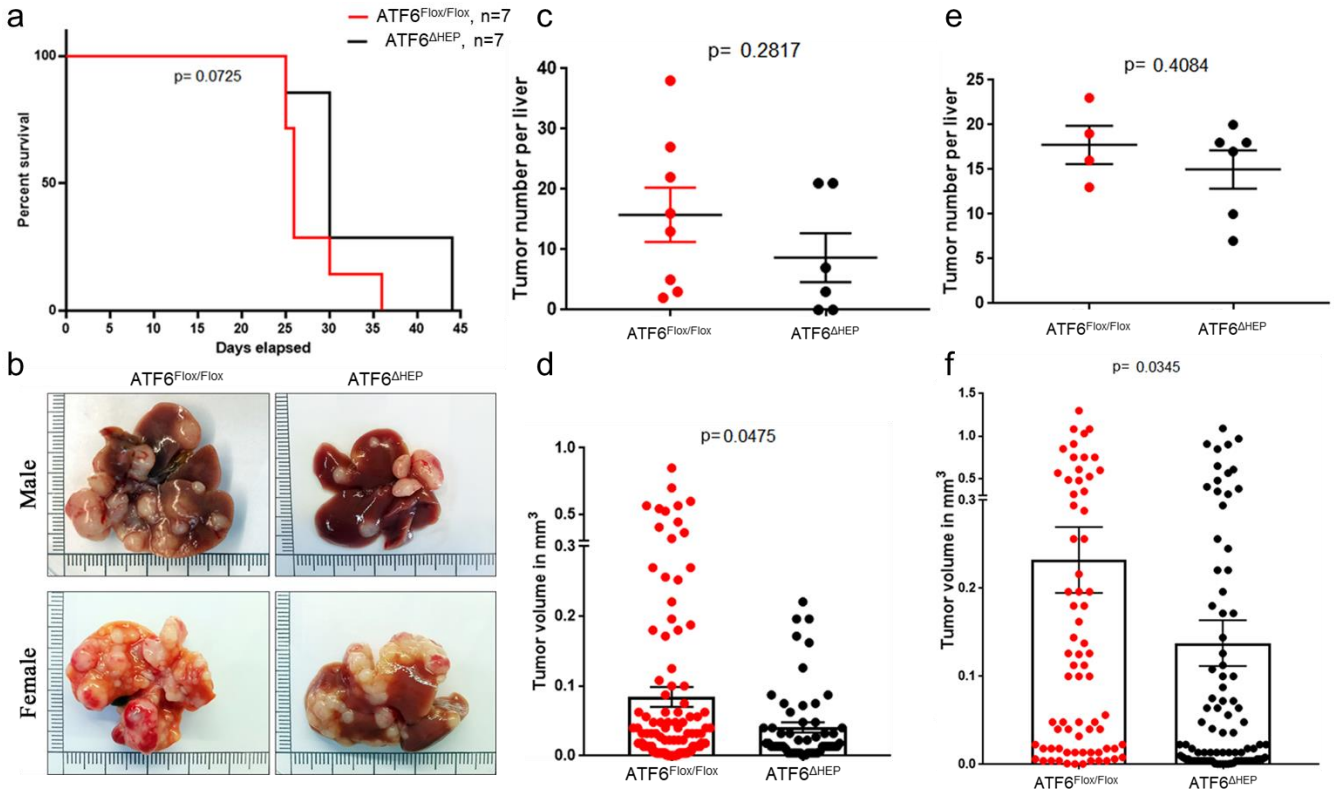

Figure 50: ATF6 knockout protects mice from oncogene-induced HCC. a). Survival curve of indicated mice groups treated with HDTVi (Kras/p53). **b).** Representative liver pictures in **a**. **c).** Hepatic tumor numbers and **d).** Hepatic tumor volumes of male ATF6$^{Flox/Flox}$ and ATF6$^{\Delta HEP}$ mice treated with HDTVi (Kras/p53). **e).** Hepatic tumor numbers and **f).** Hepatic tumor volumes of female ATF6$^{Flox/Flox}$ and ATF6$^{\Delta HEP}$ mice treated with HDTVi (Kras/p53). All data are shown as mean ± SEM. All data were analyzed by unpaired T-test. p-Value indicated in the graph.

8 Discussion

Being the primary site for lipid and glucose metabolism, hepatocytes are abundant in the amount of ER and other organelles (e.g. mitochondria) to fulfill their metabolic functions. In the face of various disturbances, which lead to ER stress and dysregulation of liver metabolic functions, such as inflammation, hyperglycemia, viral infection, and excessive nutrition, hepatocytes initiate an evolutionarily conserved pathway – the adaptive UPR – to maintain its homeostasis and to preserve essential functions of the liver.

However, unsolved ER stress, characterized by chronic and persistent stress or acute and substantial stress, overwhelms the adaptive UPR and switches the response to “terminal UPR”, which induces apoptosis[130] and concomitant adverse pathophysiologies - including inflammation, regenerative processes and metabolic dysfunction. Given this context-dependent feature of the UPR, the role of ER stress in liver pathophysiology varies – also depending on the time frame of the insults. When talking about ER stress or the UPR in the context of liver cancer, it is necessary to discuss their functions in tumorigenesis and tumor development separately. Here, I should highlight three emerging perspectives of the UPR relevant to tumor biology.

- First, as tumors often arise and establish in stressful surroundings, the activation of UPR may already exist in the host cell prior to its malignant transformation.
- Second, the quality or the type of UPR may differ in premalignant cells and transformed cells. For example, cells affected by the inflammatory microenvironment may employ the UPR to restore their physiological functions and maintain survival. However, malignant cells or tumor cells often hijack the UPR to fulfill its high demands in protein, nutrition, or other building blocks for colony expansion.
- Third, the extent of ER stress burden or the type of UPR activation also shows the spatiotemporal difference.

Indeed, in my mouse model with sustained activation of nATF6 in hepatocytes, the long-lasting and unsolved stress leads to cell death in hepatocytes, which I believe is the starting point of liver inflammation. Given the regenerative nature of the liver, dying hepatocytes will soon be replaced by ‘newly generated’ hepatocytes differentiated from hepatic progenitor cells, evidenced by Ki67 staining and ductular reaction in livers of nATF6$^{tg/wt}$ mice. Interestingly, nATF6$^{tg/wt}$ mice are protected from acute stress-induced liver damage (data not shown), whereas in the long-term and upon chronic stress, these animals developed liver cancer. Indicating that the quality of UPR in ‘aged’ hepatocytes and ‘newly generated’ hepatocytes in nATF6$^{tg/wt}$ mice is very likely to be

different. Probably the UPR in 'newly generated' hepatocytes is more to the adaptive direction, and it switches to "the terminal UPR" as the stress can not be resolved. This is especially the case in situations where the chronic insult (e.g. high caloric diet; chronic virus infection) is not interrupted. The diversity in quality of the UPR originates not only from different "ages" of hepatocytes but also reveals a spatial difference. The latter is mainly induced by hepatic vascular distribution, which entitles hepatocytes from different Zones with distinct levels of stimuli and oxygen supply[15]. Indeed, hepatocytes around the central vein are challenged more often by molecules from the digestive tracts than their counterparts in the portal triads.

Except for the pro-survival effects of the UPR in tumor cells and the pro-inflammatory effects of the UPR in pre-malignant cells, ER stress is barely linked directly to liver cancer. In my opinion, it should not be misinterpreted that the UPR can initiate and drive the malignant transformation of normal cells on its own. Usually, ER stress leverages UPR-related mechanisms, like ROS production, oncogenic signaling activation, or metabolic remodeling to participate in the pro-tumorigenic process. In my study, the protumorigenic effect of persistent ATF6 activation is mediated or partially contributed by ROS production. Anti-ROS BHA diet can limit the level of liver damage in nATF6$^{tg/wt}$ mice dramatically regardless of the animals' age. When talking about oxidative stress, it is worth mentioning NRF2, the master regulator of cellular redox status. Same as ATF6, the role of NRF2 in tumorigenesis is also under debate. Karin et al. hold the opinion that activation of NRF2 turns on oncogenic signalings and thus is protumorigenic[131], whereas others see it differently. We have tried to either knockout NRF2 or activate NRF2 in nATF6$^{tg/wt}$ mice. The knockout of NRF2 in nATF6$^{tg/wt}$ mice is not affordable as even a heterozygous knockout of NRF2 in the presence of nATF6 transgene is lethal to the animals. Whereas mild activation of NRF2 by cross CMVcaNrf2 mice with nATF6$^{tg/wt}$ mice is feasible, we have seen a reduced tumor burden in the mouse liver (data not shown); indicating that in nATF6$^{tg/wt}$ mice, the hepatic tumorigenesis is indeed a consequence of ROS generation.

The neoplastic transformation of the liver has never been the sole responsibility of hepatocytes. Other cell types, such as KCs and hepatic infiltrating immune cells, are also intensively involved. It is commonly accepted that liver cancer arises exclusively as a result of underlying chronic inflammation[12]. Hepatic immune cells are the leading force in anti-tumor immunosurveillance in the liver. Meanwhile, they also act as the primary perpetrator in generating pro-tumorigenic inflammatory microenvironment. In the context of NASH-induced HCC, the adaptive immune cells (T and B cells) are key mediators for NASH-induced liver cancer, given that Rag1$^{-/-}$ mice are protected from NASH-diet induced HCC[72]. Unlike NASH-induced HCC, the lack of adaptive

immune cells boosts the tumor burden in murine liver cancer model induced by ATF6 activation, indicating that anti-tumor immune-surveillance is still working among the inflammatory hepatic microenvironment in nATF6$^{tg/wt}$ mice. Once we depleted mature T and B cells in nATF6$^{tg/wt}$ mice by crossing them with RAG1$^{-/-}$ mice, the tumor onset occurs when the mice were 6 months old, whereas the earliest tumor found in nATF6$^{tg/wt}$ mice with complete adaptive immune response was at 9 months time point. Similarly, the tumor burden in nATF6$^{tg/wt}$Rag1$^{-/-}$ mice at 9 months is more severe compared to it in nATF6$^{tg/wt}$ mice. The opposite functions of adaptive immune response in NASH-induced HCC and ATF6 activation-mediated HCC might be explained by the different origins of the malignant cells. In NASH-induced HCC, the transformation of hepatocytes is driven by the inflammatory milieu generated by hyperactive immune cells. Not all NASH liver will develop liver cancer as the malignant transformation promoted by the inflammatory surrounding can not always be successful. However, in nATF6$^{tg/wt}$ mice, the oncogenic events occur in every hepatocyte expressing the truncated form of ATF6. At the early stage, the immune system is capable of eliminating pre-malignant cells; however, with the establishment of the inflammatory microenvironment, immune escape occurs and finally results in liver cancer formation. In this scenario, it would be informative to understand the mechanisms of how the immune surveillance in nATF6$^{tg/wt}$ mice fails to eliminate the pre-cancerous cells.

The mechanisms involved in the immune escape of pre-malignant cells include the immunosuppressive microenvironment and the dysfunction of immune cells. By checking these aspects in livers of nATF6$^{tg/wt}$ mice, I found in the first place, the PDL1 expressing cells from the myeloid lineage accumulated in livers of nATF6$^{tg/wt}$ mice. Additionally, immunosuppressive cells, namely MDSCs and M2 macrophages, are found to accumulate in livers of nATF6$^{tg/wt}$ mice. Last but not least, it is exciting to see hepatocytes themselves also express a low amount but detectable PDL1, which means, throughout the liver, more than 70% of the cells are able to suppress the function of T cells. I have not figured out yet whether the function of the immune cells is compromised or not while writing this thesis. I performed a TUNEL assay meant to see the death of hepatocytes. However, more robust signaling in immune cells has been observed compared to dying hepatocytes (data not shown). Thus I hypothesized that ATF6 activation-induced phenotype in hepatocytes also affects the fate and function of other cell types in the liver.

In the next step, I tried to answer how ATF6 activation in hepatocytes affects the function of neighboring cells. I have shown the hyperproliferation of hepatocytes in nATF6$^{tg/wt}$ mice, which requires a huge amount of energy and building blocks. Thus, I hypothesized that hyperproliferation of hepatocytes exhausts nutrition storage in hepatocytes and nutrition supply

for other non-parenchymal cells. To test this, I performed NMR-based metabolic analyses, RNA-seq analyses, and proteomic analyses of livers from nATF6$^{tg/wt}$ mice. I proved that hepatocytes with persistent ATF6 activation shift their metabolic preference towards aerobic glycolysis. Moreover, I also showed in vitro that the metabolic shift is induced by persistent ATF6 activation, but not environmental factors. However, the relationship between nutrient deprivation and immune-cell dysfunction still requires further investigation.

In my study, I could identify that ATF6 activation is involved not only in the regulation of glucose metabolism but also of lipid and amino acids metabolism, indicating a central role of the ATF6 branch of UPR in controlling cellular metabolism. For further studies, given the vast difference in bile acid concentration and components in nATF6$^{wt/wt}$ and nATF6$^{tg/wt}$ mice, the remodeling of cholesterol metabolism by ATF6 is of the highest interest for me. Importantly, I thought that the cholesterol and bile acid metabolism is closely related to the gender disparity phenotype I saw in nATF6$^{wt/wt}$ and nATF6$^{tg/wt}$ mice, revealing the human situation primary biliary cholangitis is mainly founded in females.

In the end, by using a genetically ATF6 knockout mouse model, I proved that knockout of ATF6 confers broad-spectrum protection in different tumor models in mice, indicating the potential clinical application of ATF6 inhibitors. Thus, understanding the molecular mechanisms of how the ATF6 arm of UPR contributes to hepatic tumorigenesis is essential for its therapeutic usage. In addition, it is also worth noting that ATF6 may react to acute and chronic ER stress differently, as other scientists have reported that ATF6 activation protects the host from other types of disease (e.g. ischemia/reperfusion injury)[132].

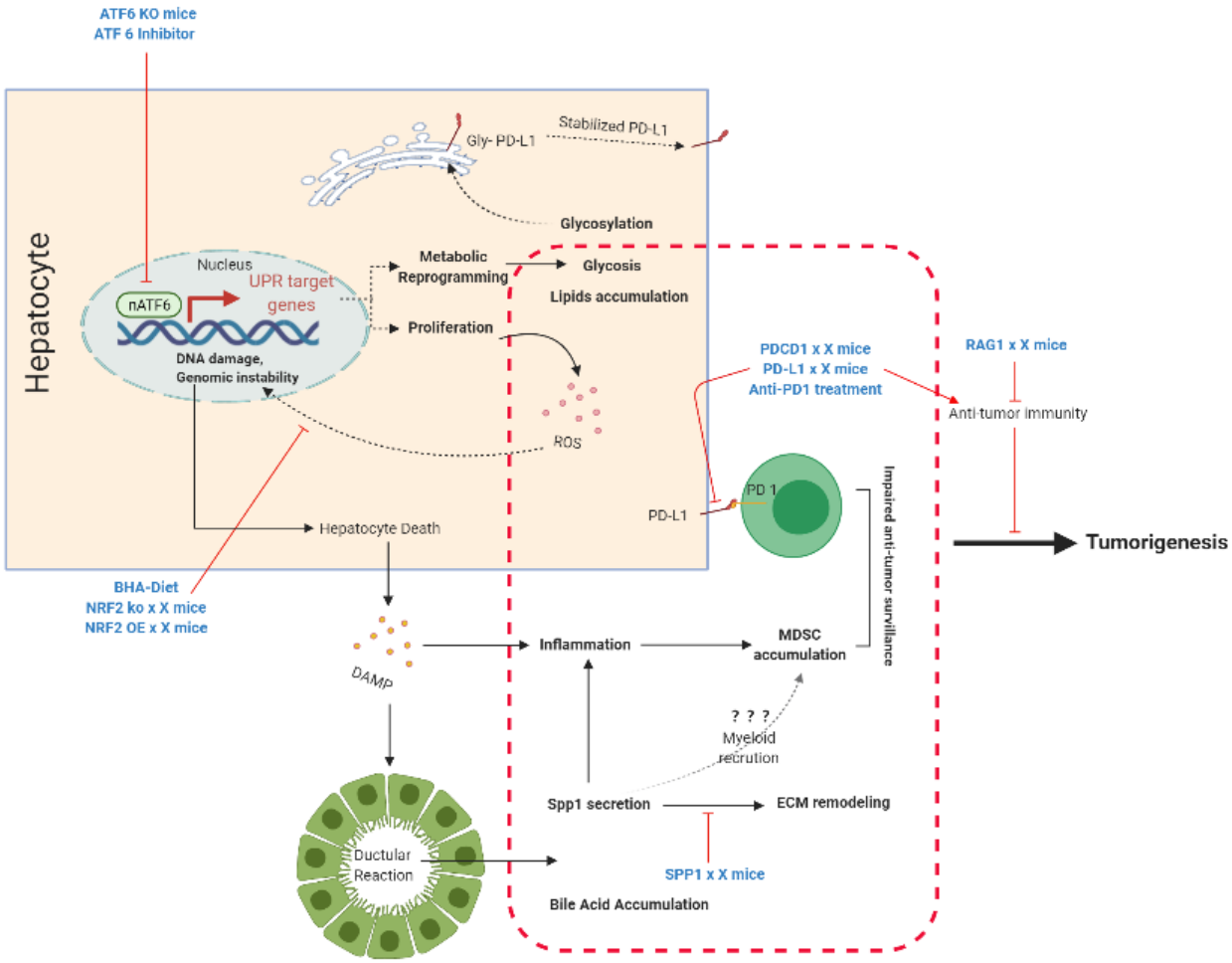

Figure 51: A schematic representation shows biological events involved in ATF6 activation-induced tumorigenesis. In brief, persistent ATF6 activation in hepatocytes induces the expression of UPR target genes which re-modulate the metabolic programs and benefits cell proliferation. Cellular ROS has been generated in this process, causing DNA damage and genomic instability in host cells, leading to cell death in hepatocytes. Dying hepatocytes release DAMPs, which can initiate the immune response and ductular reaction. The inflammatory liver microenvironment and SPP1 secreted by BECs both benefit the tumor onset. Meanwhile, metabolic reprogramming in hepatocytes burns hepatic glucose and suppresses the function of immune cells.

9 References

1 Nakagawa, H. *et al.* ER Stress Cooperates with Hypernutrition to Trigger TNF-Dependent Spontaneous HCC Development. *Cancer Cell* **26**, 331-343 (2014).

2 Lebeaupin, C. *et al.* Endoplasmic reticulum stress signalling and the pathogenesis of non-alcoholic fatty liver disease. *Journal of Hepatology* **69**, 927-947 (2018).

3 Ger, R. Surgical Anatomy of the Liver. *Surgical Clinics of North America* **69**, 179-192 (1989).

4 Mitra, V. & Metcalf, J. Functional anatomy and blood supply of the liver. *Anaesthesia & Intensive Care Medicine* **10**, 332-333 (2009).

5 Sibulesky, L. Normal liver anatomy. *Clinical liver disease* **2**, S1-S3 (2013).

6 Roan, E. The Effect of Glisson's Capsule on the Superficial Elasticity Measurements of the Liver. *Journal of Biomechanical Engineering* **132** (2010).

7 Marrone, G., Shah, V. H. & Gracia-Sancho, J. Sinusoidal communication in liver fibrosis and regeneration. *Journal of Hepatology* **65**, 608-617 (2016).

8 Rui, L. Energy metabolism in the liver. *Comprehensive Physiology* **4**, 177-197 (2014).

9 Blouin, A., Bolender, R. P. & Weibel, E. R. Distribution of organelles and membranes between hepatocytes and nonhepatocytes in the rat liver parenchyma. A stereological study. *Journal of Cell Biology* **72**, 441-455 (1977).

10 Boyer, T. D. & Lindor, K. D. *Zakim and Boyer's hepatology: A textbook of liver disease e-book*. (Elsevier Health Sciences, 2016).

11 Tabibian, J. H., Masyuk, A. I., Masyuk, T. V., O'Hara, S. P. & LaRusso, N. F. Physiology of cholangiocytes. *Comprehensive Physiology* **3**, 541-565 (2013).

12 Ringelhan, M., Pfister, D., O'Connor, T., Pikarsky, E. & Heikenwalder, M. The immunology of hepatocellular carcinoma. *Nat Immunol* **19**, 222-232 (2018).

13 Llovet, J. M. *et al.* Hepatocellular carcinoma. *Nat Rev Dis Primers*, 6-6 (2021).

14 Vogel, A. *et al.* Hepatocellular carcinoma: ESMO Clinical Practice Guidelines for diagnosis, treatment and follow-up. *Ann Oncol* **29**, iv238-iv255 (2018).

15 Li, X. *et al.* The immunological and metabolic landscape in primary and metastatic liver cancer. *Nature Reviews Cancer* **21**, 541-557 (2021).

16 Kanwal, F. *et al.* Risk of Hepatocellular Cancer in Patients With Non-Alcoholic Fatty Liver Disease. *Gastroenterology* **155**, 1828-1837.e1822 (2018).

17 Tschaharganeh, D. F. *et al.* p53-dependent Nestin regulation links tumor suppression to cellular plasticity in liver cancer. *Cell* **158**, 579-592 (2014).

18 Llovet, J. M. *et al.* Hepatocellular carcinoma. *Nat Rev Dis Primers* **2**, 16018 (2016).

19 Hu, X. *et al.* Prediction of hepatic metastasis and relapse in colorectal cancers based on concordance analyses with liver fibrosis scores. *Clin Transl Med* **9**, 13 (2020).

20 El-Serag, H. B., Marrero, J. A., Rudolph, L. & Reddy, K. R. Diagnosis and treatment of hepatocellular carcinoma. *Gastroenterology* **134**, 1752-1763 (2008).

21 Rizvi, S. & Gores, G. J. Pathogenesis, diagnosis, and management of cholangiocarcinoma. *Gastroenterology* **145**, 1215-1229 (2013).

22 Abou-Alfa, G. K. *et al.* Cabozantinib in Patients with Advanced and Progressing Hepatocellular Carcinoma. *N Engl J Med* **379**, 54-63 (2018).

23 Llovet, J. M., Montal, R. & Villanueva, A. Randomized trials and endpoints in advanced HCC: Role of PFS as a surrogate of survival. *Journal of Hepatology* **70**, 1262-1277 (2019).

24 Llovet, J. M. *et al.* Sorafenib in advanced hepatocellular carcinoma. *N Engl J Med* **359**, 378-390 (2008).

25 Nault, J. C., Cheng, A. L., Sangro, B. & Llovet, J. M. Milestones in the pathogenesis and management of primary liver cancer. *J Hepatol* **72**, 209-214 (2020).

26 Rizvi, S., Khan, S. A., Hallemeier, C. L., Kelley, R. K. & Gores, G. J. Cholangiocarcinoma - evolving concepts and therapeutic strategies. *Nat Rev Clin Oncol* **15**, 95-111 (2018).
27 Yamashita, T. *et al.* REFLECT-a phase 3 trial comparing efficacy and safety of lenvatinib to sorafenib for the treatment of unresectable hepatocellular carcinoma: an analysis of Japanese subset. *J Gastroenterol* **55**, 113-122 (2020).
28 Yarchoan, M. *et al.* Recent developments and therapeutic strategies against hepatocellular carcinoma. *Cancer research* **79**, 4326-4330 (2019).
29 Li, S. *et al.* The Role of Oxidative Stress and Antioxidants in Liver Diseases. *Int J Mol Sci* **16**, 26087-26124 (2015).
30 El-Khoueiry, A. B. *et al.* Nivolumab in patients with advanced hepatocellular carcinoma (CheckMate 040): an open-label, non-comparative, phase 1/2 dose escalation and expansion trial. *Lancet* **389**, 2492-2502 (2017).
31 Finn, R. S. *et al.* Atezolizumab plus Bevacizumab in Unresectable Hepatocellular Carcinoma. *N Engl J Med* **382**, 1894-1905 (2020).
32 Pfister, D. *et al.* NASH limits anti-tumour surveillance in immunotherapy-treated HCC. *Nature* **592**, 450-456 (2021).
33 Oyadomari, S., Harding, H. P., Zhang, Y., Oyadomari, M. & Ron, D. Dephosphorylation of Translation Initiation Factor 2α Enhances Glucose Tolerance and Attenuates Hepatosteatosis in Mice. *Cell Metabolism* **7**, 520-532 (2008).
34 Protzer, U., Maini, M. K. & Knolle, P. A. Living in the liver: hepatic infections. *Nature Reviews Immunology* **12**, 201-213 (2012).
35 Berg, M. *et al.* Cross-presentation of antigens from apoptotic tumor cells by liver sinusoidal endothelial cells leads to tumor-specific CD8+ T cell tolerance. *European Journal of Immunology* **36**, 2960-2970 (2006).
36 Heymann, F. *et al.* Liver inflammation abrogates immunological tolerance induced by Kupffer cells. *Hepatology* **62**, 279-291 (2015).
37 Jenne, C. N. & Kubes, P. Immune surveillance by the liver. *Nat Immunol* **14**, 996-1006 (2013).
38 Ichikawa, S., Mucida, D., Tyznik, A. J., Kronenberg, M. & Cheroutre, H. Hepatic Stellate Cells Function as Regulatory Bystanders. *The Journal of Immunology* **186**, 5549 (2011).
39 Knolle, P. A. & Thimme, R. Hepatic Immune Regulation and Its Involvement in Viral Hepatitis Infection. *Gastroenterology* **146**, 1193-1207 (2014).
40 Gabrilovich, D. I. & Nagaraj, S. Myeloid-derived suppressor cells as regulators of the immune system. *Nature Reviews Immunology* **9**, 162-174 (2009).
41 Luedde, T., Kaplowitz, N. & Schwabe, R. F. Cell death and cell death responses in liver disease: mechanisms and clinical relevance. *Gastroenterology* **147**, 765-783 e764 (2014).
42 Boege, Y. *et al.* A Dual Role of Caspase-8 in Triggering and Sensing Proliferation-Associated DNA Damage, a Key Determinant of Liver Cancer Development. *Cancer Cell* **32**, 342-359 e310 (2017).
43 Holze, C. *et al.* Oxeiptosis, a ROS-induced caspase-independent apoptosis-like cell-death pathway. *Nat Immunol* **19**, 130-140 (2018).
44 Brenner, C., Galluzzi, L., Kepp, O. & Kroemer, G. Decoding cell death signals in liver inflammation. *Journal of Hepatology* **59**, 583-594 (2013).
45 Caesar, R. *et al.* Gut-derived lipopolysaccharide augments adipose macrophage accumulation but is not essential for impaired glucose or insulin tolerance in mice. *Gut* **61**, 1701-1707 (2012).
46 Liaskou, E., Wilson, D. V. & Oo, Y. H. Innate immune cells in liver inflammation. *Mediators Inflamm* **2012**, 949157 (2012).
47 Karin, M. & Clevers, H. Reparative inflammation takes charge of tissue regeneration. *Nature* **529**, 307-315 (2016).

48 Afshar-Kharghan, V. The role of the complement system in cancer. *J Clin Invest* **127**, 780-789 (2017).
49 Yuan, D. T. *et al.* Kupffer Cell-Derived Tnf Triggers Cholangiocellular Tumorigenesis through JNK due to Chronic Mitochondrial Dysfunction and ROS. *Cancer Cell* **31**, 771-789 (2017).
50 Grivennikov, S. I., Greten, F. R. & Karin, M. Immunity, inflammation, and cancer. *Cell* **140**, 883-899 (2010).
51 Nakagawa, H. & Maeda, S. Inflammation- and stress-related signaling pathways in hepatocarcinogenesis. *World J Gastroenterol* **18**, 4071-4081 (2012).
52 Flecken, T. *et al.* Immunodominance and functional alterations of tumor-associated antigen-specific CD8+ T-cell responses in hepatocellular carcinoma. *Hepatology* **59**, 1415-1426 (2014).
53 Macdonald, R. Lifespan of Liver Cells - Autoradiographic Study Using Tritiated Thymidine in Normal, Cirrhotic, and Partially Hepatectomized Rats. *Archives of Internal Medicine* **107**, 335–343 (1961).
54 Ma, L. *et al.* Tumor Cell Biodiversity Drives Microenvironmental Reprogramming in Liver Cancer. *Cancer Cell* **36**, 418-430 (2019).
55 Stauffer, J. K., Scarzello, A. J., Jiang, Q. & Wiltrout, R. H. Chronic inflammation, immune escape, and oncogenesis in the liver: a unique neighborhood for novel intersections. *Hepatology* **56**, 1567-1574 (2012).
56 Klein, G. Cancer, apoptosis, and nonimmune surveillance. *Cell Death & Differentiation* **11**, 13-17 (2004).
57 Dhar, D. *et al.* Liver Cancer Initiation Requires p53 Inhibition by CD44-Enhanced Growth Factor Signaling. *Cancer Cell* **33**, 1061-1077 (2018).
58 Kang, T. W. *et al.* Senescence surveillance of pre-malignant hepatocytes limits liver cancer development. *Nature* **479**, 547-551 (2011).
59 Satriano, L., Lewinska, M., Rodrigues, P. M., Banales, J. M. & Andersen, J. B. Metabolic rearrangements in primary liver cancers: cause and consequences. *Nature reviews Gastroenterology & hepatology* **16**, 748-766 (2019).
60 Kietzmann, T. Metabolic zonation of the liver: The oxygen gradient revisited. *Redox biology* **11**, 622-630 (2017).
61 Berndt, N. *et al.* Functional Consequences of Metabolic Zonation in Murine Livers: Insights for an Old Story. *Hepatology* (2020).
62 Gola, A. *et al.* Commensal-driven immune zonation of the liver promotes host defence. *Nature* **589**, 131-136 (2021).
63 Manco, R. & Itzkovitz, S. Liver zonation. *Journal of Hepatology* **74**, 466-468 (2021).
64 Dobie, R. *et al.* Single-Cell Transcriptomics Uncovers Zonation of Function in the Mesenchyme during Liver Fibrosis. *Cell Rep* **29**, 1832-1847 e1838 (2019).
65 Keegan, A., Martini, R. & Batey, R. Ethanol-related liver injury in the rat: a model of steatosis, inflammation and pericentral fibrosis. *Journal of Hepatology* **23**, 591-600 (1995).
66 Hall, Z. *et al.* Lipid zonation and phospholipid remodeling in nonalcoholic fatty liver disease. *Hepatology* **65**, 1165-1180 (2017).
67 Michelotti, G. A., Machado, M. V. & Diehl, A. M. NAFLD, NASH and liver cancer. *Nature Reviews Gastroenterology & Hepatology* **10**, 656-665 (2013).
68 Kudo, Y. *et al.* PKCλ/ι loss induces autophagy, oxidative phosphorylation, and NRF2 to promote liver cancer progression. *Cancer Cell* **38**, 247-262 (2020).
69 Wilson, G. K., Tennant, D. A. & McKeating, J. A. Hypoxia inducible factors in liver disease and hepatocellular carcinoma: current understanding and future directions. *Journal of Hepatology* **61**, 1397-1406 (2014).

70 Wing, P. A. C. *et al.* Hypoxia inducible factors regulate hepatitis B virus replication by activating the basal core promoter. *J Hepatol* **75**, 64-73 (2021).
71 Moreau, M. *et al.* Hepatitis C viral proteins perturb metabolic liver zonation. *Journal of Hepatology* **62**, 278-285 (2015).
72 Wolf, Monika J. *et al.* Metabolic Activation of Intrahepatic CD8+ T Cells and NKT Cells Causes Nonalcoholic Steatohepatitis and Liver Cancer via Cross-Talk with Hepatocytes. *Cancer Cell* **26**, 549-564 (2014).
73 Cairns, R. A., Harris, I. S. & Mak, T. W. Regulation of cancer cell metabolism. *Nature Reviews Cancer* **11**, 85-95 (2011).
74 Wang, M. *et al.* Dysregulated fatty acid metabolism in hepatocellular carcinoma. *Hepatic oncology* **3**, 241-251 (2016).
75 Xia, S., Pan, Y., Liang, Y., Xu, J. & Cai, X. The microenvironmental and metabolic aspects of sorafenib resistance in hepatocellular carcinoma. *EBioMedicine* **51**, 102610 (2020).
76 Ma, C. *et al.* NAFLD causes selective CD4+ T lymphocyte loss and promotes hepatocarcinogenesis. *Nature* **531**, 253-257 (2016).
77 Zhang, Q. *et al.* Fatty acid oxidation contributes to IL-1β secretion in M2 macrophages and promotes macrophage-mediated tumor cell migration. *Molecular immunology* **94**, 27-35 (2018).
78 Pacella, I. *et al.* Fatty acid metabolism complements glycolysis in the selective regulatory T cell expansion during tumor growth. *Proceedings of the National Academy of Sciences* **115**, E6546-E6555 (2018).
79 Li, T. E. *et al.* PKM2 Drives Hepatocellular Carcinoma Progression by Inducing Immunosuppressive Microenvironment. *Front Immunol* **11**, 589997 (2020).
80 Friedman, J. R. & Voeltz, G. K. The ER in 3D: a multifunctional dynamic membrane network. *Trends in cell biology* **21**, 709-717 (2011).
81 Hetz, C., Chevet, E. & Harding, H. P. Targeting the unfolded protein response in disease. *Nature Reviews Drug Discovery* **12**, 703-719 (2013).
82 Walter, P. & Ron, D. The Unfolded Protein Response: From Stress Pathway to Homeostatic Regulation. *Science* **334**, 1081 (2011).
83 Hetz, C. The unfolded protein response: controlling cell fate decisions under ER stress and beyond. *Nature Reviews Molecular Cell Biology* **13**, 89-102 (2012).
84 Harding, H. P. *et al.* Regulated Translation Initiation Controls Stress-Induced Gene Expression in Mammalian Cells. *Molecular Cell* **6**, 1099-1108 (2000).
85 Kozutsumi, Y., Segal, M., Normington, K., Gething, M.-J. & Sambrook, J. The presence of malfolded proteins in the endoplasmic reticulum signals the induction of glucose-regulated proteins. *Nature* **332**, 462-464 (1988).
86 Lee, A. S. GRP78 Induction in Cancer: Therapeutic and Prognostic Implications. *Cancer research* **67**, 3496 (2007).
87 Hotamisligil, G. S. Endoplasmic Reticulum Stress and the Inflammatory Basis of Metabolic Disease. *Cell* **140**, 900-917 (2010).
88 Kaneko, M., Niinuma, Y. & Nomura, Y. Activation signal of nuclear factor-kappa B in response to endoplasmic reticulum stress is transduced via IRE1 and tumor necrosis factor receptor-associated factor 2. *Biol Pharm Bull* **26**, 931-935 (2003).
89 Garg, A. D. *et al.* ER stress-induced inflammation: does it aid or impede disease progression? *Trends in Molecular Medicine* **18**, 589-598 (2012).
90 Yamazaki, H. *et al.* Activation of the Akt-NF-κB Pathway by Subtilase Cytotoxin through the ATF6 Branch of the Unfolded Protein Response. *The Journal of Immunology* **183**, 1480 (2009).

91 Gargalovic, P. S. *et al.* The Unfolded Protein Response Is an Important Regulator of Inflammatory Genes in Endothelial Cells. *Arteriosclerosis, Thrombosis, and Vascular Biology* **26**, 2490-2496 (2006).
92 Verfaillie, T. *et al.* PERK is required at the ER-mitochondrial contact sites to convey apoptosis after ROS-based ER stress. *Cell Death & Differentiation* **19**, 1880-1891 (2012).
93 Cuozzo, J. W. & Kaiser, C. A. Competition between glutathione and protein thiols for disulphide-bond formation. *Nature Cell Biology* **1**, 130-135 (1999).
94 Tu, B. P. & Weissman, J. S. The FAD- and O2-Dependent Reaction Cycle of Ero1-Mediated Oxidative Protein Folding in the Endoplasmic Reticulum. *Molecular Cell* **10**, 983-994 (2002).
95 Zeeshan, H. M., Lee, G. H., Kim, H.-R. & Chae, H.-J. Endoplasmic Reticulum Stress and Associated ROS. *Int J Mol Sci* **17** (2016).
96 Zhang, K. Integration of ER stress, oxidative stress and the inflammatory response in health and disease. *International journal of clinical and experimental medicine* **3**, 33-40 (2010).
97 Vecchi, C. *et al.* ER stress controls iron metabolism through induction of hepcidin. *Science* **325**, 877-880 (2009).
98 Wang, M. & Kaufman, R. J. The impact of the endoplasmic reticulum protein-folding environment on cancer development. *Nature Reviews Cancer* **14**, 581-597 (2014).
99 Liu, J. *et al.* Endoplasmic reticulum stress modulates liver inflammatory immune response in the pathogenesis of liver ischemia and reperfusion injury. *Transplantation* **94**, 211-217 (2012).
100 Ren, F. *et al.* Endoplasmic reticulum stress-activated glycogen synthase kinase 3β aggravates liver inflammation and hepatotoxicity in mice with acute liver failure. *Inflammation* **38**, 1151-1165 (2015).
101 Wei, C. *et al.* Tumor Microenvironment Regulation by the Endoplasmic Reticulum Stress Transmission Mediator Golgi Protein 73 in Mice. *Hepatology* **70**, 851-870 (2019).
102 Ron, D. & Walter, P. Signal integration in the endoplasmic reticulum unfolded protein response. *Nature Reviews Molecular Cell Biology* **8**, 519-529 (2007).
103 Scheuner, D. *et al.* Translational Control Is Required for the Unfolded Protein Response and In Vivo Glucose Homeostasis. *Molecular Cell* **7**, 1165-1176 (2001).
104 Lee, A. H., Scapa, E. F., Cohen, D. E. & Glimcher, L. H. Regulation of hepatic lipogenesis by the transcription factor XBP1. *Science* **320**, 1492-1496 (2008).
105 Acosta-Alvear, D. *et al.* XBP1 Controls Diverse Cell Type- and Condition-Specific Transcriptional Regulatory Networks. *Molecular Cell* **27**, 53-66 (2007).
106 Wang, Y., Vera, L., Fischer, W. H. & Montminy, M. The CREB coactivator CRTC2 links hepatic ER stress and fasting gluconeogenesis. *Nature* **460**, 534-537 (2009).
107 Bobrovnikova-Marjon, E. *et al.* PERK-dependent regulation of lipogenesis during mouse mammary gland development and adipocyte differentiation. *Proceedings of the National Academy of Sciences* **105**, 16314 (2008).
108 Rutkowski, D. T. *et al.* UPR Pathways Combine to Prevent Hepatic Steatosis Caused by ER Stress-Mediated Suppression of Transcriptional Master Regulators. *Developmental Cell* **15**, 829-840 (2008).
109 Polak, P. & Hall, M. N. mTOR and the control of whole body metabolism. *Current Opinion in Cell Biology* **21**, 209-218 (2009).
110 Cubillos-Ruiz, J. R., Bettigole, S. E. & Glimcher, L. H. Tumorigenic and Immunosuppressive Effects of Endoplasmic Reticulum Stress in Cancer. *Cell* **168**, 692-706 (2017).
111 Bobrovnikova-Marjon, E. *et al.* PERK promotes cancer cell proliferation and tumor growth by limiting oxidative DNA damage. *Oncogene* **29**, 3881-3895 (2010).
112 Carrasco, D. R. *et al.* The Differentiation and Stress Response Factor XBP-1 Drives Multiple Myeloma Pathogenesis. *Cancer Cell* **11**, 349-360 (2007).

113 Niederreiter, L. *et al.* ER stress transcription factor Xbp1 suppresses intestinal tumorigenesis and directs intestinal stem cells. *Journal of Experimental Medicine* **210**, 2041-2056 (2013).
114 Galanis, A. *et al.* Reactive oxygen species and HIF-1 signalling in cancer. *Cancer Letters* **266**, 12-20 (2008).
115 Cubillos-Ruiz, Juan R. *et al.* ER Stress Sensor XBP1 Controls Anti-tumor Immunity by Disrupting Dendritic Cell Homeostasis. *Cell* **161**, 1527-1538 (2015).
116 Thuerauf, D. J., Marcinko, M., Belmont, P. J. & Glembotski, C. C. Effects of the isoform-specific characteristics of ATF6 alpha and ATF6 beta on endoplasmic reticulum stress response gene expression and cell viability. *J Biol Chem* **282**, 22865-22878 (2007).
117 Hillary, R. F. & FitzGerald, U. A lifetime of stress: ATF6 in development and homeostasis. *Journal of Biomedical Science* **25**, 48 (2018).
118 Schindler, A. J. & Schekman, R. In vitro reconstitution of ER-stress induced ATF6 transport in COPII vesicles. *Proceedings of the National Academy of Sciences* **106**, 17775 (2009).
119 Nault, J. C. *et al.* A hepatocellular carcinoma 5-gene score associated with survival of patients after liver resection. *Gastroenterology* **145**, 176-187 (2013).
120 Wu, X. *et al.* A missense polymorphism in ATF6 gene is associated with susceptibility to hepatocellular carcinoma probably by altering ATF6 level. *International Journal of Cancer* **135**, 61-68 (2014).
121 Coleman, O. I. *et al.* Activated ATF6 Induces Intestinal Dysbiosis and Innate Immune Response to Promote Colorectal Tumorigenesis. *Gastroenterology* **155**, 1539-1552.e1512 (2018).
122 Malehmir, M. *et al.* Platelet GPIbα is a mediator and potential interventional target for NASH and subsequent liver cancer. *Nature Medicine* **25**, 641-655 (2019).
123 Matyash, V., Liebisch, G., Kurzchalia, T. V., Shevchenko, A. & Schwudke, D. Lipid extraction by methyl-tert-butyl ether for high-throughput lipidomics. *Journal of Lipid Research* **49**, 1137-1146 (2008).
124 Godon, J. J., Zumstein, E., Dabert, P., Habouzit, F. & Moletta, R. Molecular microbial diversity of an anaerobic digestor as determined by small-subunit rDNA sequence analysis. *Applied and Environmental Microbiology* **63**, 2802-2813 (1997).
125 Lagkouvardos, I. *et al.* IMNGS: A comprehensive open resource of processed 16S rRNA microbial profiles for ecology and diversity studies. *Scientific Reports* **6**, 33721 (2016).
126 Edgar, R. C., Haas, B. J., Clemente, J. C., Quince, C. & Knight, R. UCHIME improves sensitivity and speed of chimera detection. *Bioinformatics* **27**, 2194-2200 (2011).
127 Edgar, R. C. UPARSE: highly accurate OTU sequences from microbial amplicon reads. *Nature Methods* **10**, 996-998 (2013).
128 Lagkouvardos, I., Fischer, S., Kumar, N. & Clavel, T. Rhea: a transparent and modular R pipeline for microbial profiling based on 16S rRNA gene amplicons. *PeerJ* **5**, e2836 (2017).
129 Naugler, W. E. *et al.* Gender Disparity in Liver Cancer Due to Sex Differences in MyD88-Dependent IL-6 Production. *Science* **317**, 121 (2007).
130 Hetz, C. & Papa, F. R. The Unfolded Protein Response and Cell Fate Control. *Molecular Cell* **69**, 169-181 (2018).
131 Umemura, A. *et al.* p62, Upregulated during Preneoplasia, Induces Hepatocellular Carcinogenesis by Maintaining Survival of Stressed HCC-Initiating Cells. *Cancer Cell* **29**, 935-948 (2016).
132 Blackwood, E. A. *et al.* Pharmacologic ATF6 activation confers global protection in widespread disease models by reprograming cellular proteostasis. *Nature Communications* **10**, 187 (2019).

10 Acknowledgements

I would like to show my grateful thanks to the people who supported me over the last four years during my Ph.D. studies.

I want to thank Professor. Dr. Mathias Heikenwalder for offering me the chance to conduct my Ph.D. study under his supervision. Joining this group is the wisest choice I have ever made during my career, and it is a great fortune to find a place where I could always work motivated to explore my potential. I developed from a fresh Ph.D. student into a scientist who could conduct and organize ambitious research projects; I owe my development to my supervisor, who trusted me and gave me enough freedom in my research. I have made numerous mistakes on the journey to my Ph.D. degree; some of them are small misconducts people repeat every day, some are serious problems that people could get fired. But my supervisor has never criticized a single word on me. I appreciate and cherish your forgiveness.

I want to thank Professor. Dr. Ralf Bartenschlager, my first supervisor in my thesis advisory committee (TAC) and my Ph.D. thesis defense, who has supported me with his wise ideas and suggestions and has shown me the scientific demeanor of a world-leading scientist. Thank you, Ralf, for your guidance during my long journey to my Ph.D. degree.

I want to thank Professor. Dr. Dirk Haller, my external TAC member and the most important collaborator in my Ph.D. project. Thank you, Dirk, for providing me the precious experimental material and countless support throughout my whole Ph.D. study. The mouse lines generated by AG. Haller usually give fantastic phenotypes, which are always more attractive in the liver than the gut. I would like to be a life-long collaborator with you.

I want to thank my Ph.D. examination committee, Dr. Guoliang Cui, for his tremendous support in helping me with genetically modified animals and his expertise in immunology and T cell metabolism.

I want to thank my Ph.D. examination committee, Dr. Wilhelm Palm, for his great insights on the modification of cellular metabolism by activating intrinsic signaling pathways.

Special thanks to Ms. Ulrike Rothermel, our animal manager, who offered me the first helping hand in the early stages of my Ph.D. study and provided me numerous support in the past three years. Thank you, Ulli; it is a great pleasure to meet and work together with you.

I would like to thank:

- Dr. Pierluigi Ramadori, who taught me experimental skills hand-by-hand and helped me massively with animal experiments and scientific writing. Thank you for your lenience and generosity in sharing knowledge; you are the most vital support I have ever had.
- Ms. Danijela Heide, who helped me with all the histological stainings and the establishment of new antibodies. Your hands helped me with more than 30% of the data in my project. And you have done many extra works for me, which is beyond your job. I always keep them in my heart, and I really appreciate it.
- Ms. Sandra Prokosch, the “mother of the Ph.D. students”, thank you for being the first person who witnessed the ATF6 phenotype and your dedicated support in helping me with the animal works. It is your professional organization of the lab issues which makes our work more accessible and more efficient.
- Mr. Luqing Li, who worked side-by-side with me on the ATF6 project and took care of the animal issues when I was blocked in China for 7 months, I wish you all the best in your career.
- Ms. Mirian Fernandez, who helped me with the injection of the animals, and we had inspiring discussions in the Ph.D. office, which released much of my pressure.
- Dr. Jan Kosla, who helped me with the generation of genetically modified cell lines and offered me a lot of chance for travelling.
- Ms. Michaela Hart, who helped me massively with organization and paperwork. It is impossible to focus on my work without your efforts.
- Ms. Anja Rathgeb and her team of animal caretakers in Barrier D have been taking care of my mouse lines from the beginning of my Ph.D. study. I can not manage my work without their support.
- Dr. Suchira Gallage and Adnan Ali. Dr. Suchira Gallage taught me the basic knowledge of mice and critical scientific thinking. Adnan Ali, who started the Ph.D. together with me and is the best person I could imagine who will always offer me his help.
- The technical team, Ms. Jenny Hetzer and Ms. Corinna Leuchtenberger, for the professional cutting of liver sections; Mr. Florian Müller for the FACS sorting; Ms. Anna-Lena Eck for the genotyping; Mr. Tim Machauer for the histology staining. All of your support will not be taken for granted.

- All dedicated collaborators, namely Dr. Christoph Trautwein, Dr. Praveen Baskaran, Dr. Olivia Coleman and Dr. Maike Hofmann. And all other collaborators who have helped me on this long path.
- Former lab members that helped me on my path, namely Dr. Marta Szydlowska and Ms. Lena Beideck.
- All group members of F180, who companied me during my Ph.D. and shared scientific discoveries with me.

Finally, I want to thank my whole family members and loved ones for their selfless and extraordinary support. Providing you a better and decent life is the strongest motivation in my 26 years of study. I also want to thank myself for my courage in facing challenges, my patience when encountering failures, my hard-working to generate opportunities, and my ambitions to become a better myself; I will keep moving!

Sincerely,

Xin Li

2021.08.06, Heidelberg.

11 Appendix

This appendix contains one published publication to which I contributed writing during my Ph.D.

The immunological and metabolic landscape in primary and metastatic liver cancer

Xin Li[1,6], Pierluigi Ramadori [1,6], Dominik Pfister [1], Marco Seehawer [2,3], Lars Zender[2,4,5] and Mathias Heikenwalder [1] ✉

Nature Reviews Cancer volume 21, pages541–557 (2021)[15]

The immunological and metabolic landscape in primary and metastatic liver cancer

Xin Li[1,6], Pierluigi Ramadori[1,6], Dominik Pfister[1], Marco Seehawer[2,3], Lars Zender[2,4,5] and Mathias Heikenwalder[1]

Abstract | The liver is the sixth most common site of primary cancer in humans, and generally arises in a background of cirrhosis and inflammation. Moreover, the liver is frequently colonized by metastases from cancers of other organs (particularly the colon) because of its anatomical location and organization, as well as its unique metabolic and immunosuppressive environment. In this Review, we discuss how the hepatic microenvironment adapts to pathologies characterized by chronic inflammation and metabolic alterations. We illustrate how these immunological or metabolic changes alter immunosurveillance and thus hinder or promote the development of primary liver cancer. In addition, we describe how inflammatory and metabolic niches affect the spreading of cancer metastases into or within the liver. Finally, we review the current therapeutic options in this context and the resulting challenges that must be surmounted.

[1]Division of Chronic Inflammation and Cancer, German Cancer Research Center (DKFZ), Heidelberg, Germany.

[2]Department of Medical Oncology and Pneumology (Internal Medicine VIII), University Hospital Tuebingen, Tuebingen, Germany.

[3]Department of Medical Oncology, Dana-Farber Cancer Institute, Harvard Medical School, Boston, MA, USA.

[4]Cluster of Excellence iFIT (EXC 2180) "Image-Guided and Functionally Instructed Tumor Therapies", University of Tuebingen, Tuebingen, Germany.

[5]German Cancer Research Consortium (DKTK), Partner Site Tübingen, German Cancer Research Center (DKFZ), Heidelberg, Germany.

[6]These authors contributed equally: Xin Li, Pierluigi Ramadori.

✉e-mail: m.heikenwalder@dkfz.de

https://doi.org/10.1038/s41568-021-00383-9

Liver cancer is the fourth leading cause for cancer-related mortality worldwide, despite the liver being the sixth most common site of primary cancer[1]. Hepatocellular carcinoma (HCC) accounts for 80–90% of primary liver cancers, and cholangiocarcinoma (CCA) accounts for 10–15%[2]. Angiosarcoma and paediatric hepatoblastoma account for a relatively small proportion of primary liver cancers and are not discussed in this Review. The most important risk factor for the development of primary liver cancer comes from chronic inflammatory aetiologies that lead to chronic necro-inflammation[3]. These distinct chronic inflammatory processes can originate from viral infections (hepatitis B virus (HBV) and HCV), metabolic alterations (alcoholic steatohepatitis (ASH) and nonalcoholic steatohepatitis (NASH)[4]), chronic toxin exposure (for example, aflatoxin) or parasite infection (for example, flukes)[5]. Whereas vaccination and new antiviral therapeutic approaches dampened the rise of HBV-associated or HCV-associated liver cancer[6,7], lifestyle factors such as chronic alcohol consumption, dietary habits and sedentary lifestyles fuel chronic inflammation and therefore the incidence of hepatic tumours. Indeed, lifestyle-related liver cancer is particularly found in Western societies, but is also rising epidemically in developing countries[8].

The unique anatomical localization, the endothelial fenestration and the immunosuppressive environment of the liver[9] predispose this organ to seeding by tumour metastases from extrahepatic cancers, termed secondary liver cancers. Strikingly, metastatic liver cancer occurs 18–40 times more often than primary hepatic malignancies[10]. Most secondary liver cancers originate from tumours of the gastrointestinal tract (colorectal, oesophageal, stomach and pancreatic), as well as breast and lung tumours, and melanoma[11]. In general, the occurrence of liver metastases correlates significantly with a drop in 5-year survival rate and reduced quality of life[12].

Owing to the genetic, metabolic and inflammatory heterogeneity of liver cancer, the development of therapies is challenging; chemotherapy (for example, cisplatin, gemcitabine or doxorubicin) or treatment with multikinase inhibitors (for example, first-line sorafenib, second-line regorafenib, lenvatinib or third-line cabozantinib) provides only minor prolongation of overall survival and a marginal increase in quality of life[6,13–18]. A better understanding of the complex cellular and molecular immune networks that characterize the hepatic microenvironment prompted the development of novel therapeutic interventions, including immunotherapy[3,19]. Immune checkpoint blockade in combination with other treatments has already changed and will further transform the approach to treating primary and secondary liver cancer[20].

In this Review, we provide insights into the physiological, immunological and metabolic nature of the liver. We highlight the mechanisms by which specific aetiologies alter liver homeostasis, and we discuss how this altered microenvironment promotes tumour initiation, sustains tumour growth and regulates surveillance of

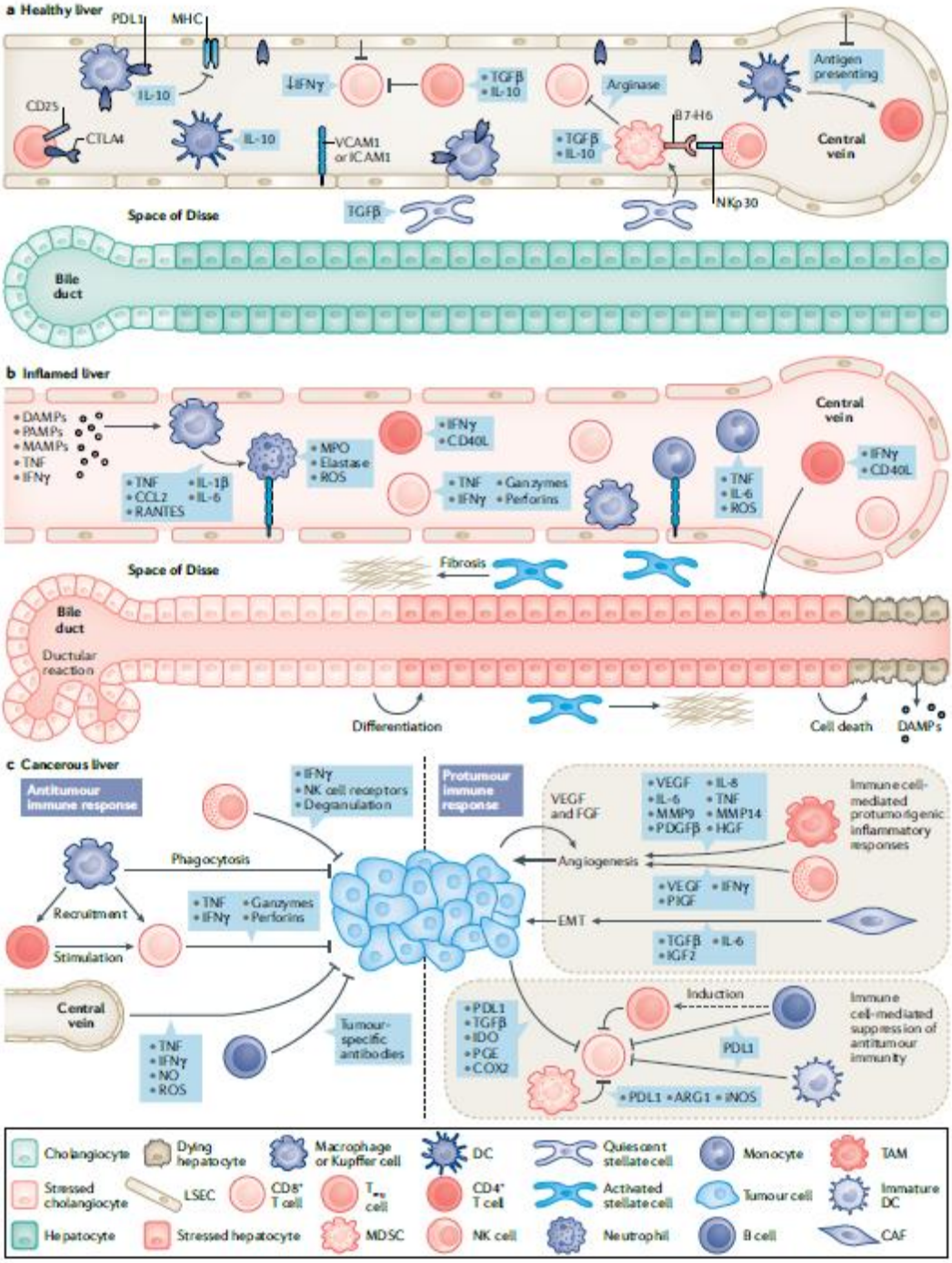
a Healthy liver
PDL1
MHC
IL-10
CD25
CTLA4
IL-10
↓IFNγ
• TGFβ
• IL-10
VCAM1
or ICAM1
Arginase
• TGFβ
• IL-10
B7-H6
NKp30
Antigen presenting
Central vein
Space of Disse
TGFβ
Bile duct
b Inflamed liver
• DAMPs
• PAMPs
• MAMPs
• TNF
• IFNγ
• TNF
• CCL2
• RANTES
• IL-1β
• IL-6
• MPO
• Elastase
• ROS
• IFNγ
• CD40L
• TNF
• IFNγ
• Granzymes
• Perforins
• TNF
• IL-6
• ROS
Central vein
• IFNγ
• CD40L
Space of Disse
Fibrosis
Bile duct
Ductular reaction
Differentiation
Cell death
DAMPs
c Cancerous liver
Antitumour immune response
• IFNγ
• NK cell receptors
• Degranulation
Phagocytosis
Recruitment
Stimulation
• TNF
• IFNγ
• Granzymes
• Perforins
Central vein
• TNF
• IFNγ
• NO
• ROS
Tumour-specific antibodies
Protumour immune response
VEGF and FGF
• VEGF
• IL-6
• MMP9
• PDGFβ
• IL-8
• TNF
• MMP14
• HGF
Immune cell-mediated protumorigenic inflammatory responses
Angiogenesis
• VEGF
• PlGF
• IFNγ
EMT
• TGFβ
• IGF2
• IL-6
Induction
• PDL1
• TGFβ
• IDO
• PGE
• COX2
PDL1
• PDL1
• ARG1
• iNOS
Immune cell-mediated suppression of antitumour immunity
Cholangiocyte
Stressed cholangiocyte
Hepatocyte
Dying hepatocyte
LSEC
Stressed hepatocyte
Macrophage or Kupffer cell
CD8+ T cell
MDSC
DC
CD4+ T cell
NK cell
Quiescent stellate cell
Activated stellate cell
Neutrophil
Monocyte
Tumour cell
B cell
TAM
Immature DC
CAF

Necro-inflammation
A pathological condition characterized by cell death (necrosis) that triggers the activation of the immune system, thereby sustaining a local inflammatory response.

primary tumours or invasive metastatic cells. Finally, we discuss strategies to improve the efficacy of anticancer therapies by modulating the hepatic microenvironment.

The precancerous liver microenvironment

To successfully treat primary liver cancer, it is essential to first understand how this arises almost exclusively as a result of underlying chronic inflammation[2]. Chronic hepatitis is triggered and sustained by events such as activation of immune cells in response to viral infections, innate immune cell-triggered generation of a pro-inflammatory cytokine milieu in response to chronic damage, and destabilization of intrinsic hepatic cell types including hepatocytes and liver sinusoidal endothelial cells (LSECs) by exogenous toxins, fatty acid-mediated lipotoxicity and excessive iron deposition[2]. All of the above over time lead to overproduction of reactive oxygen species (ROS) and reactive nitrogen species, causing destabilization of organelle-related, metabolic-related and cell cycle-related control mechanisms contributing to dysfunction of DNA-damage repair[4]. Continuous regenerative response leads to activation of hepatic stellate cells (HSCs), collagen deposition, fibrosis and subsequent cirrhosis[8].

Immunosuppressive orientation of the liver

As the systemic metabolic gatekeeper organ, the liver is constantly targeted by gut-derived pathogens, microorganism-associated molecular patterns, Toll-like-receptor (for example, TLR4 or TLR9) agonists and diverse metabolites. Thus, the liver has an immunosuppressive polarization, which impairs efficient T cell-mediated antigen responses and is maintained by resident liver cell populations, including Kupffer cells (KCs), HSCs, dendritic cells (DCs), regulatory T (T_{reg}) cells and LSECs[5] (FIG. 1a).

KCs are the largest population of tissue-resident macrophages and are key mediators of the immunosuppressive orientation of the liver, by expressing programmed cell death ligand 1 (PDL1) and low levels of costimulatory molecules (CD80 and CD86), paired with the capability to prime T_{reg} cells[21]. Bacterial-derived pathogens keep KCs polarized towards an anti-inflammatory state, as evidenced by IL-10 expression[22], which can further decrease major histocompatibility complex (MHC) expression on LSECs to restrict their immunostimulatory capacity[22]. Indeed, depletion of KCs in vivo abolishes the induction of hepatic tolerance against particulate antigens[23].

HSCs were also shown to contribute to the tolerant immune orientation of the liver by producing anti-inflammatory cytokines such as transforming growth factor-β (TGFβ), thereby activating tissue regeneration pathways and supporting the differentiation of inflammatory monocytes into myeloid-derived suppressor cells (MDSCs)[23,24].

Compared with DCs from other tissues, hepatic DCs are less effective in activating T cells because of their 'immature' character and the high levels of IL-10 combined with low levels of IL-12 in the hepatic microenvironment[22]. Interestingly, hepatic DCs were described to have a higher ability to produce IL-10 than were splenic DCs[22,25]. The liver accommodates two major subtypes of DCs: conventional DCs and plasmacytoid-derived DCs[26]. Whereas plasmacytoid-derived DCs seem to be responsible for the tolerogenic milieu of the liver by displaying hyporesponsiveness to TLR stimulation and expressing low levels of costimulatory molecules[26], a pro-inflammatory immune phenotype can be attributed to $CD141^+$ conventional DCs in humans or $CD103^+XCR1^+$ conventional DCs in mice — mainly because of the high expression of MHC class II and because of their activating interaction with naive $CD8^+$ T cells[27,28].

Resident natural killer (NK) cells in the liver represent a heterogeneous cell population with important roles in infection as well as tumour immunosurveillance. In the mouse liver, NK cells can be subdivided into two main cell populations: conventional NK cells (which lack CD49a (also known as α1 integrin) and express DX5 (also known as α2 integrin)), and liver-specific resident NK cells, which express CD49a but not DX5 (REF.[29]). Liver-specific resident NK cells were shown to behave like a classical memory cell population[30] and

◀ Fig. 1 | **The immune microenvironment of the healthy, inflamed and cancerous liver. a** | In a healthy liver, cooperation between liver-resident cells and peripheral leukocytes or myeloid cells generates and maintains the immunosuppressive orientation. **b** | In the progression of inflammatory liver disease, metabolic or inflammatory aberrations promote the activation of innate immune responses (for example, activation of Kupffer cells, and recruitment of neutrophils, dendritic cells (DCs) and monocytes) and adaptive immune responses in the stressed sites of the liver. This immune activation further alters the homeostasis of liver-resident cells as evidenced by hepatocyte turnover, activation of hepatic stellate cells and increased expression of adhesion molecules on liver sinusoidal endothelial cells (LSECs), and, in turn, triggers hepatic fibrogenesis. **c** | In cancerous liver tissue, LSECs kill tumour cells by secreting TNF, interferon-γ (IFNγ), nitric oxide (NO) and reactive oxygen species (ROS). Kupffer cells kill tumour cells via phagocytosis and recruit T cells to the liver to exert an antitumour immune response. B cells and natural killer (NK) cells are also involved in the antitumour immune response. Conversely, hepatic regulatory T (T_{reg}) cells, immature DCs and myeloid-derived suppressor cells (MDSCs) suppress immunosurveillance by modulating the function of tumour-specific T cells. Cancer-associated fibroblasts (CAFs) promote an immunosuppressive environment and epithelial-to-mesenchymal transition (EMT) in cancer cells to support progression. Tumour-associated macrophages (TAMs) and NK cells accelerate blood vessel formation in the hepatic tumour microenvironment. Tumour cells themselves also support angiogenesis and inhibit cytotoxicity of $CD8^+$ T cells. CCL2, CC-chemokine ligand 2; CTLA4, cytotoxic T lymphocyte protein 4; DAMPs, damage-associated molecular patterns; ICAM1, intercellular adhesion molecule 1; MAMPs, microorganism-associated molecular patterns; MHC, major histocompatibility complex; MMP, matrix metalloproteinase; PAMPs, pathogen-associated molecular patterns; PDL1, programmed cell death 1 ligand 1; TGFβ, transforming growth factor-β; VCAM1, vascular cell adhesion molecule 1; VEGF, vascular endothelial growth factor.

to possess cytotoxic activity by producing a high amount of interferon-γ (IFNγ). Although these cells can become activated by different pro-inflammatory stimuli, they are maintained in a hyporesponsive state[31], mainly orchestrated by the immunosuppressive environment of the liver. MDSCs, which produce immunosuppressive cytokines (for example, IL-10 and TGFβ) and express arginase to suppress T cell proliferation as well as ROS production[32], are also found in the healthy liver[33]. It has been shown in vitro that MDSCs inhibit NK cell function via interaction with the NKp30 (also known as NCR3) receptor[32].

T_{reg} cells express high levels of CD25 (also known as IL-2RA) and cytotoxic T lymphocyte protein 4 (CTLA4), to compete with potential effector T cells for IL-2, CD80 and CD86 (REF. [34]). T_{reg} cells can also produce anti-inflammatory cytokines (TGFβ and IL-10)[2] to maintain the immunosuppressive character. Finally, LSECs express PDL1, pattern recognition receptors and adhesion molecules (for example, intercellular adhesion

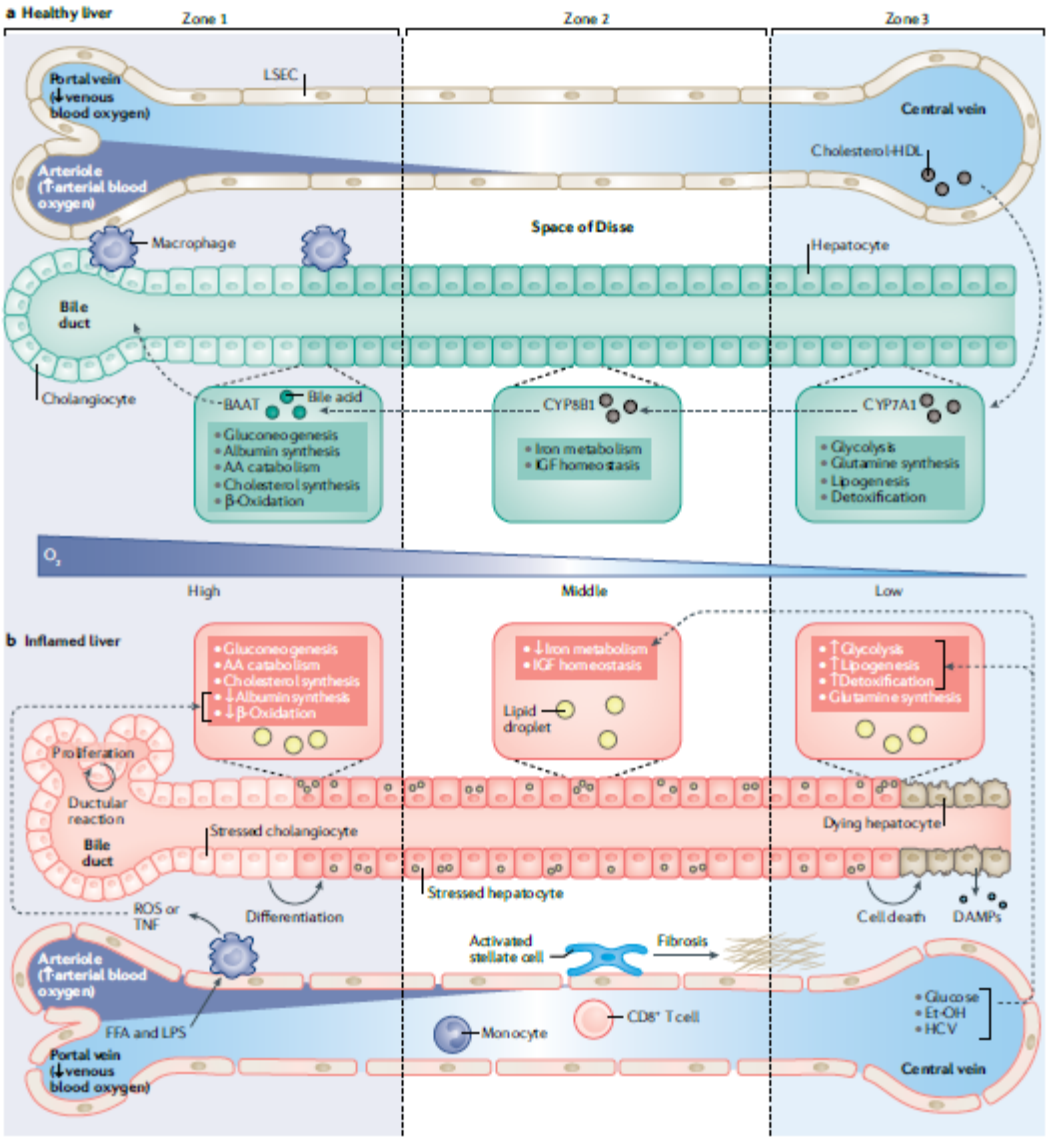

Liver sinusoids
Specific capillaries characterized by a particular distribution of endothelial cells presenting a typical fenestration that enables arterial and venous blood to mix.

Steatosis
Abnormal cytosolic accumulation of lipids in more than 5% of the total hepatocyte content in the liver.

Nonalcoholic fatty liver disease
(NAFLD). Metabolic disease of the liver related to abnormal accumulation of lipids, encompassing a wide spectrum of pathologies from simple fatty liver to nonalcoholic steatohepatitis (characterized by hepatic inflammatory infiltrate (steatohepatitis)), fibrosis and cirrhosis.

molecule 1 (ICAM1) and vascular cell adhesion molecule 1 (VCAM1)), mediating lymphocyte tissue infiltration and MHC class I or class II expression[5]. Insufficient expression of costimulatory molecules after antigen presentation by LSECs leads to T cell anergy instead of activation, further underlining the importance of the immunosuppressive hepatic polarization[35,36].

Metabolic microenvironment of the liver

The liver has a crucial role in the maintenance of systemic homeostasis. To accomplish this, the liver architecture is organized in functional units known as hepatic lobules, which present a well-defined spatial distribution in concentric layers of hepatocytes in relation to the blood supply and other non-parenchymal cells (FIG. 2a). Each lobule is composed of hexagonal-shaped structures bordered by portal spaces. The blood flows concentrically through the liver sinusoids to be drained in the central vein and directed towards the cava vein. In this setting, an oxygen gradient is generated by high tension in the portal spaces, progressively decreasing towards the central vein; this gradient determines the different distribution of functions in the hepatic lobule that is defined as hepatic zonation[37,38]. Hence, although all hepatocytes appear similar, they are subjected to different microenvironments according to their distribution along the lobule and therefore are functionally different. Hepatocytes located around the portal spaces (zone 1) are exposed to a higher concentration of oxygen and therefore carry out tasks that require higher ATP consumption, such as protein synthesis or secretion, gluconeogenesis, or fatty acid β-oxidation. Hepatocytes distributed around the pericentral vein (zone 3) are supplied with low oxygen and undertake functions that are less energy-demanding such as detoxification, lipogenesis and glycolysis[39]. Moreover, the use of single-cell spatial resolution analysis has revealed a specific distribution along the porto–central axis of sequential enzymes involved in metabolic cascades, resulting in the transfer of intermediate metabolites from different zones of the lobule[40]. An example is the production of bile acids from cholesterol, starting with cholesterol uptake in the pericentral blood followed by sequential conversion to bile acids that then flow in the bile canaliculi to finally be secreted in the intestine. Furthermore, it has recently been shown that expression of almost 50% of hepatocyte genes is not only spatially but also temporally regulated under healthy conditions[41]. In this regard, it has been shown that the WNT–β-catenin pathway has a central role in the regulation of zonation in the liver and that its expression, mainly limited to the pericentral area, regulates important metabolic genes such as glutamine synthetase[42]. A recent elegant study combining spatial cell sorting with transcriptomic and proteomic approaches identified a spatially defined TIE1–WNT signalling axis in the liver endothelium, which was critical in the angiocrine control of hepatocyte functions[43]. Similarly, non-parenchymal hepatic cell populations were also suggested to have a definite spatial distribution (BOX 1).

The spatial organization of hepatocyte functions can be altered in different contexts and during the development of liver diseases (FIG. 2b). A typical example is alcohol-related liver damage that is mostly restricted to pericentral areas where detoxification enzymes (for example, cytochrome P450 2E1 (CYP2E1)) are present at high levels and where most of the lipogenic genes responsible for lipid deposition are expressed[44]. As the liver is the central organ in glucose and lipid metabolism, these metabolic reactions occur according to a precise spatiotemporal zonation that mirrors the functional efficiency of the organ. Metabolic stress generated by excessive nutrition (high fat, fructose and caloric intake) disturbs the metabolic homeostasis and leads to steatosis and hepatocyte dysfunction starting from the pericentral areas, where key metabolic enzymes involved in glucose and lipid metabolism are found[44]. Indeed, in diet-induced and genetically induced mouse models of NASH, it was reported that lipid zonation is gradually lost with disease progression[45], indicating that changes of the metabolic microenvironment result in decreased organ functionality. Nonalcoholic fatty liver disease (NAFLD) is one of the most representative and frequent types of hepatic dysfunction that increases the susceptibility to liver cancer[46]. Increased levels of free fatty acids and their metabolites within the liver induce lipotoxicity, leading to cellular damage and hepatocyte death[8]. Around the pericentral areas where oxygenation is scarce, ballooning hepatocytes in the NASH liver might lose the ability to go through the cell cycle or cell death programmes properly due to their injured cytoskeleton, thereby becoming precancerous[47]. In mouse models, it was shown that the persistent compensatory cell death and proliferation cycles induce oxidative stress and KC activation, resulting in immune cell infiltration and disease progression. At the same time, chronic inflammation can also remodel the hepatic metabolic programme, as infiltrating immune cells secrete cytokines that suppress β-oxidation and hepatic lipid turnover[48,49]. In the context of NASH and ASH, oxidative stress and hypoxia could occur as consequences of metabolic alterations related to the oxygen gradient originating throughout the porto–central axis[50]. This microenvironment, orchestrated by two key transcription factors mainly expressed in pericentral areas, namely, HIF1α and NRF2, not only determines the progression of NASH and NASH-derived HCC[51,52] but also generates favourable conditions for viral infections and chronic hepatitis[53]. Indeed, the oxygen gradient and specific

◀ Fig. 2 | **The metabolic microenvironment of the healthy and inflamed liver. a** | In a healthy liver, the organization of hepatocytes along spatial zones and an oxygen gradient enables the accomplishment of metabolic, detoxifying and synthesizing functions. Most of these functions are compartmentalized according to their energetic and, therefore, oxygen requirements. **b** | The liver displays a well-defined metabolic microenvironment that is specifically altered in pathological conditions and that shapes disease progression. Activation of the innate immune response contributes to disruption of the metabolic microenvironment to sustain the inflammatory process. These changes in turn lead to metabolic adaptations of hepatocytes that, in the context of chronic necro-inflammation, acquire precancerous characteristics and undergo metabolic reprogramming. The dashed arrows indicate the transport of metabolites and their intermediates from the circulation through the different zones of the hepatic acinus. AA, amino acid; BAAT, bile acid-CoA:amino acid N-acyltransferase; CYP, cytochrome P450 family; DAMPs, damage-associated molecular patterns; FFA, free fatty acid; HCV, hepatitis C virus; LPS, lipopolysaccharide; LSEC, liver sinusoidal endothelial cell; ROS, reactive oxygen species.

Box 1 | Metabolic zonation of liver non-parenchymal cells

Parenchymal and non-parenchymal cells have a close relationship in the liver, with the latter displaying a characteristic spatial distribution affecting hepatocyte functionality and renewal. More than 60% of the genes expressed by liver sinusoidal endothelial cells (LSECs) seem to display zonation[17]. Pericentral LSECs express WNT ligands, RSPO3 and DKK3, which shape hepatocyte zonation and dictate spatial functionality within the hepatic parenchyma as well as expression of genes involved in immunoregulatory functions. By contrast, periportal LSECs express genes involved in hormone metabolism. LSECs and hepatocytes also seem to be crucial in the context of metabolic alterations, as in nonalcoholic steatohepatitis[203]. Kupffer cells were initially shown to be predominantly located around the portal spaces where — directly exposed to the intestinal circulation — they seem to form a protective pro-inflammatory niche, producing more TNF and exhibiting higher phagocytic activity. Conversely, the pericentral counterpart seems to produce more IL-1β and to exert more cytotoxic activity[204,205]. The liver macrophage population displays substantial heterogeneity that is particularly highlighted in the context of chronic inflammation, such as nonalcoholic steatohepatitis[206]. A sophisticated single-cell transcriptomic approach identified two distinct populations of human liver-resident macrophages: one of tolerogenic character (expressing the macrophage receptor MARCO), resembling classical Kupffer cells located near the portal spaces, and a second population characterized by a pro-inflammatory monocytic profile (expressing CD1c), circumscribing the central vein[207]. Recently, it has been shown that the zonation of innate and adaptive immune cells in the liver is controlled by commensal bacteria[204]. Hepatic stellate cells have also recently been shown to have a characteristic spatial distribution in the form of portal vein-associated hepatic stellate cells (expressing high levels of NGFR) and central vein-associated hepatic stellate cells (expressing high levels of ADAMTSL2), with the latter being the most important source of collagen in CC-chemokine ligand 4 (CCL4)-induced experimental fibrosis[208].

metabolite production in the hepatic lobule might also indicate a precise hepatic tropism for HBV–HCV infections. In fact, HCV can induce steatosis by altering lipogenic signalling and by disrupting the hepatic metabolic zonation[54].

This spatiotemporal distribution of liver metabolic functions defines an evolutionarily optimal level of organization, creating a microenvironment that defines the interaction between parenchymal and non-parenchymal cells. Alterations of this equilibrium are critical in the pathogenesis of liver inflammation and support the progression of carcinogenic changes. Moreover, the functional heterogeneity of hepatocytes along the porto–central axis indicates differential susceptibility to hepatic insults, potentially leading to distinct sites of oncogenic transformation.

Cell death as a driver of necro-inflammation

Hepatocyte death is a process that accompanies chronic liver diseases such as NASH, viral hepatitis and cirrhosis[55]. It is executed mainly in the form of apoptosis, necroptosis or necrosis[55,56]. Recent findings indicate an involvement of additional cell death pathways in shaping the liver microenvironment in chronic hepatitis, such as ferroptosis, oxeiptosis and pyroptosis. The latter forms are of high interest but are as yet understudied in the context of different forms of chronic hepatitis[57]. Notably, the type of cell death executed can affect the type of primary liver cancer that develops[58].

Extracellular stimuli trigger extrinsic apoptosis by activation of cell death receptors such as FAS via bile acids in cholestatic livers[58], by FAS ligand (FASL) expressed by activated T cells[55,60], or by activation of the tumour necrosis factor receptor superfamily through pro-inflammatory immune cell-encoded ligands (for example, TNF, lymphotoxin and TNFRSF12 (also known as TNFRSF25))[55,58,61,62]. Intracellular toxic conditions such as high levels of ROS, DNA damage or replicative stress due to exhausted regenerative capacity activate intrinsic apoptosis, which has similar executing processes as the extrinsic form[63–65].

The second main form of cell death can be divided into controlled (necroptosis) and uncontrolled (necrosis) subtypes. Necroptosis, or controlled necrosis, has been described in several liver diseases characterized by ethanol-induced liver damage and fibrosis underlying cholestasis or NASH[55,58,66]. Necroptosis can be activated by extrinsic factors via several receptors such as TNFRSF1A, TNFRSF1B, FAS, TLR3 and TLR4, or intrinsically via DNA sensors such as Z-DNA-binding protein 1 (ZBP1; also known as DAI) and stimulator of interferon genes (STING)[67–69]. This induces activation of receptor-interacting serine/threonine protein kinase 3 (RIPK3), which subsequently phosphorylates mixed-lineage kinase domain-like pseudokinase (MLKL). Phosphorylated MLKL forms multimeric pores that integrate into and disrupt the plasma membranes[70,71]. Conversely, necrosis is induced under stressful conditions such as physical-induced, chemical-induced or heat-induced damage. These conditions can be found in humans after alcohol or drug intoxication (for example, acetaminophen) or ischaemia–reperfusion injury, which directly disrupts cellular integrity, for example, via increased mitochondrial permeability and reduced ATP production[72].

Thus, depending on the aetiological stimulus, different pathways of cell death contribute to inflammation and cell transformation in the liver. Of note, a direct link between molecules involved in chronic inflammation-induced programmed cell death and DNA-damage repair and genomic stability was identified in a rodent model of liver cholestasis[55]. It has been shown that caspase 8 executes chronic inflammation-induced cell death by its well-known catalytic cleavage function. At the same time, caspase 8 functions as a scaffold for a multiprotein complex as the full-length protein, independent of its catalytic domain, to enable efficient DNA-damage repair. Thus, a direct link between genomic instability and cell death can be found in chronic liver disease that, at least in preclinical models, depends on caspase 8. The caspase 8-containing complex triggers γH2AX phosphorylation, controlling DNA integrity and therefore potentially preventing malignant transformation[56]. Hepatocytes that have become apoptosis-resistant downregulate (for example, by epigenetic mechanisms) the expression of caspase 8 and thus at the same time accumulate more DNA damage over time, as the DNA-damage repair complex stabilized by caspase 8 is impaired.

Owing to the loss of an intact cell membrane, dying hepatocytes release high amounts of damage-associated molecular patterns[60]. Together with bioproducts and aberrant metabolites derived from excessive alcohol or fatty acid catabolism, these 'endogenous antigens' contribute to the collapse of the balanced immune-tolerant character[22,73]. KCs react foremost by turning on pattern recognition receptor signalling and producing a wide

spectrum of pro-inflammatory cytokines including IL-1, IL-6 and TNF, as well as chemokines including CC-chemokine ligand 1 (CCL1), CCL2 and CCL5 (REF.[22]). This leads to increased expression of the cell adhesion molecules ICAM1 and VCAM1 and down-regulation of platelet/endothelial cell adhesion molecule 1 (PECAM1) on LSECs for recruiting monocytes, neutrophils and platelets to the sites of stress[48]. Following the activation of resident innate immune cells, adaptive immune cells and inflammatory monocytes are recruited to the inflamed liver (FIG. 1b). The actual role of adaptive immunity in chronic liver inflammation varies according to the pathological context or aetiology and still needs further investigation. Hepatic accumulation of $CD4^+$ and $CD8^+$ T cells has been detected in a mouse model[74] of NASH and in patients with NASH[75]. $CD4^+$ T cells have been shown to contribute to the high level of IFNγ and therefore acceleration in hepatic inflammation. Similarly, metabolically activated $CD8^+$ T cells were reported to exacerbate NASH progression, as immunological depletion of $CD8^+$ T cells prevents NASH-induced liver damage in dietary mouse models[48,49]. Intriguingly, in the context of HBV infection, $CD4^+$ T cells have recently been identified as a dominant TNF-producing population in patients with chronic viral infection associated with liver damage[76].

Oncogenic transformation in the liver

Tumour initiation is a process through which normal cells acquire survival advantages and progressively accumulate oncogenic mutations[77]. Chronic liver injury and inflammation induce a unique hepatic response, termed ductular reaction, which is characterized by hyper-proliferation of hepatic $A6^+KRT19^+$ progenitor-like cells around bile ducts near to the portal vein[55]. This compensatory regeneration process helps to restore the organ architecture and to maintain its functionality[78,79]. However, as cells proliferate rapidly in an environment that favours the accumulation of genetic mutations[80] and the induction of oncogenic signalling pathways, proliferating cells are endowed with malignant potential[81,82].

Box 2 | Hepatic inflammation and endoplasmic reticulum stress

In many chronic inflammatory liver disorders with procarcinogenic potential (including hepatic viral infections and primary sclerosing cholangitis), the coexistence of oxidative stress and endoplasmic reticulum (ER) stress has been extensively observed. The onset of oxidative stress and induction of ER stress seem to occur in parallel due to the tight connection between mitochondria and ER via mitochondrion-associated ER membranes[209]. The unfolded protein response functions to resolve ER stress. Sustained and massive ER stress triggers unfolded protein response-mediated cell death in hepatocytes, which releases damage-associated molecular patterns, thereby inducing inflammatory responses and contributing to the progression of liver disease. Hepatic ER stress exhibits a high level of pro-inflammatory potential as hepatocytes with ER stress are more susceptible to TNF-induced cell death[210], and ER stress in macrophages activates pro-inflammatory GSK3β, NF-κB and the MAPK pathway[211]. The stress signal propagating from a single hepatic parenchymal cell can be transmitted to the neighbouring microenvironment by effective mediators, such as the soluble form of Golgi membrane protein 73 (GP73; also known as GOLM1), that activate the unfolded protein response in nearby non-parenchymal cells[212]. This process gives rise to the release of a broad spectrum of cytokines and chemokines, generating a procarcinogenetic microenvironment.

Tumour-promoting inflammatory signals

In vivo studies show that sustained and unresolved hepatic inflammation is procarcinogenic[83]. Pro-inflammatory TNF secreted by KCs was shown to trigger tumorigenesis via activation of JNK signalling in the presence of oxidative stress[84] and via activation of WNT–β-catenin signalling. In an *Mdr2* (also known as *Abcb4*) mouse knockout[85] and diet-induced or genetically induced obesity[86] models, HCC formation was promoted by TNF-mediated inflammation. Genes encoding lymphotoxin-β, TNFSF14 and their targets CCL17 and CCL20 were found to be highly overexpressed in human and mouse liver cancer, indicating activation of the NF-κB pathway by lymphotoxin[87]. Other inflammatory mediators including IL-1β, IL-6 (REF.[86]), IL-11 and IL-23 are also tumour-promoting cytokines[77]. Among them, IL-6 was proposed as the most relevant candidate in diethylnitrosamine-induced hepatic carcinogenesis[77,86] and as a reliable marker to predict the transition from viral hepatitis to HCC[86]. Moreover, enriched levels of angiopoietin 2, vascular endothelial growth factors (VEGFs), CXC-chemokine ligand 1 (CXCL1) and CXCL8 in the inflammatory environment can stimulate angiogenesis, an essential process for liver tumorigenesis[77].

Inflammation-induced persistent compensatory cell death and proliferation exacerbate oxidative stress, which results in DNA damage and gene mutation in hepatic parenchymal cells[74]. The mutagenic lesions 8-oxo-7,8-dihydro-20-deoxyguanosine (8-oxodG) and 8-nitroguanine, which are generated by ROS or reactive nitrogen species, inhibit key enzymes in DNA repair machinery. Without proper repair machinery, damaged DNA leads to genomic instability[96] and further elevates the rate of mutation. For instance, alteration of the most commonly mutated gene in liver cancer — *TP53* — was suggested to be induced by oxidative stress[88,89], which also induces inactivation of mismatch repair enzymes by epigenetic remodelling (for example, microRNA (miRNA)-based silencing and DNA methylation)[77]. Hypermethylation of genes encoding mismatch repair proteins and tumour suppressors such as mutL homologue 1 (MLH1) and p53 silences their expression and favours tumour initiation[80]. In the presence of oxidative stress, activation of cellular oncogenes and cell–cell fusion induces hepatocyte senescence. Without efficient elimination by the genetic and immunosurveillance systems, these senescent cells acquire premalignant potential[81]. Similar to endoplasmic reticulum stress (BOX 2), oxidative stress can also contribute to inflammation, as well as being a consequence of it. Activated immune cells act as a source of ROS production as well as reactive nitrogen intermediates, and increased ROS production has been shown to induce T cell protein tyrosine phosphatase (TCPTP; also known as PTPN2) to activate both STAT1 and STAT3 signalling in mouse models of NASH-induced HCC. STAT1 transcriptional activation promotes hepatic inflammation by upregulating the expression of CXCL9 and lipocalin 2, which are responsible for the recruitment of neutrophils and T lymphocytes. Conversely, activation of STAT3 seems to drive the malignant transformation of cancer progenitor cells via an IL-6–STAT3 autocrine loop[82].

Liver cell plasticity and transformation

Understanding lineage origin and cell plasticity of primary liver cancer becomes important as tumours with a mixed HCC and CCA phenotype are increasing, and these display elevated malignancy with poor prognosis[97]. Initially, HCC was proposed to originate from hepatocytes and CCA from cholangiocytes but not vice versa[94]. Recent data indicate that these hypotheses are less stringent and that lineage commitment in liver tumorigenesis is plastic[84,95] (FIG. 3).

A unique feature of the liver is its regenerative capacity upon damage-induced death of hepatocytes. Even today, it is still unclear whether hepatic stem cells are the only source of liver regeneration or whether mature hepatocytes and cholangiocytes also contribute to this process[78]. Some studies have shown that the microenvironment can affect the lineage decision of these different cell types, highlighting liver cell plasticity[58]. In a thioacetamide-induced liver damage mouse model, it could be shown that KC-derived Jagged1 is required for Notch-mediated conversion of hepatocytes into cholangiocytes[96]. Other studies also identified the Notch signalling pathway and its downstream activation of SOX9 or the RBPJ–HES1 axis as the main regulator of hepatocyte plasticity[79,97]. Another pathway that might have an important role in hepatocyte plasticity is WNT–β-catenin signalling. In a murine model of 3,5-diethoxycarboncyl-1,4-dihydrocollidine diet-induced liver injury, the authors suggested that activation of WNT–β-catenin signalling in cholangiocytes is responsible for the transdifferentiation of hepatocytes into cholangiocytes via paracrine signalling[98]. Further results from a mouse model of carbon tetrachloride-induced liver injury and in vitro studies using Hep3B cells suggest a cooperative function of YAP1 and IGFBP3 in the induction of hepatocyte dedifferentiation[98]. In this study, the authors described a feedback loop regulation of IGF2BP3 via the miRNA family Let7 or the splicing factor ESRP2 (REF.[98]). These studies suggested an interchangeable network of cells of origin and final tumour lineages. Indeed, an in vivo study showed that mitochondrial dysfunction in hepatocytes leads to ROS production, thereby activating macrophages, which release TNF and cause JUN–JNK pathway activation in biliary cells, resulting in CCA development[84]. However, molecular profiling showed that the majority of human CCA displayed a cholangiocyte-specific pattern while the remainder shared the feature of hepatic stem cells[100], suggesting that hepatic stem cells are also able to give rise to CCA[101,102]. Interestingly, activation of the Hippo–YAP pathway in hepatocytes induces HCC development via Jagged1–Notch signalling, which is also activated via KCs[78,94]. Another study showed that specific cytokine profiles in the microenvironment, which are induced by either apoptotic or necroptotic hepatocytes, can drive transformed hepatocytes into HCC or CCA lineage, respectively, in mice[58]. This lineage is influenced by epigenetic regulation of the transcription factors TBX3 and PRDM5 (REF.[58]). Of note, patients with HCC showed increased cholangiocellular characteristics on the periphery of presumed HCC lesions after undergoing transarterial chemoembolization, a method that induces massive cell death in the liver[103].

A recent study analysing large cohorts of patients with combined or mixed HCC–CCA showed that this type of tumour has a monoclonal origin and that even CCA-like regions might be derived from HCC areas within the same tumour[97]. Together, these results underline the critical role for liver cancer plasticity and the role of microenvironmental influences on the development of liver cancer subtypes, affecting treatment response and patient survival in the clinic[58,97].

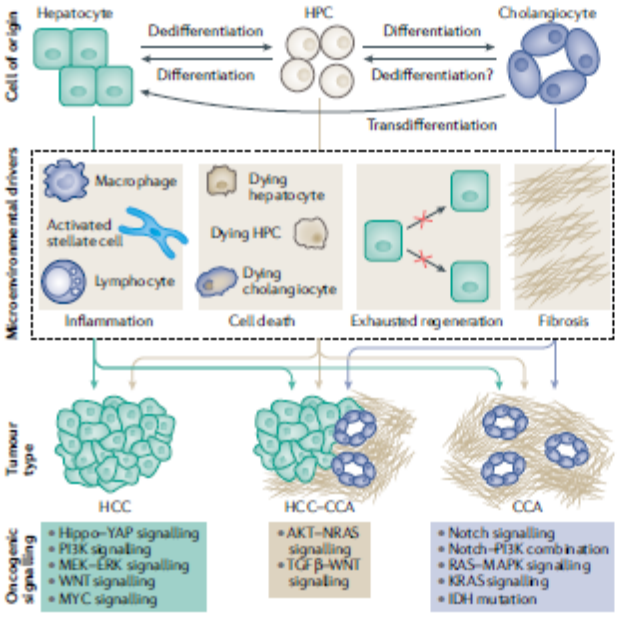

Fig. 3 | **Liver cell plasticity and oncogenic transformation.** Hepatocytes and cholangiocytes can both originate from hepatic progenitor cells (HPCs). Hepatocytes are bipotential cells; they can give rise to newly formed hepatocytes but can also transdifferentiate into cholangiocytes, which can ultimately form bile ducts. During liver injury, hepatocytes can dedifferentiate into HPCs. Whether cholangiocytes can dedifferentiate into HPCs is still a matter of debate. With different environmental factors having different effects on cell plasticity, HPCs and hepatocytes can give rise to both hepatocellular carcinoma (HCC) and cholangiocarcinoma (CCA), whereas cholangiocytes are reported to give rise only to CCA. All three mentioned cell types can also contribute to a mixed tumour type with combined features of HCC and CCA. The development of different primary liver cancer subtypes seems to be related to different oncogenic signalling depending on the environmental or disease context. Enhanced signalling within Hippo–YAP, PI3K or MEK–ERK pathways promotes HCC development. Activation of Notch signalling alone or in combination with PI3K signalling specifically in hepatocytes induces CCA outgrowth after reprogramming of the hepatocytes into a biliary-like phenotype. Moreover, mutations in isocitrate dehydrogenase (IDH) genes have been found to be unique to CCA. Oncogenic signalling related to mixed HCC–CCA remains elusive and requires further characterization. TGFβ, transforming growth factor-β.

The metabolic landscape in liver cancer

Alterations in glucose, lipid and nucleotide metabolism have been frequently observed in hepatic tumours irrespective of aetiology. Rather than oxidative

phosphorylation, tumour cells favour glycolysis (which burns glucose 15 times less efficiently than aerobic respiration) to fulfill their energetic and anabolic requirements for hyper-proliferation[104]. Accumulated metabolites from glycolysis can be directed to the hexosamine biosynthetic pathway, the pentose phosphate pathway, the tricarboxylic acid cycle, lipid synthesis and amino acid synthesis pathways, all of which are commonly dysregulated in liver cancer[104]. The metabolism of glucose and nucleotides has been reviewed elsewhere[106]; therefore, here, we focus on the metabolic changes of lipids and the metabolic reprogramming of immune cells in the hepatic tumour microenvironment.

Mechanisms of metabolic reprogramming are critical in the context of NASH and ASH-induced liver cancer, where alterations in metabolic substrates on the one hand fuel the proliferative capacity of transformed hepatocytes[105] and on the other hand alter the activity of the immune compartment. These mechanisms include unbalanced lipid intake and fatty acid mobilization from peripheral adipose tissue, thus resulting in high levels of circulating fatty acids and glucose, which induce adaptation of cancer cells to favour glucose and lipid catabolism as the major sources of energy[106]. This metabolic reprogramming not only confers hepatic cancer cells a strong ability to proliferate and spread within the parenchyma but also generates resistance to chemotherapeutic reagents[107]. Therefore, targeting specific enzymes involved in critical metabolic pathways may render cancer cells vulnerable to treatment. For instance, inhibition of stearoyl-CoA desaturase (SCD), a rate-limiting enzyme of lipogenesis, has been shown to sensitize HCC tumours in vivo to sorafenib treatment via increased endoplasmic reticulum stress[108]. In line with this, pharmacological activation of liver X receptor-α (LXRα; also known as NR1H3) in combination with RAF inhibition has recently been shown to induce cancer cell lipotoxicity related to a reduction in SCD activity and accumulation of saturated fatty acids[109]. Similarly, administration of a liver-specific synthetic inhibitor of acetyl-CoA carboxylase (ACC), another rate-limiting enzyme of lipogenesis, has been shown to slow the development of HCC alone or in combination with sorafenib in a high-calorie-induced in vivo HCC model[110]. Intriguingly, alterations in the isocitrate dehydrogenase 1 (*IDH1*) or *IDH2* genes represent about 20% of the genetic predispositions identified in CCA. As a key enzyme in the tricarboxylic acid cycle, mutations in *IDH1* and *IDH2* can lead to the accumulation of the oncometabolite 2-hydroxyglutarate (2HG), which abrogates differentiation of primary mouse hepatoblasts in vitro by blocking hepatocyte nuclear factor 4-α (HNF4α)[111]. Inhibition of SRC kinase signalling by dasatinib in CCA harbouring *IDH1* or *IDH2* mutations showed promising therapeutic potential in preclinical models[112].

In the context of metabolic alterations promoting oncogenic transformation, it is worth mentioning that the incidence of liver cancer is higher in men than in women[113]. An interesting concept was recently proposed in a study showing that, in the setting of obesity, testosterone inhibits the production of adiponectin from white adipose tissue; in a mouse model of chemically induced liver cancer, this results in a derepression of AMPK signalling with increased tumour progression in male mice[114]. Although sex hormones seem to have a critical role in this process, the mechanisms that form the basis of sex disparity in liver cancer are still poorly understood.

The metabolic environment can also shape the immune response in the liver, enabling tumour cells to escape mechanisms of immunosurveillance (FIG. 4). In mice fed a diet deficient in methionine choline, linoleic acid-mediated lipotoxicity causes selective loss of hepatic $CD4^+$ T cells and promotes hepatocarcinogenesis[115]. Moreover, immune cells undergo metabolic reprogramming that is responsible for changes in their functionality. Macrophages in the HCC microenvironment have been shown to acquire M2 polarization; this phenotype was associated with increased capacity for fatty acid oxidation and favoured tumour cell migration in vitro[116]. Changes in T cell metabolism also affect their orientation and antitumour activity; expansion of T_{reg} cells in the HCC microenvironment correlates with their increased capacity to exploit energetic substrates such as lipids and glucose[117]. Pro-inflammatory immune cells also display an increased rate of aerobic glycolysis in the tumour microenvironment. In this direction, overexpression of pyruvate kinase M2 (PKM2) was detected in patients with HCC where it was associated with poor outcome and immunosuppressive polarization of $CD8^+$ T cells, T_{reg} cells and M2 macrophages[118], thus sustaining HCC progression. Similarly, peritumoural monocytes have recently been shown to display an increased glycolytic activity in human HCC and this metabolic stimulus induces PDL1 expression in these cells, thereby dampening the cytotoxic activity of T lymphocytes against tumour cells[119].

Surveillance of early and primary tumours

Activation of specific oncogenes or mutation of tumour suppressors defines a premalignant status, inducing cell-intrinsic (genetic) or cell-extrinsic (immune cell-mediated) surveillance programmes[81].

Genetic surveillance. Oncogene-driven or stress-driven malignant cells are eliminated via apoptosis, usually mediated by non-immunosurveillance pathways — known as 'genetic surveillance' (REF.[120]). The most well-known genetic surveillance pathway involves the p53 recognition system for DNA damage. Wild-type p53 protein binds to damaged DNA and induces growth arrest in hepatocytes until DNA repair is successful. The cells that escape this checkpoint process undergo p53-mediated apoptosis. Molecules such as CD44, which induces phosphorylation of MDM2 to inhibit the genetic surveillance function of p53, accelerate the onset of HCC[121]. In a liver-specific *Trp53*-knockout mouse model, loss of p53 accelerated hepatocyte dedifferentiation and tumorigenesis[122].

Immunosurveillance. If intrinsic genetic surveillance of primary tumorigenesis fails, immune cell-mediated surveillance might come into play[81] (FIG. 1c). For example,

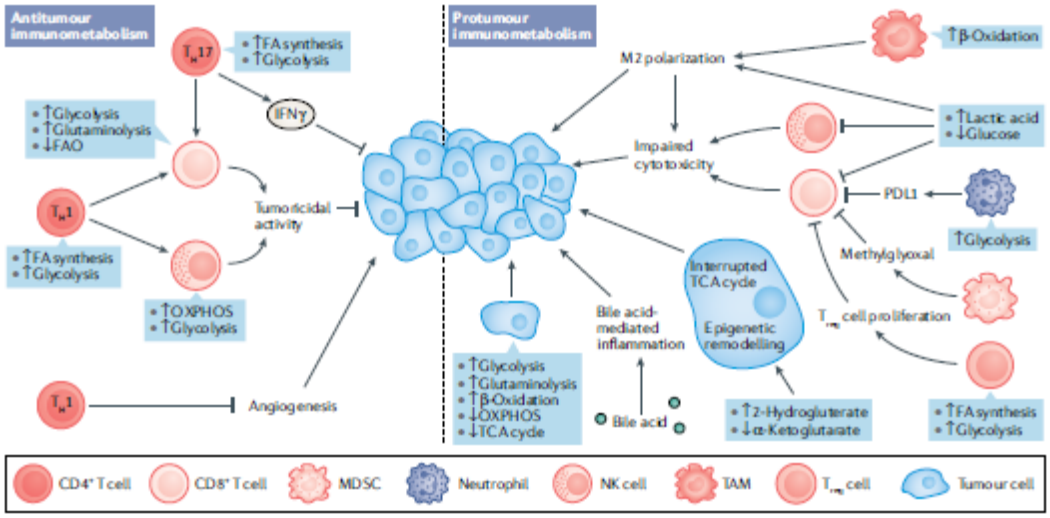

Fig. 4 | The immunometabolic microenvironment of cancerous liver. In liver cancer, metabolic reprogramming has a central role in the progression of the disease through supporting the energetic requirements of cancer cells and of the tumour immune microenvironment. Tumour cells upregulate glycolysis, gluconeogenesis and β-oxidation to support rapid proliferation, resulting in a glucose-deprived and lactate-enriched microenvironment. This glucose deprivation restricts glycolysis in tumour-infiltrating lymphocytes such as CD8+ T cells and natural killer (NK) cells. By contrast, regulatory T (T_{reg}) cells increase glycolysis and fatty acid (FA) synthesis to support their expansion, monocytes increase glycolytic activity, which induces programmed cell death 1 ligand 1 (PDL1) expression, and myeloid-derived suppressor cells (MDSCs) produce the immunosuppressive metabolite methylglyoxal; all of these dampen the antitumour immunity of CD8+ T cells. Moreover, tumour-associated macrophages (TAM2s) increase FA oxidation (FAO) and become polarized towards an M2 phenotype. Disrupted bile acid signalling and accumulation of oncometabolites (for example, 2-hydroxyglutarate) epigenetically and metabolically remodel tumour cells. Conversely, in tumours that are not glucose deprived, lymphocytes can display increased aerobic glycolysis in the tumour microenvironment to support their antitumour immunity. In particular, T helper 1 (T_H1) cells inhibit angiogenesis and promote recruitment of CD8+ T cells and NK cells. Besides recruitment of immune cells, T_H17 cells can produce interferon-γ (IFNγ) to exert tumoricidal function. OXPHOS, oxidative phosphorylation; TCA, tricarboxylic acid.

hepatocyte-specific deletion of *TAK1* (also known as *NR2C2*) was shown to trigger cellular dysplasia and hepatocarcinogenesis related to repression of canonical NF-κB-dependent signalling. In this murine model, a robust increase in senescent hepatocytes was detected after antibody-mediated depletion of CD4+ T cells[123], indicating that adaptive immune responses are essential in the surveillance of cells with cancerous potential. Key hallmarks of successful immune-mediated premalignant cell removal include sufficient T cell responses, dependent on presentation of tumour-associated antigens (for example, PPIB, SART2, SART3, p53, ABCC3, AFP, GPC3 and hTERT[124]) and costimulatory signals.

Generally, increased tumour infiltration of CD8+ T cells predicts improved clinical outcome in patients with HCC, whereas patients with HBV infection exhibiting T_{reg} cell accumulation in the liver have a high risk of HCC development[125–127], probably owing to the fact that T_{reg} cells modulate the function of tumour-specific T cells and suppress their antitumour immune responses. A high ratio of infiltrating tumour CD4+CD25+FOXP3+ T cells, which cripple the proliferation and function of CD8+ T cells, was found in the tumour microenvironment of patients with HCC and were predictive of poor prognosis[128–130]. In line with this, the intratumoural ratio of T_{reg} cells relative to cytotoxic T cells has the potential to be an independent marker for predicting HCC recurrence and patient survival[131]. Remarkably, single-cell transcriptomic analysis identified an innate-like CD8+ T cell population with high KLRB1 expression in early-relapse HCC. Compared with the well-characterized exhausted CD8+ T cells in primary HCC, this group of CD8+ T cells shows diminished antitumour cytotoxicity, low capacity of clonal expansion and correlates with poor prognosis[132]. Of note, a more in-depth understanding of hepatic T cells is needed, as NASH has been described as a CD8+ T cell-triggered liver disease that limits the efficacy of immunotherapy in NASH-driven liver cancer, indicating an aetiology-dependent disruption of immunosurveillance[133–135].

NK cells and natural killer T cells, which patrol the hepatic environment, represent another line of defence and mode of immunosurveillance. A decreased population of tumour-infiltrating NK cells has been shown in the peripheral blood and intratumoural tissue of patients with HCC compared with healthy controls, as well as functional impairment of NK cells in terms of cytokine production and cytotoxicity[2,32]. The underlying mechanism was clarified as the abnormal expression of KLRC1 and its ligand HLA-E. Notably, it has also been shown that HSCs can reduce the activity of NK

Natural killer T cells
A heterogeneous population of T cells that share characteristics of classical T cells and natural killer cells. Their classical function relates to antibacterial activity; upon activation, they produce large amounts of interferon-γ (IFNγ), IL-4 and many other cytokines.

cells via extracellular matrix (ECM) remodelling[136], and affect HCC development via different mechanisms in the setting of fibrosis (BOX 3). Natural killer T cells are a rich resource of IFNγ and are capable of activating NK cells[3]; therefore, they are commonly thought to inhibit tumour growth. However, recent evidence also suggests that $CD4^+$ natural killer T cells could secrete T helper 2 cytokines and inhibit the proliferation of $CD8^+$ T cells in both in vitro and in vivo conditions[137,138].

Similarly, the polarization of macrophages is extremely heterogeneous. Inflammatory-associated macrophages and infiltrating monocytes may induce antitumour responses[139]. However, in the tumour microenvironment, these cells are known as tumour-associated macrophages; they have an immunosuppressive phenotype[140] and facilitate tumour progression via tissue remodelling (for example, angiogenesis and wound healing), invasion and metastasis[141,142]. Recently, a group of $TREM2^+CD9^+$ profibrogenic macrophages was identified by spatially mapped single-cell RNA sequencing of patient-derived fibrotic liver tissue[143]. Although pharmacological blockade of the activity of tumour-associated macrophages seems to improve the outcome of patients with HCC, efficient and selective targeting of these cells is challenging[140,144,145].

Microenvironment-driven metastasis

Chronic alterations of the hepatic immune microenvironment accompanied by progressive changes of the metabolic profile can promote and trigger the development of primary liver cancer. Meanwhile, the apparently tumour-hostile environment of the healthy liver can also be modified acutely and transiently for homing and hosting of metastatic cells originating from extrahepatic malignancies[146]. In fact, the liver is the most frequent organ affected by metastasis after lymph nodes[147], and nearly 50% of patients with colorectal cancer (CRC) develop CRC liver metastasis, as a result of the bidirectional gut–liver relationship and the immunosuppressive orientation of the liver.

The generation of a premetastatic niche in the target organ seems to be an essential prerequisite for invasion and dissemination of cancer cells (the 'seed and soil' theory[148]). This process involves crosstalk between cancer cells and the microenvironment in the secondary target organ. Therefore, an intercellular communication between primary sites of malignant transformation and the heterogeneous cell populations present in the liver microenvironment seems to determine the capability of metastatic cells to colonize the hepatic parenchyma. In this section, we describe the dynamic interactions between specific components of the hepatic microenvironment and circulating metastases.

Liver sinusoidal endothelial cells and hepatocytes promote metastasis

Malignancies from other organs release circulating tumour cells (CTCs) into the blood or lymphatic system in a process known as intravasation, enabling them to spread to the whole body[149]. When CTCs endeavour to extravasate from the circulation to the liver, LSECs present the first barrier, with the LSEC–CTC interaction determining whether the latter forms a metastatic niche[150]. Activated LSECs increase the expression of endothelial ICAM1, CLEC4M (also known as DC-SIGNR), VCAM1 or E-selectin[151,152], which supports efficient extravasation[153] (FIG. 5). One hypothesis states that LSECs are activated by cytokines (for example, TNF and IL-1) released by KCs, whereas studies have also shown that tumour cells can induce expression of ICAM1 or VCAM1 on LSECs[154,155]. Furthermore, LSEC-derived fibronectin extra domain A or MIF can trigger prometastatic pathways in tumour cells, thereby increasing extravasation efficacy[156,157].

A direct hepatocyte–CRC cell interaction has been observed in a rat CRC model, indicating that hepatocytes contribute to metastasis spreading in the parenchyma[150]. Hepatocytes interact with tumour cells via claudin 2, or express αv integrin and CD44 isoform v6 to trap tumour cells via osteopontin, or form desmosomes with metastasizing tumour cells, enabling them to settle in the liver[158–160]. Hepatocyte-derived neuregulin 1 (also known as heregulin) can activate ERBB3 signalling and subsequently the PI3K–AKT pathway, thereby increasing the metastatic potential of CRC cells[161]. Furthermore, paracrine activation of STAT3 signalling in hepatocytes by pancreatic tumours results in the production of metastasis-supporting serum amyloid A1 (SAA1) or SAA2, which were also found to be overexpressed in liver metastases of patients with CRC[160,161].

Finally, the metabolic microenvironment has been shown to affect metastasis spreading in the liver parenchyma; in a mouse model of metastatic CRC, cancer cells were shown to boost fructose metabolism in hepatocytes by upregulating the enzyme aldolase B and therefore providing fuel for cell proliferation[162].

Box 3 | Fibrogenic response in hepatocellular carcinoma development

Most human hepatocellular carcinomas (HCCs) develop in the context of liver fibrosis or advanced cirrhosis. Activated hepatic stellate cells (HSCs) are found between endothelial cells and cancer cell trabeculae in patients with HCC, suggesting an important role for HSCs and the extracellular matrix (ECM) in the development of liver cancer[21,123,124]. In genetically modified mice expressing human platelet-derived growth factor C (to induce cirrhosis) specifically in hepatocytes, activated HSCs and collagen deposition have been observed before HCC formation, further implicating the hepatic fibrogenic response in development of fibrosis-associated HCC[21].

Hepatic parenchymal cell death and the resulting immunological response leads to activation of HSCs. Activated HSCs acquire a myofibroblastic phenotype and act as the main force driving liver ECM remodelling. The ECM molecules generate a platform for the communication of tumour cells with stromal cells[126], in which tumour cells can activate myofibroblasts and reorganize the ECM by secreting PDGF and transforming growth factor-β (TGFβ), which is beneficial for tumour growth and invasion[21,7]. ECM components such as type I and type III collagens are particularly abundant in HCC clinical samples[23,6]. Mechanotransduction mediators (for example, integrins) and ECM-associated glycoproteins, both of which contribute to the adhesion capacity of tumour cells, are also found to be highly expressed in HCC tissues[7,10].

Inflammation-related cytokines and chemokines were reported to intensively modulate liver fibrogenic responses[7,10]. For example, CC-chemokine ligand 2 (CCL2), CCL5, IL-17 and IL-33 were documented as profibrogenic, while IL-10, IL-22 and interferon-γ (IFNγ) exert the opposite effect[7,10]. PDGF and TGFβ, both of which can be secreted by HSCs and other non-parenchymal cells, promote liver fibrosis through various mechanisms[21,10] and thus contribute to HCC development. In addition, HSC-derived vascular endothelial growth factor (VEGF), PDGF and CXC-chemokines (CXCL8, CXCL9, CXCL10 and CXCL12) were shown to accelerate angiogenesis, a crucial process during HCC development.

Moreover, accumulation of lipids in hepatocytes of mice with NAFLD has been shown to influence the invasive capacity of metastatic cells by shaping the hepatic microenvironment[163]. Although data in this direction are still controversial, these findings indicate that metastatic cells exploit their reprogrammed metabolism in the new microenvironment, gaining particular benefits in metabolically active organs such as the liver.

Hepatic immune cells form a prometastatic niche

During the early phase of metastasis, KCs exert tumoricidal functions[150]. When their phagocytic capacity is overloaded, they change polarization and support CTC extravasation by secreting TNF to enhance the expression of LSEC-derived receptors[150]. Intriguingly, depletion of KCs before metastasis aggravates tumour burden in a mouse CRC liver metastasis model, while depletion of KCs in established CRC liver metastases ameliorates disease burden[164]. KCs can be activated by tumour-derived exosomes containing αvβ5 integrin, MIF[165] and/or miR-21, thus releasing promigratory and pro-inflammatory factors (such as S100 family proteins, hepatocyte growth factors, TNF, IL-6 and IL-10), which enhance liver tropism of metastases[166,166]. In fact, circulating exosomes containing miR-21 were detected in the serum of patients with CRC and were found to correlate with increased liver metastases[167]. In this specific case, the activation of a miR-21–TLR7–IL-6 axis in the liver was responsible for the generation of an inflammatory prometastatic niche. Moreover, KC-derived TGFβ and matrix metalloproteinase 9 (MMP9), together with tumour cell-derived exosomes, facilitate the production of fibronectin by HSCs, forming prometastatic conditions[165]. In mouse and human liver metastasis, HSCs transdifferentiate into cancer-associated fibroblasts[168]. Besides fibronectin, several other ECM proteins (for example, collagens, laminin and proteoglycans)[169,170] released by HSCs help to increase the efficiency of CRC cells seeding in the liver in vivo[171]. The increased deposition of ECM components activates integrin signalling-dependent cellular responses, further facilitating malignant cell growth via PI3K–MAPK signalling[172,175]. The continuous remodelling of matrix alters tissue stiffness, which was found to be increased in tumours of patients with CRC liver metastases compared with primary colorectal tumours[174]. Activated HSCs also have pro-angiogenic functions and stimulate endothelial tube formation in vivo[171], which was shown

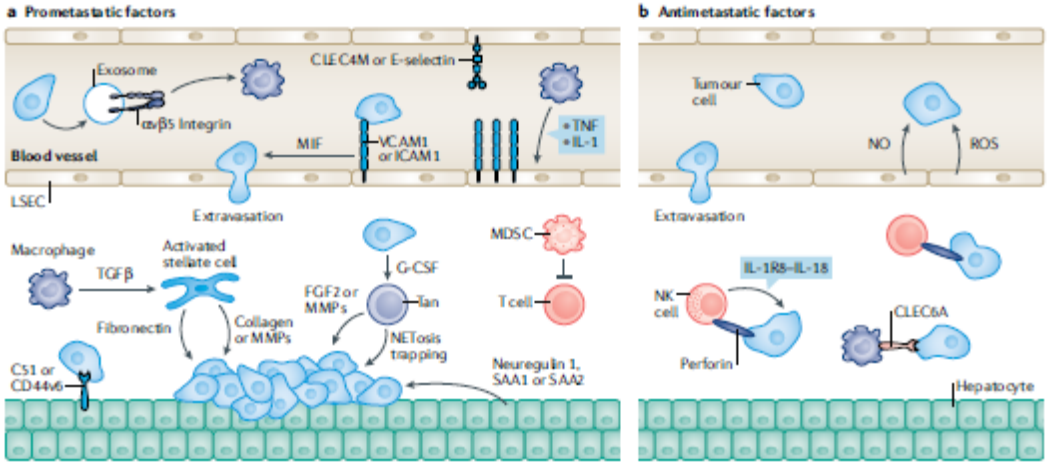

Fig. 5 | The prometastatic and antimetastatic microenvironment of the liver. a | Liver sinusoidal endothelial cells (LSECs) express surface receptors (intercellular adhesion molecule 1 (ICAM1), CLEC4M, vascular cell adhesion molecule 1 (VCAM1) or E-selectin), which are utilized by circulating tumour cells (CTCs) to adhere to the inner vessel layer, enabling efficient extravasation. CTC-derived αvβ5 integrin-expressing exosomes trigger the activation of Kupffer cells[166]. Activated Kupffer cells release TNF (which enhances the expression of LSEC-derived adhesion molecules) and transforming growth factor-β (TGFβ; which activates fibronectin production) to form a prometastatic niche; meanwhile, tumour cells can also actively increase the expression of ICAM1 or VCAM1 on LSECs, which both promote CTC extravasation. Transdifferentiation of hepatic stellate cells (HSCs) into myofibroblasts results in increased production of collagens and matrix metalloproteinases (MMPs) to enhance tumour cell extravasation and migration. Hepatocytes express αv integrin and CD44 isoform v6, and release soluble factors (for example, neuregulin 1, serum amyloid A1 (SAA1) and SAA2) into the microenvironment to form prometastatic niches. Myeloid-derived suppressor cells (MDSCs) can inhibit T cell proliferation and activation, thereby protecting metastatic cells in the liver from immune clearance. Activation of neutrophils by tumour cell-derived granulocyte colony-stimulating factor (G-CSF) enhances release of neutrophil extracellular traps (NETosis), which helps to engraft tumour cells in the hepatic tissue[176]. Furthermore, neutrophils can express fibroblast growth factor 2 (FGF2), leading to tumour cell and vascular growth. **b** | Antimetastatic factors include direct killing of CTCs by LSEC-released nitric oxide (NO) or reactive oxygen species (ROS) before extravasation, or perforin-mediated killing through T cells and natural killer (NK) cells. NK cells show antimetastatic functions mediated by the IL-1R8–IL-18 axis, leading to reduced liver metastases. A liver-specific subset of immature NK cells can kill metastatic cancer cells through a perforin-dependent cytotoxic mechanism. Furthermore, Kupffer cells can also promote killing of metastatic cells via CLEC6A, contributing to the immunosurveillance of tumour invasion. However, in summary, antimetastatic conditions in the liver microenvironment are less pronounced than prometastatic conditions.

to be mediated in a CCR2–CCL2-dependent manner[153]. Another prometastatic function of HSCs is the modulation of immune cell infiltration, as they can attract immunosuppressing T_{reg} cells and MDSCs, which inhibit T cell proliferation and activation, thereby protecting metastatic cells in the liver from immune clearance[175].

Initially, neutrophils were considered to be involved in immune clearance; however, recent studies have shown that their effects depend on the inflammatory context[153]. Neutrophils were attracted to the metastatic niche by S100A8 and S100A9 (REF.[153]) and activated by tumour-derived granulocyte colony-stimulating factor (G-CSF), displaying an increased energy metabolism that enhances NETosis, a process in which neutrophils form extracellular traps enabling engraftment of tumour cells in the hepatic tissue[176]. Furthermore, neutrophils can express fibroblast growth factor 2 (FGF2) and MMPs, promoting tumour cell proliferation and vascular growth[177]. Interestingly, platelets have recently been shown to enable metastatic cells to adhere to endothelial cells and to extravasate via P-selectin in the liver[48], and interaction with platelets shield tumour cells from TNF-mediated and NK cell-mediated killing in circulation[178].

Immunosurveillance of metastases

Despite facilitating many processes that support the onset and growth of metastases, the liver microenvironment also harbours opposing mechanisms for the surveillance of metastases (FIG. 5).

The tumoricidal functions of LSECs towards CTCs were exerted via secretion of nitric oxide, ROS, IFNγ and TNF, directly leading to tumour cell cytotoxicity before extravasation[150]. Meanwhile, they also contribute to neovascularization of metastases and inhibition of angiogenesis[179], and can reduce the formation of CRC liver metastases in a syngeneic rat model[180]. KCs can directly kill tumour cells via CLEC6A (also known as dectin 2)-mediated phagocytosis[181]. Interestingly, another study has shown that KC-mediated phagocytosis of tumour cells also depends on their interaction with NK cells[182]. NK cells show further antimetastatic functions mediated by the IL-1R8 (also known as SIGIRR)–IL-18 axis, leading to reduced CRC liver metastases after intrasplenic injection of tumour cells in a mouse model[183]. Furthermore, TRAIL-expressing NK cells also suppress hepatic metastasis of renal cell carcinoma in a FASL-dependent and IFNγ-dependent manner in both in vitro and in vivo conditions[184]. In addition, a liver-specific subset of $CD27^+CD11b^-$ immature NK cells was reported to be able to prevent melanoma from metastasizing to the liver through a perforin-dependent cytotoxic mechanism in vivo[185]. An interesting recent study has shown that conventional NK cells and type 1 innate lymphoid cells can synergistically act to limit metastasis invasion in the liver[186]. Intriguingly, single-cell transcriptomic analysis revealed that different metastatic entities from different primary sites differentially shape the liver microenvironment, inducing specific changes in these two cell populations.

The surveillance of metastases by $CD4^+$ helper and $CD8^+$ cytotoxic T cells depends largely on the liver microenvironment. Indeed, a recent study demonstrated that CRC liver metastases assimilate tolerance mechanisms that promote immunotherapy resistance in patients and mice. The authors reported that systemic T cell loss was induced by immunosuppressive macrophages recruited to CRC liver metastases via the FAS–FASL apoptotic pathway[147]. This highlights the need to investigate therapies targeting microenvironmental factors to treat metastases in the liver. In this direction, blockade of TGFβ shows potential in restoring T cell cytotoxicity and preventing CRC liver metastasis[187]. Liver-directed radiotherapy has also been reported to reshape the microenvironment of CRC liver metastases and to render tumours susceptible to anti-PDL1 therapy[147].

Targeting the hepatic microenvironment

The complex network of cells and mediators enabling efficient liver functionality characterizes a microenvironment that sustains the progression of the liver disease up to its end-stage condition: hepatic cancer. Intercepting the components of this network yields potential strategies for targeting liver cancer vulnerabilities.

The polarization of immune cells is a key component of the liver microenvironment. Despite the poor immunogenicity of HCC, the presence of lymphocyte infiltrates seem to correlate with a lower risk of recurrence and better prognosis[10]. Thus, chimeric antigen receptor (CAR) T cells or genetically modified T cell receptors (TCRs), as well as cell-based therapy using expanded tumour-infiltrated lymphocytes (for example, cytotoxic-induced killer cells) might foster the release of tumour-associated antigens by standard-of-care therapies, generating an immune defence that can potentially be bolstered by adoptive transfer of DCs[10,188,189]. Detection of uniquely expressed antigens on aberrant cells or identification of tumour-associated cell death pathways triggering a feed-forward tumour inflammatory cycle might emerge as new therapeutic weapons to overcome anti-inflammatory microenvironments and reactivate the tumour immunosurveillance[190,191]. Thus, anti-CTLA4 targeted immunotherapy in combination with transarterial chemoembolization was shown to enhance progression-free survival in patients with advanced HCC[192,193]. Monotherapeutic targeting of programmed cell death protein 1 (PD1) showed initial promising results but failed in large-scale phase III trials for treatment of HCC[135]. However, combinations of anti-CTLA4 and anti-PD1 targeted immunotherapy have shown promising efficacy and have been granted FDA approval, as have combinations of anti-PDL1 and anti-VEGF therapies[6,16,194–197].

Using immunotherapy in combination with multikinase inhibitors not only as second-line or third-line treatment option but also in first-line anticancer therapy might not only prolong survival but might also reveal a curative potential. Unfortunately, however, the individual response to immunotherapy still represents a substantial challenge[198]. Furthermore, systemic therapy might cause unfavourable side effects, which further threatens the health of patients with metastasis. As metabolic disease and NASH are associated with

disrupted immunosurveillance, stratification of patients according to the underlying chronic inflammatory aetiology might increase the patient response rate to immunotherapy — chronic HBV and HCV being positive predictors of response, and NASH being a negative predictor of response[134,135].

Targeting specific metabolic alterations that characterize the heterogeneous mutational profiles of liver cancers might present a valid option to increase the individual response to immunotherapy. Reducing glutamine availability with the glutaminase inhibitor CB-839 in combination with the inhibitor of a glutamine transporter (V-9302) seems to render tumour cells more vulnerable to oxidative stress as shown in human HCC cell lines and xenograft mouse models; therefore, it might be adopted as a complementary treatment for liver cancer[189]. Moreover, drugs targeting metabolic pathways (for example, lipogenesis and glycolysis) that shape the immune microenvironment of liver cancer could be introduced in different combined therapies. For example, metformin, ritonavir or LXRα agonists, which affect both glucose and lipid metabolism, have already been tested clinically for other indications and could be repurposed.

Conclusion

Although our knowledge of the origins and detailed molecular characterization of liver cancer has progressed tremendously in the past years, treatment options that confer substantial survival and improvement in quality of life for patients have remained scarce[200]. Only recently, a new standard-of-care therapy for advanced liver cancer has been successfully implemented with the approval of the PDL1 inhibitor atezolizumab combined with the anti-VEGF agent bevacizumab[196]. Recent data demonstrated that this combinatorial immunotherapy efficiently supports tumour surveillance in the context of viral-induced liver cancer. By contrast, non-viral aetiologies of liver cancer appear to limit the efficacy of immunotherapy-triggered immunosurveillance[133,135]. Thus, targeting and reshaping sequentially the hepatic inflammatory and/or metabolic microenvironment, as well as better understanding of and precisely targeting angiogenesis, fibrosis and nutrient supply could allow for enhanced lymphocyte infiltration into tumours — thus re-establishing effective immunosurveillance and response to immune checkpoint blockade[134,135,188,201,202].

Published online 29 July 2021

1. Llovet, J. M. et al. Hepatocellular carcinoma. *Nat. Rev. Dis. Prim.* **7**, 6 (2021).
This article provides the latest progress in the pathogenic mechanisms of HCC and its therapy.
2. Ringelhan, M., Pfister, D., O'Connor, T., Pikarsky, E. & Heikenwalder, M. The immunology of hepatocellular carcinoma. *Nat. Immunol.* **19**, 222–232 (2018).
3. Keenan, B. P., Fong, L. & Kelley, R. K. Immunotherapy in hepatocellular carcinoma: the complex interface between inflammation, fibrosis, and the immune response. *J. Immunother. Cancer* **7**, 1–13 (2019).
4. Kanwal, F. et al. Risk of hepatocellular cancer in patients with non-alcoholic fatty liver disease. *Gastroenterology* **155**, 1828–1837.e2 (2018).
5. Protzer, U., Maini, M. K. & Knolle, P. A. Living in the liver: hepatic infections. *Nat. Rev. Immunol.* **12**, 201–213 (2012).
6. European Association for the Study of the Liver. EASL clinical practice guidelines: management of hepatocellular carcinoma. *J. Hepatol.* **69**, 182–236 (2018).
7. Carrat, F. et al. Clinical outcomes in patients with chronic hepatitis C after direct-acting antiviral treatment: a prospective cohort study. *Lancet* **393**, 1453–1464 (2019).
8. Anstee, Q. M., Reeves, H. L., Kotsiliti, E., Govaere, O. & Heikenwalder, M. From NASH to HCC: current concepts and future challenges. *Nat. Rev. Gastroenterol. Hepatol.* **16**, 411–428 (2019).
9. Steeg, P. S. Tumor metastasis: mechanistic insights and clinical challenges. *Nat. Med.* **12**, 895–904 (2006).
10. Milette, S., Sicklick, J. K., Lowy, A. M. & Brodt, P. Molecular pathways: targeting the microenvironment of liver metastases. *Clin. Cancer Res.* **23**, 6390–6399 (2017).
11. de Ridder, J. et al. Incidence and origin of histologically confirmed liver metastases: an explorative case-study of 23,154 patients. *Oncotarget* **7**, 55368–55376 (2016).
12. Siegel, R. L., Miller, K. D. & Jemal, A. Cancer statistics, 2020. *CA Cancer J. Clin.* **70**, 7–30 (2020).
13. Abou-Alfa, G. K. et al. Cabozantinib in patients with advanced and progressing hepatocellular carcinoma. *N. Engl. J. Med.* **379**, 54–63 (2018).
14. Llovet, J. M., Montal, R. & Villanueva, A. Randomized trials and endpoints in advanced HCC: role of PFS as a surrogate of survival. *J. Hepatol.* **70**, 1262–1277 (2019).
15. Llovet, J. M. et al. Sorafenib in advanced hepatocellular carcinoma. *N. Engl. J. Med.* **359**, 378–390 (2008).
16. Nault, J. C., Cheng, A. L., Sangro, B. & Llovet, J. M. Milestones in the pathogenesis and management of primary liver cancer. *J. Hepatol.* **72**, 209–214 (2020).
This paper summarizes important events in the medical history of primary liver cancer and discusses the most current discoveries.
17. Rizvi, S., Khan, S. A., Hallemeier, C. L., Kelley, R. K. & Gores, G. J. Cholangiocarcinoma — evolving concepts and therapeutic strategies. *Nat. Rev. Clin. Oncol.* **15**, 95–111 (2018).
18. Vogel, A. et al. Hepatocellular carcinoma: ESMO clinical practice guidelines for diagnosis, treatment and follow-up. *Ann. Oncol.* **29**, iv238–iv255 (2018).
19. Mizukoshi, E. & Kaneko, S. Immune cell therapy for hepatocellular carcinoma. *J. Hematol. Oncol.* **12**, 52 (2019).
20. Kudo, M. Combination cancer immunotherapy in hepatocellular carcinoma. *Liver Cancer* **7**, 20–27 (2018).
21. Heymann, F. et al. Liver inflammation abrogates immunological tolerance induced by Kupffer cells. *Hepatology* **62**, 279–291 (2015).
22. Jenne, C. N. & Kubes, P. Immune surveillance by the liver. *Nat. Immunol.* **14**, 996–1006 (2013).
23. Knolle, P. A. & Thimme, R. Hepatic immune regulation and its involvement in viral hepatitis infection. *Gastroenterology* **146**, 1193–1207 (2014).
24. Winau, F. et al. Ito cells are liver-resident antigen-presenting cells for activating T cell responses. *Immunity* **26**, 117–129 (2007).
25. Thomson, A. W. & Knolle, P. A. Antigen-presenting cell function in the tolerogenic liver environment. *Nat. Rev. Immunol.* **10**, 753–766 (2010).
26. Thomson, A. W., Vionnet, J. & Sanchez-Fueyo, A. Understanding, predicting and achieving liver transplant tolerance: from bench to bedside. *Nat. Rev. Gastroenterol. Hepatol.* **17**, 719–739 (2020).
27. Krueger, P. D., Kim, T. S., Sung, S. S., Braciale, T. J. & Hahn, Y. S. Liver-resident CD103$^+$ dendritic cells prime antiviral CD8$^+$ T cells in situ. *J. Immunol.* **194**, 3213–3222 (2015).
28. Dadkowska, A. et al. XCR1$^+$ type 1 conventional dendritic cells drive liver pathology in non-alcoholic steatohepatitis. *Nat. Med.* **27**, 1043–1054 (2021).
29. Peng, H. et al. Liver-resident NK cells confer adaptive immunity in skin-contact inflammation. *J. Clin. Invest.* **123**, 1444–1456 (2013).
30. Paust, S. et al. Critical role for the chemokine receptor CXCR6 in NK cell-mediated antigen-specific memory of haptens and viruses. *Nat. Immunol.* **11**, 1127–1135 (2010).
31. Lassen, M. G., Lukens, J. R., Dolina, J. S., Brown, M. G. & Hahn, Y. S. Intrahepatic IL-10 maintains NKG2A$^+$Ly49$^-$ liver NK cells in a functionally hyporesponsive state. *J. Immunol.* **184**, 2693–2701 (2010).
32. Hoechst, B. et al. Myeloid derived suppressor cells inhibit natural killer cells in patients with hepatocellular carcinoma via the NKp30 receptor. *Hepatology* **50**, 799–807 (2009).
33. Gabrilovich, D. I. & Nagaraj, S. Myeloid-derived suppressor cells as regulators of the immune system. *Nat. Rev. Immunol.* **9**, 162–174 (2009).
34. Curiel, T. J. Tregs and rethinking cancer immunotherapy. *J. Clin. Invest.* **117**, 1167–1174 (2007).
35. Diehl, L. et al. Tolerogenic maturation of liver sinusoidal endothelial cells promotes B7-homolog 1-dependent CD8$^+$ T cell tolerance. *Hepatology* **47**, 296–305 (2008).
36. Limmer, A. et al. Efficient presentation of exogenous antigen by liver endothelial cells to CD8$^+$ T cells results in antigen-specific T-cell tolerance. *Nat. Med.* **6**, 1348–1354 (2000).
37. Aizarani, N. et al. A human liver cell atlas reveals heterogeneity and epithelial progenitors. *Nature* **572**, 199–204 (2019).
38. Peng, W. C. et al. Inflammatory cytokine TNFα promotes the long-term expansion of primary hepatocytes in 3D culture. *Cell* **175**, 1607–1619.e15 (2018).
39. Berndt, N. et al. Functional consequences of metabolic zonation in murine livers: insights for an old story. *Hepatology* **73**, 795–810 (2021).
40. Halpern, K. B. et al. Single-cell spatial reconstruction reveals global division of labour in the mammalian liver. *Nature* **542**, 352–356 (2017).
41. Droin, C. et al. Space–time logic of liver gene expression at sub-lobular scale. *Nat. Metab.* **3**, 43–58 (2021).
This article reveals how liver function is compartmentalized spatiotemporally at the sub-lobular scale.
42. Planas-Paz, L. et al. The RSPO–LGR4/5–ZNRF3/RNF43 module controls liver zonation and size. *Nat. Cell Biol.* **18**, 467–479 (2016).
43. Inverso, D. et al. A spatial vascular transcriptomic, proteomic, and phosphoproteomic atlas unveils an angiocrine Tie–Wnt signaling axis in the liver. *Dev. Cell* **56**, 1677–1693.e10 (2021).
44. Keegan, A., Martini, R. & Batey, R. Ethanol-related liver injury in the rat: a model of steatosis, inflammation and pericentral fibrosis. *J. Hepatol.* **23**, 591–600 (1995).
45. Hall, Z. et al. Lipid zonation and phospholipid remodeling in nonalcoholic fatty liver disease. *Hepatology* **65**, 1165–1180 (2017).
46. Michelotti, G. A., Machado, M. V. & Diehl, A. M. NAFLD, NASH and liver cancer. *Nat. Rev. Gastroenterol. Hepatol.* **10**, 656–665 (2013).

47. Lackner, C. Hepatocellular ballooning in nonalcoholic steatohepatitis: the pathologist's perspective. *Expert Rev. Gastroenterol. Hepatol.* **5**, 223–231 (2011).
48. Malehmir, M. et al. Platelet GPIbα is a mediator and potential interventional target for NASH and subsequent liver cancer. *Nat. Med.* **25**, 641–655 (2019).
This paper provides a rationale for antiplatelet therapy in reverting NASH and preventing NASH-to-HCC transition.
49. Wolf, M. J. et al. Metabolic activation of intrahepatic CD8+ T cells and NKT cells causes nonalcoholic steatohepatitis and liver cancer via cross-talk with hepatocytes. *Cancer Cell* **26**, 549–564 (2014).
50. Kietzmann, T. Liver zonation in health and disease: hypoxia and hypoxia-inducible transcription factors as concert masters. *Int. J. Mol. Sci.* **20**, 2347 (2019).
51. Kudo, Y. et al. PKCλ/ι loss induces autophagy, oxidative phosphorylation, and NRF2 to promote liver cancer progression. *Cancer Cell* **38**, 247–262.e11 (2020).
52. Wilson, G. K., Tennant, D. A. & McKeating, J. A. Hypoxia inducible factors in liver disease and hepatocellular carcinoma: current understanding and future directions. *J. Hepatol.* **61**, 1397–1406 (2014).
53. Wing, P. A. C. et al. Hypoxia inducible factors regulate hepatitis B virus replication by activating the basal core promoter. *J. Hepatol.* **75**, 64–73 (2021).
54. Moreau, M. et al. Hepatitis C viral proteins perturb metabolic liver zonation. *J. Hepatol.* **62**, 278–285 (2015).
55. Gautheron, J. et al. A positive feedback loop between RIP3 and JNK controls non-alcoholic steatohepatitis. *EMBO Mol. Med.* **6**, 1062–1074 (2014).
56. Boege, Y. et al. A dual role of caspase-8 in triggering and sensing proliferation-associated DNA damage, a key determinant of liver cancer development. *Cancer Cell* **32**, 342–359.e10 (2017).
This article illustrates diverging mechanistic links of caspase 8 to cancer biology in the liver.
57. Holze, C. et al. Oxeiptosis, a ROS-induced caspase-independent apoptosis-like cell-death pathway. *Nat. Immunol.* **19**, 130–140 (2018).
58. Seehawer, M. et al. Necroptosis microenvironment directs lineage commitment in liver cancer. *Nature* **562**, 69–75 (2018).
This article sheds light on lineage commitment during liver carcinogenesis and elucidates the molecular basis for common liver-damaging risk factors that result in either HCC or CCA.
59. Faubion, W. A. et al. Toxic bile salts induce rodent hepatocyte apoptosis via direct activation of Fas. *J. Clin. Invest.* **103**, 137–145 (1999).
60. Brenner, C., Galluzzi, L., Kepp, O. & Kroemer, G. Decoding cell death signals in liver inflammation. *J. Hepatol.* **59**, 583–594 (2013).
61. Assiah, T. et al. In vivo hepatic endoplasmic reticulum stress in patients with chronic hepatitis C. *J. Pathol.* **221**, 264–274 (2010).
62. Merquiol, E. et al. HCV causes chronic endoplasmic reticulum stress leading to adaptation and interference with the unfolded protein response. *PLoS ONE* **6**, e24660 (2011).
63. Roos, W. P., Thomas, A. D. & Kaina, B. DNA damage and the balance between survival and death in cancer biology. *Nat. Rev. Cancer* **16**, 20–33 (2016).
64. Brumatti, G., Salmanidis, M. & Ekert, P. G. Crossing paths: interactions between the cell death machinery and growth factor survival signals. *Cell Mol. Life Sci.* **67**, 1619–1630 (2010).
65. Farazi, P. A. & DePinho, R. A. Hepatocellular carcinoma pathogenesis: from genes to environment. *Nat. Rev. Cancer* **6**, 674–687 (2006).
66. Roychowdhury, S., McMullen, M. R., Pisano, S. G., Liu, X. & Nagy, L. E. Absence of receptor interacting protein kinase 3 prevents ethanol-induced liver injury. *Hepatology* **57**, 1773–1783 (2013).
67. Linkermann, A., Stockwell, B. R., Krautwald, S. & Anders, H. J. Regulated cell death and inflammation: an auto-amplification loop causes organ failure. *Nat. Rev. Immunol.* **14**, 759–767 (2014).
68. Newton, K. et al. Cleavage of RIPK1 by caspase-8 is crucial for limiting apoptosis and necroptosis. *Nature* **574**, 428–431 (2019).
69. Upton, J. W., Kaiser, W. J. & Mocarski, E. S. DAI/ZBP1/DLM-1 complexes with RIP3 to mediate virus-induced programmed necrosis that is targeted by murine cytomegalovirus vIRA. *Cell Host Microbe* **11**, 290–297 (2012).
70. Li, J. et al. The RIP1/RIP3 necrosome forms a functional amyloid signaling complex required for programmed necrosis. *Cell* **150**, 339–350 (2012).
71. Murphy, J. M. et al. The pseudokinase MLKL mediates necroptosis via a molecular switch mechanism. *Immunity* **39**, 443–453 (2013).
72. Malhi, H., Gores, G. J. & Lemasters, J. J. Apoptosis and necrosis in the liver: a tale of two deaths? *Hepatology* **43**, S31–S44 (2006).
73. Caesar, R. et al. Gut-derived lipopolysaccharide augments adipose macrophage accumulation but is not essential for impaired glucose or insulin tolerance in mice. *Gut* **61**, 1701–1707 (2012).
74. Sutti, S. et al. Adaptive immune responses triggered by oxidative stress contribute to hepatic inflammation in NASH. *Hepatology* **59**, 886–897 (2014).
75. Sutti, S. & Albano, E. Adaptive immunity: an emerging player in the progression of NAFLD. *Nat. Rev. Gastroenterol. Hepatol.* **17**, 81–92 (2020).
76. Wang, H. et al. TNF-α/IFN-γ profile of HBV-specific CD4 T cells is associated with liver damage and viral clearance in chronic HBV infection. *J. Hepatol.* **72**, 45–56 (2020).
77. Grivennikov, S. I., Greten, F. R. & Karin, M. Immunity, inflammation, cancer. *Cell* **140**, 883–899 (2010).
78. Kopp, J. L., Grompe, M. & Sander, M. Stem cells versus plasticity in liver and pancreas regeneration. *Nat. Cell Biol.* **18**, 238–245 (2016).
79. Yanger, K. et al. Robust cellular reprogramming occurs spontaneously during liver regeneration. *Genes Dev.* **27**, 719–724 (2013).
80. Sakurai, T. et al. Hepatocyte necrosis induced by oxidative stress and IL-1α release mediate carcinogen-induced compensatory proliferation and liver tumorigenesis. *Cancer Cell* **14**, 156–165 (2008).
81. Flecken, T. et al. Immunodominance and functional alterations of tumor-associated antigen-specific CD8+ T-cell responses in hepatocellular carcinoma. *Hepatology* **59**, 1415–1426 (2014).
82. Macdonald, R. Lifespan of liver cells — autoradiographic study using tritiated thymidine in normal, cirrhotic, and partially hepatectomized rats. *Arch. Intern. Med.* **107**, 335–343 (1961).
83. Karin, M. & Clevers, H. Reparative inflammation takes charge of tissue regeneration. *Nature* **529**, 307–315 (2016).
84. Yuan, D. T. et al. Kupffer cell-derived Tnf triggers cholangiocellular tumorigenesis through JNK due to chronic mitochondrial dysfunction and ROS. *Cancer Cell* **31**, 771–789 (2017).
85. Pikarsky, E. et al. NF-κB functions as a tumour promoter in inflammation-associated cancer. *Nature* **431**, 461–466 (2004).
86. Park, E. J. et al. Dietary and genetic obesity promote liver inflammation and tumorigenesis by enhancing IL-6 and TNF expression. *Cell* **140**, 197–208 (2010).
87. Finkin, S. et al. Ectopic lymphoid structures function as microniches for tumor progenitor cells in hepatocellular carcinoma. *Nat. Immunol.* **16**, 1235–1244 (2015).
88. Takai, A. et al. A novel mouse model of hepatocarcinogenesis triggered by AID causing deleterious p53 mutations. *Oncogene* **28**, 469–478 (2009).
89. Marrogi, A. J. et al. Oxidative stress and p53 mutations in the carcinogenesis of iron overload-associated hepatocellular carcinoma. *J. Natl Cancer Inst.* **93**, 1652–1655 (2001).
90. Elinav, E. et al. Inflammation-induced cancer: crosstalk between tumours, immune cells and microorganisms. *Nat. Rev. Cancer* **13**, 759–771 (2013).
91. Stauffer, J. K., Scarzello, A. J., Jiang, C. & Wiltrout, R. H. Chronic inflammation, immune escape, and oncogenesis in the liver: a unique neighborhood for novel intersections. *Hepatology* **56**, 1567–1574 (2012).
92. Grohmann, M. et al. Obesity drives STAT-1-dependent NASH and STAT-3-dependent HCC. *Cell* **175**, 1289–1306.e20 (2018).
This article demonstrates that obesity-related hepatic oxidative stress might contribute independently to the aetiology of NASH, fibrosis and HCC.
93. Xue, R. et al. Genomic and transcriptomic profiling of combined hepatocellular and intrahepatic cholangiocarcinoma reveals distinct molecular subtypes. *Cancer Cell* **35**, 932–947.e8 (2019).
This paper demonstrates that combined and mixed forms of HCC–CCA exhibit distinct clinical and molecular characteristics and identifies Nestin as a potential marker for diagnosis of HCC–CCA.
94. Mu, X. et al. Hepatocellular carcinoma originates from hepatocytes and not from the progenitor/biliary compartment. *J. Clin. Invest.* **125**, 3891–3903 (2015).
95. Sia, D., Villanueva, A., Friedman, S. L. & Llovet, J. M. Liver cancer cell of origin, molecular class, and effects on patient prognosis. *Gastroenterology* **152**, 745–761 (2017).
96. Ko, S., Russell, J. O., Molina, L. M. & Monga, S. P. Liver progenitors and adult cell plasticity in hepatic injury and repair: knowns and unknowns. *Annu. Rev. Pathol.* **15**, 23–50 (2020).
97. Marquardt, J. U., Andersen, J. B. & Thorgeirsson, S. S. Functional and genetic deconstruction of the cellular origin in liver cancer. *Nat. Rev. Cancer* **15**, 653–667 (2015).
98. Okabe, H. et al. Wnt signaling regulates hepatobiliary repair following cholestatic liver injury in mice. *Hepatology* **64**, 1652–1666 (2016).
99. Hyun, J. et al. Dysregulated activation of fetal liver programme in acute liver failure. *Gut* **68**, 1076–1087 (2019).
100. Komuta, M. et al. Histological diversity in cholangiocellular carcinoma reflects the different cholangiocyte phenotypes. *Hepatology* **55**, 1876–1888 (2012).
101. Banales, J. M. et al. Expert consensus document: cholangiocarcinoma: current knowledge and future perspectives consensus statement from the European Network for the Study of Cholangiocarcinoma (ENS-CCA). *Nat. Rev. Gastroenterol. Hepatol.* **13**, 261–280 (2016).
102. Komuta, M. et al. Clinicopathological study on cholangiolocellular carcinoma suggesting hepatic progenitor cell origin. *Hepatology* **47**, 1544–1556 (2008).
103. Brunt, E. et al. cHCC-CCA: consensus terminology for primary liver carcinomas with both hepatocytic and cholangiocytic differentiation. *Hepatology* **68**, 113–126 (2018).
104. Satriano, L., Lewinska, M., Rodrigues, P. M., Banales, J. M. & Andersen, J. B. Metabolic rearrangements in primary liver cancers: cause and consequences. *Nat. Rev. Gastroenterol. Hepatol.* **16**, 748–766 (2019).
This review discusses the impact of metabolic liver disturbances and the effects on primary liver cancer.
105. Yamashita, T. et al. Activation of lipogenic pathway correlates with cell proliferation and poor prognosis in hepatocellular carcinoma. *J. Hepatol.* **50**, 100–110 (2009).
106. Wang, M. et al. Dysregulated fatty acid metabolism in hepatocellular carcinoma. *Hepat. Oncol.* **3**, 241–251 (2016).
107. Xia, S., Pan, Y., Liang, Y., Xu, J. & Cai, X. The microenvironmental and metabolic aspects of sorafenib resistance in hepatocellular carcinoma. *EBioMedicine* **51**, 102610 (2020).
108. Ma, M. K. F. et al. Stearoyl-CoA desaturase regulates sorafenib resistance via modulation of ER stress-induced differentiation. *J. Hepatol.* **67**, 979–990 (2017).
109. Rudalska, R. et al. LXRα activation and Raf inhibition trigger lethal lipotoxicity in liver cancer. *Nat. Cancer* **2**, 201–217 (2021).
110. Lally, J. S. V. et al. Inhibition of acetyl-CoA carboxylase by phosphorylation or the inhibitor ND-654 suppresses lipogenesis and hepatocellular carcinoma. *Cell Metab.* **29**, 174–182.e5 (2019).
111. Saha, S. K. et al. Mutant IDH inhibits HNF-4α to block hepatocyte differentiation and promote biliary cancer. *Nature* **513**, 110–114 (2014).
This article establishes a functional relationship between IDH mutations and CCA pathogenesis, and provides a novel genetically engineered mouse model of IDH-driven malignancy.
112. Saha, S. K. et al. Isocitrate dehydrogenase mutations confer dasatinib hypersensitivity and SRC dependence in intrahepatic cholangiocarcinoma. *Cancer Discov.* **6**, 727–739 (2016).
113. Wu, E. M. et al. Gender differences in hepatocellular cancer: disparities in nonalcoholic fatty liver disease/steatohepatitis and liver transplantation. *Hepatoma Res.* **4**, 66 (2018).
114. Manieri, E. et al. Adiponectin accounts for gender differences in hepatocellular carcinoma incidence. *J. Exp. Med.* **216**, 1108–1119 (2019).
115. Ma, C. et al. NAFLD causes selective CD4+ T lymphocyte loss and promotes hepatocarcinogenesis. *Nature* **531**, 253–257 (2016).
The findings from this article, for the first time, connect lipid dysregulation with decreased antitumour surveillance in CD4+ T cells.
116. Zhang, Q. et al. Fatty acid oxidation contributes to IL-1β secretion in M2 macrophages and promotes

macrophage-mediated tumor cell migration. *Mol. Immunol.* **94**, 27–35 (2018).
117. Pacella, I. et al. Fatty acid metabolism complements glycolysis in the selective regulatory T cell expansion during tumor growth. *Proc. Natl Acad. Sci. USA* **115**, E6546–E6555 (2018).
118. Li, T.-E. et al. PKM2 drives hepatocellular carcinoma progression by inducing immunosuppressive microenvironment. *Front. Immunol.* **11**, 2722 (2020).
119. Chen, D. P. et al. Glycolytic activation of peritumoral monocytes fosters immune privilege via the PFKFB3–PD-L1 axis in human hepatocellular carcinoma. *J. Hepatol.* **71**, 333–343 (2019).
120. Klein, G. Cancer, apoptosis, and nonimmune surveillance. *Cell Death Differ.* **11**, 13–17 (2004).
121. Dhar, D. et al. Liver cancer initiation requires p53 inhibition by CD44-enhanced growth factor signaling. *Cancer Cell* **33**, 1061–1077.e6 (2018).
122. Tschaharganeh, D. F. et al. p53-Dependent Nestin regulation links tumor suppression to cellular plasticity in liver cancer. *Cell* **158**, 579–592 (2014).
123. Kang, T. W. et al. Senescence surveillance of pre-malignant hepatocytes limits liver cancer development. *Nature* **479**, 547–551 (2011).
124. Mizukoshi, E. et al. Comparative analysis of various tumor-associated antigen-specific T-cell responses in patients with hepatocellular carcinoma. *Hepatology* **53**, 1206–1216 (2011).
125. Endig, J. et al. Dual role of the adaptive immune system in liver injury and hepatocellular carcinoma development. *Cancer Cell* **30**, 308–323 (2016).
126. Fu, J. et al. Impairment of CD4+ cytotoxic T cells predicts poor survival and high recurrence rates in patients with hepatocellular carcinoma. *Hepatology* **58**, 139–149 (2013).
127. Garnelo, M. et al. Interaction between tumour-infiltrating B cells and T cells controls the progression of hepatocellular carcinoma. *Gut* **66**, 342–351 (2017).
128. Chen, K. J. et al. Selective recruitment of regulatory T cell through CCR6–CCL20 in hepatocellular carcinoma fosters tumor progression and predicts poor prognosis. *PLoS ONE* **6**, e24671 (2011).
129. Fu, J. et al. Increased regulatory T cells correlate with CD8 T-cell impairment and poor survival in hepatocellular carcinoma patients. *Gastroenterology* **132**, 2328–2339 (2007).
130. Gallimore, A. M. & Simon, A. K. Positive and negative influences of regulatory T cells on tumour immunity. *Oncogene* **27**, 5886–5893 (2008).
131. Chiriglioni, F., Menard, C., Martin, F. & Zitvogel, L. The role of regulatory T cells in the control of natural killer cells: relevance during tumor progression. *Immunol. Rev.* **214**, 229–238 (2006).
132. Sun, Y. et al. Single-cell landscape of the ecosystem in early-relapse hepatocellular carcinoma. *Cell* **184**, 404–421.e16 (2021).
This paper uses single-cell analysis of primary and recurrent HCC tumours to produce deep insights into immune evasion mechanisms.
133. Dudek, M. et al. Auto-aggressive CXCR6+ CD8 T cells cause liver immune pathology in NASH. *Nature* **592**, 444–449 (2021).
This article reveals that the mechanisms behind auto-aggression by CD8+ T cells are separate from those of antigen-specific killing by CD8+ T cells.
134. Heinrich, B. et al. Steatohepatitis impairs T-cell-directed immunotherapies against liver tumors in mice. *Gastroenterology* **160**, 331–345.e6 (2021).
135. Pfister, D. et al. NASH limits anti-tumour surveillance in immunotherapy-treated HCC. *Nature* **592**, 450–456 (2021).
This paper supports stratifying patients with HCC according to their underlying aetiology, before using immunotherapy as a main or adjuvant treatment.
136. Albertsson, P. A. et al. NK cells and the tumour microenvironment: implications for NK-cell function and anti-tumour activity. *Trends Immunol.* **24**, 603–609 (2003).
137. Bricard, G. et al. Enrichment of human CD4+ Va24/Vβ11 invariant NKT cells in intrahepatic malignant tumors. *J. Immunol.* **182**, 5140–5151 (2009).
138. Crowe, N. Y. et al. Differential antitumor immunity mediated by NKT cell subsets in vivo. *J. Exp. Med.* **202**, 1279–1288 (2005).
139. Pommier, A. et al. Inflammatory monocytes are potent antitumor effectors controlled by regulatory CD4+ T cells. *Proc. Natl Acad. Sci. USA* **110**, 13085–13090 (2013).
140. Lee, J. W. et al. Hepatocytes direct the formation of a pro-metastatic niche in the liver. *Nature* **567**, 249–252 (2019).
141. Condeelis, J. & Pollard, J. W. Macrophages: obligate partners for tumor cell migration, invasion, and metastasis. *Cell* **124**, 263–266 (2006).
142. Noy, R. & Pollard, J. W. Tumor-associated macrophages: from mechanisms to therapy. *Immunity* **41**, 49–61 (2014).
143. Ramachandran, P. et al. Resolving the fibrotic niche of human liver cirrhosis at single-cell level. *Nature* **575**, 512–518 (2019).
144. Budhu, A. et al. Prediction of venous metastases, recurrence, and prognosis in hepatocellular carcinoma based on a unique immune response signature of the liver microenvironment. *Cancer Cell* **10**, 99–111 (2006).
145. Zhu, X. D. et al. High expression of macrophage colony-stimulating factor in peritumoral liver tissue is associated with poor survival after curative resection of hepatocellular carcinoma. *J. Clin. Oncol.* **26**, 2707–2716 (2008).
146. Ciner, A. T., Jones, K., Muschel, R. J. & Brodt, P. The unique immune microenvironment of liver metastases: challenges and opportunities. *Semin. Cancer Biol.* **71**, 143–156 (2021).
147. Yu, J. et al. Liver metastasis restrains immunotherapy efficacy via macrophage-mediated T cell elimination. *Nat. Med.* **27**, 152–164 (2021).
This paper shows that hepatic metastases utilize host peripheral tolerance mechanisms to promote CD8+ T cell depletion.
148. Fidler, I. J. Timeline — the pathogenesis of cancer metastasis: the 'seed and soil' hypothesis revisited. *Nat. Rev. Cancer* **3**, 453–458 (2003).
149. Lorentzen, A. et al. Single cell polarity in liquid phase facilitates tumour metastasis. *Nat. Commun.* **9**, 887 (2018).
150. Clark, A. M., Ma, B., Taylor, D. L., Griffith, L. & Wells, A. Liver metastases: microenvironments and ex-vivo models. *Exp. Biol. Med.* **241**, 1639–1652 (2016).
151. Benedicto, A., Romayor, I. & Arteta, B. Role of liver ICAM-1 in metastasis. *Oncol. Lett.* **14**, 3883–3892 (2017).
152. Khatib, A. M. et al. Rapid induction of cytokine and E-selectin expression in the liver in response to metastatic tumor cells. *Cancer Res.* **59**, 1356–1361 (1999).
153. Brodt, P. Role of the microenvironment in liver metastasis: from pre- to prometastatic niches. *Clin. Cancer Res.* **22**, 5971–5982 (2016).
154. Wohlfeil, S. A. et al. Hepatic endothelial notch activation protects against liver metastasis by regulating endothelial-tumor cell adhesion independent of angiocrine signaling. *Cancer Res.* **79**, 598–610 (2019).
155. Mendoza, L. et al. Hydrogen peroxide mediates vascular cell adhesion molecule-1 expression from interleukin-18-activated hepatic sinusoidal endothelium: implications for circulating cancer cell arrest in the murine liver. *Hepatology* **34**, 298–310 (2001).
156. Hu, C. T. et al. MIF, secreted by human hepatic sinusoidal endothelial cells, promotes chemotaxis and outgrowth of colorectal cancer in liver prometastasis. *Oncotarget* **6**, 22410–22423 (2015).
157. Ou, J. et al. Endothelial cell-derived fibronectin extra domain A promotes colorectal cancer metastasis via inducing epithelial–mesenchymal transition. *Carcinogenesis* **35**, 1661–1670 (2014).
158. Huang, J., Pan, C., Hu, H., Zheng, S. & Ding, L. Osteopontin-enhanced hepatic metastasis of colorectal cancer cells. *PLoS ONE* **7**, e47901 (2012).
159. Tabariès, S. et al. Claudin-2 promotes breast cancer liver metastasis by facilitating tumor cell interactions with hepatocytes. *Mol. Cell Biol.* **32**, 2979–2991 (2012).
160. Shimizu, S. et al. Ultrastructure of early phase hepatic metastasis of human colon carcinoma cells with special reference to desmosomal junctions with hepatocytes. *Pathol. Int.* **50**, 953–959 (2000).
161. Yoshioka, T. et al. Significance of integrin α9β5 and erbB3 in enhanced cell migration and liver metastasis of colon carcinomas stimulated by hepatocyte-derived heregulin. *Cancer Sci.* **101**, 2011–2018 (2010).
162. Bu, P. et al. Aldolase B-mediated fructose metabolism drives metabolic reprogramming of colon cancer liver metastasis. *Cell Metab.* **27**, 1249–1262.e4 (2018).
163. Li, Y. et al. Hepatic lipids promote liver metastasis. *JCI Insight* **5**, e136215 (2020).
164. Wen, S. W., Aper, E. L. & Christophi, C. Bimodal role of Kupffer cells during colorectal cancer liver metastasis. *Cancer Biol. Ther.* **14**, 606–613 (2013).
165. Costa-Silva, B. et al. Pancreatic cancer exosomes initiate pre-metastatic niche formation in the liver. *Nat. Cell Biol.* **17**, 816–826 (2015).
166. Hoshino, A. et al. Tumour exosome integrins determine organotropic metastasis. *Nature* **527**, 329–335 (2015).
167. Shao, Y. et al. Colorectal cancer-derived small extracellular vesicles establish an inflammatory premetastatic niche in liver metastasis. *Carcinogenesis* **39**, 1368–1379 (2018).
168. Bhattacharjee, S. et al. Tumor restriction by type I collagen opposes tumor-promoting effects of cancer-associated fibroblasts. *J. Clin. Invest.* **131**, e146987 (2021).
169. Iredale, J. P., Thompson, A. & Henderson, N. C. Extracellular matrix degradation in liver fibrosis: biochemistry and regulation. *Biochim. Biophys. Acta* **1832**, 876–883 (2013).
170. Friedman, S. L. Seminars in medicine of the Beth Israel Hospital, Boston. The cellular basis of hepatic fibrosis. Mechanisms and treatment strategies. *N. Engl. J. Med.* **328**, 1828–1835 (1993).
171. Evano, C. et al. Proof of prometastatic niche induction by hepatic stellate cells. *J. Surg. Res.* **194**, 496–504 (2015).
172. Cox, D., Brennan, M. & Moran, N. Integrins as therapeutic targets: lessons and opportunities. *Nat. Rev. Drug Discov.* **9**, 804–820 (2010).
173. Zhang, D. Y. & Friedman, S. L. Fibrosis-dependent mechanisms of hepatocarcinogenesis. *Hepatology* **56**, 769–775 (2012).
174. Shen, Y. et al. Reduction of liver metastasis stiffness improves response to bevacizumab in metastatic colorectal cancer. *Cancer Cell* **37**, 800–817.e7 (2020).
175. Zhao, W. et al. Hepatic stellate cells promote tumor progression by enhancement of immunosuppressive cells in an orthotopic liver tumor mouse model. *Lab. Invest.* **94**, 182–191 (2014).
176. Hsu, B. E. et al. Immature low-density neutrophils exhibit metabolic flexibility that facilitates breast cancer liver metastasis. *Cell Rep.* **27**, 3902–3915.e6 (2019).
177. Gordon-Weeks, A. N. et al. Neutrophils promote hepatic metastasis growth through fibroblast growth factor 2-dependent angiogenesis in mice. *Hepatology* **65**, 1920–1935 (2017).
178. Haemmerle, M., Stone, R. L., Menter, D. G., Afshar-Kharghan, V. & Sood, A. K. The platelet lifeline to cancer: challenges and opportunities. *Cancer Cell* **33**, 965–983 (2018).
179. Verheul, H. M. et al. Vascular endothelial growth factor trap blocks tumor growth, metastasis formation, and vascular leakage in an orthotopic murine renal cell cancer model. *Clin. Cancer Res.* **13**, 4201–4208 (2007).
180. Gervaz, P. et al. Angiogenesis of liver metastases: role of sinusoidal endothelial cells. *Dis. Colon Rectum* **43**, 980–986 (2000).
181. Kimura, Y. et al. The innate immune receptor Dectin-2 mediates the phagocytosis of cancer cells by Kupffer cells for the suppression of liver metastasis. *Proc. Natl Acad. Sci. USA* **113**, 14097–14102 (2016).
182. Timmers, M. et al. Interactions between rat colon carcinoma cells and Kupffer cells during the onset of hepatic metastasis. *Int. J. Cancer* **112**, 793–802 (2004).
183. Molgora, M. et al. IL-1R8 is a checkpoint in NK cells regulating anti-tumour and anti-viral activity. *Nature* **551**, 110–114 (2017).
184. Takeda, K. et al. Involvement of tumor necrosis factor-related apoptosis-inducing ligand in surveillance of tumor metastasis by liver natural killer cells. *Nat. Med.* **7**, 94–100 (2001).
185. Ballas, Z. K., Buchta, C. M., Rosean, T. R., Heusel, J. W. & Shay, M. R. Role of NK cell subsets in organ-specific murine melanoma metastasis. *PLoS ONE* **8**, e65599 (2013).
186. Ducimetière, L. et al. Conventional NK cells and tissue-resident ILC1s join forces to control liver metastasis. *Proc. Natl Acad. Sci. USA* **118**, e2026271118 (2021).
187. Tauriello, D. V. F. et al. TGFβ drives immune evasion in genetically reconstituted colon cancer metastasis. *Nature* **554**, 538–543 (2018).
188. Lee, J. H. et al. Adjuvant immunotherapy with autologous cytokine-induced killer cells for hepatocellular carcinoma. *Gastroenterology* **148**, 1383–1391.e6 (2015).
189. Lee, J.-H., Oh, S.-Y., Kim, J. Y. & Nishida, N. Cancer immunotherapy for hepatocellular carcinoma. *Hepatoma Res.* **4**, 51 (2018).

190. Zhang, Z. et al. Gasdermin E suppresses tumour growth by activating anti-tumour immunity. *Nature* **579**, 415–420 (2020).
191. Crowther, M. D. et al. Genome-wide CRISPR–Cas9 screening reveals ubiquitous T cell cancer targeting via the monomorphic MHC class I-related protein MR1. *Nat. Immunol.* **21**, 178–185 (2020).
192. Sangro, B. et al. A clinical trial of CTLA-4 blockade with tremelimumab in patients with hepatocellular carcinoma and chronic hepatitis C. *J. Hepatol.* **59**, 81–88 (2013).
193. Duffy, A. G. et al. Tremelimumab in combination with ablation in patients with advanced hepatocellular carcinoma. *J. Hepatol.* **66**, 545–551 (2017).
194. Finn, R. S. et al. Atezolizumab plus bevacizumab in unresectable hepatocellular carcinoma. *N. Engl. J. Med.* **382**, 1894–1905 (2020).
This article reports an improvement of overall survival and progression-free survival in patients with advanced unresectable HCC who were treated with atezolizumab and bevacizumab when compared with sorafenib.
195. Llovet, J. M. et al. Hepatocellular carcinoma. *Nat. Rev. Dis. Primers* **2**, 16018 (2016).
196. El-Khoueiry, A. B. et al. Nivolumab in patients with advanced hepatocellular carcinoma (CheckMate 040): an open-label, non-comparative, phase 1/2 dose escalation and expansion trial. *Lancet* **389**, 2492–2502 (2017).
197. Yarchoan, M. et al. Recent developments and therapeutic strategies against hepatocellular carcinoma. *Cancer Res.* **79**, 4326–4330 (2019).
198. Harding, J. J. et al. Prospective genotyping of hepatocellular carcinoma: clinical implications of next-generation sequencing for matching patients to targeted and immune therapies. *Clin. Cancer Res.* **25**, 2116–2126 (2019).
199. Jin, H. et al. A powerful drug combination strategy targeting glutamine addiction for the treatment of human liver cancer. *eLife* **9**, e56749 (2020).
200. Rizvi, S. & Gores, G. J. Pathogenesis, diagnosis, and management of cholangiocarcinoma. *Gastroenterology* **145**, 1215–1229 (2013).
201. Rothwell, P. M. et al. Effects of aspirin on risks of vascular events and cancer according to bodyweight and dose: analysis of individual patient data from randomised trials. *Lancet* **392**, 387–399 (2018).
202. Simon, T. G. et al. Association of aspirin with hepatocellular carcinoma and liver-related mortality. *N. Engl. J. Med.* **382**, 1018–1028 (2020).
203. Xiong, X. et al. Landscape of intercellular crosstalk in healthy and NASH liver revealed by single-cell secretome gene analysis. *Mol. Cell* **75**, 644–660.e5 (2019).
This article reports unprecedented insights into intercellular interaction and reprogramming of liver cells in health and disease.
204. Gola, A. et al. Commensal-driven immune zonation of the liver promotes host defence. *Nature* **589**, 131–136 (2021).
This paper explains the link between the localization of hepatic immune cells and host protection.
205. Manco, R. & Itzkovitz, S. Liver zonation. *J. Hepatol.* **74**, 466–468 (2021).
206. Krenkel, O. et al. Myeloid cells in liver and bone marrow acquire a functionally distinct inflammatory phenotype during obesity-related steatohepatitis. *Gut* **69**, 551–563 (2020).
207. MacParland, S. A. et al. Single cell RNA sequencing of human liver reveals distinct intrahepatic macrophage populations. *Nat. Commun.* **9**, 4383 (2018).
208. Dobie, R. et al. Single-cell transcriptomics uncovers zonation of function in the mesenchyme during liver fibrosis. *Cell Rep.* **29**, 1832–1847.e8 (2019).
209. Verfaillie, T. et al. PERK is required at the ER–mitochondrial contact sites to convey apoptosis after ROS-based ER stress. *Cell Death Differ.* **19**, 1880–1891 (2012).
210. Liu, J. et al. Endoplasmic reticulum stress modulates liver inflammatory immune response in the pathogenesis of liver ischemia and reperfusion injury. *Transplantation* **94**, 211–217 (2012).
211. Ren, F. et al. Endoplasmic reticulum stress-activated glycogen synthase kinase 3β aggravates liver inflammation and hepatotoxicity in mice with acute liver failure. *Inflammation* **38**, 1151–1165 (2015).
212. Wei, C. et al. Tumor microenvironment regulation by the endoplasmic reticulum stress transmission mediator Golgi protein 73 in mice. *Hepatology* **70**, 851–870 (2019).
213. Enzan, H. et al. α-Smooth muscle actin-positive perisinusoidal stromal cells in human hepatocellular carcinoma. *Hepatology* **19**, 895–903 (1994).
214. Seitz, H. K. & Stickel, F. Risk factors and mechanisms of hepatocarcinogenesis with special emphasis on alcohol and oxidative stress. *Biol. Chem.* **387**, 349–360 (2006).
215. Heindryckx, F., Colle, I. & Van Vlierberghe, H. Experimental mouse models for hepatocellular carcinoma research. *Int. J. Exp. Pathol.* **90**, 367–386 (2009).
216. Carloni, V., Luong, T. V. & Rombouts, K. Hepatic stellate cells and extracellular matrix in hepatocellular carcinoma: more complicated than ever. *Liver Int.* **34**, 834–843 (2014).
217. Bagliери, J., Brenner, D. A. & Kisseleva, T. The role of fibrosis and liver-associated fibroblasts in the pathogenesis of hepatocellular carcinoma. *Int. J. Mol. Sci.* **20**, 1723 (2019).
218. Rosenberg, W. M. et al. Serum markers detect the presence of liver fibrosis: a cohort study. *Gastroenterology* **127**, 1704–1713 (2004).
219. Wu, Y., Qiao, X., Qiao, S. & Yu, L. Targeting integrins in hepatocellular carcinoma. *Expert. Opin. Ther. Targets* **15**, 421–437 (2011).
220. Dhar, D., Baglieri, J., Kisseleva, T. & Brenner, D. A. Mechanisms of liver fibrosis and its role in liver cancer. *Exp. Biol. Med.* **245**, 96–108 (2020).

Acknowledgements
The authors thank S. Gallage for his critical proofreading of the manuscript. M.H. was supported by an European Research Council (ERC) Consolidator grant (Hepato-MetaboPath), SFBTR179 project ID 272983813, SFB/TR 209 project ID 314905040, SFBTR1335 project ID 360372040, SFB 1479 (Project ID: 441891347), the Wilhelm Sander-Stiftung, the Rainer Hoenig Stiftung, a Horizon 2020 grant (Hepcar), Research Foundation Flanders (FWO) under grant 30826052 (EOS Convention MODEL-IDI), Deutsche Krebshilfe projects 70113166 and 70113167, German-Israeli Cooperation in Cancer Research (DKFZ-MOST) and the Helmholtz-Gemeinschaft, Zukunftsthema 'Immunology and Inflammation' (ZT-0027).

Author contributions
All authors contributed to all aspects of the article.

Competing interests
The authors declare no competing interests.

Peer review information
Nature Reviews Cancer thanks J. Fan, J. Moscat and the other, anonymous, reviewer(s) for their contribution to the peer review of this work.

Publisher's note
Springer Nature remains neutral with regard to jurisdictional claims in published maps and institutional affiliations.